

Timing and Spectral Studies of Accretion Powered X-ray Pulsars

A Thesis

submitted for the Award of Ph.D. degree of
MOHANLAL SUKHADIA UNIVERSITY

in the
Faculty of Science

By
Gaurava Kumar Jaisawal



Under the supervision of
Dr. Sachindranatha Naik
Associate Professor
Astronomy and Astrophysics Division
Physical Research Laboratory, Ahmedabad, India

DEPARTMENT OF PHYSICS
FACULTY OF SCIENCE
MOHANLAL SUKHADIA UNIVERSITY
UDAIPUR (RAJ)

Year of submission: 2016

DECLARATION

I, **Mr. Gaurava Kumar Jaisawal**, s/o Mr. Arun Kumar Jaisawal and Mrs. Vidhya Basani Jaisawal, resident of 105, PRL Thaltej Hostel, Ahmedabad 380054, hereby declare that the research work incorporated in the present thesis entitled, “**Timing and Spectral Studies of Accretion Powered X-ray Pulsars**” is my own work and is original. This work (in part or in full) has not been submitted to any University for the award of a Degree or a Diploma. I have properly acknowledged the material collected from secondary sources wherever required. I solely own the responsibility for the originality of the entire content.

Date:

Gaurava Kumar Jaisawal
(Author)

CERTIFICATE

I feel great pleasure in certifying that the thesis entitled, “**Timing and Spectral Studies of Accretion Powered X-ray Pulsars**” embodies a record of the results of investigations carried out by Mr. Gaurava Kumar Jaisawal under my guidance. He has completed the following requirements as per Ph.D regulations of the University.

- (a) Course work as per the university rules.
- (b) Residential requirements of the university.
- (c) Regularly submitted six monthly progress reports.
- (d) Presented his work in the departmental committee.
- (e) Published minimum of one research paper in a referred research journal.

I recommend the submission of thesis.

Date:

Dr. Sachindranatha Naik

Associate Professor,

Astronomy and Astrophysics Division,

Physical Research Laboratory,

Ahmedabad - 380 009.

Countersigned by

Head of the Department

Dedicated
to my family

Contents

List of Figures	xi
List of Tables	xv
Acknowledgements	xvii
Abstract	xxi
1 Introduction	1
1.1 X-ray binaries	3
1.2 Basics of accretion and Eddington luminosity	7
1.3 Accretion mechanisms in X-ray binaries	8
1.3.1 Roche-lobe overflow	10
1.3.2 Stellar wind accretion	11
1.3.3 Be/X-ray binaries: Another type of mass accretion	13
1.4 Neutron star X-ray binaries	17
1.5 Accretion powered X-ray pulsars	19
1.6 Properties of accretion powered X-ray pulsars	23
1.6.1 Spectral formation	23
1.6.2 Cyclotron resonance scattering feature	25
1.6.3 Pulse profiles	28
1.7 Spectral continuum models for pulsar	31
1.8 Outline of the thesis	33
2 Instruments, Observations and Data Analysis	35
2.1 <i>Suzaku</i> : A soft to hard X-ray observatory	37

2.1.1	X-ray Imaging Spectrometer	38
2.1.2	Hard X-ray Detector	40
2.2	<i>Nuclear Spectroscopic Telescope Array (NuSTAR)</i>	40
2.3	Overview and the observational details of X-ray sources	42
2.3.1	EXO 2030+375	42
2.3.2	4U 1909+07	43
2.3.3	Cep X-4	44
2.3.4	GX 304-1	45
2.3.5	SMC X-2	46
2.3.6	OA0 1657-415	47
2.3.7	4U 1700-37	47
2.4	Data extraction	48
2.5	X-ray timing and spectral techniques	50
3	Absorption dips in the pulse profiles of Be/X-ray	
	binary pulsars	53
3.1	Energy dependent pulse profiles of Be/X-ray binary pulsars . . .	54
3.1.1	EXO 2030+375	55
3.1.2	Cep X-4	59
3.1.3	GX 304-1	62
3.2	Broad-band spectroscopy of Be/X-ray binary pulsars	66
3.2.1	Phase-averaged and Phase-resolved spectroscopy of EXO 2030+375	67
3.2.2	Phase-averaged and Phase-resolved spectroscopy of Cep X-4	71
3.2.3	Phase-averaged and Phase-resolved spectroscopy of GX 304-1	73
3.3	Results and Discussion	75
4	Cyclotron resonance scattering features and	
	Magnetic field of pulsars	79
4.1	Detection of cyclotron line in X-ray pulsars	82

4.1.1	The fundamental cyclotron line in 4U 1909+07	83
4.1.2	The first harmonic of cyclotron line in Cep X-4	89
4.1.3	The cyclotron absorption feature in SMC X-2	96
4.1.4	Luminosity dependence of cyclotron line energy in GX 304-1	100
4.2	Phase-resolved spectroscopy of cyclotron line features	103
4.2.1	Cep X-4	103
4.2.2	SMC X-2	105
4.2.3	GX 304-1	107
4.3	Results and Discussion	109
4.3.1	Anharmonic cyclotron line energies	109
4.3.2	Luminosity dependent cyclotron line energy	111
4.3.3	Pulse-phase dependence of cyclotron line parameters	113
5	Time-resolved properties of OAO 1657-415 and 4U 1700-37	115
5.1	OA0 1657-415	117
5.1.1	Pulse profiles	117
5.1.2	Spectral analysis	121
5.1.3	Implication of clumpy wind model	128
5.1.4	Location of the Fe fluorescence line emitting region in OAO 1657-415	131
5.2	4U 1700-37	132
5.2.1	Timing properties	132
5.2.2	Time-resolved spectroscopy	139
5.3	Results and Discussion	142
6	Summary and Future Work	147
6.1	Summary	148
6.2	Scope of future study	152
	References	155

List of Publications	183
Publications attached with Thesis	187

List of Figures

1.1	Classification of X-ray binaries	3
1.2	Equipotential surfaces of two star and Roche lobe overflow	9
1.3	Stellar wind accretion	11
1.4	Representation of Be/X-ray binary system	14
1.5	<i>Swift</i> -BAT light curves of A 0535+262 and EXO 2030+375	16
1.6	Corbet diagram	16
1.7	The interaction of accretion disk with the magnetized neutron star	18
1.8	Accretion powered X-ray pulsar	20
1.9	Emission beam patterns from the poles of the neutron star	22
1.10	Systematic view of accretion column formed at poles of neutron star	23
1.11	Theoretical spectrum of Her X-1	24
1.12	Pulse profiles of the accreting X-ray pulsars	30
2.1	<i>Suzaku</i> : soft to hard X-ray observatory	38
2.2	Schematic view of <i>Suzaku</i> observatory on-board instruments	39
2.3	<i>NuSTAR</i> : the first hard X-ray focusing observatory	41
3.1	<i>Swift</i> /BAT light curves of EXO 2030+375 during 2007 and 2012 Type I outbursts	55
3.2	Pulse profiles of EXO 2030+375 in broad energy bands during 2007 and 2012 observations with <i>Suzaku</i>	56

3.3	Energy resolved pulse profiles of EXO 2030+375 up to 10 keV during 2007 May observation with <i>Suzaku</i>	57
3.4	Energy resolved pulse profiles of EXO 2030+375 from 10 to 600 keV during 2007 May observation with <i>Suzaku</i>	58
3.5	Energy resolved pulse profiles of EXO 2030+375 during 2012 May observation with <i>Suzaku</i>	59
3.6	<i>Swift</i> /BAT light curve of Cep X-4 during its 2014 outburst along with the pulse profiles of pulsar at two different luminosity epochs with <i>Suzaku</i>	60
3.7	Energy resolved pulse profiles of Cep X-4 during first <i>Suzaku</i> observation in 2014 outburst	61
3.8	Energy resolved pulse profiles of Cep X-4 during second <i>Suzaku</i> observation in 2014 outburst	62
3.9	<i>Swift</i> /BAT light curves of GX 304-1 during its 2010 and 2012 outbursts along with the pulse profiles of pulsar obtained from <i>Suzaku</i> observations	63
3.10	Energy resolved pulse profiles of GX 304-1 during first <i>Suzaku</i> observation in 2010 outburst	64
3.11	Energy resolved pulse profiles of GX 304-1 during second <i>Suzaku</i> observation performed in 2012 outburst	65
3.12	Spectral parameters obtained from phase resolved spectroscopy of 2007 <i>Suzaku</i> observation of EXO 2030+375	68
3.13	Spectral parameters obtained from phase resolved spectroscopy of 2012 <i>Suzaku</i> observation of EXO 2030+375	69
3.14	Spectral parameters obtained from phase-resolved spectroscopy of <i>Suzaku</i> observations of Cep X-4 during 2014 outburst	72
3.15	Spectral parameters obtained from phase-resolved spectroscopy of first and second <i>Suzaku</i> observations of GX 304-1	74
3.16	MHD simulations of matter flow in stable and unstable regime of accretion	77

4.1	The 1-70 keV energy spectrum of 4U 1909+07 from <i>Suzaku</i> observation fitted with a partial covering HECut model	84
4.2	The 1-70 keV energy spectrum of 4U 1909+07 from <i>Suzaku</i> observation fitted with a partial covering NPEX model.	85
4.3	Crab ratio for 4U 1909+07	88
4.4	<i>Swift</i> /BAT light curve of Cep X-4 during 2014 outburst, including the date of observations with <i>Suzaku</i> and <i>NuSTAR</i>	89
4.5	Energy spectrum of Cep X-4 in the 0.8-70 keV range obtained from second <i>Suzaku</i> observation in 2014 outburst	91
4.6	Energy spectrum of Cep X-4 in the 3-79 keV range obtained from first <i>NuSTAR</i> observation in 2014 outburst	94
4.7	Crab ratio performed for Cep X-4 from <i>NuSTAR</i> observations	96
4.8	Luminosity dependence of fundamental and first harmonics cyclotron line energies of Cep X-4	97
4.9	<i>MAXI</i> light curve of SMC X-2 during its 2015 outburst	98
4.10	Energy spectra of SMC X-2 in 1-70 keV range obtained <i>NuSTAR</i> and <i>Swift</i> /XRT observations	99
4.11	Broadband energy spectra of GX 304-1 during 2010 and 2012 observations	101
4.12	Phase-resolved spectroscopy of cyclotron line parameters of Cep X-4 during <i>Suzaku</i> observations in 2014 outburst	104
4.13	Phase-resolved spectroscopy of cyclotron line parameters of SMC X-2 during first <i>NuSTAR</i> observation in 2015 outburst	106
4.14	Phase-resolved spectroscopy of cyclotron line parameters of GX 304-1 during <i>Suzaku</i> observations	108
4.15	Reflection model for negative correlation between cyclotron line energy and luminosity	112
5.1	<i>Swift</i> /BAT light curve of OAO 1657-415	118
5.2	Light curves of OAO 1657-415 in different energy bands obtained from <i>Suzaku</i> observation	119

5.3	Energy-resolved pulse profiles of OAO 1657-415 in four region obtained from <i>Suzaku</i> observation	120
5.4	Spectral ratio in 1.8-70 keV energy range obtained for different regions of <i>Suzaku</i> observation of OAO 1657-415	122
5.5	Energy spectrum of OAO 1657-415 at four different flux levels as seen during <i>Suzaku</i> observation	124
5.6	Spectral parameters obtained from the time-resolved spectroscopy of <i>Suzaku</i> observation of OAO 1657-415	126
5.7	Change in the fluxes of iron emission lines and its equivalent widths with respect to the 2-70 keV flux obtained from time resolved spectroscopy of OAO 1657-415	127
5.8	Light curves and hardness ratio obtained from the <i>Suzaku</i> ob- servation of 4U 1700-37	133
5.9	Power density spectrum of 4U 1700-37 obtained from <i>Suzaku</i> observation	134
5.10	The 1-70 keV energy spectrum of 4U 1700-37 fitted with a par- tial covering NPEX continuum model	135
5.11	The 1-70 keV energy spectrum of 4U 1700-37 fitted with a par- tial covering HECut continuum model	136
5.12	Spectral parameters obtained from the time-resolved spectroscopy for <i>Suzaku</i> observation of 4U 1700-37	140
5.13	Variation in the fluxes of iron emission lines and its equivalent widths with respect to the 8-70 keV flux obtained from time resolved spectroscopy of 4U 1700-37.	141
5.14	Change in equivalent widths of iron emission lines with respect to the column density obtained from time-resolved spectroscopy of 4U 1700-37	141

List of Tables

1.1	Properties of HMXBs and LMXBs	5
1.2	List of the cyclotron line sources	26
3.1	Log of Be/X-ray binary pulsars EXO 2030+375, Cep X-4 and GX 304-1 with <i>Suzaku</i>	54
4.1	Observational details of pulsars 4U 1909+07, Cep X-4, SMC X-2 and GX 304-1	82
4.2	Best-fit parameters of the phase-averaged spectra for 4U 1909+07 from <i>Suzaku</i>	86
4.3	Spectral parameters obtained from the fitting of spectra of Cep X- 4 during second <i>Suzaku</i> observation in 2014 outburst	92
4.4	Best-fitting parameters obtained from <i>Suzaku</i> and <i>NuSTAR</i> ob- servations of Cep X-4 during 2014 outburst.	95
4.5	Spectral parameters obtained from the spectral fitting of three <i>NuSTAR</i> and <i>Swift</i> /XRT observations of SMC X-2 during 2015 outburst	100
4.6	Spectral parameters obtained from the spectral fitting of two <i>Suzaku</i> observations of GX 304-1	102
5.1	Log of <i>Suzaku</i> observations of eclipsing high mass X-ray binaries OAO 1657-415 and 4U 1700-37	117
5.2	Best-fitting spectral parameters obtained from the four regions seen during <i>Suzaku</i> observation of OAO 1657-415	123

5.3	Best-fitting parameters obtained from the spectral fitting of	
	<i>Suzaku</i> observation of 4U 1700-37	137

Acknowledgements

My five years journey of this thesis has been memorable because of many people who supported in all possible ways to achieve the dream of highest academic degree of my life.

First and foremost, I would like to thank my adviser Dr. Sachindra Naik, for introducing me to the exciting field of X-ray Astronomy. His deep understanding and vast experience helped me immensely in learning the subject. He allowed me to grow and explore the subject on my own, while nurturing with valuable suggestions and help whenever required. His constant guidance, support, encouragement and patience kept me motivated that finally emerged in the form of this manuscript. I have reason to be thankful to him throughout my life.

I was lucky to interact with Prof. Biswajit Paul, Prof. A.R. Rao and Prof. Dipankar Bhattacharya during my visits to IUCAA. Fruitful discussions and suggestions with them developed a more clear understanding about several areas of the high energy astrophysics. I express my sincere gratitude to my doctoral committee members, Prof. K.S. Baliyan and Dr. Santosh Vadawale for carefully reading this thesis, and their useful comments.

I am obliged to have diverse research groups in the Astronomy and Astrophysics Division that helped me to learn about ongoing researches in other branches of astronomy. I take this opportunity to thank Prof. N.M. Ashok, Dr. Ashok Singal, Prof. U.C. Joshi, Prof. D.P.K. Banerjee, Prof. Chandrashekhar, Prof. Hari Om Vats, Prof. P. Janardhan, Dr. A. Chakraborty, Dr. Shashikiran Ganesh, Dr. Mudit Srivastava, Dr. Venkat, Dr. Veeresh Singh, Dr. Lokesh Dewangan, Dr. Arvind Rajpurohit, Dr. Vishal Joshi, Dr. Aveek Sarkar, Dr. Kinshuk Acharyya, Dr. Jayesh Pabari, Mr. A.B. Shah, Mr. S. H. Doshi and Mr. Vishal Shah for their support and scientific discussion on the various topics during area seminars and canteen times. I am grateful to my seniors at division Ashish, Arun, Sunil, Susanta, Tapas and Blesson for their advice and guidance whenever required. I also thank Priyanka and Tanmoy for being such a nice and supportive seniors. I am happy to have wonderful juniors like Prahlad, Navpreet, Kumar, Shivangi, Archita and Aarthy for their cheering talks. I would also like to acknowledge the aid and academic interactions with Nilkanth, Vishal Gajjar, Shweta, Pragya, Alam Vaibhav, Samir, Mithun, Raj Laxmi, Ratna, Anjali and Suruchi at various stages. I thank to Bhagirath Bhai for

the administrative assistance at Thaltej campus. I would like to thank all the staff members of Mt. Abu observatory, Mr. Rajesh Shah, Mr. S. N. Mathur, Mr. J. K. Jain, Mr. G. S. Rajpurohit and Nafeesbai for their help during my visit to the observatory for Near-infrared observations. This list would not be complete without mentioning the name of my teachers, starting from my grandmother as my first teacher, Mr. Jeet Bahadur Singh, Mr. Dayaram Pandey, Mr. Ravindra Pratap Singh and Mr. Satish Sharma, for their constant encouragement and motivational words. I am deeply indebted to Dr. B.K. Verma and Dr. A.P. Srivastva for introducing me to the beautiful world of Physics and Mathematics during my undergraduate days. I revered to have supportive mentors like Prof. A.K. Singh, Prof. B.K. Singh and Dr. Y.C. Joshi during graduation. They familiarized me the Astronomy and Space physics research cultures.

I would like to thank the past and current Directors of PRL, Dean, Academic Committee Chairmen and other members, Registrar, coursework instructors for their support, facilities and science-based suggestions related to my research work at PRL. I am also thankful to the Dean and Head of Physics Dept. at MLSU, Udaipur for their extended co-operation. I would greatly acknowledge the resources readily available at internet (Google, NASA ADS, SIMBAD data base, arxiv, HEASoft, HEASARC Online Service) which widely helped me with present thesis. I extend my thanks to the members of computer centre, library, account section, transport section, purchase, workshop facilities and the entire administrative services of PRL for their prompt and uninterrupted services. I am gratified to the Thaltej canteen and CISF who have provided unceasing services.

I have been fortunate to have many good friends who have been always by my side. I will forever cherish the the wonderful memories, parties and brainstorming discussion on several open topics with Lalit, Anand and Prashant. I am gratified towards my close buddies Sushil, Alok, Pankaj, Nurain, Vishal and Sanjeev for always being patient listeners and unconditional supporters in time of need. I am grateful to my batch mates Anirban, Ikshu, Arun, Girish, Abhaya, Guru, Sanjay, Alok, Shraddha, Saweeta, Tanmoy, Chitra (Swapna), Kuldeep and Manu for many memorable and enjoyable moments during my years at PRL. I spent five pleasant years at Thaltej hostel and it would not be possible without the hostel mates. I would like to thank Amrendra, Arko, Rajeev, Naveen, Manojit, Girish C., Yashpal, Gaurav Tomar,

Bhavya, Gulab, Gaurav Sharma, Lekshmy, Midhun, Avdhesh, Upendra, Wageesh, Aadhi, Shrema, Batuk, Sneha, Rahul Yadav, Asim, Jinia, Chandana, Vikas, Apurv, Bivin, Dipti, Deepak, Newton, Pankaj, Shivali, Wriju, Abhishek, Subha, Chandan Gupta, Arvind Singh, Chandan Hati, Rukmani, Kuldeep Pandey, Satish, Jabir, Ali, Sudha, Rishabh, Dharak, Abdul, Ketan, Pikky, Gulshan, Rahul Kushwaha, Shefali, Nidhi, Ranadeep, Akanksha, Subir, Kaustav, Richa and Varun for their good company. I can not forget to thanks my friends KMT, Rudresh, Satyam, Prabhakar, Durgesh, Jalim, Cambodge, Sumit, Ashish and Amit Jaiswal for their best wishes.

My parents and grandparents (Amma and Babuji) have been very supportive and cooperative to my each and every decisions. They have always inspired and motivated me for hard work and, this dissertation is the end result of that. Thanks would be a small word for their untiring devotion and belief in me. I would also like to thank my relatives specially Dilip Mama for continuous support and guidance. I owe a big thanks to my sister Shalu and her husband Pankaj for their unconditional supports and frequent visit with my cute nephew 'Aarav'. Finally last but not least I thank my younger brother Saurabh for his love and affection.

Gaurava

ABSTRACT

This thesis focuses on the timing and spectral studies of accretion powered X-ray pulsars. X-ray pulsars are rotating neutron stars that emit pulsed beam of radiation along the line of sight of the observer. These sources are considered to be the unique astrophysical laboratory to test the properties of matter under extreme conditions such as high pressure, extreme density and strong magnetic field. The pulsars with strong magnetic field ($\sim 10^{12}$ G) are generally found in high mass X-ray binary systems. During the process of accretion, matter accreted from the optical companion interacts with the strong magnetic field of neutron star and follows the field lines to hot magnetic poles beyond the magnetospheric radius. A column like structure, known as accretion column, is expected to form on the top of neutron star that hosts numerous complex processes for X-ray emissions. The observational studies of these processes were carried out in this thesis for several accretion powered X-ray pulsars. The beam function or geometry of emission region is investigated through the luminosity and energy dependence of pulse profiles. Effect of the surrounding medium on the emitted radiation is also explored with the studies of pulse profiles. Detailed broad-band spectroscopy of the accretion powered X-ray pulsars can provide important information on the physical processes involved in the emission of radiation, characteristic properties of the matter distribution in accretion column, accretion stream, accretion disk, photosphere and stellar wind of the high mass companion star. Apart from the continuum spectra, several other spectral components are required to explain the pulsar spectra. In addition to fluorescence emission lines from matter distributed around the neutron star, an important interaction between magnetic field and electrons is also observed in pulsars' spectra in the form of absorption lines, known as cyclotron lines. Detection of these lines provide a direct and more accurate estimation of the magnetic field of the pulsars.

Using *Suzaku* and *NuSTAR* observations, timing and spectral studies of several X-ray pulsars have been carried out in this thesis. Luminosity and energy dependence of pulse profiles in Be/X-ray binary pulsars such as EXO 2030+375,

Cep X-4 and GX 304-1 have been studied to understand the cause of absorption dips observed in the pulse profiles. Pulse profiles of pulsars are expected to be simple and single peaked. However, Be/X-ray binaries show complex pulse profiles due to the presence of several narrow absorption dips at different pulse phases of the pulsars. Pulse profiles of above mentioned three Be/X-ray binary pulsars were studied in detail to understand the cause of absorption dips even up to higher energies by performing phase-resolved spectroscopy. In the course of this thesis work, it has been found that the value of additional column density was relatively high at dip phases in the pulse profiles. This indicates that matter is inhomogeneously distributed around the neutron star in the form of narrow streams that are phase-locked with the pulsar.

Apart from the investigation of shape of pulse profiles with energy and luminosity, broad-band spectra of several pulsars were carefully examined for the detection of cyclotron resonance scattering features in several sources in which the feature had not been detected earlier. Significant results that have obtained from this work are the detection of cyclotron absorption lines in high mass X-ray binary pulsars 4U 1909+07 and SMC X-2 along with luminosity dependence properties of these lines in pulsars like Cep X-4, SMC X-2 and GX 304-1. From this study, the first harmonic of cyclotron line was also discovered in Cep X-4. The interesting result is that the first harmonic cyclotron line was detected at an energy which is less than twice the fundamental line energy. Geometry of the magnetic field around the pulsars was also studied by performing phase resolved spectroscopy of cyclotron lines in Cep X-4, SMC X-2 and GX 304-1. The results obtained from our analysis showed that the cyclotron line parameters are variable with pulse phase of the pulsars. The observed variation was attributed to the effect of viewing angle or the role of complicated magnetic field of the pulsars.

Supergiant X-ray binaries show flare like activities in their light curves on several time scales. To probe the cause of the intensity variation in these objects, two eclipsing high mass X-ray binaries OAO 1657-415 and 4U 1700-37 were studied in this thesis. Time-resolved spectroscopy was performed to un-

derstand the observed intensity variation. It was found that inhomogeneous accretion of clumps of matter from the stellar wind of the supergiant companion was the cause of the observed variation. Using the clumpy stellar wind model, the physical parameters of the clumps causing the observed intensity variation were derived and discussed in the thesis. Apart from this, the properties of iron emission lines were also investigated in both the supergiant binaries at various orbital phases.

Keywords: X-ray binaries, Accretion, Accretion powered pulsars, Pulse profiles, Absorption, Spectroscopy, Pulse phase resolved spectroscopy, Cyclotron lines, Magnetic fields

Chapter 1

Introduction

X-ray astronomy started with the advent of rocket technology. The very first detector designed for the high energy observations was flown with V-2 sounding rocket in 1949 that discovered X-ray emission from the Sun. During this experiment, estimated X-ray flux was found to be significantly lower compared to that in the optical band. Following this, a majority of astronomers speculated that it is extremely difficult to detect high energy radiation from distant sun-like stars. In 1962, a group led by Riccardo Giacconi, later who was awarded 2002 Nobel prize in physics, proposed to investigate the solar radiation reflected from the surface of the moon. This was a historic step towards the dawn of X-ray astronomy. In addition to the expected emission, an intense beam of X-rays was recorded from a cosmic source known as Sco X-1, located in Scorpius constellation (Giacconi *et al.*, 1962). This experiment discovered X-ray emission from an extraterrestrial source that led to the origin of X-ray astronomy. Further studies suggested that Sco X-1 was about ten thousand times more luminous than the Sun. The optical counterpart of Sco X-1 was later found to be a fainter star of 13 magnitude which puzzled astronomers to understand the cause of X-ray emission from the source. On the basis of these sparkling results, the concept of mass accretion on to the compact object was considered to explain the presence of high energy emission from extra-solar sources.

A rapid growth in this branch of astronomy occurred when NASA launched its first X-ray satellite *Uhuru* in December 1970 which was dedicated to survey the sky in 2-20 keV range. *Uhuru* discovered more than 300 extra-solar X-ray sources within 27 months of its life-time and provided the first catalog of the high energy sky (Forman *et al.*, 1978). A crucial discovery of pulsation in X-ray emission was made by *Uhuru* in January 1971. Cen X-3 was discovered as the first X-ray pulsar with pulsations at a period of 4.84 s (Giacconi *et al.*, 1971). X-ray pulsars are rotating neutron stars that consist of strong magnetic field. Although neutron stars were theoretically predicated in 1934 (Baade and Zwicky, 1934), observational evidence of presence of such sources was lacking until the discovery of radio pulsar PSR 1919+21 by Jocelyn Bell (Hewish *et al.*, 1968). The detection of pulsar proved the formation of neutron stars as one of the final product of stellar evolution of massive stars. The identification of such sources in binary systems introduced a new branch of high energy astrophysics, called as X-ray binaries. After *Uhuru*, several X-ray observatories (*Einstein*, *EXOSAT*, *Ginga*, *ASCA*, *RXTE*, *BeppoSAX*, *Suzaku*) with onboard detectors of imaging and non-imaging capabilities have significantly enriched the understanding of X-ray binary systems as well as other areas of high energy astrophysics such as studies of Active Galactic Nuclei (AGN), supernova remnants, rotation powered pulsars, magnetars, Gamma-Ray Burst etc. Dedicated X-ray missions such as *Chandra X-ray observatory* (CXO), *XMM-Newton*, *INTEGRAL*, *Swift*, *NuSTAR*, *ASTROSAT* are actively operating in the sky and providing astonishing results everyday.

This thesis is aimed to explore the properties of accretion powered X-ray pulsars with the help of timing and spectral characteristics. A portion of the thesis mainly concerns the causes of absorption dips in pulse profiles of Be/X-ray binary pulsars at different luminosity levels, which is not well understood yet. Among fundamental properties, the strength and complex geometry of the magnetic field of neutron stars can be thoroughly investigated by probing the cyclotron resonance scattering features in the broad-band energy spectrum. However, these features are rare and only known for a couple of tens

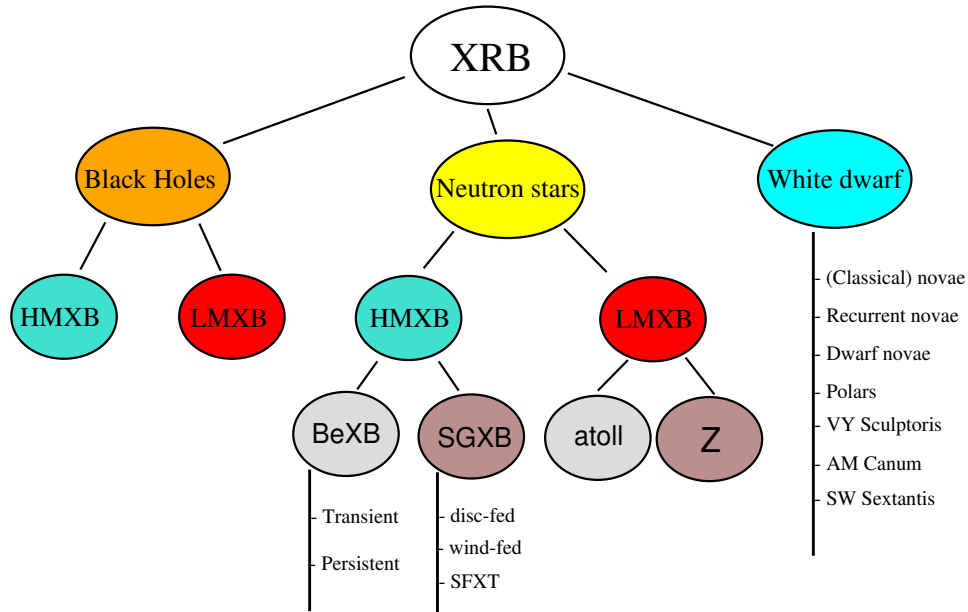


Figure 1.1: Classification of X-ray binaries based on the nature of the compact object. Further subdivisions are made depending on the nature of optical companion (Reig, 2011).

of such pulsars. A detailed investigation of the cyclotron line and its related properties in less studied or unknown pulsars is the main motivation for this research work. The current introductory chapter describes an overview of X-ray binaries, basics of mass accretion, mass transfer mechanisms, accretion powered pulsars and their properties i.e. pulse profiles, spectral formation and cyclotron resonance scattering in the following sections.

1.1 X-ray binaries

X-ray binary (XRB) is a system of two stars in which a compact object i.e. black-hole, neutron star or white dwarf and an optical companion co-rotate around the common centre of mass (Nagase, 1989; Lewin, van Paradijs and van den Heuvel, 1995; Liu, van Paradijs and van den Heuvel, 2007; Paul and Naik, 2011). They are considered to be the brightest objects in the X-ray sky with luminosities in the range of 10^{33} - 10^{38} erg s $^{-1}$. In these systems, X-ray photons are emitted because of the accretion of matter from the optical companion to

the compact object. Depending on the nature and evolutionary state of the optical star, the mass accretion can occur through different processes, such as (i) Roche-lobe overflow, (ii) capture of stellar wind or (iii) Be-disk accretion. However, the observed characteristic properties of X-ray emission are primarily governed by the nature of the compact object. If the accreting object is a neutron star, its strong magnetic field ($\sim 10^{12}$ G) truncates the accretion flow at several hundreds of neutron star radii and funnels matter onto its magnetic poles. A thermal mound is formed at poles which acts as a major source of X-ray emission. However, in case of low magnetic field neutron star, an accretion disk is expected to be formed during the accretion process that extends closer to the surface of neutron star. The boundary layer between the neutron star and the accretion disk produces high energy radiation. Moreover, if the compact object is a black hole, X-rays are produced from the hot inner accretion disk around it. The reprocessing of hard X-ray photons from accretion disk also shapes the broadband spectrum of black holes.

Depending on the nature of compact objects, XRBs are broadly divided into three major groups such as (1) Black hole X-ray binaries, (2) Neutron star X-ray binaries and (3) White dwarf X-ray binaries or cataclysmic variables (CVs) (Lewin, van Paradijs and van den Heuvel, 1995; Reig, 2011). A categorization of XRBs is depicted as family-tree with three main branches and shown in Figure 1.1. Another kind of sub-division can also be implemented on the black hole and neutron star X-ray binaries. This classification is based on the mass of the optical companion. If the optical companion is an early type massive star with mass $\geq 10 M_{\odot}$, then such XRB is known as high mass X-ray binary (HMXB). If the optical companion is relatively less massive ($\leq 3 M_{\odot}$) main sequence star of later than A-type, the system is categorized as low mass X-ray binary (LMXB).

HMXBs and LMXBs are powered by different kind of mass transfer mechanisms. Mass accretion through the capture of stellar wind or Be-disk mechanism generally takes place in HMXBs. However, the Roche-lobe overflow is considered as the dominant mode of mass transfer in LMXBs. As a result,

Table 1.1: Properties of HMXBs and LMXBs

Characteristics	HMXBs	LMXBs
Compact object	NS (BH in a few cases)	NS and BH
Optical companion	O or B	later than A
Mass of companion	$>10 M_{\odot}$	$<3 M_{\odot}$
Orbital period	1 d - 1 yr	10 m - 10 d
L_{opt}/L_x	0.1 - 1000	0.001 - 0.01
Optical spectrum	stellar like	reprocessing
X-ray outbursts	less	more
X-ray eclipses	common	less
X-ray spectra	hard (kT >15 keV)	soft (kT <5 keV)
Accretion disk	usually no or small	yes
Accretion mechanism	stellar wind/ Be-disk	Roche-lobe overflow
Pulsations (NS)	common	in a few cases
Magnetic field (NS)	high (10^{12} G)	relatively low (10^{8-9} G)
Age	$<10^7$ yr	$\sim 10^9$ yr
Distribution	Galactic plane	Galactic centre, Galactic plane, Galactic bulge, globular clusters

LMXBs and HMXBs exhibit different X-ray properties in their light curves and spectra. LMXBs are assumed to be highly variable on various time scales as compared to HMXBs. There are several LMXBs which show two type of thermonuclear X-ray bursts such as Type I (thermonuclear explosions on neutron star surface) and Type II (giant outburst due to accretion instabilities; Lewin, van Paradijs and Taam, 1993). On the other hand, HMXBs appear as transient as well as persistent X-ray sources depending on the properties of optical companion and binary orbital parameters (Reig, 2011). Although most of the HMXBs are known to possess neutron stars as compact object, a

few of them are also discovered with black hole as the primary star. Therefore, the population of HMXBs are generally referred as the neutron star X-ray binaries. We have summarized observational properties of HMXBs and LMXBs in Table 1.1. A comprehensive review on CVs can be found in Lewin, van Paradijs and van den Heuvel (1995). In this thesis, the observational studies of accretion powered X-ray pulsar in HMXB systems are presented.

HMXBs can be further classified into two classes – Supergiant X-ray Binaries (SGXBs) and Be/X-ray Binaries (BeXBs). This classification is based on the luminosity and type of the optical companion. SGXB consists of a supergiant optical companion (luminosity class I, II), while BeXB has a dwarf, subdwarf or giant OB star of luminosity class III-V as the optical companion. A supergiant companion is a strong source of stellar wind (10^{-6} – 10^{-8} M_{\odot} yr^{-1}) with supersonic velocity of up to 2000 km s^{-1} . Capture of the stellar wind by the compact object is the major source of X-ray emission in SGXB systems. Due to their supergiant size, the possibility of mass transfer through Roche-lobe overflow, however, can not be overruled. Based on the accretion processes, SGXBs can be further sub-divided into wind-fed and disk-fed SGXBs. The wind-fed SGXBs appeared to be transient and have a largest population (up to a few tens in number). However, only three sources, SMC X-1, LMC X-4 and Cen X-3, are known as disk-fed SGXBs. They show persistent X-ray activity.

On the other hand, BeXBs represent the largest sub-class ($\sim 60\%$) of HMXBs. The optical companion in these system is a Be star which shows emission lines in their optical and infrared spectra. These emission lines are believed to originate from a circumstellar disk around the Be star (Porter and Rivinius, 2003; Balona, 2000; Slettebak, 1988). Although BeXBs generally host a neutron star as compact object, recently a BeXB system (MWC 656) with a black hole and a Be star is discovered (Casares *et al.*, 2014). The mass transfer from the Be circumstellar disk to the compact object causes X-ray outbursts in these systems. A detailed description on the properties of BeXBs are discussed in section 1.3.3.

1.2 Basics of accretion and Eddington luminosity

Zeldovich and Guseynov (1966) suggested that mass accretion is the most efficient process of high energy emission in XRBs and can explain the observations of X-ray sources. It converts the gravitational potential energy of accreting matter into the kinetic energy. A simple calculation can show the power of accretion mechanism. Suppose a particle of mass m is moving from infinity towards a compact object of mass M and radius R . The energy released during this process can be estimated as

$$E_{\text{acc}} = \frac{GMm}{R} \quad (1.1)$$

where G is the gravitational constant. For a canonical neutron star of $M=1.4 M_{\odot}$ and $R=10$ km, the accretion of 1 gm matter produces an enormous amount of energy $E_{\text{acc}} \sim 10^{20}$ erg. This is ~ 20 times more than the energy produced during nuclear fusion of hydrogen to helium, which is $E_{\text{nucl}} \sim 6 \times 10^{18}$ erg (Frank, King and Raine, 1992). The accretion energy depends on the M/R ratio of the compact object. Therefore, the process of accretion onto neutron star and black hole is considered to be the efficient source of energy with an efficiency factor of up to $\sim 15\%$ and 40% , respectively (Frank, King and Raine, 1992).

The luminosity produced during this process is known as accretion luminosity which is defined as

$$L_{\text{acc}} = \frac{GM\dot{m}}{R} \quad (1.2)$$

For a given compact object, accretion luminosity is proportional to the mass accretion rate \dot{m} . It means that for higher accretion rate, the accretion luminosity is higher. However, there is an upper limit to the accretion luminosity that an accreting object can attain. This limiting luminosity is known as *Eddington luminosity* L_{Edd} . In other words, the Eddington luminosity represents limiting luminosity at which gravitational and radiation forces acting

on an electron-proton pair are in equilibrium condition. The expression for Eddington luminosity can be written as

$$L_{\text{Edd}} = \frac{4\pi GMm_p c}{\sigma_T} \approx 1.3 \times 10^{38} \frac{M}{M_\odot} \text{erg s}^{-1} \quad (1.3)$$

where m_p is the proton mass and σ_T is Thomson scattering cross-section ($\sigma_T = 6.6 \times 10^{-25} \text{ cm}^{-2}$). This expression assumes the scenario of spherical geometry and steady flow accretion. However, in cases of non-spherical geometry and non-steady accretion like supernova explosion, luminosity of a compact object can exceed the Eddington luminosity. Accretion of matter from the companion star to the compact object is considered as main cause of X-ray emission. In general, there are three methods by which matter can be transferred from companion to the compact object. These processes are described in details in the following section.

1.3 Accretion mechanisms in X-ray binaries

To understand the process of accretion mechanism, we need to know about the geometry of gravitational potential surfaces of both the stars in a binary. A star of certain mass and radius consists of spherical equipotential surfaces around it. In the presence of second star, the equipotential surfaces of a star appear no longer symmetric. They distort from spherical geometry and represent by a combined effective potential of both the stars, known as the Roche potential. The Roche potential is given by

$$\phi_R = -\frac{GM_1}{|r - r_1|} - \frac{GM_2}{|r - r_2|} - \frac{1}{2}(\omega \wedge r)^2 \quad (1.4)$$

where M_1 and M_2 are masses of two stars, and r_1 and r_2 are the position vectors of star centers. The first two terms in the expression show the potential of individual stars acting on a test particle at distance r . The third term represents the centrifugal potential because of binary rotation at angular velocity ω . The contribution of Coriolis force is not included in the expression. For a certain mass ratio, the geometry of Roche potential is shown in Figure 1.2. It can

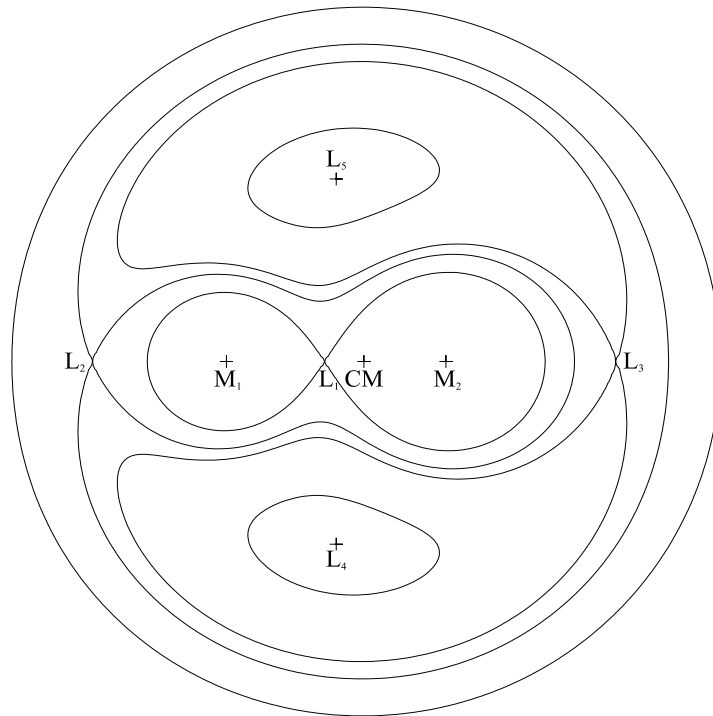


Figure 1.2: The equipotential surfaces of a binary system is shown for a given mass ratio. M_1 and M_2 represent the masses of stars in the binary system. Mass transfer from the companion to the compact object takes place through the L_1 point. Image courtesy: Kuster (2004).

be seen that the lobes of both the stars are connected at a point called inner Lagrange L_1 or saddle point. At this point, the gravitational forces exerted by both the stars are equal but in opposite direction. In other words, a test particle feels zero gravitational force at a Lagrangian point. Total five Lagrangian points are possible in a binary system. Three points L_1 , L_2 & L_3 are located in the binary plane and other two points L_4 & L_5 are in perpendicular direction of the plane as shown in Figure 1.2. If one of the star is evolving and exceeding its own Roche lobe, this extra mass is no longer bound to the star. This can get transferred into the gravitational well of other star through L_1 point (Frank, King and Raine, 1992; Longair, 1994). Such type of mass transfer mechanism is known as Roche-lobe overflow. A discussion on the Roche-lobe overflow and other types of mass transfer processes are presented in the following sections.

1.3.1 Roche-lobe overflow

The Roche lobe overflow is the primary mode of mass accretion in LMXBs. In these systems, the optical companion is a late type low mass star that have weak stellar wind. Due to evolution of the optical companion or orbit-shrink, matter from the surface of optical companion exceeds its own Roche-lobe and falls into the gravitational pull of compact object via inner Lagrange point (see Figure 1.2). Such type of mass transfer is known as Roche-lobe overflow. Due to the rotation of donor star, accreting matter carries significant amount of angular momentum. As a result, instead of directly falling, the accreted matter starts spiraling around the compact object in the lowest energy orbit i.e. circular orbit. An accretion disk is expected to form around the compact object only if circularization radius (R_{cir}) is greater than the radius of accreting object. In general the circularization radius is defined as,

$$R_{cir} = \frac{J^2}{GM_X} \quad (1.5)$$

where, J is the specific angular momentum (angular momentum per unit mass) and M_X is the mass of the compact object (Pringle, 1981). The estimation of circularization radius can also constrain the upper limit of the disk size. In other words, this relates to a distance from where disk begins to form. The matter orbiting around the compact object losses angular momentum by dissipative processes such as collision, shock, viscosity in a circular ring (Shakura and Sunyaev, 1973; Pringle, 1981). This causes the orbit to shrink towards a lower circular orbit and an accretion disk starts to form around the compact object.

For LMXBs, the circularization radius can be simply described as

$$R_{cir}^{roche} \simeq 3.5 \times 10^9 M_O^{1/3} P_{hr}^{2/3} \text{ cm} \quad (1.6)$$

here, P_{hr} is the orbital period of binary in hours and M_O is the mass of companion star in the unit of solar mass (Frank, King and Raine, 1992). For typical parameters, the circularization radius can be estimated as $R_{cir} > 10^9$ cm. Since the radius of a compact object can not be larger than the radius of white

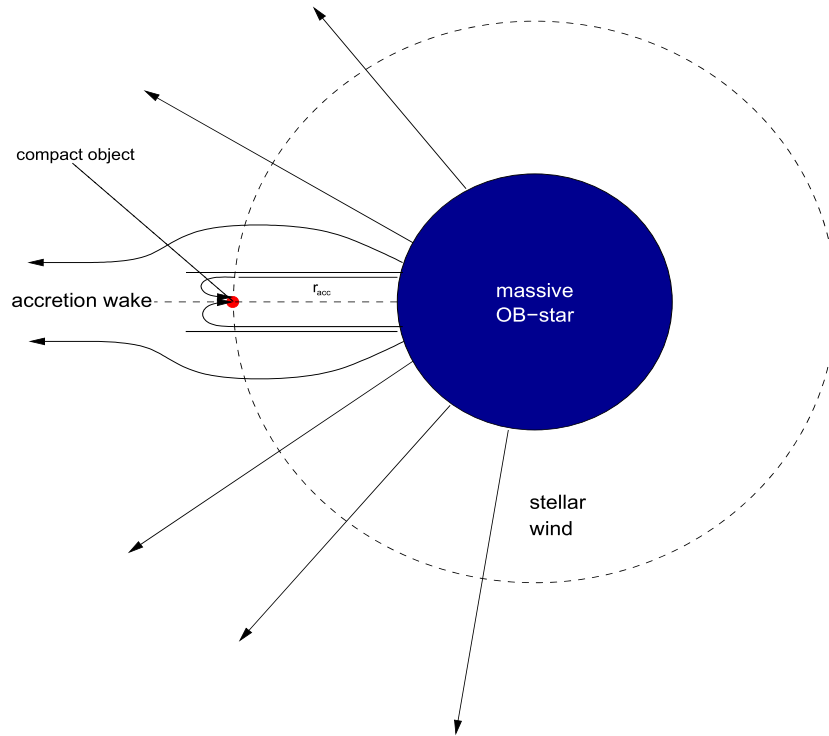


Figure 1.3: Stellar wind accretion in high mass X-ray binaries. The compact object orbits close to the OB companion star. The matter captured within accretion radius r_{acc} is accreted by the compact object. An accretion wake, as shown in figure, is formed behind the compact object. This figure is not to scale and adopted from Kreykenbohm *et al.* (2004).

dwarf ($\sim 10^9$ cm), an accretion disk is expected to form during the process of Roche-lobe overflow. When the accreted matter touches the surface of compact object, X-ray emission takes place.

1.3.2 Stellar wind accretion

Accretion of matter through Roche-lobe overflow is considered to be rare in HMXBs because of the massive and non-supergiant optical companion. However, accretion via the capture of stellar wind is possible in these systems. This process was first suggested by Bondi and Hoyle (1944) even before the discovery of XRBs. The optical companion in HMXBs is an early OB-type star which is the rich source of stellar wind. These stars throw matter from

their surface through the stellar winds at a rate of 10^{-6} – $10^{-8} M_{\odot} \text{ yr}^{-1}$ with terminal velocities up to 2000 km s^{-1} . Due to high wind loss rate, the orbit of compact object appears as deeply embedded in the wind. The compact object, generally a neutron star or a blackhole in HMXBs, orbits close to the donor star and captures matter due to its own gravitational field. Only a small fraction of matter within a cylindrical radius is accreted by the compact object. The radius of accretion cylinder r_{acc} is given by

$$r_{acc} = \frac{2GM_X}{v_{rel}^2} \quad (1.7)$$

with M_X is the mass of compact object and v_{rel} is relative wind velocity. The relative wind velocity is the quadrature sum of stellar wind velocity and compact object velocity (considering a neutron star) and mathematically expressed as $v_{rel}^2 = v_w^2 + v_{ns}^2 \approx v_w^2$. v_{rel} is assumed to be nearly same as the stellar wind velocity due to relatively low velocity of neutron star.

For a given binary separation ($a \sim 10^{12} \text{ cm}$), the rate of mass captured by compact object within accretion cylinder can be calculated as

$$\dot{M} \sim \frac{\pi r_{acc}^2}{\Omega a^2} \dot{M}_w \quad (1.8)$$

where solid angle Ω is 4π for isotropic distribution of stellar wind in the orbit. \dot{M}_w represents the mass loss rate from the optical companion. Using these parameters in equation 1.7 and 1.8, the accretion radius can be estimated as $\sim 10^{10} \text{ cm}$, which is found to be much smaller than the orbital separation. It implies that only a tiny fraction of mass $\dot{M}/\dot{M}_w \leq 10^{-4}$ is accreted by the compact object. The luminosity produced during the process of wind-fed accretion can be expressed as,

$$L \sim 10^{37} \left(\frac{\dot{M}}{10^{-4} \dot{M}_w} \right) \left(\frac{\dot{M}_w}{10^{-5} M_{\odot} \text{ yr}^{-1}} \right) \quad (1.9)$$

Although, the stellar wind accretion appeared to be an inefficient process of mass accretion compared to the Roche-lobe overflow, the high value of wind loss rate \dot{M}_w produces a higher luminosity that reaches close to the Eddington luminosity of a compact object (Davidson and Ostriker, 1973; Frank, King

and Raine, 1992). Two bright sources such as Vela X 1 and 4U 1700-37 are the typical examples of wind-fed systems. During the process of accretion, a strong bow shock is usually seen at r_{acc} in these systems as a result of interaction between supersonic wind and the compact object. An accretion wake is also expected to form behind the compact object due to the focusing of stellar wind, as shown in Figure 1.3.

An accretion disk can be formed in HMXBs if accreting matter carries some amount of angular momentum. The condition for disk formation is governed by the circularization radius R_{cir}^{wind} . For HMXBs, this radius is defined as

$$R_{cir}^{wind} \simeq 1.3 \times 10^6 M_O^{1/3} P_{10}^{2/3} \text{ cm} \quad (1.10)$$

with an orbital period P_{10} in unit of 10 d. The accretion disk can only form if R_{cir}^{wind} is greater than the radius of the compact object. In general the formation of disk is rare in these systems. Sometimes a small disk is expected to form during accretion of matter (Boerner *et al.*, 1987).

1.3.3 Be/X-ray binaries: Another type of mass accretion

BeXBs represent the largest population (about >60%) of HMXBs. These sources are transient in nature. In these systems, the compact object is mainly a neutron star whereas the optical companion is non-supergiant Oe or Be type star of III-V luminosity class with mass in the range of 10-20 M_\odot (see e.g., Coe, 2000; Reig, 2011 for a review). A Be star shows prominent Balmer and Paschen series hydrogen emission lines in the optical and infrared spectra. Sometimes line emissions from He and Fe atoms are also seen. On the other hand, a classical B star of same spectral type is known to show absorption lines in the optical/infrared spectra. Therefore qualifier ‘e’ is introduced to differentiate these stars from classical one. Be stars also show an excess in infrared emission (Reig, 2011). The presence of emission lines and infrared excess are thought to originate from a quasi Keplerian circumstellar disk along the equatorial plane of the Be star (see Figure 1.4). The ultimate formation of this Be-disk is not

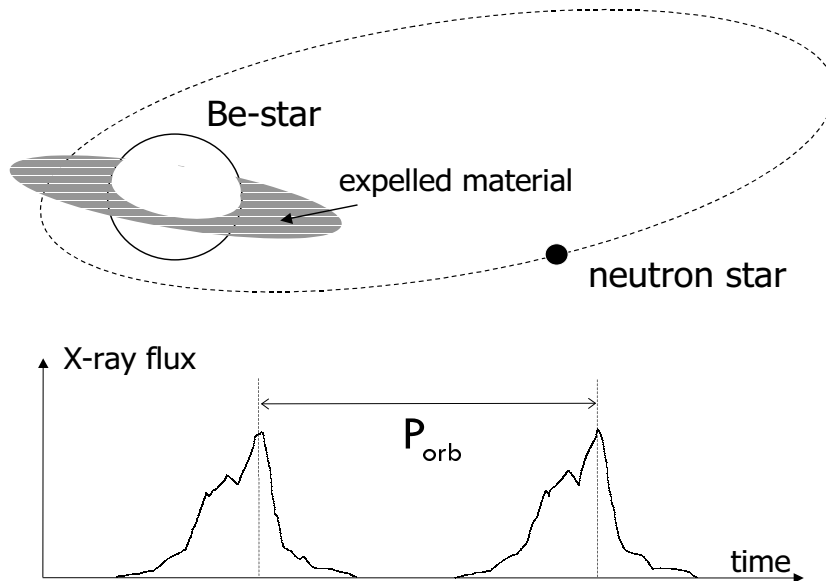


Figure 1.4: Representation of Be/X-ray binary system. The neutron star orbits in eccentric orbit and accretes matter from circumstellar disk of Be star at periastron. This results in the periodic X-ray outbursts (Type-I), which often lasts from several days to weeks. Image courtesy: Tauris and van den Heuvel (2006).

clear. However, it is believed that rapid rotation of these stars expels matter equatorially forming a decretion disk (Porter and Rivinius, 2003; Townsend, Owocki and Howarth, 2004). This disk occasionally extends up to 6-20 times of the stellar radii and covers whole binary separation (Negueruela, 1998). In general, BeXBs are in eccentric orbits ($e \geq 0.3$) with orbital periods in the range of 16-300 d. As a result of large orbital period and non-supergiant companion, Be star underfills its Roche-lobe. Mass transfer in these systems takes place through accretion of matter from the Be-disk. At the periastron passage, neutron star passes closest to or through the circumstellar disk of Be star and captures a copious amount of matter. This matter is accreted by the compact object and shows X-ray outbursts in these systems (Figure 1.4). The Be star rarely losses its entire disk during the process of mass transfer. As a consequence, emission lines disappear from the spectrum and absorption lines are observed in the IR/optical spectra. In addition, X-ray activities are ceased from the system.

Two different types of X-ray outbursts, Type-I and Type-II, have been observed from the BeXB systems. Type-I outbursts are periodic and observed at periastron passage of the binary. The source luminosity during Type-I outbursts is observed to be moderate, in the range of ($L_X \leq 10^{35} - 10^{37}$ erg s⁻¹). These outbursts are short-lived and last for a few days to weeks. They cover a small fraction e.g. $\sim 0.2 - 0.3 P_{orb}$ of the binary orbit. During these outbursts, accretion rate increases up to ~ 100 times than the quiescence phase (Stella, White and Rosner, 1986). On the other hand, Type-II outbursts are rare and most luminous outbursts in BeXBs. The luminosity during these outburst reaches up to the Eddington luminosity of neutron star $L_X \sim 10^{38}$ erg s⁻¹ or more. These outbursts last for more than several weeks to a few months. They cover a significant fraction of binary orbit or even up to several orbital periods. Unlike Type-I outbursts, Type-II outbursts are independent of orbital phase of the binary. It is believed that due to increased companion activity, most of Be-disk gets accreted during Type-II outburst (Coe, 2000; Ziolkowski, 2002). However, the actual causes of Type II outbursts are not known. During these outbursts, quasi-periodic oscillations (QPOs) have been observed in several BeXBs such as A 0535+26, 4U 0115+634. This confirmed the formation of accretion disk around the neutron star in giant outbursts (see Paul and Naik, 2011). *Swift*/BAT monitoring light curves of two BeXB pulsars A0535+26 and EXO 2030+375 exhibiting Type I and Type II outbursts are shown in Figure 1.5.

Apart from transient behavior, a fraction of BeXBs show persistent X-ray activities at a luminosity level of $L_X \leq 10^{36}$ erg s⁻¹ viz. X Per and LS +61°235 (Negueruela, 1998; Reig and Roche, 1999). The neutron stars in these persistent BeXBs are usually a slow rotator ($P_{spin} \geq 200$ s) having a wide orbit $P_{orb} > 200$ d. The spin and orbital periods of neutron star in BeXBs show a positive correlation in Corbet diagram (Corbet, 1986). Corbet diagram represents a relation between spin period and orbital period of pulsars in the binary system. In this diagram, different systems follow different trends indicating differences in the mass transfer mechanism. For example, wind-fed SGXBs show

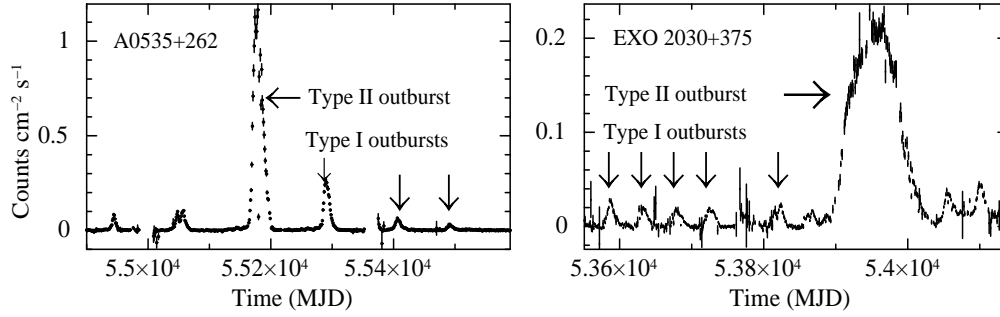


Figure 1.5: *Swift-BAT* light curves of A 0535+262 and EXO 2030+375, showing the presence of Type I and Type II outbursts. The figure is taken from Paul and Naik (2011).

no correlation whereas an anticorrelation is seen in case of disk-fed SGXB (see Figure 1.6). There are only three disk-fed SGXBs which have short orbital as well as spin periods. Due to well-evolved companion and small orbital separation, disk-fed SGXBs appear to fill their Roche lobe and mass transfer can occur through Roche-lobe overflow. Wind-fed SGXBs with long spin period and short orbital period populate a separate region in this diagram. In these systems, the mass accretion from the companion takes place through the capture of stellar wind. However, the spin and orbital periods of BeXB show a

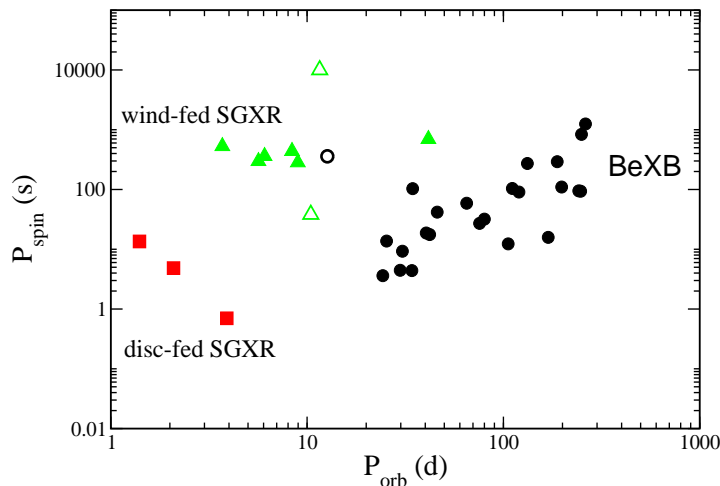


Figure 1.6: A diagram between spin period (P_{spin}) and orbital period (P_{orb}) of accretion powered X-ray pulsars in binary system known as Corbet diagram (figure from Reig, 2011).

clear correlation in this diagram. For a wide orbit, it is possible that neutron star accretes matter only from low dense/ outer part of Be circumstellar disk. This can explain the causes of observed low X-ray luminosity in persistent BeXBs (Negueruela, 1998).

1.4 Neutron star X-ray binaries

Neutron star X-ray binaries is a sub-class of XRBs, where the compact object is a neutron star. Neutron star is born as a final product of massive star of mass in the range of $11 M_{\odot} < M \leq 40M_{\odot}$ after stellar evolution (Iben, 1991; Lewin, van Paradijs and van den Heuvel, 1995). They have a strong magnetic field in the order of $\sim 10^8$ – 10^{15} G. They are considered to be ideal candidates to probe the properties of matter in extreme conditions such as high density, strong gravity, powerful magnetic field and extreme velocity regimes by offering an unique astrophysical laboratory. Irrespective of mass transfer mechanisms, accreted matter is influenced by the magnetic field when it reaches closer to the neutron star. According to current understanding, strong magnetic field disrupts the accretion flow at certain radius and funnels matter towards the magnetic poles of the neutron star.

For a dipole geometry, the magnetic field strength can be described as a function of distance r as follows,

$$B(r) \sim \frac{\mu}{r^3} \quad (1.11)$$

here μ is the magnetic dipole moment. Corresponding magnetic pressure poses by the field lines can be defined as

$$P_{mag} = \frac{B^2}{8\pi} = \frac{\mu^2}{8\pi r^6} \quad (1.12)$$

From the expression it is clear that the strength of magnetic pressure is extremely high at a distance closer to the neutron star. As the accreting matter approaches the neutron star, the ram pressure $P_{ram} = \rho v^2$ due to the thermal motion of electrons try to counter balance the magnetic pressure. The distance

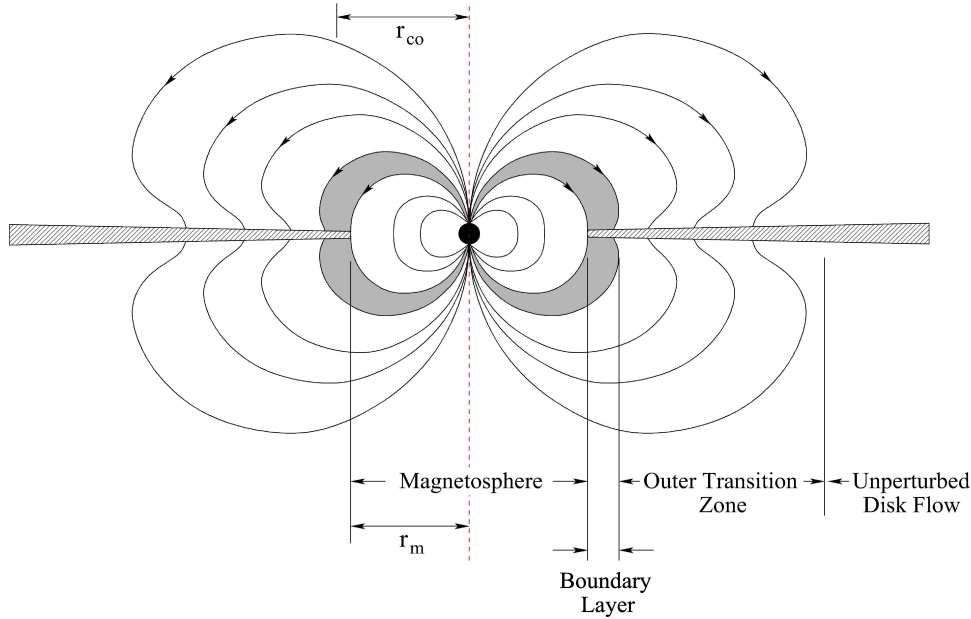


Figure 1.7: The interaction of accretion disk with the magnetized neutron star (Ghosh and Lamb, 1978). At the magnetospheric radius (r_M transition layer) matter from disk follows the field lines towards poles of neutron star only if co-rotation radius $r_{co} > r_M$ (figure from Kuster, 2004).

at which the ram pressure becomes equal to the magnetic pressure in spherically symmetric accretion is known as Alfvén radius or magnetospheric radius r_M (Lamb, Pethick and Pines, 1973). Beyond this radius, magnetic pressure dominates over the ram pressure and accreting matter is forced to follow the field lines towards the poles of neutron star.

$$P_{ram} = \frac{(2GM)^{1/2} \dot{M}}{4\pi r_M^{5/2}} = \frac{\mu^2}{8\pi r^6} = P_{mag} \quad (1.13)$$

For a typical neutron star, the magnetosphere radius is expressed in term of luminosity:

$$r_M = 2.9 \times 10^8 M_X^{1/7} R_6^{-2/7} L_{37}^{-2/7} \mu_{30}^{4/7} \text{ cm} \quad (1.14)$$

where M_X is the mass of neutron star in M_\odot , R_6 is radius in unit of 10^6 cm, L_{37} is luminosity in unit of 10^{37} erg s $^{-1}$, μ_{30} is magnetic dipole moment in unit of 10^{30} gm cm 3 . This expression is slightly modified for disk accretion scenario (Kiraly and Meszaros, 1988). Due to spinning of the neutron star, magnetosphere also rotates with the same velocity. The co-rotation radius

r_{co} is defined at the position where centrifugal force balances the gravity. In other words, the angular velocity of magnetosphere, ωr , would be equal to the Keplerian velocity of disk at the co-rotation radius, r_{co} ,

$$r_{co} = \left(\frac{GM_X}{\omega^2} \right)^{1/3} \quad (1.15)$$

This radius is important in order to probe the accretion-regimes in neutron stars. When the angular velocity of neutron star is smaller than the disk Keplerian velocity $\omega r < \sqrt{GM/r_{co}}$ or $r_m < r_{co}$, matter is allowed to accrete on to the compact object. On the other hand, when neutron star rotates faster than the disk velocity i.e. $r_m > r_{co}$, a centrifugal barrier arises which prevents mass accretion on to the neutron star and ceases X-ray emission. This mechanism is known as *propeller effect* (Illarionov and Sunyaev, 1975).

1.5 Accretion powered X-ray pulsars

The fate of accreting matter is governed by the strong magnetic field of the neutron star. The matter captured at the Alfvén radius follows the field lines to magnetic poles. A column like structure, accretion column, is expected to form at the poles of the neutron star from where the X-ray emissions takes place as a result of various physical processes. Due to rotation of neutron star, these emission regions appear as pulsating only if the rotation and magnetic axes are misaligned. These pulsating neutron stars are known as accretion powered X-ray pulsars. A geometric representation of X-ray pulsar is shown in Figure 1.8.

X-ray photons are emitted from a small accreting spot $0.1 R_{ns}$ (~ 1 km) within the accretion column (Davidson and Ostriker, 1973). The exact shape of accretion column and the formation physics are still a matter of debate. However, different geometries such as filled column, hallow column and partial hallow column have been proposed (Basko and Sunyaev, 1976; Meszaros, 1984). During the process of accretion, matter gains sufficient amount of kinetic energy (up to $\sim 0.6 c$) till it reaches the magnetic poles This energy is

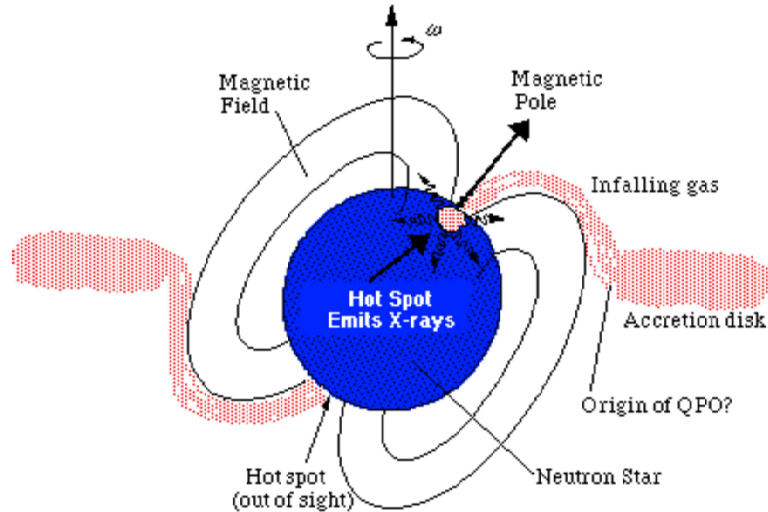


Figure 1.8: The accretion in magnetized neutron star. The hotspot formed at the poles of neutron star is pulsate due to rotation of neutron star. These are known as accretion powered X-ray pulsars. Figure courtesy: *NASA-Imagine* http://imagine.gsfc.nasa.gov/science/objects/binary_flash.html.

released in the form of radiation when the matter hits the poles of the neutron star (Basko and Sunyaev, 1976; Becker *et al.*, 2012). Close to the neutron star, accreting gas interacts with the surface and produces X-ray photons through deceleration in a radiation dominated or collision-less shock (Basko and Sunyaev, 1976). The process of interaction as well as the geometry of emission regions depend on the accretion rate i.e. X-ray luminosity of the pulsar. At lower accretion rate, a thermal hot spot formed on the surface of neutron star is the source of emission. While at higher accretion rate, a radiation dominated shock front and thermal mound are the main sources of emission through complex processes such as thermal and bulk Comptonization in the column.

Basko and Sunyaev (1976) introduced critical luminosity L_{crit} to differentiate the transition between these two accretion scenario. X-ray pulsars with luminosity lower than L_{crit} (sub-critical regime) are known as sub-critical sources. However, pulsars with luminosity $>L_{crit}$ (super-critical regime) are called as super-critical sources. The critical luminosity is strongly dependent on properties of the pulsar and related to Eddington luminosity (Becker *et al.*, 2012). The critical luminosity, calculated in terms of magnetic field (for cy-

clotron absorption line sources) by Becker *et al.* (2012) considering the physical processes within the accretion column, can be written as

$$L_{crit} = 1.49 \times 10^{37} \text{ erg sec}^{-1} \left(\frac{\Lambda}{0.1} \right)^{-7/5} w^{-28/15} \times \left(\frac{M_*}{1.4M_\odot} \right)^{29/30} \left(\frac{R_*}{10 \text{ km}} \right)^{1/10} \left(\frac{B_*}{10^{12} \text{ G}} \right)^{16/15} \quad (1.16)$$

where, the constant $\Lambda=1$ assumes the spherical accretion scenario and $\Lambda<1$ indicates the case of disk accretion. The parameter w shows the bremsstrahlung spectrum at $w\sim 1$, whereas Planck spectrum can be produced for $w\sim 3$. Other parameters such as M_* , R_* and B_* are mass, radius and magnetic field of the neutron star, respectively. For typical parameters of $w\sim 1$ and $\Lambda=0.1$, above equation is dominated by bremsstrahlung radiation (Becker and Wolff, 2007) and reduces to a simple expression

$$L_{crit} = 1.49 \times 10^{37} B_{12}^{16/15} \text{ erg s}^{-1} \quad (1.17)$$

Luminosity of a source depends on the mass accretion rate. As a result, the properties of X-ray emission mechanisms can change with mass accretion rate. Due to these variations, three major luminosity regimes can be considered for the pulsars which are being discussed here in detail.

At low accretion rate $L \ll L_{crit}$ ($\sim 10^{34} - 10^{35} \text{ erg s}^{-1}$), matter is almost free to fall until hydrodynamical shock halts the plasma closer to the surface of neutron star. The gas is decelerated in shock region via Coulomb interactions before reaching the surface (Langer and Rappaport, 1982). An accretion mound/ hot spot formed at poles produces X-ray emissions that escape vertically along the accretion column. The observed emission pattern is known as *pencil-beam*, as shown in right side of Figure 1.9.

If accretion rate of pulsar increases such that luminosity is lower than or close to critical luminosity ($L_X \leq L_{crit}$) in the order of $\sim 10^{35} - 10^{37} \text{ erg s}^{-1}$, a radiation dominated shock is expected to form in the accretion column (Figure 1.10). Thermal photons emitted from the mound (hotspot) gets upscattered by inverse Compton scattering in accretion column. The radiation which is emitted below the shock region diffuse through side-walls of accretion column

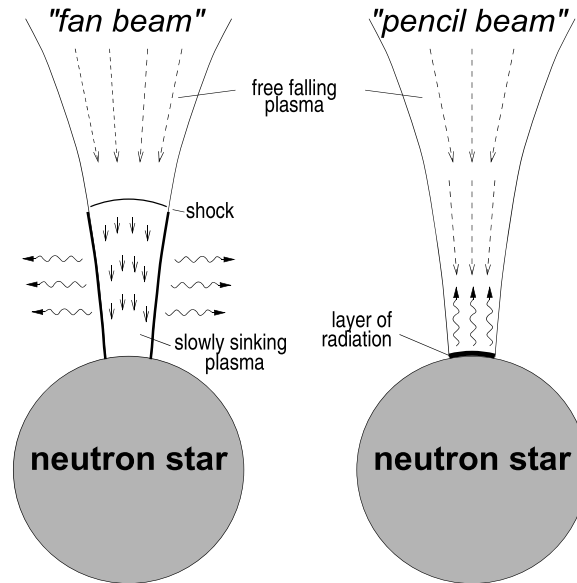


Figure 1.9: Emission beam patterns from the poles of the neutron star. For high accretion rate, a radiation dominated shock is formed in the column. Photons below the shock region escape from the side of the wall in form of *fan beam* pattern (left-panel). The *pencil beam* pattern is formed in case of low accretion rate where photons propagate vertically along the accretion column (right-panel). Figure is taken from Kretschmar (1996).

in *fan-beam* pattern. X-ray photons above the shock region, however, move upward in the column in *pencil-beam* pattern. This results a mixture of *pencil and fan* beam patterns for the pulsar in this luminosity regime (Blum and Kraus, 2000). Close to the surface of neutron star, the gas sinks slowly and decelerates again via Coulomb interactions before settling (Nelson, Salpeter and Wasserman, 1993). The shock or emission region can drift in the accretion column depending on accretion rate.

For very high luminosity of $\sim 10^{37} - 10^{38} \text{ erg s}^{-1}$ ($L > L_{crit}$), accreting gas loses its energy in radiation dominated shock and decelerates completely via radiation field below the shock region (Basko and Sunyaev, 1976). In this regime, shock can drift upwards in accretion column with increasing accretion rate. X-ray photons are emitted only through the side walls of optically thick column in pure *fan-beam* pattern, as shown in Figure 1.9.

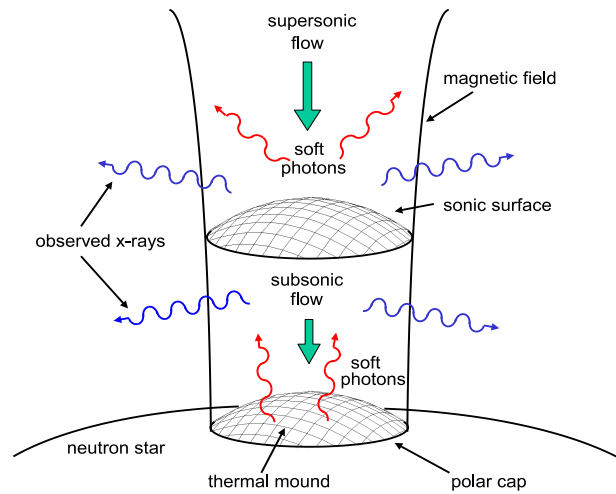


Figure 1.10: Systematic view of accretion column in neutron star based on Becker and Wolff (2007). A radiation dominated shock front is formed above the surface of neutron star. Seed photons, produced at the base of accretion column (thermal mound) and via bremsstrahlung and cyclotron emission all over the column, interact with accreting gas near the shock region, resulting thermal and bulk Comptonization spectrum. Figure courtesy: Becker and Wolff (2007).

1.6 Properties of accretion powered X-ray pulsars

In this section, current understanding of empirical and theoretical models used to describe the continuum spectrum of accretion powered X-ray pulsars is discussed. Description about the cyclotron line and properties of pulse profiles is also presented in the following sections.

1.6.1 Spectral formation

Standard shape of X-ray continuum for accretion powered pulsar is generally described by a power-law modified with a cutoff in the energy range 10-30 keV

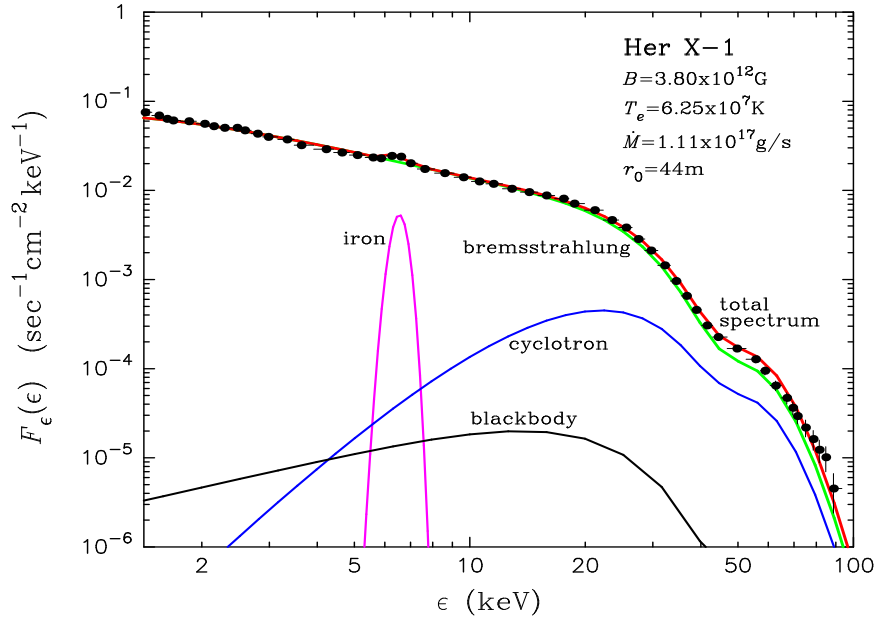


Figure 1.11: Theoretical spectrum of Her X-1 compared to observational data of pulsar from *BeppoSAX* observation (black points). Figure courtesy: Becker and Wolff (2007).

and a blackbody component in soft X-rays < 5 keV (White, Swank and Holt, 1983; Coburn *et al.*, 2002; Becker and Wolff, 2005). In addition to photoelectric absorbed continuum, fluorescence emission lines from Fe and other atoms such as Ni, Si, Ar etc., and absorption like features known as *cyclotron absorption lines* (discussed in section 1.6.2) are also observed in pulsar spectrum. The observed spectrum can be explained with phenomenological models irrespective of complex physical processes occurring in magnetosphere and accretion column. Various attempts have been made to develop a standard theoretical model that can produce observed spectrum of X-ray pulsars (Nagel, 1981a,b; Meszaros *et al.*, 1983; Meszaros and Nagel, 1985; Burnard, Klein and Arons, 1988; Burnard, Arons and Klein, 1991; Becker and Wolff, 2005). However, it is extremely difficult to develop a self-consistent model that can reproduce the spectra of all X-ray pulsars. Becker and Wolff (2007) introduced a model which successfully produced the continuum for high luminous sources, Her X-1, LMC X-4 and Cen X-3. Figure 1.11 shows the continuum spectrum for Her X-1 produced by the model which matches well with the *BeppoSAX* observation.

This model considers scattering via bulk and thermal Comptonization in radiation dominated shock within accretion column (shown in Figure 1.10). Seed photons emitted from thermal mound (blackbody) and inside the accretion column (bremsstrahlung and cyclotron emission) are assumed to be up-scattered with energetic electrons in gas via bulk Comptonization. In addition, the cut-off and flatten soft X-ray spectrum are resulted by thermal Comptonization of photons.

1.6.2 Cyclotron resonance scattering feature

Cyclotron resonance scattering feature (CRSF) is absorption-like feature, observed in hard X-ray (10-100 keV) spectrum of pulsars with magnetic field of $\sim 10^{12}$ G. These features are originated due to resonant scattering of X-ray photons with electrons in discrete quantized levels (Meszaros, 1992). Detection of CRSFs is the direct and powerful method to determine the magnetic field of neutron stars. The first cyclotron absorption line was discovered in the spectrum of Her X-1 (Truemper *et al.*, 1978). Cyclotron absorption lines have been detected in 29 pulsars till today (including the new detection from this thesis and other references from Coburn *et al.*, 2002; Pottschmidt *et al.*, 2012). However, there are eight pulsars in which detection are not well established. The list of all these sources are given in Table 1.2 in increasing order of cyclotron line energies.

The formation of cyclotron line is a quantum mechanical phenomenon. In presence of magnetic field, electron follows a helical trajectory due to the Lorentz force and gyrates at a frequency known as gyration frequency or *Larmor frequency*. The gyration radius of electron can be expressed as,

$$r_L = \frac{m_e v_{\perp}}{eB}, \quad (1.18)$$

This radius decreases with increasing magnetic field. As the gyration radius approaches de-Broglie wavelength ($\lambda_{deBroglie} = \frac{h}{mv}$), quantum mechanical effects become important (Araya and Harding, 1996). As a result, energy states of electron become quantized along perpendicular direction of magnetic field in

Table 1.2: List of the cyclotron line sources

	Source name	CRSFs energies (keV)	Spin period (s)	Orbital period (d)	Type	References
1	Swift J1626.6-5156	10	15	132.9	HMXB	DeCesar <i>et al.</i> (2013)
2	XMMU J054134.7-682550	10,	61.6	80?	BeXB?	Manousakis <i>et al.</i> (2009)
3	KS 1947+300	12.5	18.7	41.5	BeXB	Fürst <i>et al.</i> (2014)
4	4U 0115+634	14, 24, 36 48, 62	3.61	24.31	BeXB	Wheaton <i>et al.</i> (1979), Ferrigno <i>et al.</i> (2011)
5	IGR J17544-2619	17	71.49	4.9	HMXB	Bhalerao <i>et al.</i> (2015)
6	4U 1907+09	19, 40	438	838	HMXB	Rivers <i>et al.</i> (2010)
7	4U 1538-52	22, 47	530	3.73	HMXB	Rodes-Roca <i>et al.</i> (2009)
8	IGR J18179-1621	22	11.8	?	HMXB?	Li <i>et al.</i> (2012)
9	2S 1553-542	23.5	9.28	30.6	BeXB	Tsygankov <i>et al.</i> (2016)
10	Vela X-1	25, 50	283	8.96	HMXB	Maitra and Paul (2013b)
11	V 0332+53	27, 51, 74	4.37	34.25	BeXB	Nakajima <i>et al.</i> (2010)
12	SMC X-2	27	2.37	18	BeXB	Jaisawal and Naik (2016)
13	Cep X-4	28, 45	66.2	?	BeXB	Jaisawal and Naik (2015b)
14	4U 0352+309 (X Per)	29	837	250.3	BeXB	Coburn <i>et al.</i> (2001)
15	IGR J16393-4643	29.3	904	4.2	HMXB?	Bodaghee <i>et al.</i> (2016)
16	Cen X-3	30	4.84	2.09	HMXB	Burderi <i>et al.</i> (2000)
17	IGR J16493-4348	30	1069	6.7	HMXB	D’Ai <i>et al.</i> (2011)
18	RX J0520.5-6932	31.5	8.04	23.9	BeXB	Tendulkar <i>et al.</i> (2014)
19	LS V+44 17	32	202	155?	BeXB	Tsygankov <i>et al.</i> (2012)
20	MXB 0656-072	33	160	?	BeXB	McBride <i>et al.</i> (2006)
21	XTE J1946+274	36	15.8	169.2	BeXB	Heindl <i>et al.</i> (2001)
22	4U 1626-67	37	7.66	0.028	LMXB	Orlandini <i>et al.</i> (1998)
23	GX 301-2	37	690	41.48	HMXB	Suchy <i>et al.</i> (2012)
24	Her X-1	39, 73	1.24	1.7	LMXB	Enoto <i>et al.</i> (2008)
25	MAXI J1409-619	44, 73, 128	500	?	HMXB?	Orlandini <i>et al.</i> (2012)
26	1A 0535+262	45, 100	105	110.6	BeXB	Terada <i>et al.</i> (2006)
27	GX 304-1	54	272	132.5	BeXB	Yamamoto <i>et al.</i> (2011)
28	1A 1118-615	55, 112?	408	24	BeXB	Doroshenko <i>et al.</i> (2010)
29	GRO J1008-57	76	93.5	249.5	BeXB	Yamamoto <i>et al.</i> (2014)
1	EXO 2030+375	11? 61?	41.8	46	BeXB	Wilson <i>et al.</i> (2008)
2	GS 1843+009	20?	29.5	?	BeXB	Mihara (1995)
3	2S 0114+650	22?, 44?	9600	11.6	HMXB	Bonning and Falanga (2005)
4	GX 1+4	34?	138	1161?	LMXB	Ferrigno <i>et al.</i> (2007)
5	OA0 1657-415	36?	38	10.2	HMXB	Orlandini <i>et al.</i> (1999)
6	4U 1700-37	37?	?	3.4	HMXB	Jaisawal and Naik (2015a)
7	4U 1909+07	44?	604	4.4	HMXB	Jaisawal, Naik and Paul (2013)
8	LMC X-4	100?	13.5	1.41	HMXB	La Barbera <i>et al.</i> (2001)

discrete energy levels known as *Landau levels*. The energy of electron in Landau levels is described as

$$E_n = \frac{m_e c^2}{\sin^2 \theta} \left(\sqrt{1 + 2n \frac{B}{B_c} \sin^2 \theta} - 1 \right) \quad (1.19)$$

with θ is the angle between photon direction and magnetic field axis. The critical magnetic field $B_c = \frac{m_e^2 c^3}{e \hbar} \approx 4.4 \times 10^{13}$ G is the magnetic field at which electron kinetic energy (or energy of Landau level) becomes equal to the rest mass energy of the electron. From equation 1.19, it can be seen that the cyclotron energy is strongly dependent on angle θ . The relativistic corrections become important to describe the motion of electrons in high magnetic field $B \geq B_c$ (Araya-Góchez and Harding, 2000). However, at low magnetic field $B \ll B_c$ (non-relativistic case), the quantized levels appear as equispaced at energy difference of

$$E_{\text{cyc}} = \hbar \omega = \frac{\hbar e}{m_e c} B = 11.6 \text{ keV} \left(\frac{B}{10^{12} \text{ G}} \right) \quad (1.20)$$

This can be simply described by *12-B-12 rule*. In presence of gravitational redshift (z), above expression is slightly modified as $E_{\text{cyc,obs}} = E_{\text{cyc}} (1 + z)^{-1}$. Using this simple formula, we can estimate the magnetic field of a neutron star at corresponding cyclotron line energy.

In general, electron energy states are quantized at Landau energy levels corresponding to magnetic field of the neutron star. The photons having energies of nE_{cyc} are get absorbed in the plasma by exciting electrons to the higher energy states $n > 1$ of Landau levels. These states have relatively shorter life time in comparison to collision de-excitation time scale of electrons (Latal, 1986). As a result, the absorbed photon is instantaneously re-emitted at the same energy. This process is generally considered as *resonant scattering* rather than the absorption of photon. Due to the continuity of absorption and emission processes in plasma, the photons of energies close to nE_{cyc} appear to be trapped in the column. These photons can only escape from the accretion column/ plasma if inelastic scattering slightly changes their energy. This process leads to the formation of a broad absorption like features (cyclotron resonant

scattering feature or simply cyclotron lines) at energies nE_{cyc} in X-ray pulsars. Cyclotron line at energy of E_{cyc} is known as fundamental line. The harmonics of cyclotron lines are also observed in many pulsars (see Table 1.2). The formation of cyclotron line is a complex process and not fully understood yet. Numerous simulation studies show that the shape of cyclotron line is non-trivial. This depends on various factors such as plasma properties, emission region geometry, optical depth (Araya and Harding, 1999; Schönherr *et al.*, 2007). Sometimes emission wing-like features near fundamental cyclotron line are also seen. These wings are thought to be originated by photon spawning effect. Due to lack of accurate cyclotron model, the observed feature is used to model with simple Gaussian or Lorentzian absorption profiles without taking complex structures like emission wings in to account.

It has been found that the energy of cyclotron line is dependent on luminosity for a few X-ray pulsars. A positive dependence between cyclotron line energy and luminosity was observed for only two pulsars such as Her X-1 (Staubert *et al.*, 2007) and GX 304-1 (Klochkov *et al.*, 2012). However, a negative correlation was seen in two Be/X-ray binary pulsars 4U 0115+63 (Nakajima *et al.*, 2006; Tsygankov *et al.*, 2007) and V 0332+53 (Tsygankov, Lutovinov and Serber, 2010). The observed correlation for 4U 0115+63 is uncertain and model dependent (Müller *et al.*, 2013). In addition, there are also pulsars which show no significant trend between these parameters, for example Be/X-ray binary pulsar A 0535+26 (Caballero *et al.*, 2007). Several models have been proposed to explain the observed correlations by considering changes in the shock region or height of accretion column or changes in the beam pattern or in term of reflection from neutron star surface, discussed in the section 4.3.2 of Chapter-4 (Staubert *et al.*, 2007; Poutanen *et al.*, 2013; Nishimura, 2014).

1.6.3 Pulse profiles

The pulse profiles are characteristic features of a pulsar. Studies of these profiles provide important information regarding the emission geometry and beam

pattern. It also reflects the signature of physical environment around the pulsar. The properties of pulse profiles depend on numerous factors such as angle between rotation and magnetic axes, properties of accretion column, emission geometry, mass accretion rate, gravitational light bending effect (Nagase, 1989; Kraus *et al.*, 2003). The shape of pulse profiles can be reproduced simply by considering the beam pattern and varying the geometrical aspect of rotation axis, magnetic axis and line of sight (Wang and Welter, 1981). One or both the magnetic poles are visible if $\alpha + \beta < \pi/2$ or $> \pi/2$, where α and β are the angles of magnetic axis and line of sight with respect to rotation axis. In general, single or double peaked profiles are observed in several pulsars and assigned to emission from one or both the poles, respectively (Bulik *et al.*, 2003). However, multiple peaks are also observed in some cases. These peaks are mostly seen in soft X-rays (< 10 keV). Figure 1.12 shows pulse profiles of accretion powered pulsars in 20-35 keV ranges consisting of single-peaked (GX 1+4, GRO J1008-57, 4U 0115+634 etc.; first and second panels), single-peaked with inter-pulse (Cen X-3 and Her X-1; third panel) and double-peaked profiles (A 0535+26, GX 301-2, 2S 1417-62; fourth panel).

Theoretical efforts have been made to model the observed pulse profiles (Leahy, 1991; Kraus *et al.*, 2003). The presence of single/ double peaked pulse profiles was explained in a simple picture of emission from one/ both poles, respectively. Modeling results showed that the inclusion of gravitation light bending effects produce a complex pulse profile which is strongly dependent on geometry of neutron star (Kraus *et al.*, 1995, 2003). Moreover, some pulsars can have asymmetry between two pulse peaks. This indicates an asymmetry in magnetic field of neutron star which can form accretion columns at different locations rather than poles (Leahy, 1991). Depending on the mass accretion rate, the beam pattern of pulse profile can change at different luminosity states, as discussed in section 1.5. The pulse profiles appearing from fan-beam geometry are assumed to be complex. However, pencil beam produces a relatively simpler pulse profile of sinusoidal nature.

In general, the pulse profiles of Be/X-ray binary pulsars appear to be com-

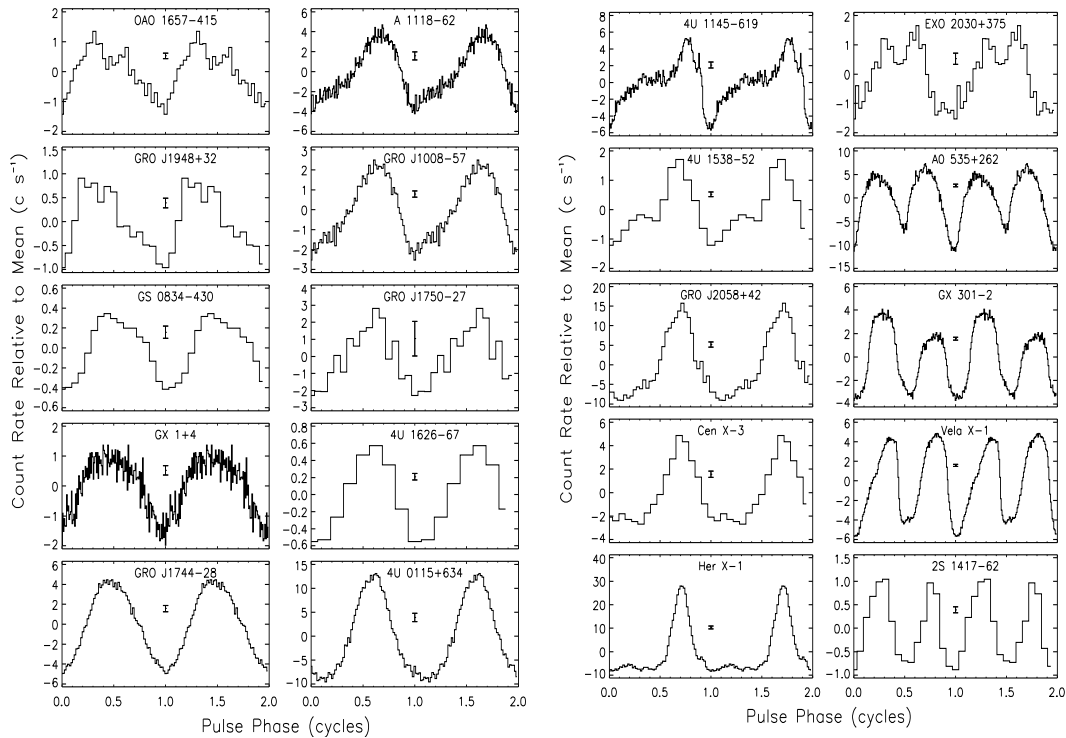


Figure 1.12: Pulse profiles of the accreting X-ray pulsars in 20-35 keV range. This figure is taken from Nagase (1989) and Devasia (2014).

plex. They show a strong dependence on energy and luminosity. At soft X-rays, pulse profiles consist of multiple absorption dips which disappear at hard X-rays. These absorption dips are observed at certain phases of pulsars. It is thought that the presence of narrow streams of matter that are phase-locked with the pulsar, causes absorption dips at certain phases of pulse profiles (Galloway *et al.*, 2001; Paul and Naik, 2011). These dips are observed up to higher energies depending on the density and opacity of matter in the streams. With phase-resolved spectroscopy, the causes of absorption dips or distribution of matter surrounding pulsars can be probed in detail.

In some cases, pulse profiles show sudden changes or phase-shift at energy close to the cyclotron line energy of the pulsar. Numerical simulation studies show that the presence of strong cyclotron absorption feature can influence the beam function and produce the change in pulse profiles closer to cyclotron energy (Schönherr *et al.*, 2014). These effects have been observed in two other

Be/X-ray binary pulsars such as V 0332+53 (Tsygankov *et al.*, 2006) and 4U 0115+63 (Ferrigno *et al.*, 2011) in form of phase-shift in the pulse profiles.

1.7 Spectral continuum models for pulsar

The broadband spectrum of X-ray pulsar originates as a result of complicated processes occurring near magnetic poles of neutron star. However, the spectrum can be easily described with several empirical models based on power-law, modified with other components. In general, a simple model with three parameters are inadequate to describe the continuum well. Other parameters are also included in the empirical models for reasonable description of observed spectra. These models are described below.

- **The cutoff power-law (Cutoffpl):**

This model consists of a simple power-law modified with a cutoff energy in the range of ~ 5 -30 keV. X-ray pulsars generally show a cutoff, which originates due to Comptonization or Bremsstrahlung process of electrons in thin thermal plasma, as discussed in section 1.6.1. The simulated spectrum produced by Becker and Wolff (2007) consistent with this empirical model, can be mathematically expressed as,

$$\text{Cutoffpl}(\mathbf{E}) = N E^{-\Gamma} e^{-E/E_{cut}} \quad (1.21)$$

where, Γ is a dimensionless quantity and known as photon-index of power-law. N is the normalization constant of power-law and represents the flux in the unit of photons/s/cm²/keV. E_{cut} represents a parameter which corresponds to the thermal temperature of the electrons in accreting plasma.

- **High energy cutoff model (HECut):**

HECut model is one of the most widely used model after the discovery of X-ray pulsars (White, Swank and Holt, 1983). This model includes

one more fit parameters and is expressed as,

$$\mathbf{HECut}(\mathbf{E}) = \begin{cases} E^{-\Gamma} & \text{for } E \leq E_{cut} \\ E^{-\Gamma} e^{-\left(\frac{E-E_{cut}}{E_{fold}}\right)} & \text{for } E > E_{cut} \end{cases} \quad (1.22)$$

The high energy rollover, E_{cut} or E_{break} , is typically seen around 10 keV energies. This model sometime results a nonphysical kink around E_{cut} , which can easily be misinterpreted.

- **The Fermi Dirac Cutoff (FDCut):**

FDCut is another empirical continuum model based on the power-law modified with the Fermi-Dirac Cutoff (Tanaka, 1986). This model is represented as,

$$\mathbf{FDCut}(\mathbf{E}) = NE^{-\Gamma} \frac{1}{1 + e^{\left(\frac{E-E_{cut}}{E_{fold}}\right)}} \quad (1.23)$$

The model parameters have same physical meaning.

- **The Negative and Positive power-law with EXponential cutoff (NPEX):**

NPEX model consists of two cutoff power-law models with same cutoff energy. This model is motivated with the physical phenomena occurring in the accretion column. As discussed in previous sections, the soft X-ray photons are produced from the hot spot at magnetic poles of neutron star and described as a blackbody spectrum. The hard X-ray part is originated through the inverse Compton scattering of soft X-ray photons that lead towards a power-law distribution. In NPEX model, power-law has different photon-indexes: positive and negative. The positive power-law is generally fixed at a photon index of 2, representing Wien's peak (Mihara, 1995; Nakajima *et al.*, 2006). However, the hard X-ray spectrum is described by the negative power-law which is kept free. The mathematical form of NPEX model is

$$\mathbf{NPEX}(\mathbf{E}) = (N_1 E^{-\alpha_1} + N_2 E^{+\alpha_2}) \exp\left(-\frac{E}{kT}\right)$$

where N_1 , α_1 and N_2 , α_2 are the normalization and photon indices of the negative and positive power laws, respectively. kT represents the cutoff energy in the unit of keV.

1.8 Outline of the thesis

The emission from the accreting X-ray pulsars resulted due to the complicated processes occurring in the magnetosphere and closer to the neutron star. The accretion column, formed at the poles of the neutron star, is the main source of X-ray emissions. This thesis is aimed to study the X-ray properties of high mass X-ray binary pulsars e.g. to probe the properties of pulse profiles, its dependence on energy and luminosity (mass accretion rate), surroundings of the pulsars, changes in the accretion column geometry, magnetic field strength of neutron star and magnetic field geometry. The detection of cyclotron line is known to be the only direct way to estimate the magnetic field of the pulsar, technically the magnetic field at the line-forming region. It is assumed that the neutron star has dipolar magnetic field, which is a good approximation for a distant observer. However, the magnetic field close to neutron star is far more complex and may be distorted due to accretion instability (Mukherjee and Bhattacharya, 2012). The phase-resolved spectroscopy of the cyclotron absorption line can be the effective way to map the geometry of magnetic field of the pulsar. The environment close to the neutron star can also be studied through phase-resolved spectroscopy. Sometimes the absorption dips are observed in the soft X-ray pulse profiles. These dips appear due to absorption of photons by narrow streams of matter which is locked with the pulsar. As discussed earlier, SGXBs (a sub-class of HMXBs) are powered by the capture of stellar wind. In this thesis, we have also focused on the properties of these sources in order to understand the origin of flare-like episodes in their light curves. The outline of the thesis is given below.

Chapter-2 deals with the description of instruments on-board the satellites from which data have been used in this thesis. We have also described

the list of the sources studied in this thesis.

In **Chapter-3**, we have studied the pulse profiles of a few Be/X-ray binary pulsars at different luminosity levels with *Suzaku*. The causes of multiple absorption dips seen in the soft X-ray pulse profiles of these pulsars are also probed.

Chapter-4 is dedicated to the study of cyclotron lines in X-ray pulsars. We have presented the results from phase-averaged as well phase-resolved spectroscopy of the cyclotron line parameters.

Chapter-5 describes the time-resolved spectral properties of two eclipsing high mass X-ray binaries in order to study the intensity variability observed in their light curves.

In **Chapter-6**, conclusion and summary of thesis is presented.

Chapter 2

Instruments, Observations and Data Analysis

Ground based astronomical observations are limited to the optical, near infrared and radio wavebands of the electromagnetic spectrum as the the Earth's atmosphere is opaque for the high energy radiations such as UV, X-rays and Gamma-rays. In order to detect X-ray photons from the cosmic sources, instruments have been sent above the densest parts of the atmosphere. This has been done by using balloon, rocket and satellite experiments. Since the flux of high energy radiation from cosmic sources is extremely low, it is necessary to either have a large area detector or develop a technique to collect photons from a larger area and then focus them to a detector with reasonable area. As it is not possible to have sufficiently large area detectors with timing, spectral and imaging capabilities, it is required to develop focusing techniques to achieve high quality data. These energetic X-ray photons, however, can not be collected by the traditional method of focusing through mirrors or lens as used in the optical/ infrared astronomy. Because of very high energy, X-ray photons easily penetrate and even ionize the material of the focusing instrument. The ionizing capability of these photons can be used as main principle to detect them and that was the practice during early days observations in form of Geiger counters and proportional counters. New generation of X-ray

astronomy missions, e.g. *RXTE*, *Suzaku* and *ASTROSAT* often used these non-imaging instruments such as proportional counters and scintillator detectors because of their large effective area and high timing sensitivity.

Indirect detection techniques were adopted initially as the X-ray photons are difficult to focus. In principle, the electromagnetic waves can be reflected from a surface if they incident at a special angle, known as grazing angle. This process is called as the total external reflection and later used to develop the X-ray focusing telescopes. A nested shells of X-ray mirrors arranged in the geometry of paraboloid followed by a hyperboloid mirrors are able to reflect the X-ray photons if the incident angle of photons is very very small (less than a degree). Such conical arrangement of mirrors is known as the *Wolter type* configuration and first used in the *EXOSAT* observatory. Several focusing telescopes such as *XMM-Newton*, *Chandra*, *Swift/XRT*, *Suzaku/XIS*, *ASTROSAT/SXT* and *NuSTAR* are actively exploring the X-ray sky. Use of imaging instruments at the focal point of X-ray telescopes benefited the astronomical studies in terms of instantaneous detection of background radiation which is found to be several orders less than the non-imaging detectors. The morphology of the extra-solar sources can also be well probed with the imaging facilities.

Besides the technological development of X-ray detectors and X-ray telescopes, the space weather is unpredictable. In addition to the solar wind particles, the instruments on-board a satellite continuously get hit by numerous high energetic particles and photons from the cosmos. The space-based astronomical observatories are generally projected into low Earth orbits below *van Allen belts*. The *van Allen belt* is the region of trapped charged particles at a height of about 1000 km which is formed due to the interaction between solar wind particles and the Earth's magnetosphere. To avoid these effects, satellites are kept into orbits that are below this belt at altitudes of 500-600 km. However, due to the dent in the Earth's magnetic field near the south Atlantic region, these charged particles penetrate into the atmosphere up to ~ 500 km. As a result, high charge particle background is measured across

the area, known as *South Atlantic Anomaly* (SAA) region. The instruments onboard satellites are generally switch-off during the SAA passage in order to protect the detectors and associated electronics.

In this thesis, data from space based observatories such as *Suzaku* and *NuSTAR* have been used for studying the properties of high mass X-ray binary pulsars. The details about these observatories are presented in following sections of this chapter.

2.1 *Suzaku*: A soft to hard X-ray observatory

I have extensively used data from *Suzaku* observatory for studies of accretion powered X-ray pulsars. *Suzaku* is the fifth Japanese X-ray astronomy satellite launched by Japan Aerospace Exploration Agency (JAXA) on 2005 July, 10 (Mitsuda *et al.*, 2007). The name *Suzaku* was taken from the Asian mythology. It means the *red bird*, one of the four guardian animals, protecting the southern skies. This mission was in joint collaboration with Japan and US. *Suzaku* was launched in a nearly circular orbit of 96 minutes at an altitude of 570 km and inclination of 31° from the equator. It has the broad-band energy coverage, starting from 0.2 to 600 keV with the help of two sets of detectors: the X-ray Imaging Spectrometers (XISs; Koyama *et al.*, 2007) and the Hard X-ray Detectors (HXD; Takahashi *et al.*, 2007). Figure 2.1 shows the schematic view of the satellite in orbit. Description about both detectors is given in next sections. Apart from XIS and HXD detectors, *Suzaku* also carried a third instrument e.g. X-ray micro-calorimeter (X-ray Spectrometer; XRS) which was a new generation spectrometer with significantly better energy resolution than the grating used in the *XMM-Newton* and *Chandra*. But it was lost even before routine scientific observations could begin. The *Suzaku* mission was operational for nearly 10 years and provided abundance of new scientific results. JAXA announced this mission as completed on 2015 August, 26 after malfunction of the satellite in early June of the same year.

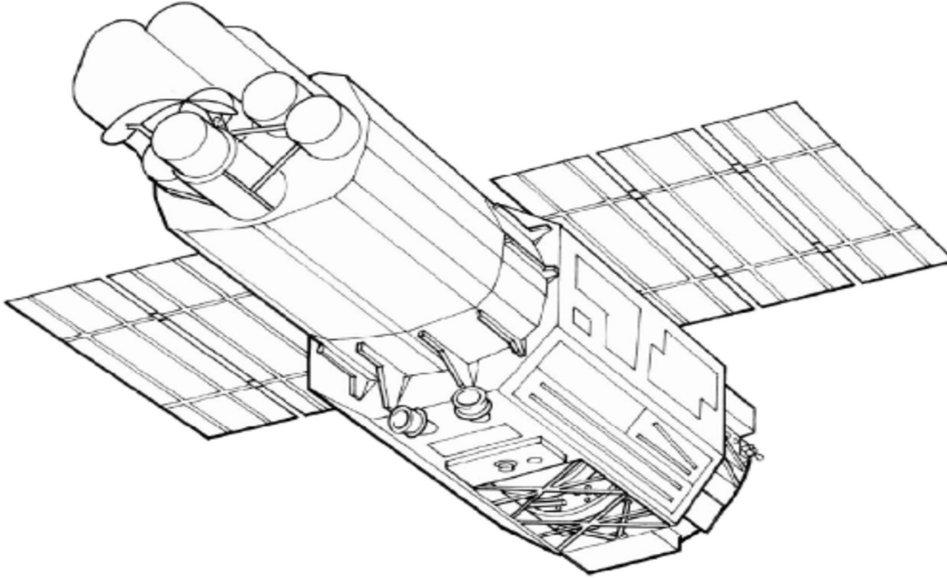


Figure 2.1: *Suzaku*, the fifth Japanese X-ray astronomy satellite launched on 2005 July, 10 in a nearly circular orbit at ~ 570 km. It has broad-band energy coverage from soft X-rays to hard X-rays in 0.2-600 keV. The figure shows schematics view of satellite in the orbit. Image is taken from Mitsuda *et al.* (2007).

2.1.1 X-ray Imaging Spectrometer

XIS is an X-ray sensitive silicon charge-coupled device (CCD) camera that operates in the photon counting mode. In general, CCD converts the energy of incident photon into charge clouds. The produced charge particles are then transferred toward an output gate with the help of electronics and recorded in the form of output voltage. The energy of the incident photon is proportional to the height of the voltage level, referred as *pulse height*. By measuring the pulse height, the energy of the incident photon can be estimated. The XIS has 1024×1024 pixel grids with $24 \times 24 \mu\text{m}^2$ as the dimension of each pixel. Total physical size of the CCD was $25 \times 25 \text{ mm}^2$ that provided a field of view of $17.8 \times 17.8 \text{ arcmin}^2$ in full window mode. The angular resolution of XIS detector is 2 arcmin. There are four XIS instruments on-board *Suzaku*, located at the focal point of X-ray telescopes (XRT; Serlemitsos *et al.*, 2007). The XRT is made of gold coated thin foils, arranged closely in the form of conical shells that focus the soft X-ray photons $< 12 \text{ keV}$ incident at a small grazing angle.

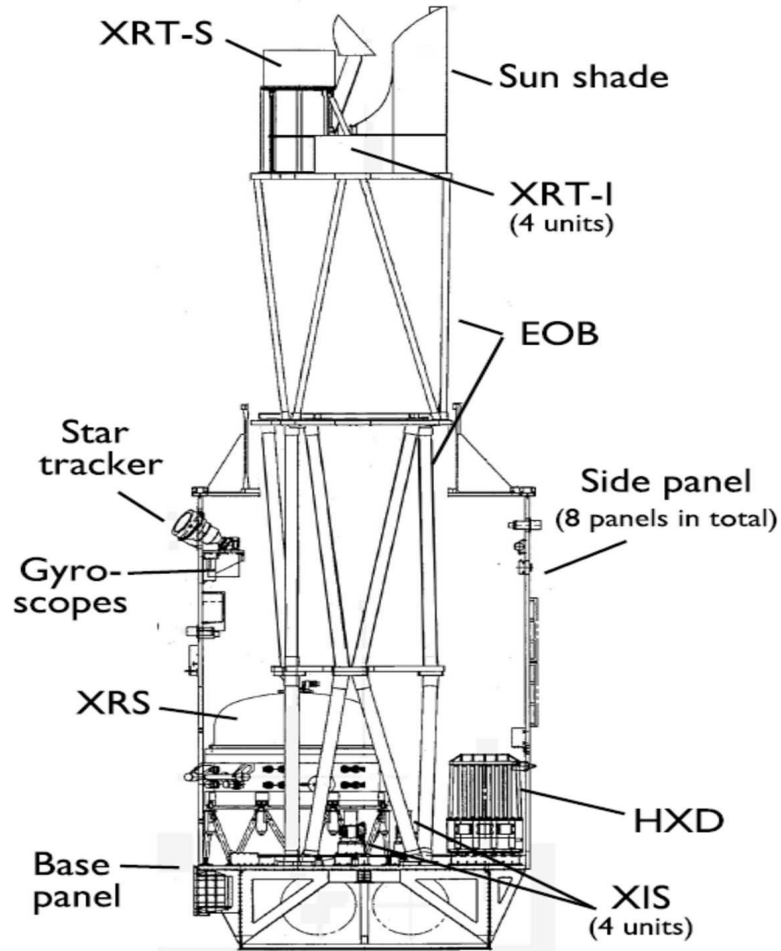


Figure 2.2: Schematic view of *Suzaku* observatory with instruments on-board it. Image credit: Mitsuda *et al.* (2007).

The XIS detector is kept at the focal point of respective XRT which has focal length of 4.75 m. Among four XISs, the XISs-0, 2 & 3 were front-illuminated (FI; 0.4-12 keV energy range), while XIS-1 was back-illuminated (BI; 0.2-12 keV energy range). The effective area for FI and BI XISs are 330 and 370 cm² at 1.5 keV, respectively. The energy resolution of XIS (preflight) was estimated to be 130 eV at 6 keV. The time resolution of XIS detector depends on its operating modes: normal mode and parallel sum clock mode. In normal mode, all the pixels have readout time of 8 s. However, the time resolution of 8, 4, 2 and 1 s can be achieved from XIS depending on the window operating mode. The time resolution of 7.8 ms can be achieved with parallel

sum clock mode.

2.1.2 Hard X-ray Detector

HXD is the non-imaging unit of detectors on-board *Suzaku* which is sensitive in the energy range of 10 to 600 keV. It is a collimating instrument and made of Bismuth Germanate (BGO) crystals that actively shield the main unit of HXD from off-axis photons. HXD comprises of 16 veto shielded detectors arranged in 4×4 arrays deep inside the collimator well. HXD sensor consists of two types of detectors: Gadolinium Silicate (GSO) phoswich counter and 2 mm-thick PIN silicon diodes. Silicon diode is located in front of GSO scintillator and has sensitivity in 10-70 keV energy range, whereas HXD/GSO operates in 40-600 keV energy range. The field of view of PIN and GSO (up to 100 keV) is 34×34 arcmin². Above 100 keV, the collimator becomes transparent and instrument acts as a wide field detector with a field of view of $4.5^\circ \times 4.5^\circ$. The effective area of HXD is ~ 160 cm² at 20 keV and ~ 260 cm² at 100 keV. The energy resolution of PIN detector is ~ 3 keV (FWHM) while GSO has $7.6/\sqrt{E_{MeV}}$ % (FWHM). Along with spectral capability, HXD has high timing sensitivity with time resolution of 61 μ s.

2.2 Nuclear Spectroscopic Telescope Array (*NuSTAR*)

NuSTAR is the first hard X-ray focusing observatory covering an energy range of 3 to 79 keV (Harrison *et al.*, 2013). It is a small explorer mission launched on 2012 June 13 into a low earth equatorial orbit at an altitude of about 600 km and an inclination of 6° . Two separate X-ray telescopes are on-board the satellite that comprise 133 nested mirror shells arranged in conical approximation to the Walter-I design for the focusing of high energy photons. The hard X-ray sensitivity up to 79 keV was achieved by multilayer coating of reflective material with Pt/SiC and W/Si on these X-ray mirrors. Above this energy, Pt starts absorbing rather than reflecting the photons. The X-rays from astronomical sources are reflected by these two telescopes and focused

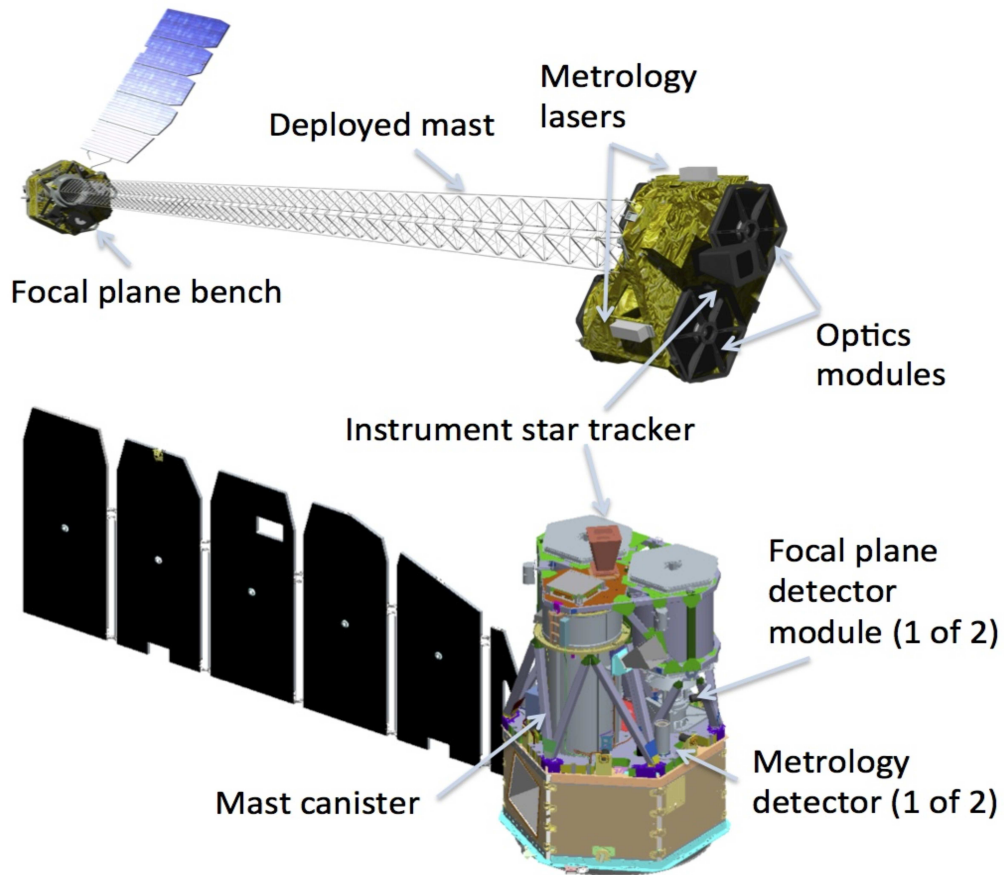


Figure 2.3: *NuSTAR*, the first hard X-ray focusing telescope operated in the 3-79 keV energy range. The figure shows schematics view of satellite in the stowed (bottom) and deployed (top) configurations. This image is taken from Harrison *et al.* (2013).

on to two different focal plane modules, FPMA and FPMB. The focal length of each telescope is 10.15 m which was attained by unique deployable mast that extended the optics after the satellite was in orbit. Figure 2.3 represents schematics view of the satellite before (bottom) and after (top) the launch.

One detector unit consists of four 32×32 pixel Cadmium-Zinc-Telluride (CZT) detectors. The total dimension of a CZT instrument is $20\text{mm} \times 20\text{mm}$ with thickness of 2mm. The energy resolution of detector is 0.4 keV at 10 keV and 0.9 keV at 68 keV (FWHM) respectively. The field of view of *NuSTAR* is 10 arcmin at 10 keV and 6 arcmin at 68 keV, respectively. The high temporal resolution of $2 \mu\text{s}$ can be achieved with *NuSTAR*.

2.3 Overview and the observational details of X-ray sources

Broad-band spectral capabilities and high timing sensitivity of *Suzaku* and *NuSTAR* are most suited for the scientific goals of my work. This allowed me to study the phase-averaged, phase-resolved and time-resolved spectroscopy of X-ray sources along with the opportunity to search the cyclotron absorption line in several unexplored pulsars. An overview and the observational details of the sources studied in this thesis are described below.

2.3.1 EXO 2030+375

EXO 2030+375 is a transient Be/X-ray binary pulsar which was observed with *Suzaku* twice during its Type-I outbursts in 2007 and 2012. EXO 2030+375 was discovered during a giant outburst in 1985 with *EXOSAT* observatory (Parmar *et al.*, 1989). Optical and near-infrared observations of the *EXOSAT* error circle identified a B0 Ve star as the counterpart of EXO 2030+375 (Motch and Janot-Pacheco, 1987; Coe *et al.*, 1988). Using the *EXOSAT* observations in 1985, the spin and orbital periods of the pulsar were estimated to be 42 s and 44.3-48.6 days, respectively. Analyzing *BATSE* monitoring data of several consecutive outbursts of the pulsar EXO 2030+375 in 1992, Stollberg (1997) derived following orbital parameters of the binary system : orbital period $P_{orb} = 46.02 \pm 0.01$ days, $e = 0.36 \pm 0.02$, $a_x \sin i = 261 \pm 14$ lt-sec and $\omega = 223^\circ.5 \pm 1^\circ.8$. The 1-20 keV pulsar spectrum consisted of two component continuum model with a blackbody component of temperature ~ 1.1 keV and a power-law (Reynolds, Parmar and White, 1993; Sun *et al.*, 1994). A spectral feature at ~ 36 keV in the hard X-ray spectrum (in 17-65 keV range) was ascribed to a possible cyclotron absorption line implying the estimated magnetic field of the pulsar to be 3.1×10^{12} Gauss (Reig and Coe, 1999). However, using regular monitoring data of EXO 2030+375 with the *RXTE* from 2006 June to 2007 May, covering the first giant outburst since its discovery in 1985, Wilson,

Finger and Camero-Arranz (2008) reported a cyclotron feature at ~ 11 keV and estimated the magnetic field strength to be 1.3×10^{12} Gauss. *INTEGRAL* and *Swift* observation of the same giant outburst was used to describe the 3–120 keV spectra by using an absorbed power-law with an exponential cut-off, an iron emission line and some peculiar features in 10–20 keV energy range (Klochkov *et al.*, 2007).

For a detailed study of timing and spectral properties, EXO 2030+375 was observed with *Suzaku* on 2007 May 14, at the peak of a regular Type I outburst. This observation was carried out at ‘HXD nominal’ pointing position for effective exposures of ~ 57 ks and ~ 53 ks for XIS and HXD, respectively. The XIS were operated with ‘burst’ clock mode in ‘1/4 window’ option, covering $17'.8 \times 4'.4$ field of view. EXO 2030+375 was observed again with *Suzaku* during a Type-I outburst on 2012 May 23. This observation was carried out at the ‘XIS nominal’ pointing position for a total exposures of ~ 78 ks and ~ 72.5 ks for XIS and HXD, respectively. The XIS was operated in the ‘1/4 window’ option during second observation.

2.3.2 4U 1909+07

High mass X-ray binary pulsar 4U 1909+07 was discovered with *Uhuru* satellite (Giacconi *et al.*, 1974). By using *RXTE*/All-Sky Monitor data, the orbital period of the binary system was reported to be 4.4 days (Wen, Remillard and Bradt, 2000). *RXTE*/ Proportional Counter Array (PCA) observations of 4U 1909+07 yielded 605 s pulsations in the X-ray light curves (Levine *et al.*, 2004). The orbital inclination, orbital separation and mass of the companion star were estimated to be in the ranges of 38° – 72° , 60–80 lt-s and 9–31 M_\odot , respectively (Levine *et al.*, 2004). The detection of an OB star in near-infrared within the X-ray error box of the pulsar confirmed the system to be a OB supergiant-neutron star HMXB (Morel and Grosdidier, 2005). The distance of the binary system was estimated to be ~ 7 kpc (Morel and Grosdidier, 2005). *RXTE* and *INTEGRAL* observations of the pulsar showed that the pulsation period of the pulsar is not stable, rather it changes erratically on time

scales of years (Fürst *et al.*, 2011). Phase averaged spectrum, obtained from above observations, were well described by a power-law with high energy cut-off continuum model along with a black-body component (Fürst *et al.*, 2011). 4U 1909+07 was observed with *Suzaku* on 2010 November 2-3 (Fürst *et al.*, 2012). The observation was carried out at ‘XIS nominal’ pointing position for effective exposures of ~ 30 ks and ~ 22 ks for XIS and HXD, respectively. XIS were operated with ‘normal’ clock mode in ‘1/4 window’ option with 2 s time resolution. The same observation was used during our study.

2.3.3 Cep X-4

Be/X-ray binary pulsar Cep X-4 (GS 2138+56) was discovered at a position near the galactic plane with *OSO-7* in 1972 (Ulmer *et al.*, 1973). X-ray pulsations were detected in the source at ~ 66 s during its 1988 March outburst (Koyama *et al.*, 1991). A cyclotron absorption feature at ~ 30 keV was discovered during *Ginga* observation of the pulsar (Mihara *et al.*, 1991). The optical companion is identified as a Be star, located at a distance of 3.8 kpc (Bonnet-Bidaud and Mouchet, 1998).

The presence of cyclotron line at ~ 30 keV was confirmed with the 2002 June *RXTE* observations of Cep X-4 (McBride *et al.*, 2007). However, no significant changes in cyclotron line energy with source luminosity was observed during these observations. The pulsar was observed with *NuSTAR* during the 2014 June-July X-ray outburst. First observation was carried out at the peak of the outburst whereas the second was at the declining phase of the outburst (Fürst *et al.*, 2015). The 1-50 keV combined spectra from *Swift/XRT* and *NuSTAR* were described by Fermi-Dirac cutoff power-law model along with an absorption component at ~ 30 keV. Addition of a simple absorption component or a pseudo-Lorentzian profile failed to explain the cyclotron absorption feature properly due to the asymmetric nature of the line profile. Along with this asymmetry profile, an absorption like feature at ~ 19 keV was also detected in the spectrum. A marginal positive dependence of cyclotron line energy with the pulsar luminosity was seen during the *NuSTAR* observations.

A Target of Opportunity observation of Cep X-4 was carried out with *Suzaku* in July 01-02 during its 2014 June-July outburst. The pulsar was observed for exposures of ~ 60 ks with XIS-3 and ~ 81 ks with HXD during the decay phase of the outburst. The XIS-3 detector was operated in ‘normal’ clock mode with ‘1/4’ window option yielding 2 s time resolution. The observation was carried out in ‘XIS nominal’ position.

2.3.4 GX 304-1

Be/X-ray binary pulsar GX 304-1 was discovered during hard X-ray sky surveys with balloon observations in 1967 (McClintock, Ricker and Lewin, 1971). Using data from *SAS-3* observations, X-ray pulsations at ~ 272 s were discovered in the source (McClintock *et al.*, 1977). The orbital period of GX 304-1 was reported to be 132.5 d (Priedhorsky and Terrell, 1983). A Be star with visual magnitude of 15 and at distance of 2.4 ± 0.5 kpc was discovered as the optical companion of the pulsar (Mason *et al.*, 1978; Parkes, Murdin and Mason, 1980).

GX 304-1 was in off-state for about 28 years (Corbet *et al.*, 1986; Pietsch *et al.*, 1986). In 2008 June, an X-ray outburst was detected from GX 304-1 with the *INTEGRAL* observatory (Manousakis *et al.*, 2008). Since then, several X-ray outbursts have been detected in the pulsar with *Swift*/BAT and *MAXI*. During the 2010 August outburst, a cyclotron absorption feature at ~ 54 keV was detected in the pulsar spectrum (Yamamoto *et al.*, 2011) and the corresponding magnetic field of the neutron star was estimated to be $\sim 4.7 \times 10^{12}$ G. A positive correlation between cyclotron energy and luminosity was seen during 2012 January-February outburst with *INTEGRAL* (Klochkov *et al.*, 2012). The orbital parameters of the binary system were estimated to be – orbital period = 132.19 d, epoch at the periastron = MJD 55425, pulse period $\simeq 275.45$ s, orbital eccentricity $\simeq 0.5$, $a_x \sin i \simeq 500$ –600 light-s and ω at periastron $\simeq 122.5^\circ$ – 130° (Sugizaki *et al.*, 2015).

GX 304-1 was observed with *Suzaku* during its outbursts in 2010 August and 2012 January. During 2010 August outburst, the *Suzaku* observation was

carried out at the peak of outburst whereas the second observation was made during the decay phase of the 2012 January outburst. The first observation was performed on 2010 August 13, in ‘HXD nominal’ position with an effective exposure of ~ 5.1 ks and ~ 12.9 ks for XIS and HXD detectors, respectively. However, the second observation was made during 2012 January 31-February 02 for longer effective exposures of ~ 16.5 ks for XIS and ~ 58.7 ks for HXD. The second observation was performed in ‘XIS nominal’ position. During both observations, the XIS detectors were operated in ‘burst’ clock mode with ‘1/4’ window option yielding 0.5 s time resolution.

2.3.5 SMC X-2

SMC X-2 is one of the brightest transient X-ray pulsar in the Small Magellanic Cloud (SMC). It was discovered with *SAS-3* in 1977 at a luminosity of 8.4×10^{37} ergs s $^{-1}$ in 2-11 keV energy band, assuming a distance of 65 kpc (Clark *et al.*, 1978). Pulsation at ~ 2.37 s was discovered with the *RXTE* and *ASCA* observations during one of the major X-ray outburst observed in 2000 (Corbet *et al.*, 2001; Yokogawa *et al.*, 2001). The optical companion is identified as O9.5 III-V spectral type emission star (Schmidtke, Cowley and Udalski, 2006; McBride *et al.*, 2008). The orbital of this system is assumed to be ~ 18.5 d based on the periodicity observed during optical and X-ray studies (Schurch *et al.*, 2011; Townsend *et al.*, 2011).

Since 2000, there was no report of any major X-ray activity (outburst) detected in the pulsar. Recently, an intense X-ray outburst was detected in 2015 September during which the pulsar luminosity reached up to as high as $\sim 10^{38}$ ergs s $^{-1}$. The pulsar spectra obtained from *XMM-Newton* and *Swift*/XRT observations during this outburst were explained with the cutoff power-law model with a soft blackbody component at ~ 0.15 keV. In addition to a hard spectrum ($\Gamma \simeq 0$), several emission lines from ionized N, O, Ne, Si and Fe were detected during this outburst (La Palombara *et al.*, 2016).

Following the report of X-ray outburst, Target of Opportunity (ToO) observations of SMC X-2 were performed with *NuSTAR* at three different epochs

in 2015 September – October. Simultaneous *Swift*/XRT (Burrows *et al.*, 2005) observations were also carried out at these epochs of the outburst.

2.3.6 OAO 1657-415

Accretion powered high mass X-ray binary pulsar OAO 1657-415 was discovered by Copernicus satellite (Polidan *et al.*, 1978). Using *HEAO 1 & Einstein* observations, a pulsation at period of 38.22 s was detected in the pulsar (White and Pravdo, 1979). Long term monitoring of the pulsar with the Burst and Transient Source Experiment (*BATSE*) onboard Compton Gamma Ray Observatory (CGRO) confirmed the system as an eclipsing binary (Chakrabarty *et al.*, 1993). The orbital parameters derived from the *BATSE* observations are : orbital period $P_{orb} = 10.444 \pm 0.004$ d, duration of the eclipse = 1.7d, $e = 0.104 \pm 0.005$, $a_x \sin i = 106 \pm 0.5$ lt-sec and $\omega = 93^\circ \pm 5^\circ$. Using these orbital parameters, the mass and radius of companion were estimated to be in the range of 14–18 M_\odot and 25–32 R_\odot , respectively (Chakrabarty *et al.*, 1993). A highly reddened B-type supergiant star was identified as binary companion of OAO 1657-415 (Chakrabarty *et al.*, 2002). The distance of the binary system was estimated to be 6.4 ± 1.5 kpc. The eclipsing HMXB pulsar OAO 1657-415 was observed with *Suzaku* on 2011 September 26–28. The effective exposures for XIS and HXD/PIN were ~ 85 ks and ~ 75 ks, respectively. XIS detectors were operated in ‘1/4 window mode’.

2.3.7 4U 1700-37

The high mass X-ray binary 4U 1700-37 was discovered by *Uhuru* satellite in December 1970 (Jones *et al.*, 1973). Extensive follow-up observations with *Uhuru* revealed the system as an eclipsing binary with an orbital period of 3.412 days. One of the most luminous and hottest optical star among the known high mass X-ray binaries, a supergiant star (HD 153919) of O6.5 Iaf spectral type was identified as the optical companion (Hutchings *et al.*, 1973). Using *BATSE* data, the orbital parameters of the binary system such as inclination

$i=66^\circ$, eccentricity $e < 0.01$, $48 < a_x \sin i < 82$ lt-sec and semi eclipse angle $\theta_E=28^\circ.6$ were derived Rubin1996. Using ultraviolet and optical spectroscopic observations, Clark *et al.* (2002) evaluated physical parameters of the optical companion and used in Monte Carlo simulation to estimate the mass of the X-ray source and optical companion to be $M_x \sim 2.44 \pm 0.27 M_\odot$ and $M_o \sim 58 \pm 11 M_\odot$. The distance of the binary system was estimated to be 1.9 kpc (Ankay *et al.*, 2001). The nature of compact object in 4U 1700-37 is uncertain.

4U 1700-37 was observed with *Suzaku* in 2006 September 13-14. The observation was carried out during out of eclipse phase of the binary covering 0.29-0.72 orbital phase range (considering mid-eclipse time as phase zero; Rubin *et al.* (1996)). The observation was performed in ‘XIS nominal’ position with an effective exposure of ~ 81.5 ks and ~ 82.1 ks for XIS and HXD, respectively.

2.4 Data extraction

High Energy Astronomy Software (HEASoft¹) package is used for the analysis of data obtained from *Suzaku* and *NuSTAR* observatories. This package is freely available and widely used by the X-ray astronomy community. Data for observed X-ray sources are available on HEASARC Archive facilities at Goddard Space Flight Center. The HEASoft package allows to analyze the data for many observatories with up to date Calibration data base (CALDB) files.

For *Suzaku*, the unfiltered events data are reprocessed by using *aepipeline* package of FTOOLS. The clean event files generated after the reprocessing of XIS and HXD unfiltered events were used in our analysis for all the sources. Due to motion of satellite around the earth, the arrival times of the X-ray photons recorded in XIS and HXD events need to be corrected for solar system barycenter, which is done by applying *aebarycen* task of FTOOLS. For the bright X-ray sources, it is possible that XISs detectors are affected by the

¹<https://heasarc.gsfc.nasa.gov/lheasoft>

pile-up, thermal flexing and wobbling effects. To correct these, we generally use S-lang scripts, *aeattcor.sl*². *pile_estimate.sl*³, to imply these correction on XISs data. As the XIS is an imaging detector, we use *DS9* to see the image and select the source and background regions. The light curves and spectra were extracted from XIS cleaned event files by applying the regions for source and background in *XSELECT* package of FTOOLS. The response matrices and effective area files, which carries the information about detector performances, for XISs are created by using *XSRMFGEN* and *XISSIMARFGEN* tasks of FTOOLS, respectively. HXD is a non-imaging detector. The light curves and spectra from the source are accumulated from cleaned HXD/PIN and HXD/GSO event data by using *XSELECT* package. Instrument teams provide the simulated non-X-ray background event files for each observations. We used these events to obtain the background light curves and spectra for HXD/PIN and HXD/GSO. A correction for cosmic X-ray background (CXB⁴) is also applied to PIN spectrum. Depending on the epoch of observation, response files for HXD/PIN and HXD/GSO released by instruments team were used. Technical details for XIS and HXD can be found in *Suzaku ABC Guide*⁵

To analyze *NuSTAR* data, we have used standard *NUSTARDAS* software inbuilt in the *HEASoft* package. Data can be reprocessed by using *nupipeline* package. The science events generated after the reprocessing are used to generate the barycentric corrected light curves, spectra, response matrices and effective area files for both detectors through *nuproducts* task. The source light curves and spectra are extracted from the FPMA and FPMB data by selecting a circular region around the source center. Background data products are accumulated in a similar manner by selecting circular regions of same size away from the source. More detail can be found in *The NuSTAR Data*

²<http://space.mit.edu/ASC/software/suzaku/aeattcor.sl>

³http://space.mit.edu/ASC/software/suzaku/pile_estimate.sl

⁴http://heasarc.nasa.gov/docs/suzaku/analysis/pin_cxb.html

⁵<http://heasarc.nasa.gov/docs/suzaku/analysis/abc/>

*Analysis Software Guide*⁶

We also used *Swift*/XRT data for spectral analysis which was done by using standard *xrtpipeline* task for reprocessing the XRT data in HEASoft package. The source and background spectra were extracted from the window timing mode event by considering the source and background regions in *XSELECT* package. The response file for XRT was generated by using the *XRTMKARF* tool.

2.5 X-ray timing and spectral techniques

Apart from imaging, X-ray detectors are developed to record the distribution of source photons in time and energy spaces i.e. producing the light curve and energy spectrum. The properties of a source and its physical phenomena that cause the high energy emission can be studied from the light curve and energy spectrum. The HEASoft package is designed to extract these information by using some specific tools.

For timing analysis, tasks from XRONOS package are used to search the presence of periodicity or quasi-periodicity in a time series data. FTOOLS provides two packages such as *powspec* and *efsearch*. The *powspec* task is based on the Fourier transform method that generates a power density spectra (PDS) in power and frequency domain. A strong power at certain frequency shows the presence of periodicity in data. If the peak in the PDS is relatively weak but above the continuum and also distributed in a Gaussian shape, this feature can be considered as quasi-periodicity in the time series data. In addition to the Fourier transform method, the periodicity can be searched by folding method which is implemented in the *efsearch* package. Using this, a distribution between χ^2 and period is plotted. The highest value of chi-square is expected at the pulsation/ rotation period of a source. At a given periodicity, the pulse profile of a pulsar can also be generated at a given epoch with the *efold* task.

Spectral analysis is aimed to study the shape of energy continuum with

⁶https://heasarc.gsfc.nasa.gov/docs/mustar/analysis/mustar_swguide.pdf

different physical models. The XSPEC (*X-ray Spectral Fitting Package*), a part of HEASoft, allows to fit the spectra considering several models present in the package itself. There are some local models which can be also implemented during the fitting. The spectra recorded by a detector do not show the real spectrum of a source due to the effect of the response of the detector and its effective area. In order to get actual source spectrum, recorded photon distribution is convoluted with the response of the detector. With proper background subtraction, response and effective area files, the source spectra are fitted in the XSPEC by using the χ^2 method. In general, the χ^2 method tests the difference between data points and model, as described

$$\chi^2 = \sum \frac{(O - M)^2}{\sigma^2}$$

where, O is the observed data and M is the model point. σ^2 indicates the variance among data points. The reduced- χ^2 , $\chi_{red}^2 = \chi^2/\nu$, is defined as the ratio of χ^2 to degree of freedom. The number of degree of freedom corresponds the total number of data points minus model parameters. If the value of χ_{red}^2 is equal to 1, the model is believed to well describe the observational data obtained from a source. For χ_{red}^2 much greater than one, the model is insignificant, while $\chi_{red}^2 < 1$ corresponds to large number of parameters in the model some of which may not be required or overestimation of error in the data.

Chapter 3

Absorption dips in the pulse profiles of Be/X-ray binary pulsars

Pulse profile is an intrinsic feature of a pulsar. It represents the geometry of the emission region and its beam pattern near the surface of the neutron star. Some pulsars have single/ double peaked profiles depending on the visibility of one or both the poles (Nagase, 1989; Bulik *et al.*, 2003). The intermediate peaks are also seen in the the pulse profiles of a few pulsars e.g. Cen X-3 and Her X-1, showing a wide range of variety among their shapes. In general, the pulse profiles of accretion powered X-rays are found to be energy dependent. In soft X-rays, they appear to be complex and become simpler at hard X-rays. Corresponding pulse fraction also evolves with the energy and expected to be maximum at energies >10 keV (White, Swank and Holt, 1983). The pulse fraction is defined as the ratio between the difference in the maximum and minimum intensities to the sum of the maximum and minimum intensities in the pulse profile. Apart from the energy, pulse profiles also show a luminosity dependence. This can help us to understand the evolution of beam function geometry with mass accretion rate (see section 1.5 of Chapter-1).

Table 3.1: Log of Be/X-ray binary pulsars studied in this thesis with *Suzaku*.

Source name	ObsID	Start Date	Exposure (ks)	Period
			XIS, HXD	(s)
EXO 2030+375	402068010	2007-05-14	58, 53	41.4106
EXO 2030+375	407089010	2012-05-23	78, 73	41.2852
Cep X-4	409037010	2014-06-18	30, 53	66.334
Cep X-4	909001010	2014-07-01	60, 81	66.334
GX 304-1	905002010	2010-08-13	5, 13	275.45
GX 304-1	406060010	2012-01-31	17, 59	274.88

Pulse profiles of Be/X-ray binary pulsars are generally found to be complex among the accretion powered pulsars. They show complicated pulse profiles which consist of multiple intensity drops at certain pulse phases, referred as *dips* in the pulse profiles. These dips are frequently seen at lower energies and become indistinguishable from profiles at higher energies. Cemeljic and Bulik (1998) first suggested that the narrow streams of accretion flow are associated with pulsar which are phase-locked and co-rotate with the pulsar. The photons propagating along the line of sight are getting absorbed/blocked by matter in these streams producing dips in the pulse profile of these pulsars. Using this, they also successfully examined the pulse profiles of A 0535+262 obtained from BATSE observations at various luminosity states. Similar explanation was also proposed by Galloway *et al.* (2001) to explain the sharp dips observed in the pulse profiles of GX 1+4 and RX J0812.4-3114 based on their finding through phase-resolved spectroscopy.

3.1 Energy dependent pulse profiles of Be/X-ray binary pulsars

To understand the nature of dips and their energy and luminosity dependence, three Be/X-ray binary pulsars EXO 2030+375, Cep X-4 and GX 304-1 were studied at different luminosity levels with *Suzaku*. We have also probed the

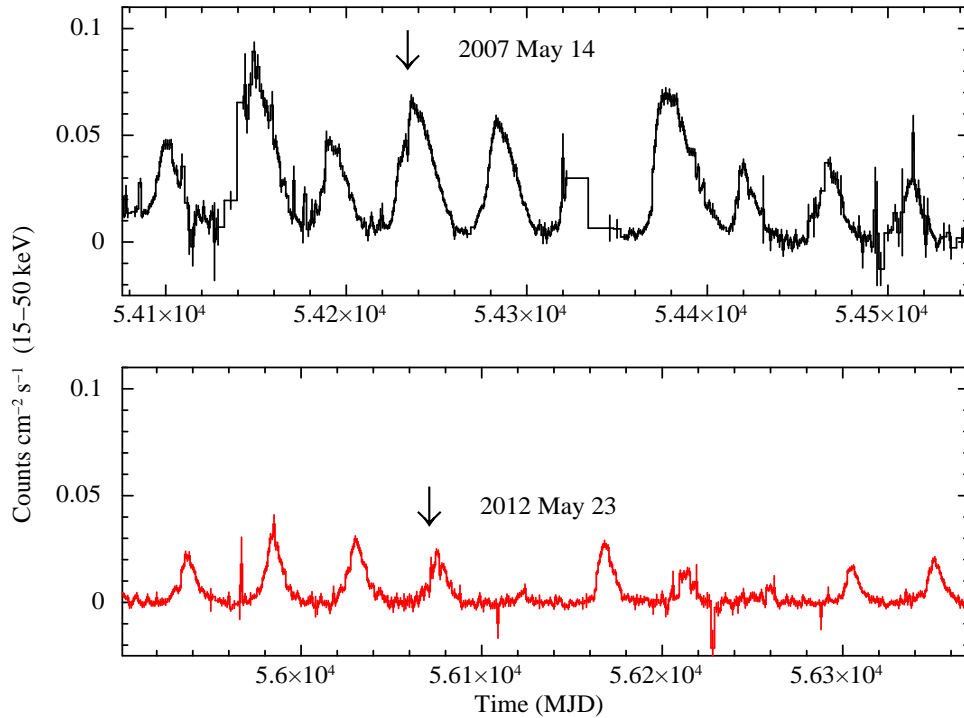


Figure 3.1: *Swift*/BAT light curves of EXO 2030+375 covering the duration of *Suzaku* observations in 2007 May (upper) and 2012 May (bottom) outbursts. The light curve is plotted for 469 days of monitoring data showing frequent Type I outbursts in the system. Arrow marks in the figure show the dates of *Suzaku* observation.

geometry of the beam function and the effect of mass accretion rate on the pulse profiles. Pulse-phase-resolved spectroscopy has been performed on these observations to explore the matter distribution around these pulsars. The log of *Suzaku* observations of these pulsars is given in Table 3.1 along with the estimated value of pulse periods during our study. An overview of these pulsars can be found in section 2.3 of Chapter-2.

3.1.1 EXO 2030+375

The transient pulsar EXO 2030+375 was observed with *Suzaku* during its 2007 May and 2012 May outbursts. We have analyzed these two observations to study the pulse profiles of this pulsar at different luminosity states. EXO 2030+375 is one of the unique Be/X-ray binary pulsar which shows

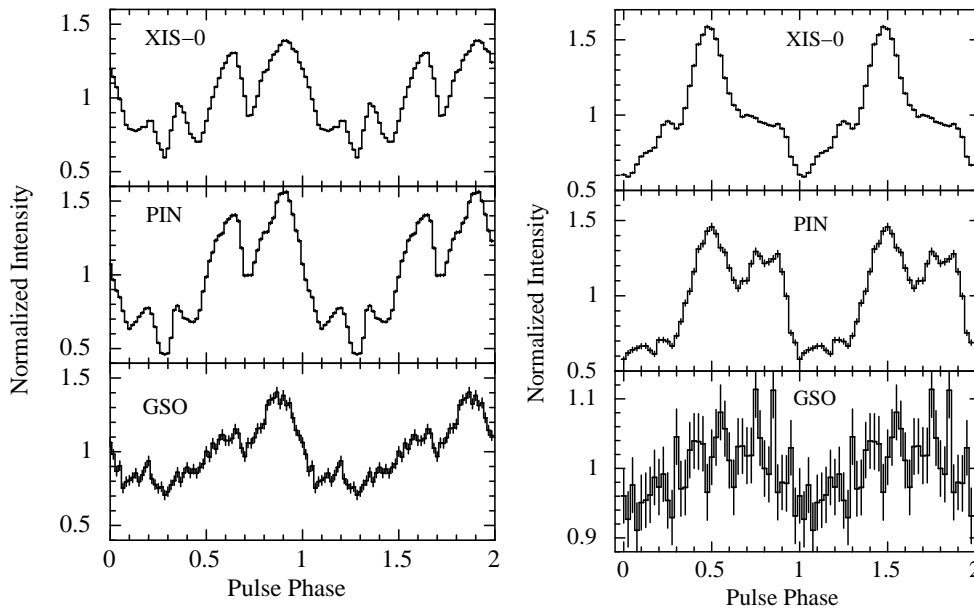


Figure 3.2: The soft to hard X-ray pulse profiles of EXO 2030+375 in different energy bands obtained from XIS-0 (top panel; in 0.2–12 keV range), PIN (second panel; in 10–70 keV range) and GSO (bottom panel; in 40–600 keV range) during 2007 May (left panel) and 2012 May (right panel) outbursts. Pulse profiles were observed to be complicated due to the presence of narrow absorption dips during the 2007 observation compared to the 2012 observation. The errors in the figure are estimated for the 1σ confidence level. Two pulses are shown for clarity.

Type I outbursts almost at each periastron passage. *Swift*/BAT monitoring light curves covering the span of 2007 and 2012 outbursts are shown in Figure 3.1. Several Type-I outbursts can be seen in both the panels of the figure.

Following the standard procedure, we extracted barycentric corrected light curves in a several energy ranges from XIS-0 (0.5–10 keV), PIN (10–70 keV) and GSO (40–600 keV) data with time resolution of 2, 1 and 1 s, respectively. The pulse period of the pulsar was estimated from these light curves by using the χ^2 maximization technique and found to be 41.4106(1) and 41.2852(3) s during first and second observations, respectively. The background subtracted light curves were then folded at the respective periods to get the pulse profiles of pulsar in various energy ranges during these observations.

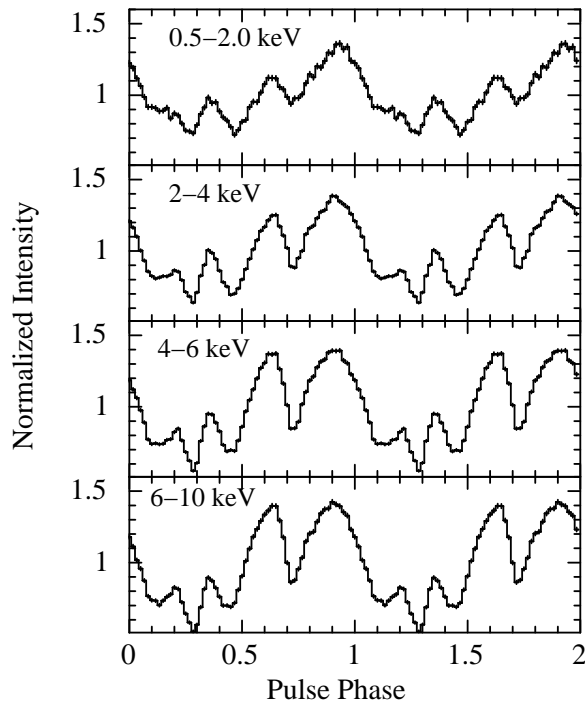


Figure 3.3: The XIS-0 pulse profiles of EXO 2030+375 at different energy ranges during 2007 May outburst. The presence of several dip-like features in 0.3-0.7 and 0.9-1.1 pulse phase ranges are clearly seen. The error bars represent 1σ uncertainties. Two pulses are shown for clarity.

The pulse profiles, shown in Figure 3.2, were found to be different during these two observations. From the figure it can be also seen that pulse profiles during 2007 May observation (left panels) are complicated than the pulse profiles during 2012 May observation. Several narrow absorption dips were seen at certain phases of profiles and were seen up to higher energies (10-70 keV range). To investigate the energy dependence of the pulse profiles, the source and background light curves were generated in various energy bands from the XIS, PIN and GSO event data and corresponding profiles are shown in Figures 3.3 & 3.4 for 2007 May observation. From these figures, it can be seen that the pulse profiles appear complex due to the presence of prominent dips at soft X-rays. The dips in the profiles are very strong and clearly distinguishable up to ~ 40 keV. After this energy, the width and depth of the dips in the pulse profiles decrease gradually up to ~ 70 keV. Beyond ~ 70 keV, however, the dips become indistinguishable and the pulse profiles appear smooth and

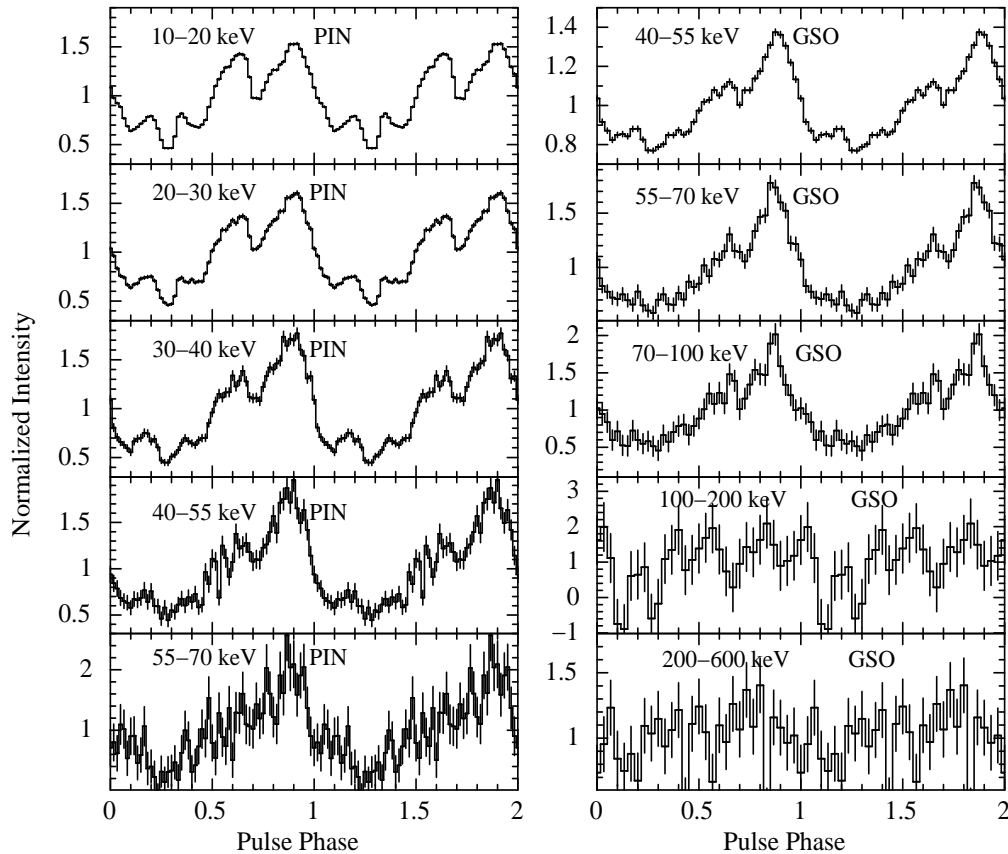


Figure 3.4: The energy resolved pulse profiles of EXO 2030+375 obtained from HXD/PIN and HXD/GSO light curves at various energy bands during 2007 May outburst. The presence/absence of dip-like structures can be seen in 0.3-0.7 and 0.9-1.1 pulse phase ranges. The error bars represent 1σ uncertainties. Two pulses in each panel are shown for clarity.

single peaked. The presence of dips in the pulse profiles up to ~ 70 keV is rarely seen in the accretion powered X-ray pulsars. The pulsations were seen clearly up to ~ 100 keV in the pulse profiles.

For 2012 May observation, the energy resolved pulse profiles were also obtained by folding the background subtracted light curves at respective pulse-period of the pulsar and are shown in Figure 3.5. It can be seen from this figure that the shape of the pulse profiles obtained from the 2012 May *Suzaku* observation was found to be significantly different from the pulse profiles of 2007 observation. The profile appeared to be single-peaked up to ~ 8 keV beyond which a hump-like structure appeared after the main peak. The pulse

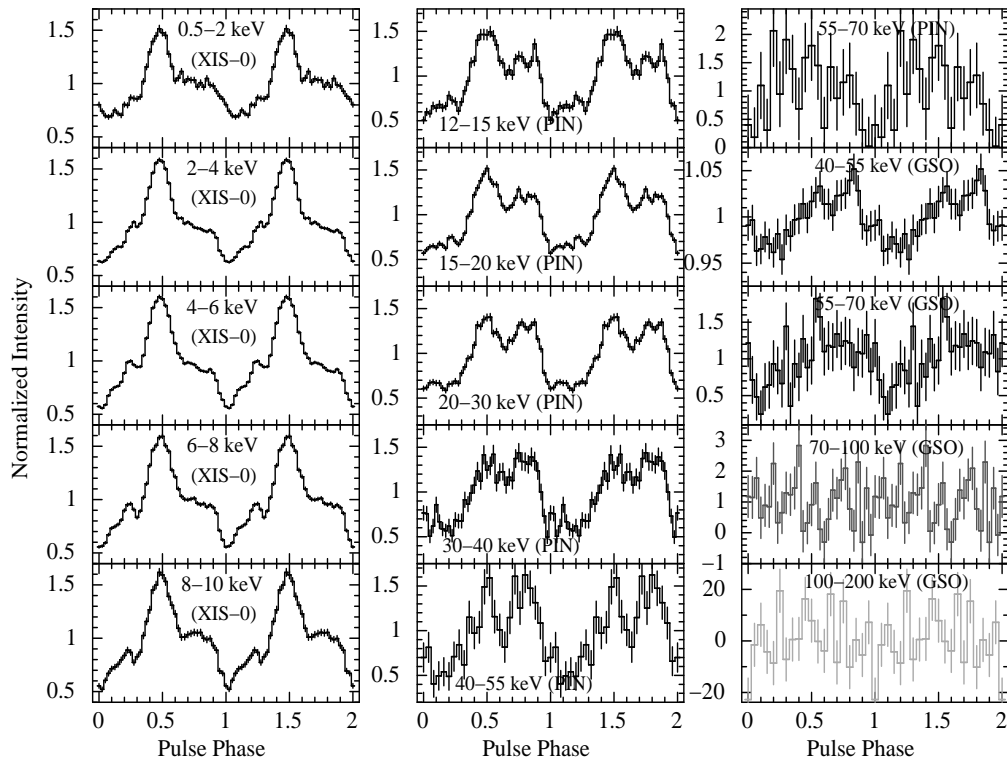


Figure 3.5: Energy-resolved pulse profiles of EXO 2030+375 obtained from XIS-0, HXD/PIN and HXD/GSO light curves at various energy ranges during 2012 May outburst. The presence of absorption dips in profiles at higher energies can be seen in 0.6–0.8 pulse phase range. The error bars represent 1σ uncertainties. Two pulses in each panel are shown for clarity.

profile became double-peaked up to ~ 40 keV beyond which it again became single-peaked. The pulsation was seen in the light curves up to ~ 70 keV range.

3.1.2 Cep X-4

Be/X-ray binary pulsar Cep X-4 was observed with *Suzaku* at two epochs during 2014 June–July outburst. The first observation was performed at peak whereas the second observation was carried out at declining phase of the outburst. *Swift*/BAT light curve covering this outburst is shown in the first panel of Figure 3.6. Using the standard procedure of data reduction, we have analyzed data from both the *Suzaku* observations of Cep X-4. The barycentric corrected light curves were generated from XIS-0, PIN and GSO events at

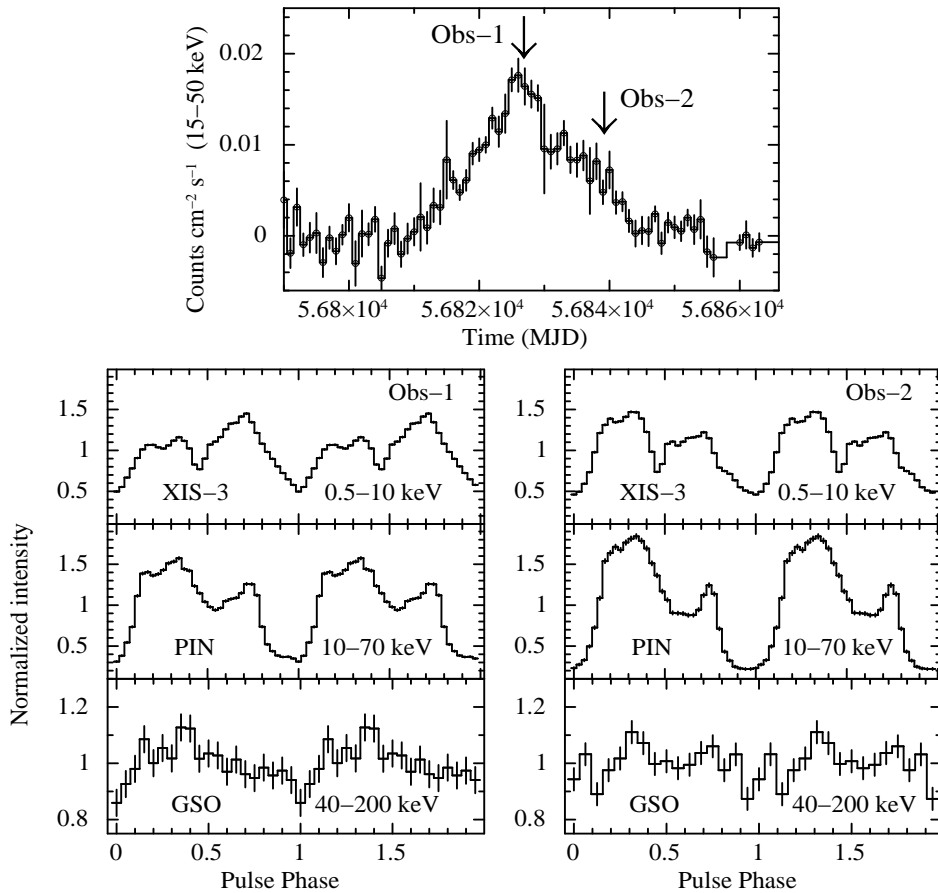


Figure 3.6: *Swift*/BAT light curve of Cep X-4 in the 15-50 keV range during its 2014 outburst is shown in the first panel. The arrow marks in the figure indicate the date of *Suzaku* observations. Corresponding pulse profiles in 0.5-10 keV, 10-70 keV and 40-200 keV obtained from both observations are shown in both sides of figure. The errors in the pulse profiles are estimated for 1σ confidence level and two pulses are shown for clarity.

time resolution of 2, 1 and 1 s, respectively. Following the χ^2 maximization technique, the pulse period of pulsar was estimated to be 66.334(1) s during both of the observations. The background subtracted XIS, PIN and GSO light curves were folded at corresponding pulse period to generate the pulse profiles in respective energy bands and are shown in second, third and fourth panels of Figure 3.6 for first (left panels) and second (right panels) observations.

During both observations, the soft X-ray pulse profile in 0.5-10 keV range were found to be simple with a dip at around 0.4 phase. However, the 10-

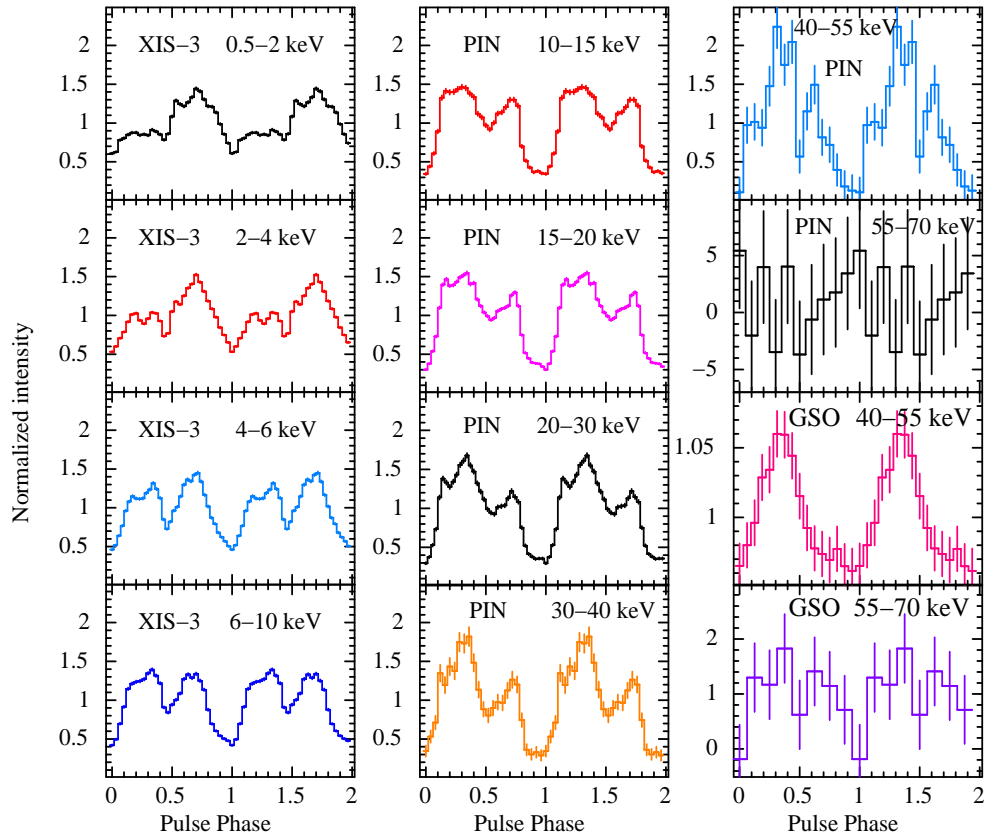


Figure 3.7: Energy-resolved pulse profiles of Cep X-4 obtained from the first *Suzaku* observation during 2014 outburst. The presence of absorption dips in profiles can be clearly seen between 0.4-0.5 pulse phases. The error bars represent 1σ uncertainties. Two pulses in each panel are shown for clarity.

70 keV pulse profiles appeared to be broad and a hump like shape. This feature was prominent during second observation of the pulsar. To explore energy dependence of the pulse profiles, we have generated energy-resolved light curves that were folded at the spin period of the pulsar. Figures 3.7 & 3.8 show the energy-resolved pulse profiles during first and second observations, respectively. It is evident from the figures that the soft X-ray pulse profiles were relatively simple with a dip feature. However with increasing energy, the depth of dip decreased and profiles were evolved into a broad peak followed by a hump like structure. Up to 40 keV, dip was clearly distinguishable in the pulse profiles. Beyond this energy, profiles become single peaked. During both observations, pulsation were seen up to 55 keV in the light curves.

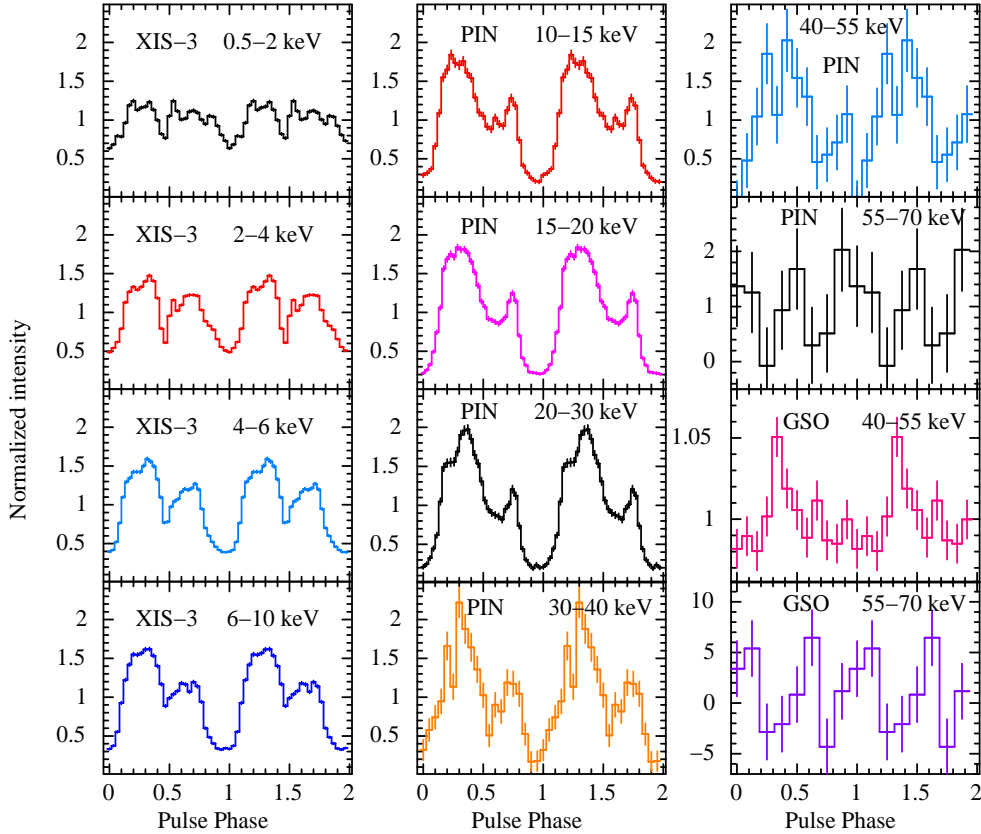


Figure 3.8: Energy-resolved pulse profiles of Cep X-4 at various energy bands, during second *Suzaku* observation in 2014 outburst. The presence of absorption dips in profiles can be clearly seen between 0.4-0.5 pulse phases (with 1σ errors). The error bars represent 1σ uncertainties. Two pulses in each panel are shown for clarity.

3.1.3 GX 304-1

GX 304-1 was observed with *Suzaku* during its outbursts in 2010 August and 2012 January. *Swift*/BAT light curves of the pulsar in 15-50 keV range, covering the outbursts are shown in top panels of Figure 3.9. Arrow marks in both panels indicate the date of *Suzaku* observation of GX 304-1 during respective outbursts. During 2010 August outburst, the *Suzaku* observation was carried out at the peak of the outburst whereas the second observation was made during the decay phase of the 2012 January outburst.

The source and background light curves with 1 s time resolution were extracted from barycentric corrected XIS-0, PIN and GSO event data for both the observations. The χ^2 -maximization technique was applied to estimate

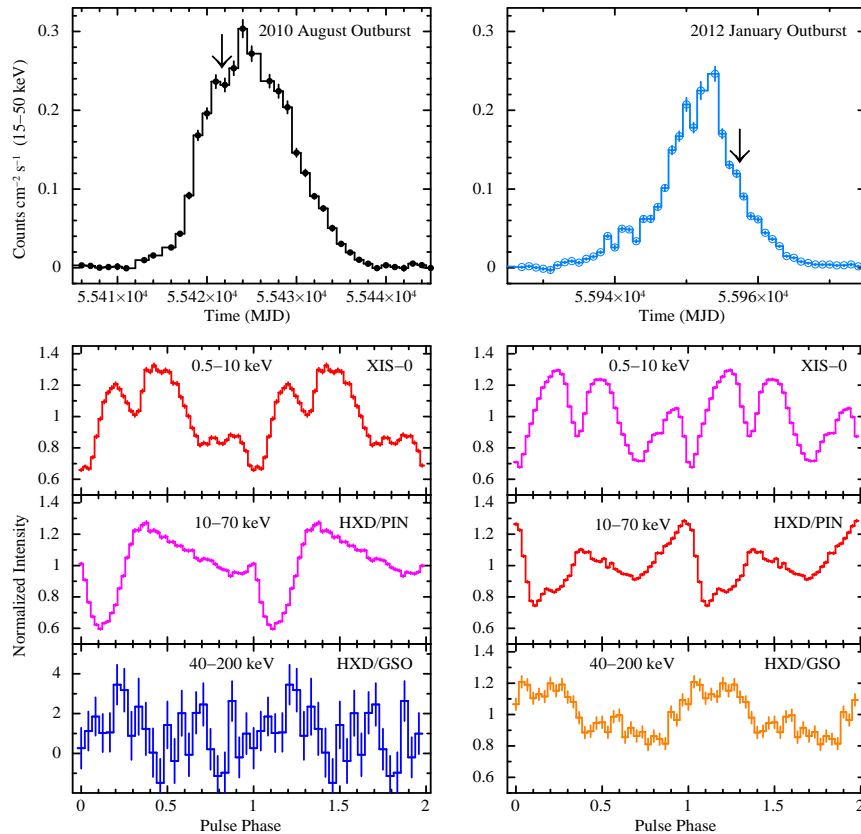


Figure 3.9: *Swift*/BAT light curves of GX 304-1 in the 15-50 keV energy band during 2010 and 2012 outbursts are shown in both sides of first panel. The arrow marks in both sides of first panel show the date of *Suzaku* observations. Corresponding pulse profiles in 0.5-10 keV, 10-70 keV and 40-200 keV obtained from both the observations are shown in both sides of the figure (Jaisawal, Naik and Epili, 2016). The errors in the pulse profiles are estimated for 1σ confidence level and two pulses are shown for clarity.

the pulse period of the pulsar. Pulsations at periods of 275.45 ± 0.05 and 274.88 ± 0.01 s were detected in the source light curves obtained from the first and second *Suzaku* observations, respectively. The estimated pulse periods were used to generate pulse profiles from background subtracted light curves from corresponding observations. Pulse profiles in 0.5-10 keV (XIS-0), 10-70 keV (PIN) and 40-200 keV (GSO) energy ranges for both the observations are shown in second, third and fourth panels of Figure 3.9, respectively.

Strong energy dependence of the pulse profiles can be clearly seen during

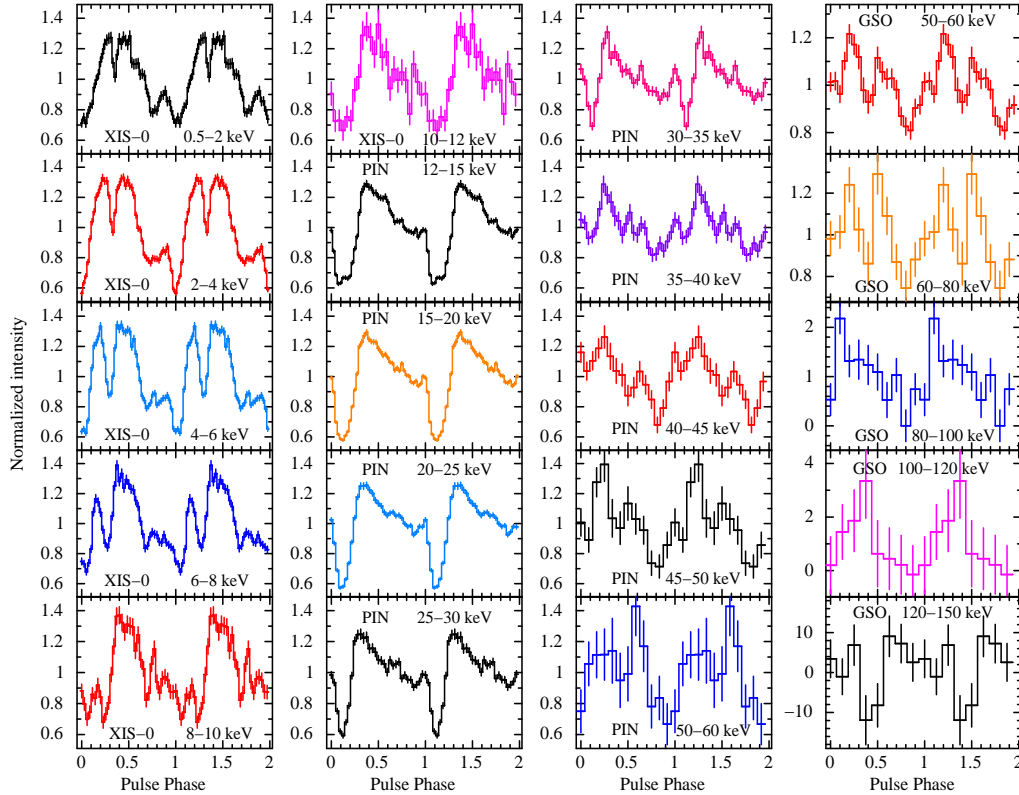


Figure 3.10: Energy-resolved pulse profiles of GX 304-1 obtained from XIS-0, HXD/PIN and HXD/GSO light curves at various energy ranges, during 2010 August *Suzaku* observation. The presence of absorption dips in profiles can be seen at various pulse phases (Jaisawal, Naik and Epili, 2016). The error bars represent 1σ uncertainties. Two pulses in each panel are shown for clarity.

both the observations (Figure 3.9). Absorption dips at certain phases were seen in the soft X-ray pulse profiles (0.5-10 keV range). However, these dips disappeared from the pulse profiles in 10-70 keV range. Pulsations were absent or marginally seen in 40-200 keV pulse profiles obtained from GSO light curves. Apart from the energy dependence, the pulse profiles are also found to be luminosity dependent. The top panels of the Figure 3.9 show that the *Suzaku* observations of the pulsar were carried out at different luminosity levels e.g. the source was comparatively brighter during the 2010 August observation than the 2012 January observation. However, the shape of the pulse profiles in soft and hard X-rays (second and third panels) are different due to the presence of absorption dips or dip-like features. Along with the energy and

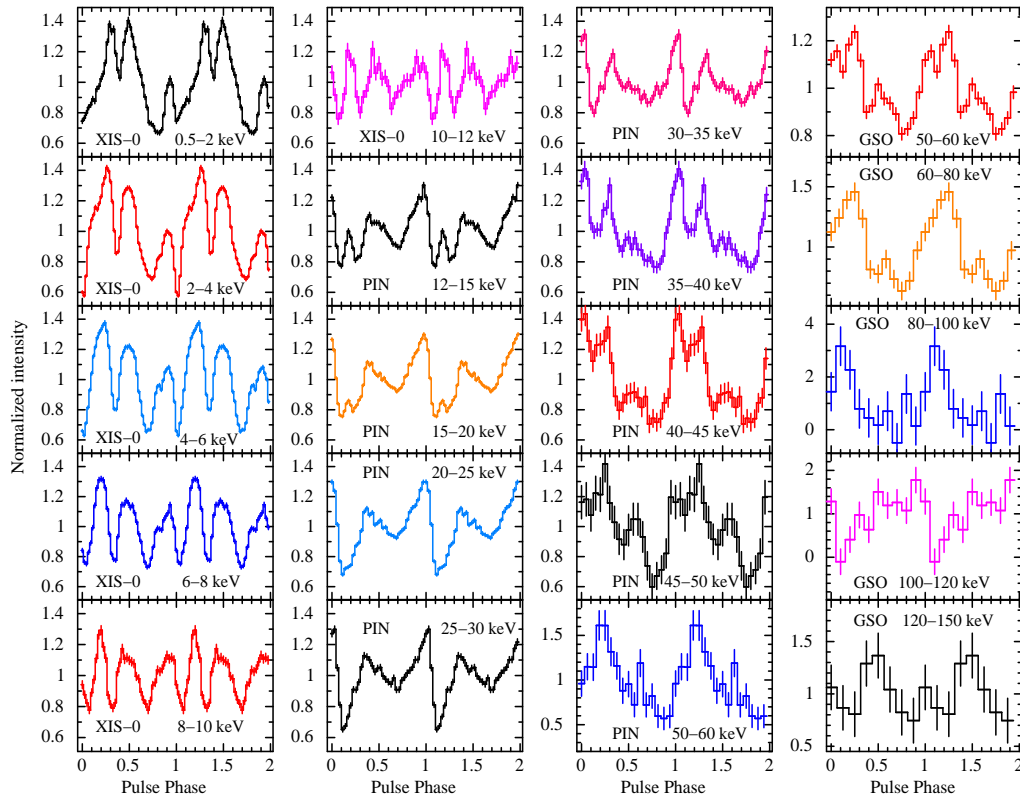


Figure 3.11: Energy-resolved pulse profiles of GX 304-1 obtained from XIS-0, HXD/PIN and HXD/GSO light curves at various energy ranges, during 2012 January *Suzaku* observation. The presence of absorption dips in profiles at higher energies can be seen at various pulse phases (Jaisawal, Naik and Epili, 2016). The error bars represent 1σ uncertainties. Two pulses in each panel are shown for clarity.

luminosity dependence of the pulse profiles in GX 304-1, a phase shift of ~ 0.1 (see Figure 3.9) was also found between the soft (XIS) and hard (PIN) X-ray pulse profiles obtained from both the observations.

To investigate the evolution of pulse profiles with energy during both *Suzaku* observations, we have generated the energy resolved pulse profiles in various energy bands and are shown in Figure 3.10 & 3.11 for first and second observations, respectively. It can be seen from Figure 3.10 that a prominent and narrow absorption dip was present in pulse profiles up to ~ 8 keV. Beyond this energy, the peak in the pulse profiles prior to the dip (≤ 0.3 phase; left panels of Figure 3.10) disappeared and broadened the minima in the pulse profile to 0.05-0.25 pulse phase range (panels in second column of Figure 3.10). We

suggest that this broadening of the minima in the pulse profile is the possible cause of observed ~ 0.1 phase shift in the soft (0.5-10 keV) and hard X-ray (10-70 keV) pulse profiles. A careful inspection of Figure 3.10 & 3.11 showed that the pulse profiles were complex due to presence of several absorption features (dips) at various pulse phases and strongly energy dependent up to ~ 12 keV beyond which the shape of the profiles became simple up to ~ 35 keV. The main dip in the pulse profiles in this energy range (12-35 keV) was observed to be phase-shifted by ~ 0.1 phase compared to that in soft X-ray profiles. In pulse profiles beyond ~ 35 keV, the main dip at ~ 0.1 phase appeared to be filled-up gradually with increase in energy. Along with the increase in the normalized intensity at ~ 0.1 phase (Figure 3.10 & 3.11), a significant decrease in intensity was observed at ~ 0.7 - 0.8 phase range which appeared as the main dip in hard X-ray pulse profiles. These hard X-ray pulse profiles (≥ 40 keV) appeared to be single-peaked and pulsations were detected up to ~ 120 keV.

3.2 Broad-band spectroscopy of Be/X-ray binary pulsars

The energy resolved pulse profiles of all the three pulsars EXO 2030+375, Cep X-4 and GX 304-1 were found to be complex during *Suzaku* observations. Presence of multiple narrow and prominent absorption dips were generally seen in the soft X-ray pulse profiles. However, during 2007 May observation of EXO 2030+375, dip was observed up to as high as ~ 70 keV which is rare in the accretion powered X-ray pulsars. To investigate the origin of these dips and explore the matter distribution surrounding the pulsars, spectral analysis is performed. First we have studied the broad-band phase-averaged spectra of these pulsars by describing their continuum with several empirical models such as high energy cutoff power-law (HECut; White, Swank and Holt, 1983), cutoff power-law (Cutoffpl), the Fermi Dirac Cutoff (FDCut; Tanaka, 1986), the negative and positive power-law with exponential cutoff (NPEX; Mihara, 1995) and CompTT (Titarchuk, 1994) models. A partial absorption component was

added in these models to explain the presence of narrow absorption dips in the pulse profiles of Be/X-ray binary pulsars. Using respective best fit model, phase-resolved spectroscopy was also performed for these pulsars.

3.2.1 Phase-averaged and Phase-resolved spectroscopy of EXO 2030+375

We have extracted the spectra of EXO 2030+375 using XIS, HXD/PIN and HXD/GSO event data for both the observations and fitted by using *XSPEC* package with appropriate background, response and effective area files. For 2007 outburst, the 1-200 energy spectra of the pulsar was best explained with the partial covering HECut model along with several emission lines at ~ 2 keV, ~ 2.5 keV, ~ 3.2 keV and ~ 6.6 keV (Naik et al. 2013). These lines were identified as emissions from Si XIII, Si XIV, S XV, Fe K_{α} and Fe XXVI at the respective energies. The reduced χ^2 obtained from the spectral fitting was found to be 1.59 (for 638 dof). As the pulsar was bright and several emission lines were detected at soft X-rays, we attempted to fit the broad-band spectra with the HECut model with partially ionized absorber *zxipcf* model in XSPEC) in place of neutral absorber component *pcfabs*. Using this, the ionization states of the absorbing medium and the corresponding covering fraction could be investigated. The spectral fitting was improved marginally with the reduced χ^2 of 1.51 (for 637 dof) for 2007 May observation of the pulsar. However, in case of 2012 May *Suzaku* observation, the 1-100 energy spectrum of the pulsar was found to be best described (χ^2 of 1.4) by three continuum models such as HECut, Cutoffpl and NPEX models along with an iron emission line at ~ 6.4 keV. During both of the observations, we did not find any signature of the presence of cyclotron resonance scattering feature at earlier reported energies in EXO 2030+375.

The pulse-phase-resolved spectroscopy was performed to investigate the possibilities of presence of additional matter at various pulse phases around the poles of the transient pulsar EXO 2030+375. We have accumulated the spectra

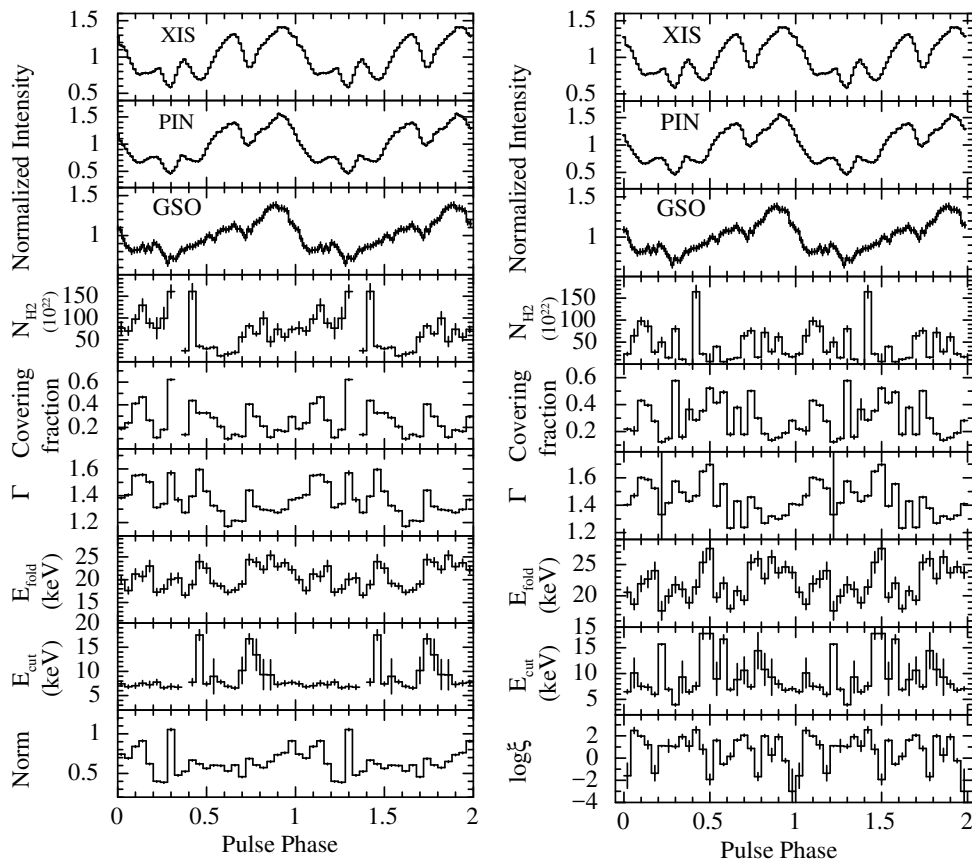


Figure 3.12: Best-fitted spectral parameters obtained from the phase resolved spectroscopy of 2007 May *Suzaku* observation of EXO 2030+375. The pulse profiles in 0.2-12 keV (XIS), 10-70 keV (PIN) 40-600 keV (GSO) ranges are shown in top three panels of both sides of the figure, respectively. The other panels in the left and right sides show the spectral parameters obtained from pulse phase-resolved spectroscopy by using partial covering HECut model with neutral and ionized absorber, respectively (Naik *et al.*, 2013). The errors shown are estimated for 1σ confidence level.

in 25 and 20 phase-bins during first and second observations, respectively. The 1-70 keV phase resolved spectroscopy was carried out by using the respective best fitted phase-averaged models. During the fitting, certain parameters such as absorption column density (N_{H1}), normalization constant of detectors, iron line energy and line width were fixed at their phase-averaged values.

Spectral parameters obtained from the simultaneous spectral fitting of 2007

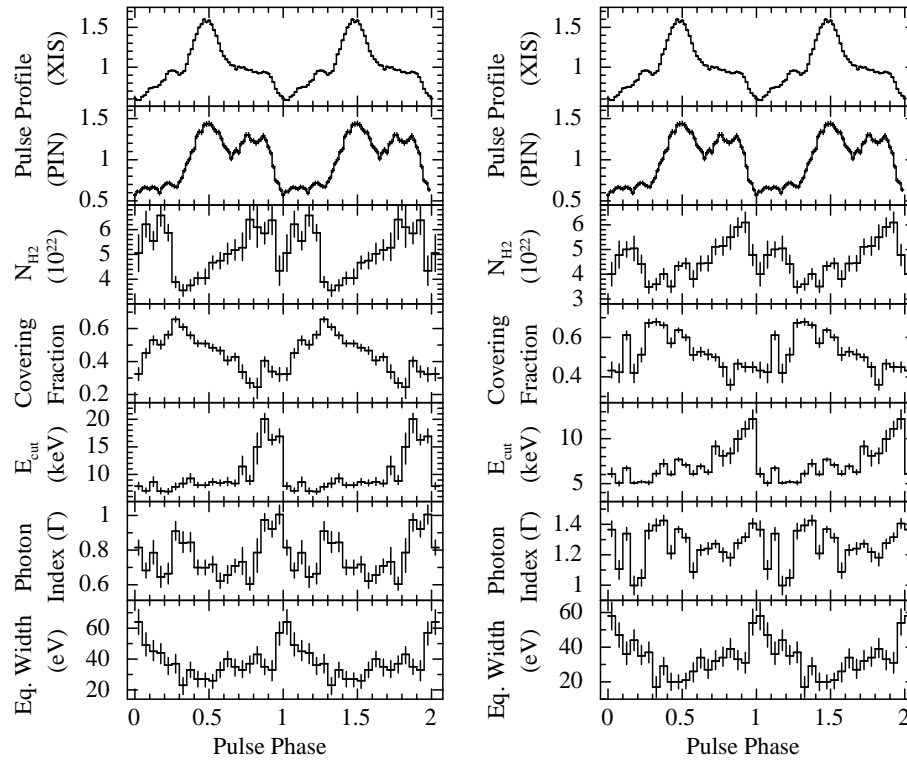


Figure 3.13: Best fitted spectral parameters obtained from the pulse-phase-resolved spectroscopy of *Suzaku* observation of EXO 2030+375 during 2012 May outburst. The XIS (in 0.4-12 keV range) and PIN (in 10-70 keV range) pulse profiles are shown in top two panels of both sides of the figure, respectively. The other panels show the spectral parameters obtained by using a partial covering NPEX and partial covering HECut continuum models in left and right panels of the figure. The errors are estimated for 1σ confidence level.

May observation are plotted in left and right panels of Figure 3.12 for the partial covering HECut model with neutral and partially ionized absorber, respectively. The top three panels in both the sides of Figure 3.12 show the pulse profiles of EXO 2030+375 obtained from XIS, PIN and GSO data. The values of additional column density (N_{H2}) and covering fraction over pulse phases are shown in fourth and fifth panels of the figure, respectively. The change in values of power-law photon index, folding and cut-off energy over pulse phases are shown in the sixth, seventh and eighth panels respectively. The left bottom panel shows the variation of power-law normalization whereas the right bottom panel of the figure shows the value of ionization parameter

$\log \xi$ over pulse phases.

Among the spectral parameters obtained from 2007 observation, most notable and systematic variability is seen in the values of additional column density and covering fraction of the absorber. The values of N_{H2} are found to be high at phases where dips are present in the pulse profiles. This pattern is seen in case of both the models i.e. partial covering HECut model with neutral as well as partially ionized absorber. In case of partial covering model with partially ionized absorber, the value of the ionization parameter was found to be relatively higher at dip phases indicating the presence of highly ionized additional absorber at several pulse phases causing dips in the pulse profiles. The higher values of cut-off energy were also found at pulse phases that are coincident with the dips in the pulse profiles. The values of the power-law photon index and e-folding energy are found to be variable over the pulse phases of the pulsar. However, it is difficult to correlate these variabilities with the dips in the pulse profiles. We did not find any variability in the flux of both the iron emission lines over the pulse phases of the pulsar. This suggests that the matter emitting the iron fluorescence lines is probably distributed symmetrically around the pulsar.

Spectral parameters obtained from the phase-resolved spectroscopy of 2012 May observation are shown in left and right panels of Figure 3.13 by using partial covering NPEX and partial covering HECut continuum models, respectively. Pulse profiles obtained from XIS and PIN data are shown in top two panels on both the sides of the figure. It can be seen that the parameters obtained from the phase-resolved spectral fitting using two different continuum models followed similar pattern over pulse phases of the pulsar. In case of both the models, the value of additional column density (N_{H2}) was found to be high in 0.6-0.9 pulse phase range. High value of additional column density can explain the absence of significant amount of soft X-ray photons in the above pulse phase range. The absorption of soft X-ray photons by the additional matter makes the pulse profile shallow in 0.6-0.9 pulse phase range (top panels of Figure 3.13). However, at hard X-rays, the effect of the additional

matter is drastically reduced making the pulse profile different compared to that in soft X-ray bands. The pulsar spectrum was found to be marginally hard in 0.8-1.1 phase range along with high value of cutoff energy and iron line equivalent width. This coincides with the presence of a dip (primary dip in the pulse profile) in the pulse profile at this phase range.

3.2.2 Phase-averaged and Phase-resolved spectroscopy of Cep X-4

Using the data from XISs and PIN detectors, we have studied the 1-70 keV energy spectra of Cep X-4 from the *Suzaku* observations carried out at two epochs of the 2014 June-July outbursts. In the beginning, standard continuum models were applied on the broad-band spectra of the pulsar. We found that the 1-70 energy continuum of pulsar can be well described with a NPEX, HECut and CompTT models along with a partial covering component. In addition to iron fluorescence line at ~ 6.4 keV, an earlier reported cyclotron line was seen at ~ 28 keV during both the observations of the pulsar. Apart from this, we have also detected an absorption like feature around ~ 45 keV (Jaisawal and Naik, 2015b). More details about these cyclotron lines are presented in the section 4.1.2 of Chapter-4.

To probe the causes of absorption dip in the pulse profiles of Cep X-4, phase-resolved spectroscopy was performed by accumulating the spectra in 10 phase bins for both the *Suzaku* observations. During the fitting, the galactic column density and iron line parameters were kept fixed at their phase-averaged values. Spectral parameters obtained from the fitting the data with partial covering NPEX model are plotted in left and right panels of Figure 3.14 for first and second observations, respectively. The first and second panels of the figure show the XIS and PIN pulse profiles. The parameters such as additional column density (N_{H2}), covering fraction, photon index, high energy cutoff and 1-10 keV flux are shown in third, fourth, fifth, sixth and seventh panels in both sides of the figure, respectively. Among these parameters, the

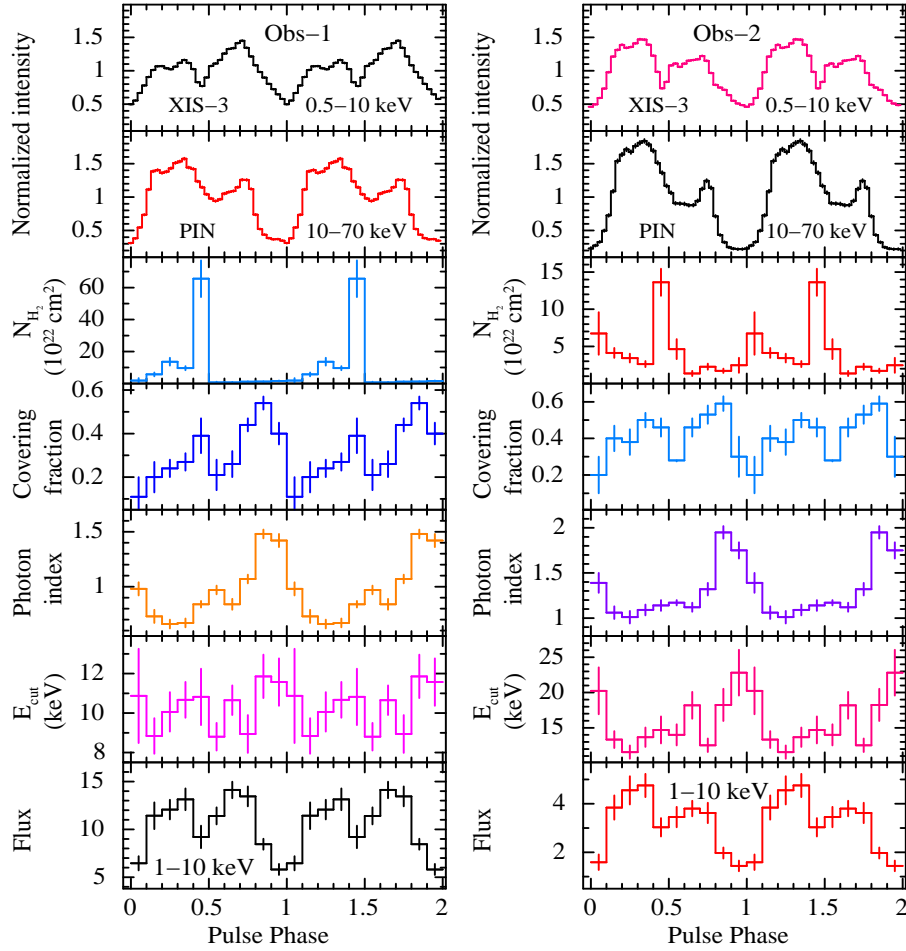


Figure 3.14: Best fitted spectral parameters obtained from the pulse-phase-resolved spectroscopy of *Suzaku* observations of Cep X-4 during 2014 outburst. The XIS (0.5-10 keV range) and PIN (10-70 keV range) pulse profiles are shown in top two panels of both sides of the figure, respectively. The left and right panels show the spectral parameters (with 90% errors) obtained from fitting of spectra with a partial covering NPEX model for first and second observations, respectively.

N_{H2} was found to be high at the dip (0.4-0.5) phase of the XIS pulse profile with the value of ~ 70 and $14 \times 10^{22} \text{ cm}^{-2}$ during the first and second observations, respectively. It can be seen that the value of N_{H2} during first observation was about five times more than the observed value during second observation at relatively low luminosity state. The higher value of N_{H2} at the dip phase indicated the presence of an accretion stream at this phase of pulsar. Other spectral parameters such as covering fraction and photon index were found to

be changing over phases and peaking close to phase 1 during both observations. The 1-10 keV flux showed similar pattern as the pulse profiles in same energy range.

3.2.3 Phase-averaged and Phase-resolved spectroscopy of GX 304-1

Phase-averaged spectroscopy of GX 304-1 was performed by using spectra from XISs, PIN and GSO data taken from the 2010 August and 2012 January observations. We have tried several standard continuum models to fit the spectra of the pulsar. Among these, a partial covering NPEX model was found to describe both the *Suzaku* observations. While fitting, an iron line at ~ 6.4 keV and a cyclotron feature were clearly seen. The cyclotron line energy was found to be ~ 53 and 50 keV during first and second *Suzaku* observations of GX 304-1, respectively (Jaisawal, Naik and Epili, 2016). The properties of cyclotron line are studied in more detail and are presented in the section 4.1.4 Chapter-4.

The pulse profiles of GX 304-1 are found to be different even when compared at same energy ranges from both *Suzaku* observations. Therefore, it is interesting to perform phase-resolved spectroscopy to probe the changes in spectral parameters with pulse phase and then compare with the observations at different luminosity levels. The phase-resolved spectroscopy was carried out by accumulating source spectra in 10 and 16 pulse-phase bins for first and second observations, respectively. We have fitted these spectra by using partial covering NPEX continuum model along with the cyclotron absorption component and Gaussian function for the iron emission line. While fitting, the values of relative instrument normalizations, equivalent hydrogen column density (N_{H_1}) and iron emission line parameters were fixed at the corresponding values obtained from phase-averaged spectroscopy. Spectral parameters obtained from fitting the XIS and PIN phase resolved spectra are shown in left and right panels of Figure 3.15 for 2010 August and 2012 January obser-

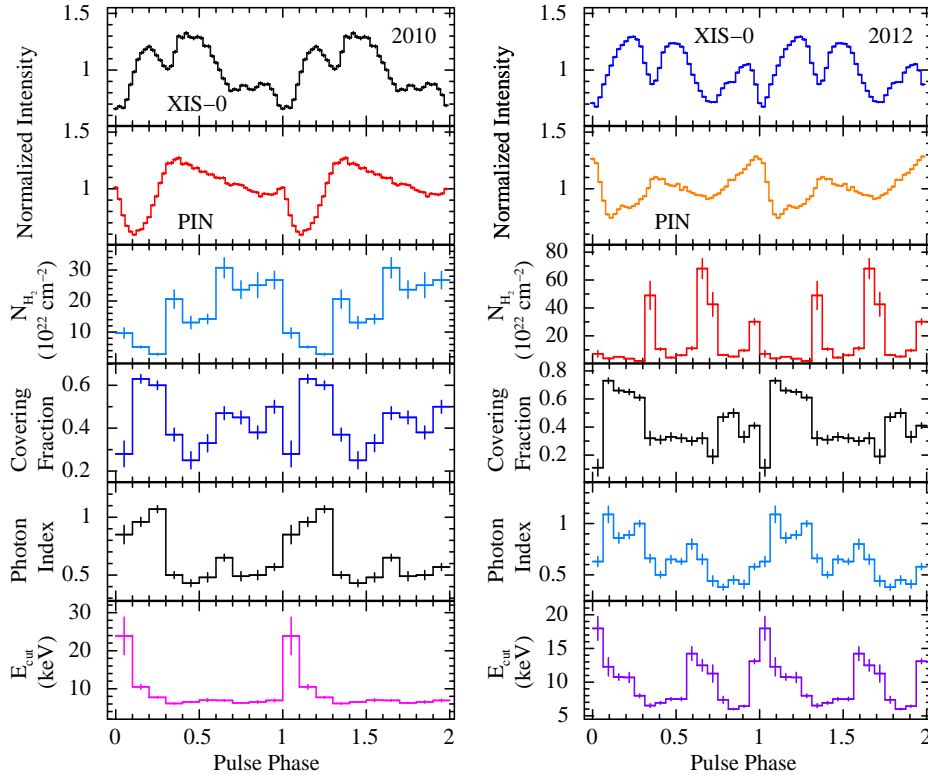


Figure 3.15: Best fitted spectral parameters obtained from the pulse-phase-resolved spectroscopy of *Suzaku* observations of GX 304-1. The XIS (0.5-10 keV range) and PIN (10-70 keV range) pulse profiles are shown in top two panels of both sides of the figure, respectively. The left and right panels show the spectral parameters obtained from fitting of spectra with a partial covering NPEX model for first and second observations, respectively. The errors are estimated for 90% of confidence level.

vations, respectively. Pulse profiles obtained from XIS-0 and PIN event data of each observation are also shown in top two panels of these figures.

During both the observations, all the spectral parameters showed significant variability with pulse-phase of the pulsar. During first observation, the value of additional hydrogen column density (N_{H_2}) varies in $1\text{-}30 \times 10^{22} \text{ cm}^{-2}$ range over pulse phases. The value of N_{H_2} was increased from 0.3 phase and became maximum in 0.6-1.0 phase range. It can be seen that normalized intensity (XIS pulse profile; top panel) was low at 0.6 phase and remain steady before reaching the minimum value at 1.0 phase. Decrease in the normalized intensity

of the pulsar during above pulse phase range and simultaneous increase in the value of N_{H_2} confirm that the plateau like feature in XIS pulse profile in 0.6-1.0 pulse phase range was due to the presence of an additional absorbing material close to the pulsar. This can also explain the presence of an absorption dip in the XIS pulse profile and an increase in the N_{H_2} value in 0.3-0.4 phase range of the pulsar. As in case of N_{H_2} , the covering fraction of the additional absorption was also found to be comparatively high during the dip and plateau region. As expected, the values of power-law photon index and cutoff energy were high during the main dip in the XIS and PIN pulse profiles.

Though the shape of XIS and PIN pulse profiles of the pulsar were significantly different during second *Suzaku* observation, the variation of spectral parameters over pulse phase was comparable. High values of absorption column density were found at phases of absorption dip in XIS pulse profile. The values of power-law photon index and cutoff energy followed similar pattern as seen during the 2010 August *Suzaku* observation of the pulsar. Although the number of absorption dips and the shape of the pulse profiles of the pulsar during both observations were different, the presence of additional matter as the cause of absorption dips in the soft X-ray profiles is supported by the findings in the present work. However, the low value ($\leq 5 \times 10^{22} \text{ cm}^{-2}$) of absorption column density at $\sim 0.1-0.2$ phase range (Figure 3.15) suggests that the cause of absorption dip at the above phase range in the hard X-ray pulse profiles was different.

3.3 Results and Discussion

In this chapter, we have discussed the properties of three Be/X-ray binary pulsars EXO 2030+375, Cep X-4 and GX 304-1 with *Suzaku*. The pulse profile of these pulsars were found to be strongly energy dependent. The presence of several prominent dips makes the soft X-ray pulse profiles complex. The strength of these dips were found to gradually decrease with energy, making the profile a smooth and single peaked at high energy bands. The presence

of dips in the pulse profile are seen in other transient X-ray pulsars such as A0535+262 (Naik *et al.*, 2008), GX 304-1 (Devasia *et al.*, 2011b), GRO J1008-57 (Naik *et al.*, 2011b), 1A 1118-61 (Devasia *et al.*, 2011a; Maitra, Paul and Naik, 2012), RX J0440.9+4431 (Usui *et al.*, 2012), Vela X-1 (Maitra and Paul, 2013b). In most of the cases, pulse-phase resolved spectral analysis showed the presence of additional absorption component at certain pulse phases that partially absorbed/obscured the emitted radiation giving rise to dips in the pulse profiles. The additional absorption is understood to be taking place by matter in the accretion streams that are phase locked with the neutron star.

Pulse-phase resolved spectroscopy of the *Suzaku* observations of these pulsars also showed that the value of additional column density (N_{H2}) due to matter local to the neutron star was higher at certain pulse phases where absorption dips are present. High values of N_{H2} , therefore, explains the presence of absorption dips in the pulse profile. We expect that the narrow streams of matter are phase-locked with the pulsars and obscuring the photons at certain phases. Depending on the density and opacity of these streams, dips are expected to be observed in the profiles even up to higher energies. This idea was first proposed by Cemeljic and Bulik (1998) to explain the absorption dips observed in the pulse profile of accretion powered pulsars. These authors also simulated the pulse profiles for A 0535+262 at different luminosity levels and successfully reproduced the profiles, similar to the observed one.

Complex nature of the pulse profiles and the presence of dips may indicate the scenario of abrupt accretion of matter. In this case, the smooth accretion flow disrupts into several narrow streams of matter that are phase locked with the neutron star. Using three-dimensional Magnetohydrodynamic (MHD) simulations of mass accretion on to low magnetic field stars, Romanova, Kulkarni and Lovelace (2008) showed that during unstable regime of accretion, the matter can penetrate into the magnetosphere leading to stochastic light curves, as seen in the right side of Figure 3.16. However, in case of stable accretion, matter gets accreted in the form of streams yielding almost periodic light curves. Although these results were obtained for low magnetic field objects, the ob-

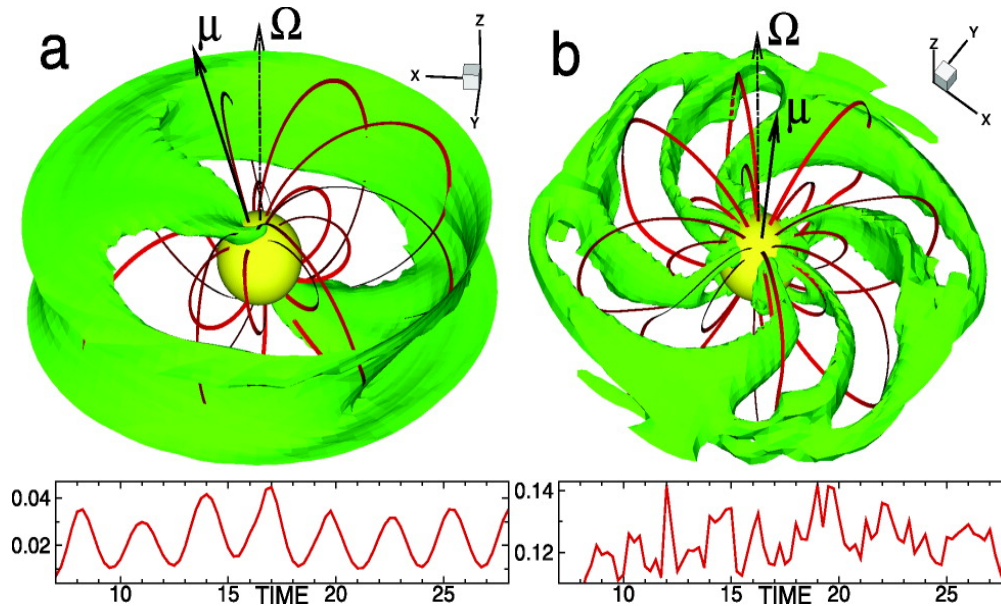


Figure 3.16: Upper panels show a 3D view of matter flow in the stable (left) and unstable (right) regime of accretion. Bottom panels show the light curves from the hot spots. This image is adopted from Romanova, Kulkarni and Lovelace (2008). In case of stable accretion, the light curve appears to be smooth in contrast to complicated light curves as seen during unstable accretion scenario.

servational evidences from our studies indicate that effect of such coupling are also possible in Be/X-ray binary pulsars. In general, the accretion from the companion to the neutron star takes place through the capture of stellar wind or matter from the Be circumstellar disk in HMXB systems. This can lead to the unstable accretion at higher mass accretion rate and resulting a complex pulse profile as seen in the Be/X-ray binary pulsars.

Although dip-like features in GX 304-1 appeared up to ~ 50 keV (see Figures 3.10 and 3.11), the low value of the additional column density at dip phases suggests that absorption is not the cause of these dips in the hard X-ray pulse profiles (Figure 3.15). The energy resolved pulse profiles of GX 304-1, obtained from both the *Suzaku* observations, revealed a significant phase-shift (~ 0.35) of the main dip in profiles at energies below and above ~ 35 keV. The observed phase-shift of the main dip happened to occur at an energy close to the cyclotron absorption line energy in GX 304-1. Such type of effects

e.g. phase-shifts (lags) or significant variations in pulse profiles close to the cyclotron absorption line energy are also seen in two other Be/X-ray binary pulsars such as V 0332+53 (Tsygankov *et al.*, 2006) and 4U 0115+63 (Ferrigno *et al.*, 2011). Using a numerical study on the effect of cyclotron resonant scattering in highly magnetized accretion powered X-ray pulsars, Schönherr *et al.* (2014) showed that a strong change in the pulse profile is expected at the cyclotron absorption line energy. This change is attributed to the effects of angular redistribution of X-ray photons by cyclotron resonant scattering in a strong magnetic field combined with relativistic effects. In GX 304-1, we observed a significant change in the phase of main dip in the pulse profile close to the cyclotron line energy. This detection, along with the reported results from V 0332+53 and 4U 0115+63 supports the results obtained from the numerical study of Schönherr *et al.* (2014).

Chapter 4

Cyclotron resonance scattering features and Magnetic field of pulsars

Accretion powered X-ray pulsars are considered to be bright X-ray sources in our Galaxy. Luminosity of these objects is in the range of 10^{33} erg s⁻¹ (quiescence) to 10^{38} erg s⁻¹ (active phase) while radiating in a broad energy range. X-ray emission from these sources is known to be originated from the accretion column formed at the magnetic poles of the neutron star. The accretion column has complicated geometry and host numerous complex processes that shape the broad-band energy spectrum of pulsars. Among these, a crucial signature of interaction between electrons and photons in high magnetic field is observed as cyclotron absorption feature in the continuum spectrum of several bright X-ray pulsars.

Cyclotron resonance scattering features (CRSFs) or simply cyclotron lines are absorption like features that are generally seen in the 10-100 keV spectrum of accretion powered X-ray pulsars with magnetic field of the order of $\sim 10^{12}$ G. These features are originated due to resonant scattering of photons with electrons in quantized energy states, known as Landau levels (Meszaros, 1992).

The energy separation of these levels are considered to be equi-spaced in non-relativistic assumption and expressed by a relation $E_{cyc} = 11.6 B_{12} \times (1 + z)^{-1}$ (keV); where B_{12} is the magnetic field in the unit of 10^{12} G and z is the gravitational red-shift. Corresponding the energy gap, cyclotron features are expected to be observed in the spectra of X-ray pulsars. Detection of fundamental CRSF thus provides the direct estimation of local magnetic field of the neutron stars in the line forming region. At the same time, the study of the harmonics (multiples of fundamental cyclotron line) gives crucial information about the optical depth of the line-forming region (Araya-Góchez and Harding, 2000; Schönherr *et al.*, 2007; Nishimura, 2013). Despite the abundance of data from earlier X-ray missions, the CRSF has been detected only in 29 accretion powered X-ray pulsars among about two hundred pulsars. There are eight more sources in which tentative detection of cyclotron line has been proposed (see Table 1.2 in Chapter-1). The harmonics of the fundamental cyclotron line are also observed in a few cases. In addition to detection, various important characteristics of cyclotron lines are also seen in pulsars. Generally the energy of harmonics of cyclotron lines are expected to observe at multiples of fundamental line energy. However, there are pulsars such as 4U 0115+63, V 0332+53, Her X-1 and Cep X-4 in which energy of the harmonics has not been not observed at expected values (Table 1.2), indicating the possibility of anharmonicity in the quantized energy levels.

Another crucial property such as positive and negative correlations between cyclotron line energy and source luminosity has been detected for a few pulsars. Two sources viz. Her X-1 (Staubert *et al.*, 2007) and GX 304-1 (Klochkov *et al.*, 2012) are known to follow a positive correlation between these parameters. However, two other Be/X-ray binary pulsars, 4U 0115+63 (Nakajima *et al.*, 2006; Tsygankov *et al.*, 2007) and V 0332+53 (Tsygankov, Lutovinov and Serber, 2010), show a negative correlation. The observed dependence for 4U 0115+63 is uncertain and found to be model dependent (Müller *et al.*, 2013). Theoretical attempts have been made to explain these observed correlations by several authors and are discussed in section 4.3.2 of this chapter.

Apart from these, the formation of cyclotron line is itself a complex process that depends on various factors such as plasma properties, emission region geometry, optical depth (Araya and Harding, 1999; Schönherr *et al.*, 2007). Although numerous simulation studies have been performed, the shape of cyclotron line is not fully understood. An emission wings like structure appear which makes the line profile complicated. In addition, asymmetric line profiles are also observed in some cases such as V 0332+53 and Cep X-4 (Nakajima, Mihara and Makishima, 2010; Fürst *et al.*, 2015). Due to lack of the proper model, a Gaussian or pseudo-Lorentzian profile is generally used to model the feature. The Gaussian profiles model *gabs* is available in *XSPEC* which can be mathematically expressed as,

$$gabs(E) = exp\left(\frac{-\tau}{\sqrt{2\pi}\sigma} exp\left(\frac{-(E - E_{cyc})^2}{2\sigma^2}\right)\right) \quad (4.1)$$

where E_{cyc} , σ and τ are centroid energy, width σ and depth of the line, respectively. This model is widely used during spectral fitting for the cyclotron line.

On the other hand, the pseudo-Lorentzian profile which is available as *cyclabs* model in *XSPEC* is also used frequently to explain the cyclotron feature during spectral fitting and described as,

$$cyclabs(E) = exp\left(-D_0 \frac{(W_0 E / E_{cyc})^2}{(E - E_{cyc})^2 + W_0^2} - D_1 \frac{(W_1 E / 2E_{cyc})^2}{(E - 2E_{cyc})^2 + W_1^2}\right) \quad (4.2)$$

where, D_0 , D_1 are the optical depths and W_0 , W_1 are the width of fundamental and first harmonics of cyclotron line (Mihara *et al.*, 1990; Makishima *et al.*, 1990). This model allows to fit the cyclotron fundamental and first harmonic line energy together with an assumption that the energy of first harmonics is the twice of fundamental energy. But, it is not always true as the cyclotron lines shows an anharmonicity in the line energies. The cyclotron line energy obtained from these two model, *gabs* and *cyclabs*, are different. The energy estimated by *cyclabs* model is about 10-20 % less than the energy obtained from *gabs*. This is due to the inclusion of line shape in the Equation 4.2.

Table 4.1: Log of accretion powered X-ray pulsars observed with *Suzaku*, *NuSTAR* and *Swift*/XRT that are used in our analysis.

Source name	Observatory/ Instrument	ObsID	Start Date	Exposure (ks)*	Period (s)
4U 1909+07	<i>Suzaku</i>	405073010	2010-11-02	29, 21	604.11
Cep X-4	<i>Suzaku</i>	409037010	2014-06-18	30, 53	66.334
Cep X-4	<i>NuSTAR</i>	80002016002	2014-06-18	41	
Cep X-4	<i>Suzaku</i>	909001010	2014-07-01	60, 81	66.334
Cep X-4	<i>NuSTAR</i>	80002016004	2014-07-01	41	
SMC X-2	<i>NuSTAR</i>	90102014002	2015-09-25	24.5	2.37197
SMC X-2	<i>Swift</i> /XRT	00034073002	2015-09-25	1.8	
SMC X-2	<i>Swift</i> /XRT	00081771002	2015-10-12	1.5	
SMC X-2	<i>NuSTAR</i>	90102014004	2015-10-12	23	2.37141
SMC X-2	<i>Swift</i> /XRT	00034073042	2015-10-21	4	
SMC X-2	<i>NuSTAR</i>	90101017002	2015-10-21	26.7	2.37257
GX 304-1	<i>Suzaku</i>	905002010	2010-08-13	5, 13	275.45
GX 304-1	<i>Suzaku</i>	406060010	2012-01-31	17, 59	274.88

* : Two effective exposure times are given for XIS and HXD instruments onboard *Suzaku*.

4.1 Detection of cyclotron line in X-ray pulsars

The properties of magnetic field of X-ray pulsars can be directly investigated through the detailed study of cyclotron resonance scattering features. These features are proxy to probe the strength of local magnetic field. The magnetic field geometry of a pulsar can also be mapped through the phase-resolved spectroscopy of cyclotron lines. In this chapter, we have studied several accretion powered X-ray pulsars in order to study the broadband continuum at different luminosity levels and search for the cyclotron scattering features in sources such as 4U 1909+07, Cep X-4 and SMC X-2. Apart from these, the properties of luminosity dependence of cyclotron energy are also discussed for

three sources such as Cep X-4, SMC X-2 and GX 304-1. The observations from *Suzaku* and *NuSTAR* are used in this study. The log of observations of these pulsars are given in Table 4.1. An overview about these sources can be found in the section 2.3 of Chapter-2.

4.1.1 The fundamental cyclotron line in 4U 1909+07

The persistent high mass X-ray binary pulsar 4U 1909+07 was observed with *Suzaku* on 2010 November 02. We have carried out broad-band spectroscopy of this poorly studied source by using data from XIS and HXD detectors of *Suzaku*. Following standard procedure of data reduction, we have extracted source spectra from XISs and PIN event data. Corresponding background, response and effective area files were also obtained. Using these, simultaneous spectral fitting was carried out in the 0.8-70 energy range by using *XSPEC* package. We attempted to fit the continuum spectrum with several models such as (i) a simple power-law model, (ii) HECut model, (iii) NPEX model and (iv) CompTT model. A partial covering absorption component *pcfabs* was also applied to above continuum models in spectral fittings. Apart from these, additional components such as photoelectric absorption, Gaussian function for iron emission line, a black-body component for soft X-ray excess were needed to describe the continuum spectrum. All these models were reasonably well fitted up to ~ 40 keV beyond which significant anomaly in residuals was noticed in the spectral fitting. We tried to obtain a suitable model that describes the broad-band spectrum of the pulsar in 0.8-70 keV energy range.

We found that the partial covering power-law continuum model with iron emission line and a black-body component of temperature ~ 3 keV fitted the pulsar spectrum well. A black-body component with temperature as high as ~ 3 keV is unusual in case of accretion powered X-ray pulsars. The addition of high energy cut-off to the partial covering power-law model fitted data well with the black-body temperature of ~ 0.2 keV. However, the partial covering NPEX continuum model with iron emission line and black-body component described the spectrum better yielding an acceptable black-body temperature

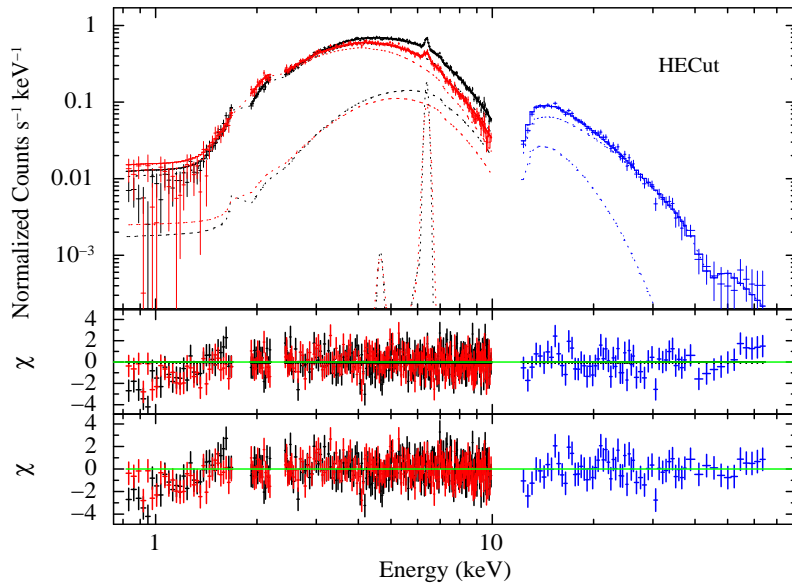


Figure 4.1: Energy spectrum of 4U 1909+07 obtained with XIS and HXD/PIN detectors of *Suzaku* observation, along with the fitted model comprising a partial covering HECut continuum model along with a black-body component, a narrow iron line emission, and a CRSF (Jaisawal, Naik and Paul, 2013). The middle and bottom panels show the contributions of the residuals to χ^2 for each energy bin for the partial covering HECut continuum model without and with CRSF component in the model, respectively.

of 0.2 keV. An absorption like feature was seen in pulsar spectrum and in the residuals at ~ 44 keV that allowed us to add a CRSF component in the spectral model. The addition of CRSF component to above continuum models improved χ^2 values for HECut and NPEX models (Table 4.2). The count rate spectra of the pulsar 4U 1909+07 are shown in Figures 4.1 and 4.2 for partial covering HECut and NPEX models along with the model components, respectively. The middle panels in above figures show the residuals to the fitted models without the CRSF whereas the bottom panels show the residuals to the best-fitting model along with the CRSF component in the spectral models. The presence of an absorption feature at ~ 44 keV can be clearly seen in the middle panels of both figures.

To test the statistical significance of the χ^2 improvement due to the addition of the CRSF component, we performed F -test. In case of emission line

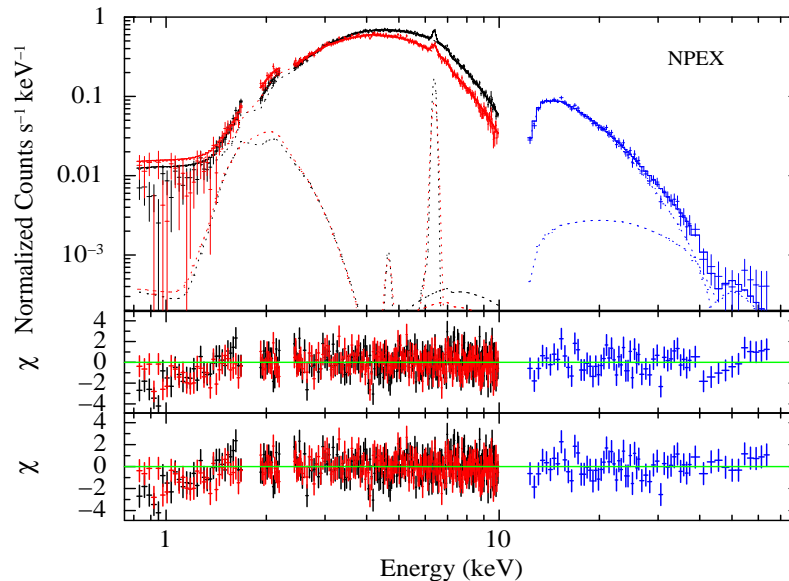


Figure 4.2: Energy spectrum of 4U 1909+07 obtained with XIS and HXD/PIN detectors of *Suzaku* observation, along with the best-fit model comprising a partial covering NPEX continuum model along with a black-body component, a narrow iron emission line and a CRSF (Jaisawal, Naik and Paul, 2013). The middle and bottom panels show the contributions of the residuals to χ^2 for each energy bin for the partial covering NPEX continuum model without and with CRSF component in the model, respectively.

features (additive components in *XSPEC*), the F -test routine incorporated in *XSPEC* package should be the best suited to perform the significance test (though care should be taken while using this - see Protassov *et al.*, 2002). However, in case of multiplicative components such as CRSF, the F -test in *XSPEC* is inappropriate for performing the null hypothesis test. The F -test in *XSPEC* is based on the assumption that the inclusion of the new component does not alter the continuum. This is true if the component is added to the continuum model whereas this is not correct if the component is multiplied by the continuum. Therefore, we used a different F -test, as described in Press *et al.* (1992), to test the statistical significance of the CRSF component in the spectrum of 4U 1909+07 (see e.g. Orlandini *et al.*, 2012). The F -test routine is available in *IDL* package (named as *mpftest*¹) and was used

¹<http://www.physics.wisc.edu/~craigm/idl/down/mpftest.pro>

Table 4.2: Best-fit parameters of the phase-averaged spectra for 4U 1909+07 from *Suzaku* observation with 1σ errors.

Parameter	Value			
	HECut	HECut×CYCL	NPEX	NPEX×CYCL
N_{H1} (10^{22} atoms cm^{-2})	7.50±0.21	7.53±0.25	7.09±0.20	7.05±0.19
N_{H2} (10^{22} atoms cm^{-2})	32.19±8.20	34.01±7.82	38.78±7.89	39.71±7.90
Covering Fraction	0.18±0.04	0.18±0.03	0.19±0.03	0.20±0.03
kT_{BB} (keV)	0.19±0.01	0.19±0.01	0.20±0.01	0.20±0.01
Norm. ^a of kT_{BB} (10^{-3})	10.59±3.25	11.07±3.10	5.65±1.70	5.27±1.82
Iron line Energy (keV)	6.39±0.01	6.39±0.01	6.39±0.01	6.39±0.01
Iron line width (keV)	0.01±0.01	0.01±0.01	0.01±0.01	0.01±0.01
Iron line eq. width (eV)	68±3	68±3	69±3	68±3
Power-law index	1.43±0.05	1.44±0.04	1.05±0.06	1.01±0.07
Norm. ^b of Power-law (10^{-2})	4.16±0.50	4.26±0.52		
High energy cut-off (keV)	7.34±0.28	7.37±0.16	13.98±1.77	12.78±1.58
Folding energy (keV)	23.42±1.51	24.23±1.10		
Cyclotron line E_a (keV)		43.10±2.09		43.85±1.58
Width of cyclotron line (keV)		1.0 ^{+2.5} _{-1.0}		2.04±2.02
Depth of cyclotron line		1.01±0.83		1.57±0.89
Flux ^c (in 1-10 keV range)	1.51±0.18	1.51±0.16	1.51±0.15	1.51±0.14
Flux ^c (in 10-70 keV range)	3.76±0.42	3.76±0.38	3.94±0.69	4.01±0.75
$C_{XIS-03}/C_{XIS-1}/C_{PIN}$	1.0/0.94/1.18	1.0/0.94/1.17	1.0/0.94/1.13	1.0/0.94/1.13
χ^2 (dofs)	576 (487)	573 (484)	578 (487)	570 (484)

N_{H1} = Equivalent hydrogen column density, N_{H2} = Additional hydrogen column density, ^a : in units of 10^{39} erg s^{-1} ($d/10$ kpc) $^{-2}$ where d is the distance to the source, ^b : photons $\text{keV}^{-1}\text{cm}^{-2}\text{s}^{-1}$ at 1 keV, ^c : Absorption uncorrected flux (in units of 10^{-10} ergs cm^{-2} s^{-1}).

for significance test of multiplicative components such as CRSF or Gaussian absorption features. The probability of chance improvement (PCI) is evaluated for each of the three models used to fit the pulsar spectrum without and with CRSF component. The estimated PCI values after addition of CRSF component to the (i) partial covering power-law model with black-body, (ii) partial covering high-energy cutoff power-law model with black-body and (iii) partial covering NPEX model with black-body are found to be 37%, 51% and 47%, respectively. Considering the high value of PCI for all three models, the CRSF is not found to be statistically significant. But the residuals shown in the middle panels of Figures 4.1 and 4.2 clearly show an absorption-like feature at ~ 44 keV. It may be noted that the goodness-of-fit estimator chosen here to assess the statistical significance of the CRSF (the χ^2) is not the best suited

as it does not take into account the “shape” of the residuals. Considering the identical distribution of residuals around 40 keV (middle panels of Figures 4.1 and 4.2, we applied run-test (also called Wald-Wolfowitz test) on the residuals obtained from the spectral fitting by using above three continuum models. *IDL* routine for run-test was used to derive the null hypothesis of the randomness in the residuals of spectral fitting in 37-65 keV energy range. It was found that the number of data points used for the run-test in 37-65 keV energy range are 12 (6 points below zero and 6 points above zero), 13 (4 points below zero and 9 points above zero) and 13 (6 points below zero and 7 points above zero) for partial covering power-law, partial covering high-energy cutoff and partial covering NPEX continuum models, respectively. The probability for getting 3 runs in above energy range was estimated to be 0.8%, 0.7% and 0.5%, respectively. Marginal difference in the values of probability is because of the use of different continuum models that can affect the residuals in the spectral fitting. The computed probability of $\leq 1\%$ for all three continuum models reject the hypothesis of random sampling of the detected absorption feature in the pulsar spectrum. Among the three continuum models, it is found that the NPEX continuum model with black-body, a Gaussian function and a CRSF feature at ~ 44 keV yields the best fit to 0.8-70 keV data. The presence of an absorption feature at ~ 44 keV in the residuals of all the models suggest that the CRSF is indeed required in the spectral fitting. The best-fit spectral parameters obtained by using three different continuum models along with additional components are given in Table 4.2. It can be seen from the table that addition of a CRSF at ~ 44 keV improved the spectral fitting in all cases.

To establish the absorption like feature seen at ~ 44 keV in the pulsar spectrum as CRSF, we evaluated the energy spectra of the pulsar 4U 1909+07 in a model-independent manner. We attempted to normalize the pulsar spectrum with that of Crab Nebula, the spectrum of which is a featureless power-law with a photon index of ~ 2.1 . The normalization (Crab ratio) has the advantage of minimizing the effects due to the detector response and the uncertainties

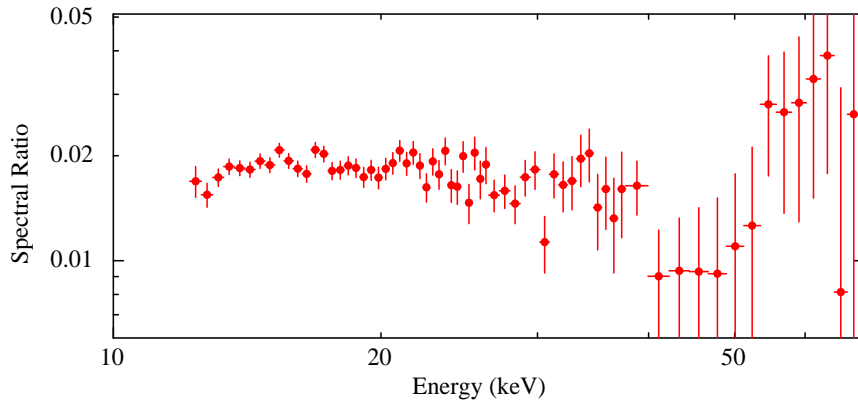


Figure 4.3: Ratio between the background subtracted HXD/PIN spectra of the HMXB pulsar 4U 1909+07 and Crab Nebula. The absorption feature at ~ 44 keV is clearly seen (Jaisawal, Naik and Paul, 2013).

in the energy response. To generate Crab ratio, we used a Crab observation with *Suzaku* (on 2010 April 5) that is nearest to the observation of the pulsar 4U 1909+07. Data reduction and background estimation for HXD/PIN data of Crab observation were done as described above and the Crab ratio was obtained to investigate the presence of the absorption feature in the pulsar spectrum. The resulting Crab ratio in 12-70 keV energy range is shown in Figure 4.3. The presence of the absorption feature at ~ 44 keV, as was seen in the spectral fitting (middle panels of Figures 4.1 and 4.2) can be clearly seen in the figure. It should be noted here that the shape of this CRSF-like feature in Crab ratio was very similar to that seen in the middle panels of above figures. In order to evaluate the statistical significance of the absorption feature, we performed a run-test on the Crab-ratio data. It was found that in 37-65 keV energy range in Crab ratio, there are 13 data points with 3 runs in which 7 points are above zero and 6 points are below zero. The probability of obtaining 3 runs is only $\sim 1\%$. This result, together with the results obtained from the analysis on the spectral residuals, strongly supports the genuine presence of absorption feature in the Crab ratio at ~ 44 keV. It confirms the presence of CRSF at ~ 44 keV in the HMXB pulsar 4U 1909+07. We estimated the corresponding surface magnetic field of the pulsar to be 3.8×10^{12} Gauss (Jaisawal, Naik and Paul, 2013).

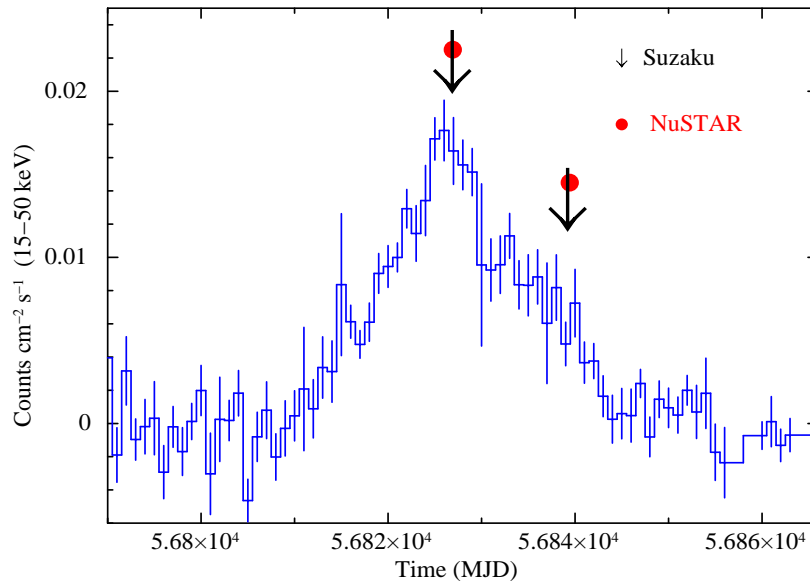


Figure 4.4: *Swift*/BAT light curve of Cep X-4 during 2014 Jun-July outburst. The arrow and solid marks in the figure indicate the date of observation with *Suzaku* and *NuSTAR*, respectively.

4.1.2 The first harmonic of cyclotron line in Cep X-4

Be/X-ray binary pulsar Cep X-4 was observed with *Suzaku* and *NuSTAR* during 2014 June – July outburst. Observations from both observatory were performed almost on the same day. As shown in Figure 4.4, the observations were carried out at two different epochs of the outburst. The first observation was performed at the peak of the outburst whereas the second observation was carried out at declining phase of the outburst. Details about the observations are provided in the Table 4.1. We followed the standard data analysis method to analyze all four observations. The spectra of the pulsar were generated from XIS and PIN event data of *Suzaku* observation whereas event data from FPMA and FPMB detectors were used to extract the spectra from both the *NuSTAR* observations. Standard continuum models such as HECut, Cutoffpl, NPEX, FDCut and CompTT were considered to fit the 0.8-70 keV and the 3-70 keV energy spectra of Cep X-4 obtained from *Suzaku* and *NuSTAR* observations, respectively. *NuSTAR* observations of Cep X-4 have been already studied by Fuerst et al. (2015) by using FDCut model with a blackbody component with

temperature of 0.9 keV. They reported the presence of asymmetry in the cyclotron line feature at ~ 30 keV and also find an evidence of another feature at around ~ 19 keV as a result of asymmetric line profile.

In our study, we first present the results obtained from the second *Suzaku* observation and later describe the results from others. Although, this observation was performed at the declining phase of the outburst, a longer effective exposure allowed us to explore the 0.8-70 keV broad-band energy spectrum in detail. We found that all standard models can explain the continuum of the pulsar obtained during the second *Suzaku* observation along with partial covering component. This component was used to explain the presence of dips in the pulse profiles of the pulsar (see section 3.1.2 of the Chapter-3). While fitting, a strong absorption like feature at ~ 28 keV was clearly seen in the spectrum. A CRSF component at above energy was added to all the continuum models. Simultaneous spectral fitting of XIS-3 and HXD/PIN data in 0.8-70 keV range showed that partial covering NPEX continuum model, partial covering high energy cutoff power-law model and partial covering CompTT model describe the spectrum well with acceptable values of reduced χ^2 (< 1.5). Iron emission lines at 6.4 and 6.9 keV were also detected in the pulsar spectrum.

Apart from ~ 28 keV cyclotron line, we found an additional absorption like feature at ~ 45 keV in the residuals obtained from all three continuum models. This feature was clearly seen at same energy range and was model independent (third panel in Figure 4.5). The inset in the figure shows the HXD/PIN spectrum of the *Suzaku* observation of the pulsar with background, without background and simulated PIN background spectrum. The absorption-like feature at ~ 45 keV can be clearly seen in the background subtracted spectrum. The inclusion of additional CRSF component (*cyclabs* model) at this energy in the model fitted the XIS-3 and HXD/PIN spectra well with significant improvement in the values of χ^2 . Absorption feature at ~ 45 keV can be considered as the first harmonic of the ~ 28 keV cyclotron absorption line. Ideally, the ratio between the energy of first cyclotron harmonic and fundamental line is expected to be a value closer to 2. However, in present case,

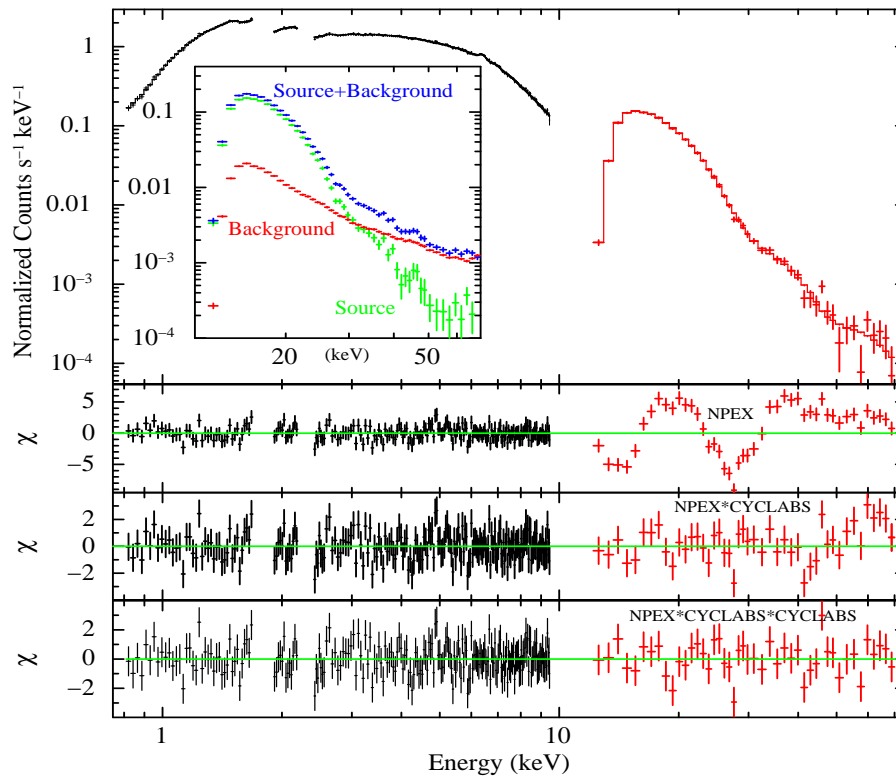


Figure 4.5: Energy spectrum of Cep X-4 in the 0.8-70 keV range obtained from XIS-3 and HXD/PIN data, along with the best-fit model comprising a partial covering NPEX model, two Gaussian functions for iron emission lines and two cyclotron absorption components. The second, third and fourth panels show the contributions of the residuals to χ^2 for each energy bin for the partial covering NPEX continuum model without, with one and with two cyclotron absorption components, respectively (Jaisawal and Naik, 2015b). The inset shows the HXD/PIN spectrum of the pulsar with background, without background and the simulated HXD/PIN background spectrum.

the ratio was estimated to be $\sim 1.7 \pm 0.1$, which can be acceptable in current understanding of the cyclotron physics. Best-fit parameters obtained from simultaneous spectral fitting are given in Table 4.3. Energy spectra obtained from simultaneous fitting of the XIS-3 and HXD/PIN data are shown in Figure 4.5. As in case of *NuSTAR* observations, a weak absorption like feature can be seen at ~ 19 keV in the spectral residue (third and fourth panels of Fig. 4.5). Addition of an absorption component at ~ 19 keV, however, did not show any significant improvement in the spectral fitting. Negligible strength

Table 4.3: Best-fitting parameters (with 90% errors) obtained from the spectral fitting of *Suzaku* observation of Cep X-4 in 2014 July. Model-1, Model-2 and Model-3 consist of the partial covering NPEX, HECut and CompTT model with two Gaussian and two cyclotron lines, respectively.

Parameter	Model-1	Model-2	Model-3
N_{H1}^a	0.78±0.03	0.80±0.02	0.77±0.03
N_{H2}^b	3.7±0.6	2.8±0.4	2.6±0.3
Cov. fraction	0.28±0.06	0.31±0.03	0.41±0.08
Photon index	1.04±0.09	1.33±0.02	–
E_{cut} (keV)	9.5±2.1	17.9±0.2	–
E_{fold} (keV)	–	25.3±9.8	–
CompTT T_0 (keV)	–	–	0.21 $^{+0.6}_{-0.21}$
CompTT kT (keV)	–	–	11.6±2.3
CompTT τ	–	–	4.4±0.4
Fe line parameters			
Energy (keV)	6.41±0.03	6.42±0.03	6.41±0.03
Eq. width (eV)	32±8	27±7	27±7
Energy (keV)	6.97±0.16	6.99±0.22	6.98±0.22
Eq. width (eV)	13±6	9±6	9±6
Cyc. line parameters			
Energy (E_{c1}) (keV)	27.5±0.4	28.0±0.4	27.7±0.4
Width (σ_{c1}) (keV)	8.9±1.0	5.3±0.9	6.1±0.8
Depth (D_{c1})	2.3±0.3	1.53±0.2	1.8±0.3
Energy (E_{c2}) (keV)	45.4±2.8	42.3±4.2	43.0±3.6
Width (σ_{c2}) (keV)	10.3±4.6	8.8±5.4	11.9±4.2
Depth (D_{c2})	1.8±0.7	1.1±0.5	1.8±0.4
Flux ^c (1-10 keV)	3.1±0.5	3.1±0.3	3.1±0.7
Flux ^c (10-70 keV)	5.5±1.1	5.5±1.2	5.6±1.2
χ^2 (dofs)	254 (244)	267 (244)	261 (244)

^a : Equivalent hydrogen column density and ^b : Additional hydrogen column density (in 10^{22} atoms cm^{-2}); ^c : Absorption uncorrected flux (in 10^{-10} ergs cm^{-2} s^{-1} .)

and width of the ~ 19 keV line against other two absorption lines at ~ 28 and ~ 45 keV, therefore, makes it difficult to accept the earlier feature as the fundamental cyclotron absorption line. Therefore, we did not include any spectral component for this feature in our fitting.

To verify the ~ 45 keV feature as additional absorption feature detected in *Suzaku* spectra, we fitted XIS-3 and HXD/PIN spectra with the spectral model (FDCut model along with black-body and Gaussian absorption *gabs*

components) as used by Fürst *et al.* (2015) to fit spectra obtained from *Swift* and *NuSTAR* observations of the source. Though the data shown in Fig. 2 of Fürst *et al.* (2015) were up to 50 keV, we used *Suzaku* data in 0.8-70 keV range to compare both the results. The spectral parameters obtained from our fitting were found to be comparable (within errors) with the parameters obtained from the *NuSTAR* observations. While fitting *Suzaku* data with the model used by Fürst *et al.* (2015), an absorption like feature at ~ 45 keV was also seen in the spectral residue. A careful look at the trend of distribution of points at ~ 45 -50 keV in the residuals obtained from the spectral fitting of Obs.1 data (second and third panels of Fig. 2 of Fürst *et al.*, 2015) indicates a hint of presence of an absorption-like feature.

Statistical significance of the ~ 45 keV absorption feature was tested by using *XSPEC* script *simftest*. Including systematic uncertainty of 0.3% (15-40 keV) and 1.9% (40-70 keV) in PIN background model, we simulated 1000 fake spectra for partial covering NPEX model and estimated the differences in χ^2 ($\Delta\chi^2$) without and with ~ 45 keV cyclotron absorption line. The maximum value of $\Delta\chi^2$ from 1000 simulations was found to be 17.8 which is less than the observed $\Delta\chi^2=27.2$ for three degree of freedom in real data. Corresponding to this, we confirmed significant detection of ~ 45 keV absorption feature at $> 4\sigma$ level in the spectrum of Cep X-4 during the second *Suzaku* observation (Jaisawal and Naik, 2015b).

As the trend of data points in spectral residual of *NuSTAR* Obs.1 from Fürst *et al.* (2015) indicates a hint of first harmonics in the spectral residue, we analyzed both *NuSTAR* and *Suzaku* observations which were performed at the peak of the outburst. The NPEX continuum model was considered to describe the 3-79 keV energy spectrum of pulsar obtained from the *NuSTAR* observations. While fitting the first *NuSTAR* observation, a fundamental cyclotron line (*cyclabs* component) was detected at ~ 28 keV in our study. However, using *gabs* component, Fürst *et al.* (2015) reported energy to be ~ 30 keV. Apart from this, an additional absorption feature in between 45-60 keV was clearly seen in the spectral residual. Addition of a CRSF component fits the

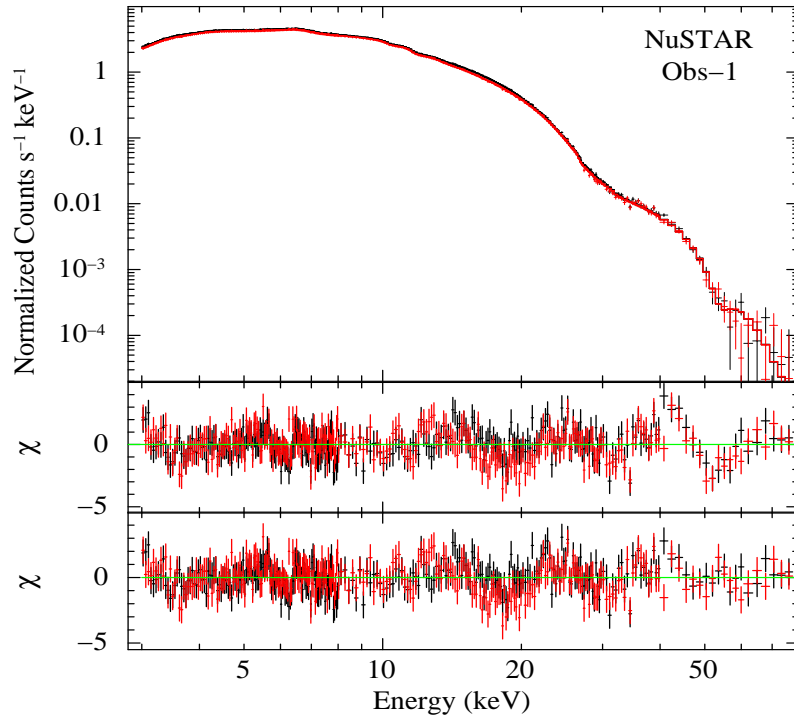


Figure 4.6: Energy spectrum of Cep X-4 in the 3-79 keV range obtained from first *NuSTAR* observation at the peak of the outburst. The spectrum was fitted with a NPEX model with a Gaussian function for iron emission line and two cyclotron absorption components. The second and third and fourth panels show the contributions of the residuals to χ^2 for each energy bin for NPEX continuum model with one and two cyclotron absorption components, respectively.

line energy at ~ 54 keV and improves the spectral fitting further from reduced χ^2 of 1.17 (1353) to 1.13 (1350). This feature was seen in a model independent manner and identified as the first harmonics of cyclotron line at ~ 28 keV. In our study, the ~ 19 keV feature was not included during spectral fitting. The energy spectra obtained from simultaneous fitting of first *NuSTAR* observation is shown in Figure 4.6. The second and third panels in the figure show the residuals to the best-fit model with one and two cyclotron lines in the continuum model, respectively. The spectral parameters obtained from the fitting by using NPEX model are given in Table 4.4.

To check further, background subtracted pulsar spectra obtained from both the *NuSTAR* observations were normalized with the spectrum of Crab pulsar,

Table 4.4: Best-fitting parameters (with 90% errors) obtained from *Suzaku* and *NuSTAR* observations of Cep X-4 during 2014 Jun-July outburst.

Parameter	Obs-1		Obs-2	
	<i>Suzaku</i>	<i>NuSTAR</i>	<i>Suzaku</i>	<i>NuSTAR</i>
N_{H1}^a	0.77 ± 0.01	0.5 ± 0.2	0.78 ± 0.03	1 ± 0.3
N_{H2}^b	–	–	3.7 ± 0.6	–
Cov. fraction	–	–	0.28 ± 0.06	–
Photon index	0.69 ± 0.04	0.81 ± 0.03	1.04 ± 0.09	0.91 ± 0.07
E_{cut} (keV)	6.8 ± 1	5.5 ± 0.2	9.5 ± 2.1	5.4 ± 0.5
<i>Fe line parameters</i>				
Energy (keV)	6.49 ± 0.03	6.46 ± 0.03	6.41 ± 0.03	6.35 ± 0.08
Eq. width (eV)	65 ± 8	98 ± 10	32 ± 8	80 ± 17
<i>Cyc. line parameters</i>				
Energy (E_{c1}) (keV)	28.8 ± 0.3	28 ± 0.1	27.5 ± 0.4	27.9 ± 0.2
Width (σ_{c1}) (keV)	10.2 ± 1.0	9.6 ± 0.6	8.9 ± 1.0	6.9 ± 1.0
Depth (D_{c1})	1.9 ± 0.2	1.5 ± 0.1	2.3 ± 0.3	1.4 ± 0.2
Energy (E_{c2}) (keV)	$52.4^{+4.9}_{-2.9}$	53.9 ± 1.1	45.4 ± 2.8	$49.8^{+3.2}_{-2.1}$
Width (σ_{c2}) (keV)	$7.8^{+9}_{-3.7}$	3.8 ± 1.2	10.3 ± 4.6	$5.9^{+6.8}_{-5.9}$
Depth (D_{c2})	$1.4^{+1}_{-0.7}$	1.3 ± 0.4	1.8 ± 0.7	$0.8^{+1}_{-0.4}$
Energy ratio (E_{c2}/E_{c1})	$1.82^{+0.17}_{-0.1}$	1.93 ± 0.04	1.7 ± 0.1	1.8 ± 0.1
Flux ^c (3-70 keV)	2.9 ± 0.4	2.7 ± 0.2	0.8 ± 0.2	0.7 ± 0.1
Luminosity ^d (3-70 keV)	5 ± 1.7	4.7 ± 1.6	1.4 ± 0.6	1.2 ± 0.4
χ^2 (dofs)	1302 (1014)	685 (549)	254 (244)	570 (541)

^a : Equivalent hydrogen column density and ^b : Additional hydrogen column density (in 10^{22} atoms cm^{-2}); ^c : Absorption corrected flux (in 10^{-9} ergs cm^{-2} s^{-1}); ^d : luminosity in 10^{36} ergs s^{-1} .

known as Crab ratio. Figure 4.7 shows the Crab ratio for first and second observations in left and right panels, respectively. Two absorption like features are clearly present in the Crab ratio at energies close to the fundamental and first harmonics of cyclotron line energies. This confirms the firm detection of first harmonics of cyclotron line in Cep X-4.

Earlier, the first harmonic of cyclotron line was detected at ~ 45 keV with a fundamental line energy at ~ 28 keV during second *Suzaku* observation which was performed in the declining phase of the outburst e.g. low luminosity phase. However, during the first *Suzaku* observation (at the peak of the outburst –

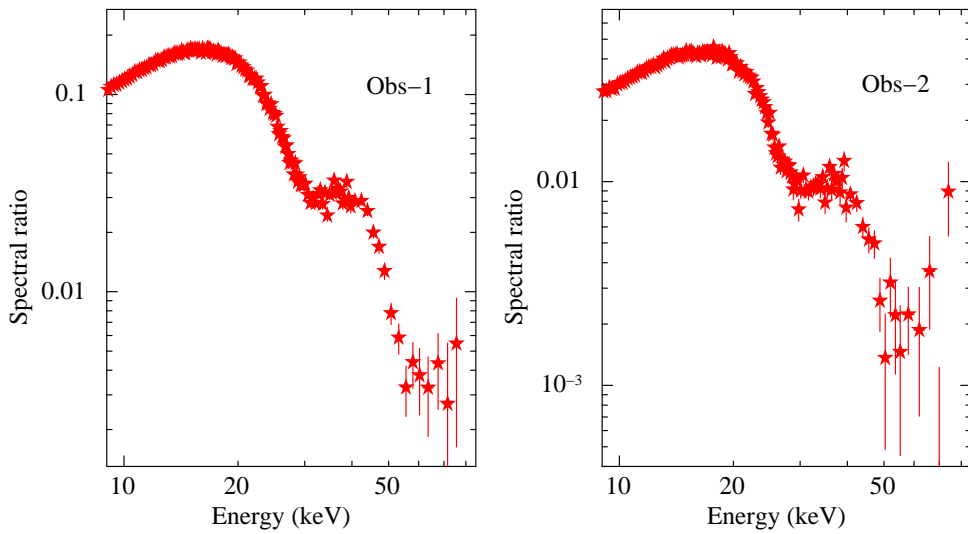


Figure 4.7: Ratio between the background subtracted FPMA spectra of Cep X-4 and Crab Nebula is shown in left and right panels of the figure for first and second *NuSTAR* observations, respectively. The absorption features close to ~ 20 -30 keV and ~ 50 -60 keV energy ranges are clearly evident in these observations.

higher luminosity), the energy of first harmonic was found to be at ~ 54 keV with the fundamental line energy at ~ 28 keV (see Table 4.4). As the source luminosity was different during both the observations, the energy of the first harmonic showed a positive dependence with the pulsar luminosity. In addition, the fundamental cyclotron line also showed a marginal positive luminosity dependence (Table 4.4). We have plotted these energies and the ratio between first harmonics to fundamental cyclotron line in the Figure 4.8. The fundamental and first harmonics energy of cyclotron line seem to follow a moderate positive correlation with luminosity. As a result, the coupling factor (E_{c2}/E_{c1}) also showed a moderate positive dependence on luminosity, varying from 1.7 to 1.93 (within error bars) during both the observations.

4.1.3 The cyclotron absorption feature in SMC X-2

SMC X-2 is one of the brightest transient X-ray pulsar in the Small Magellanic Cloud (SMC). This pulsar was observed with *NuSTAR* at three epochs during

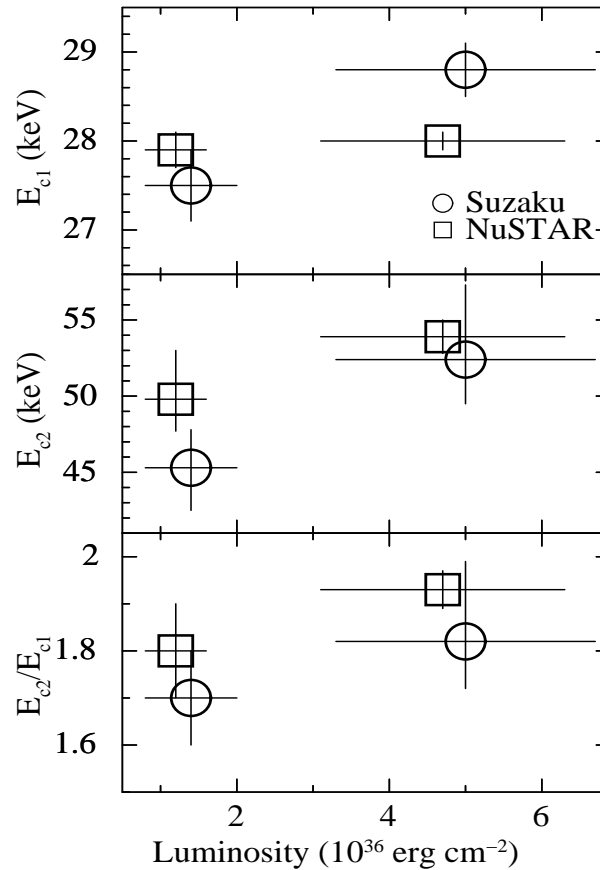


Figure 4.8: Luminosity dependence of fundamental and first harmonics cyclotron line energies of Cep X-4 is shown in the first and second panels of the figure obtained from *Suzaku* and *NuSTAR* observations. The third panel shows the energy ratio between the first harmonics and fundamental energy. A moderate positive luminosity dependence can be seen in these parameters.

2015 September – October outburst, as shown in Figure 4.9. Simultaneous *Swift*/XRT observations were also carried out at these epochs of the outburst. The details of the observations are listed in Table 4.1 and considered as first (Obs-I), second (Obs-II) and third (Obs-III) sets of simultaneous *NuSTAR* and *Swift*/XRT observations. Following standard procedure of data reduction, we extracted spectra of SMC X-2 from all three sets of observations. The spectral properties of SMC X-2 was investigated for the first time in the 1-70 keV broad energy range using data from *NuSTAR* (3-70 keV) and *Swift*/XRT (1-8 keV).

Standard continuum models such as HECut, FDCut, NPEX and Cutoffpl were used to fit the pulsar spectra obtained from three epochs of observations.

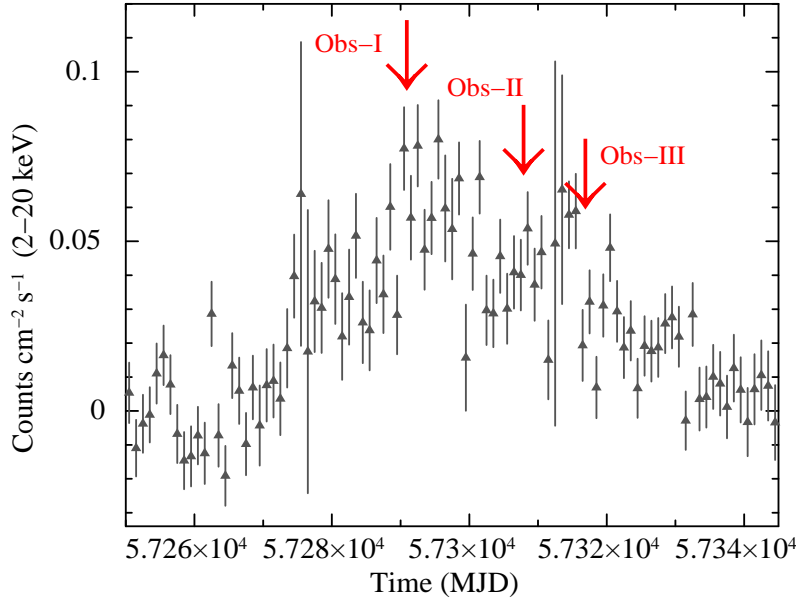


Figure 4.9: Light curve of the 2015 outburst of SMC X-2, observed with *MAXI* in 2-20 keV energy range covering the duration from 2015 August 16 (MJD 57250) to 2015 November 19 (MJD 57345), is shown. Arrows in the figure show the date of *NuSTAR* and *Swift*/XRT observations during the outburst.

We found that NPEX, FDCut and Cutoffpl models can explain the continuum spectrum well for all three epochs of observations. However, an additional blackbody component was required to fit the source spectra obtained from Obs-II & Obs-III while fitting with Cutoffpl model. An iron fluorescence emission line at ~ 6.4 keV was seen in the source spectrum. Apart from the iron emission line, an absorption-like feature at ~ 27 keV was also detected in the pulsar spectra obtained from all *NuSTAR* observations. This feature was detected in the source continuum in a model independent manner. We added a Gaussian absorption line (*gabs*) in the model to explain the absorption feature. The addition of *gabs* component in the model improved our spectral fitting significantly (reduced $\chi^2 \sim$ to 1). The residuals obtained from the spectral fitting with all three models are shown in left and right side of Figure 4.10 for Obs-I & II, respectively. A strong absorption like feature can be clearly visible in 20-30 keV energy range in second, third and fourth panels of the figures. This feature was found to be model independent and clearly detected in all three *NuSTAR*

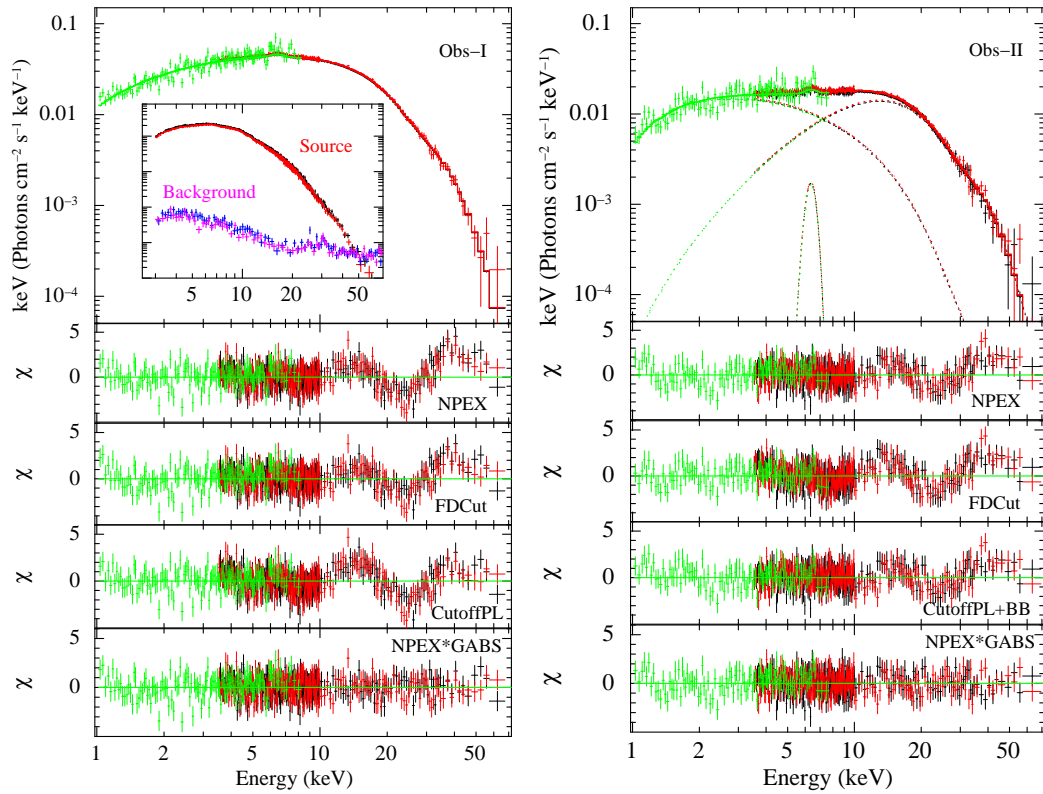


Figure 4.10: The energy spectrum of SMC X-2 in 1-70 keV range obtained from FPMA and FPMB detectors of *NuSTAR* and *Swift*/XRT data during the first (left panel) and second (right panel) observations along with the best-fit model comprising a NPEX continuum model with an iron emission line and a Gaussian absorption component for cyclotron resonance scattering feature. The second, third and fourth panels show the contributions of the residuals to χ^2 when pulsar continuum was fitted with NPEX, FDCut and CutoffPL models, respectively. In all these panels, an absorption like feature in 20-30 keV range is clearly visible (Jaisawal and Naik, 2016). The fifth panel shows the residuals for NPEX model after including a *gabs* component for cyclotron line. The background subtracted source spectra and background spectra are shown in the inset of first observation.

observations. We identified this feature as cyclotron absorption line of the pulsar at ~ 27 keV during first observation. Corresponding magnetic field of the neutron star was estimated to be $\sim 2.3 \times 10^{12}$ G. Best fitting parameters from the NPEX continuum model are given in Table 4.5 for all three observations.

Table 4.5: Best-fitting parameters (with 90% errors) obtained from the spectral fitting of three *NuSTAR* and *Swift*/XRT observations of SMC X-2 during 2015 outburst with the NPEX continuum model with an iron emission line and cyclotron absorption line.

Parameter	Obs-I		Obs-II		Obs-III	
	NPEX	NPEX×GABS	NPEX	NPEX×GABS	NPEX	NPEX×GABS
N_H^a	$0.1^{+0.03}_{-0.1}$	0.18 ± 0.06	0.7 ± 0.1	0.5 ± 0.1	0.8 ± 0.1	0.6 ± 0.1
Photon index	-0.1 ± 0.02	0.04 ± 0.04	0.78 ± 0.05	0.62 ± 0.08	1.05 ± 0.09	0.81 ± 0.09
E_{cut} (keV)	4.4 ± 0.1	4.8 ± 0.1	4 ± 0.1	4.6 ± 0.2	4 ± 0.1	4.5 ± 0.2
<i>Fe line para.</i>						
Energy (keV)	6.42 ± 0.08	6.42 ± 0.08	6.32 ± 0.09	6.35 ± 0.08	6.31 ± 0.15	6.34 ± 0.1
Eq. width (eV)	47 ± 10	72 ± 14	88 ± 18	83 ± 18	70 ± 20	70 ± 20
<i>Cycl. line para.</i>						
E_c (keV)	–	27.2 ± 0.9	–	29 ± 1.6	–	$29.8^{+2.7}_{-1.7}$
σ_c (keV)	–	6.4 ± 1.0	–	7 ± 1.5	–	$7.2^{+2.3}_{-1.4}$
τ_c	–	6 ± 2	–	9^{+5}_{-3}	–	9^{+9}_{-4}
Luminosity ^b	–	5.5 ± 0.5	–	2.7 ± 0.3	–	1.8 ± 0.2
Red.- χ^2 (dofs)	1.55 (582)	1.04 (579)	1.29 (551)	1.02 (548)	1.27 (596)	1.08 (593)

^a : Equivalent hydrogen column density (in 10^{22} atoms cm^{-2}); ^b : 1-70 keV luminosity in 10^{38} ergs s^{-1} , assuming a distance of 61 kpc (Hilditch, Howarth & Harries 2005). Here E_c , σ_c and τ_c denote the energy, width and strength of cyclotron line.

It can be seen that the cyclotron line energies during these observations are marginally different, showing a negative dependence on luminosity.

4.1.4 Luminosity dependence of cyclotron line energy in GX 304-1

Be/X-ray binary pulsar GX 304-1 was observed with *Suzaku* during its 2010 August and 2012 January Type I outbursts. Luminosity of the pulsar was higher during first observation as compared to second *Suzaku* observation. The details of the observations are given in Table 4.1. An overview about the properties of the pulsar can be found in the section 2.3 of Chapter-2. Using the standard technique of data reduction, we extracted source spectra from XIS,

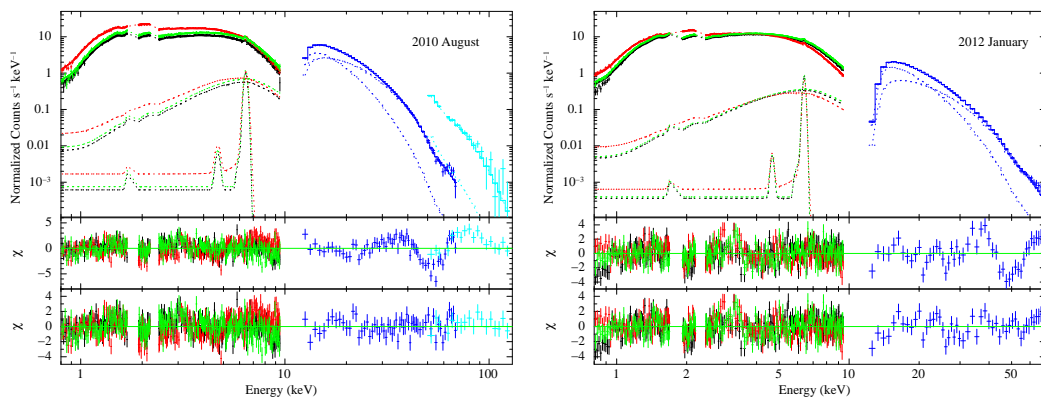


Figure 4.11: Left and right panels of the figure show the energy spectrum of GX 304-1 in the 1-130 and 1-70 keV energy ranges for first and second *Suzaku* observations, along with the best-fit model comprising a partial covering NPEX continuum model, a Gaussian function for iron emission line and a cyclotron absorption component (Jaisawal, Naik and Epili, 2016). The middle and bottom panels in both sides show the contributions of the residuals to χ^2 for each energy bin for the partial covering NPEX continuum model without and with cyclotron component in the model, respectively.

PIN and GSO data. Corresponding background, response and effective area files were also generated by following appropriate procedure. Using these files, spectral fitting was carried out in the 1-130 keV (2010 observation) and 1-70 keV (2012 observation). Several standard models such as HECut, FDCut, Cutoffpl, NPEX and CompTT were used in our spectral fitting to describe the continuum spectrum of GX 304-1. Due to the presence of narrow absorption dips in the pulse profiles of the pulsar (section 3.1.3 of Chapter-3) as seen in other Be/X-ray binary pulsars, a partial covering absorption component was added to above continuum models. Among these models, partial covering NPEX continuum model was found to fit the source spectra obtained from both the observations better than all other continuum models. We selected this model to use in phase-averaged analysis of both the *Suzaku* observations of GX 304-1.

While fitting, an absorption like feature at ~ 53 keV was clearly seen in

Table 4.6: Best-fitting parameters (with 90% errors) obtained from the spectral fitting of *Suzaku* observations of GX 304-1 during 2010 August and 2012 January outbursts. Model-1 : partial covering NPEX model with Gaussian component; Model-2 : partial covering NPEX model with Gaussian component and cyclotron absorption line.

Parameter	2010 August		2012 January	
	Model-1	Model-2	Model-1	Model-2
N_{H1}^a	1.04 ± 0.02	1.02 ± 0.02	0.98 ± 0.02	0.97 ± 0.02
N_{H2}^b	13.2 ± 1	13.7 ± 1.2	5.7 ± 0.5	5.3 ± 0.5
Cov. fraction	0.35 ± 0.02	0.32 ± 0.02	0.25 ± 0.02	0.23 ± 0.02
Photon index	0.6 ± 0.03	0.57 ± 0.03	0.42 ± 0.02	0.43 ± 0.02
E_{cut} (keV)	6.6 ± 0.1	7.1 ± 0.2	6.8 ± 0.1	7.4 ± 0.2
Fe line energy (keV)	6.41 ± 0.02	6.41 ± 0.02	6.41 ± 0.01	6.41 ± 0.01
Eq. width of Fe line (eV)	44 ± 7	43 ± 8	23 ± 2	23 ± 3
Cyclotron line energy (keV)	–	53.2 ± 0.8	–	50 ± 1
Width of cyclotron line (keV)	–	$6.5^{+2.1}_{-1.6}$	–	$5.5^{+2.6}_{-1.8}$
Depth of cyclotron line	–	0.8 ± 0.1	–	0.5 ± 0.1
Flux ^c (1-10 keV)	9.2 ± 0.5	9.2 ± 0.6	4.9 ± 0.2	4.9 ± 0.2
Flux ^c (10-70 keV)	24.5 ± 1.5	24.4 ± 2.0	9.6 ± 0.5	9.6 ± 1.1
Flux ^c (70-130 keV)	0.2 ± 0.1	0.2 ± 0.1	–	–
χ^2 (dofs)	857 (527)	638 (524)	863 (588)	765 (585)

^a : Equivalent hydrogen column density in the source direction (in 10^{22} atoms cm^{-2} units),

^b : Additional hydrogen column density (in 10^{22} atoms cm^{-2} units),

^c : Absorption corrected flux in units of 10^{-9} ergs cm^{-2} s^{-1} .

residuals obtained from spectral fittings of both the observations. Addition of a cyclotron absorption component (*cyclabs* in *XSPEC*) in the partial covering NPEX continuum model improved spectral fitting further with reduced χ^2 of 1.22 and 1.31 for first and second observations, respectively. Best-fit model parameters obtained from simultaneous spectral fitting of XIS-0 & 3, PIN and GSO data are given in Table 4.6. The energy spectra of the pulsar along with the best-fit model components are shown in left and right sides of Figure 4.11 for both observations. The middle and bottom panels in both sides of figure show the residuals to the best-fit model without and with the addition of cyclotron absorption feature in the continuum model, respectively.

The cyclotron feature was detected at ~ 53 and 50 keV during 2010 August

and 2012 January *Suzaku* observations, respectively. The observed cyclotron absorption line energies are not significantly different. However, it shows a marginal positive dependence on the pulsar luminosity, as seen in Her X-1 (Staubert *et al.*, 2007). Klochkov *et al.* (2012) studied the cyclotron line energy of GX 304-1 at different phase of 2012 January – February outbursts and found out a positive a correlation between these parameters. They explained this behavior in terms of changes in the height of emitting region with luminosity based on Staubert *et al.* (2007) and Becker *et al.* (2012), which are also discussed in detail in section 4.3.2 of this chapter.

4.2 Phase-resolved spectroscopy of cyclotron line features

Phase-resolved spectroscopy of cyclotron line provides important information about the magnetic field geometry of accretion powered X-ray pulsars. Cyclotron line energy are expected to show a few % of variation with the viewing angle or pulse phase of the pulsar (see Equation 1.19 in Chapter-1). In addition, the cyclotron line depends on various physical parameters such as plasma temperature, optical depth, geometry of the line-forming which can be different at different part of the accretion column (Araya-Góchez and Harding, 2000; Schönherr *et al.*, 2007). This can also give rise to the variation in the cyclotron line energy and other parameters with pulsar-phases. In this section, we have studied a few pulsars such as Cep X-4, SMC X-2 and GX 304-1 in order to probe the distribution of pulsar’s magnetic field and the properties of the line forming region.

4.2.1 Cep X-4

Using *Suzaku* observations of Cep X-4, we have performed phase-resolved spectroscopy by accumulating the spectra from XIS and PIN data in 10 phase-bins. The NPEX continuum model along with additional model components e.g. the

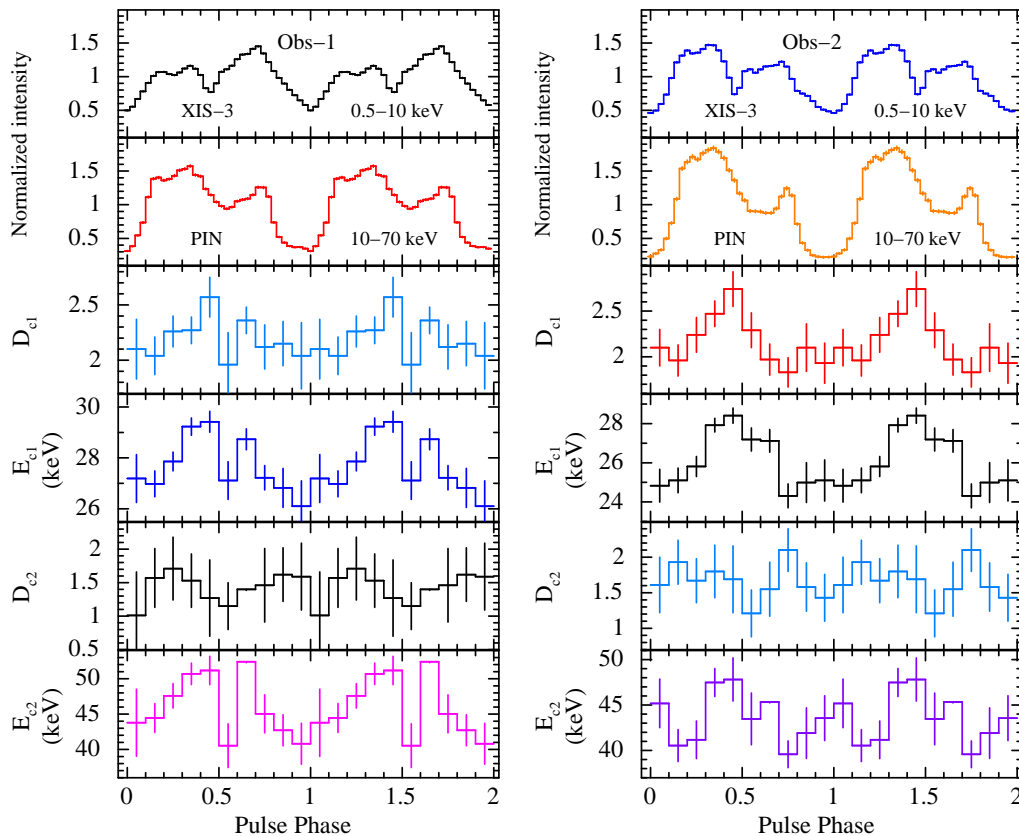


Figure 4.12: Best-fitted spectral parameters (with 90% errors) obtained from the pulse-phase-resolved spectroscopy of *Suzaku* observations of Cep X-4 during 2014 outburst. The XIS (0.5-10 keV range) and PIN (10-70 keV range) pulse profiles are shown in top two panels of both sides of the figure, respectively. The left and right panels show the cyclotron line parameters obtained from the fitting of spectra with a NPEX model for first and second observations, respectively.

model used in phase-averaged spectroscopy, was applied to fit all these phase resolved spectra. Corresponding to fundamental and first harmonics of cyclotron line, two different *cyclabs* components were added in the model. While fitting, the values of relative instrument normalizations, equivalent hydrogen column density (N_{H1}) and iron emission line parameters were fixed at the corresponding values obtained from phase-averaged spectroscopy. The width of the cyclotron absorption lines was fixed at their phase averaged value to constrain the feature. Spectral parameters obtained from fitting the XIS and PIN phase resolved spectra are shown in left and right sides of Figure 4.12 for first and

second *Suzaku* observations, respectively. Pulse profiles obtained from XIS-0 and PIN event data of each observation are also shown in top two panels of the figure.

Cyclotron line parameters such as depth and energy of both the lines were found to be significantly variable with pulse-phase with maximum values in 0.3-0.6 phase range. However, the peak values of these parameters were marginally phase shifted (0.1 phase) with respect to the peaks of 10-70 keV pulse profile and source flux. Variations in the cyclotron line parameters are clearly visible during the second observation where the values of depth and energy of fundamental line are maximum at ~ 0.4 pulse phase. The fundamental cyclotron energy was varying within 24 to 28 keV, whereas the depth of fundamental line was variable in the range of 1.8 to 2.5 in similar pattern to that of cyclotron line energy. Moreover, the energy of first harmonics line was found to be variable between 38 to 50 keV, peaking at the same phase of the fundamental line energy. The depth of this line was found to be moderately variable with the pulsar phases (within error bars).

For first observation, marginal variation of the fundamental and first harmonic cyclotron line parameters with pulse phase were seen. As in the case of second observation, the energy and depth of fundamental line were found to be maximum at 0.4 pulse phase of the pulsar. The energy of the first harmonics line was also high at this phase. The energy and depth of the first harmonic line were found to be marginally variable (within the errors). During both the observations, it was found that the cyclotron line parameters were found to be variable with pulsar-phases but within $<30\%$ of their phase-averaged values.

4.2.2 SMC X-2

Phase-resolved spectroscopy of SMC X-2 was performed for the first time to understand the variation of the parameters of cyclotron resonance scattering features with the pulse phase of the pulsar. As the pulsar was relatively bright during the first observation (see Figure 4.9 and Table 4.5), we accumulated the phase-resolved spectra in 8 pulse-phase bins from the first *NuSTAR* observa-

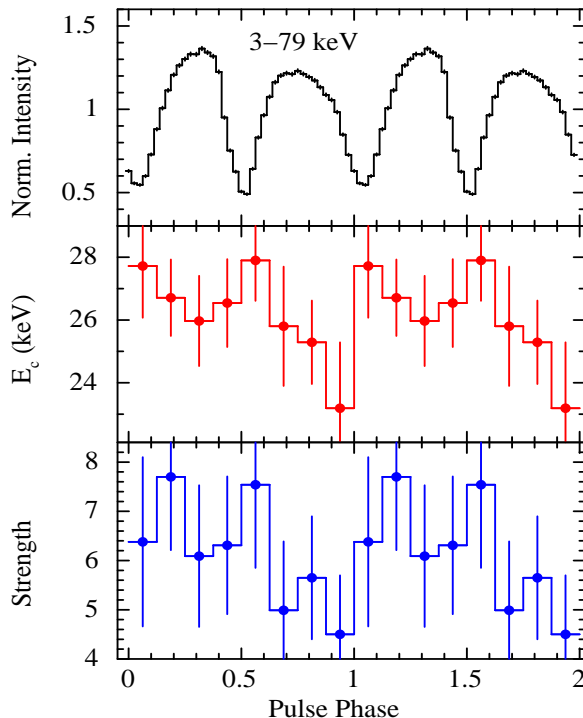


Figure 4.13: Spectral parameters (with 90% errors) obtained from the phase-resolved spectroscopy of SMC X-2 during first *NuSTAR* observation. Top panel shows the pulse profile in the 3-79 keV energy range. The values of cyclotron line parameter such as energy E_c and strength τ are shown in second and third panels, respectively.

tion. Using corresponding background, response and effective area files, phase-resolved spectroscopy was carried out in 3-70 keV energy range. The NPEX continuum model was used to fit the phase-resolved spectra. The absorption-like feature, as seen in phase-averaged spectra, was also clearly detected in each of the phase-resolved spectra. A *gabs* component was included in the continuum model for the cyclotron absorption line. While fitting, the equivalent hydrogen column density (N_H), iron line parameters and cyclotron width were fixed to corresponding phase-averaged values.

The cyclotron line parameters such as line energy and strength obtained from the phase-resolved spectroscopy are shown in Figure 4.13. Both the parameters are marginally variable with pulse-phase of the pulsar. The energy of cyclotron line was found to be variable between 23 to 28 keV (<20% of phase-

averaged value) with maximum at around 0.5 pulse phase. The strength of cyclotron line was found to be varying between 4 to 8 and following similar pattern to that of cyclotron line energy. The errors in the figure are estimated for 90% confidence level. We also checked the variation of cyclotron line energy with pulse phase by fixing the line strength at the phase-averaged value and vice versa. However, there was no notable change in the pulse phase dependence of these parameters apart from a marginal improvement in the estimated errors at each of the pulse phase values.

4.2.3 GX 304-1

We carried out phase-resolve spectroscopy of GX 304-1 by using data from instruments with good spectral resolution such as XIS and PIN onboard *Suzaku*. We have used both the observations (see Table 4.1) performed at different luminosity of 2010 August and 2012 January outbursts. As the first observation was for a relatively short exposure (~ 13 ks for HXD) compared to the second observation (~ 59 ks for HXD), phase-resolved spectroscopy was carried out by accumulating source spectra in 10 and 16 pulse-phase bins for first and second observations, respectively. Simultaneous spectral fitting was carried out on phase-resolved spectra obtained from both the observations by using partial covering NPEX continuum model along with the cyclotron absorption component and Gaussian function for the iron emission line. While fitting, the values of relative instrument normalizations, equivalent hydrogen column density (N_{H_1}) and iron emission line parameters were fixed at the corresponding values obtained from phase-averaged spectroscopy. The width of the cyclotron absorption line was fixed at the phase averaged value to constrain the feature. Spectral parameters obtained from fitting the XIS and PIN phase resolved spectra are shown in the left and right sides of Figure 4.14 for 2010 August 13 and 2012 January 31 observations, respectively. Pulse profiles obtained from XIS-0 and PIN event data of each observation are also shown in top two panels of the figure.

During both the observations, cyclotron line parameters showed a signif-

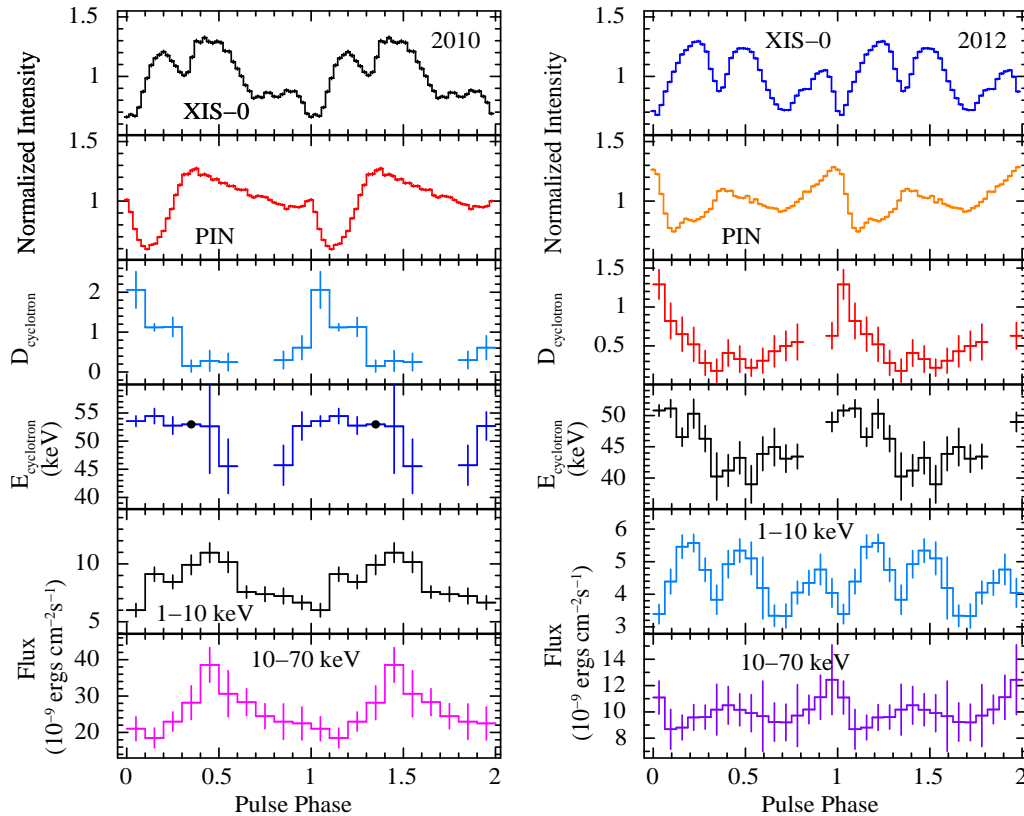


Figure 4.14: Best fitting spectral parameters obtained from the pulse-phase-resolved spectroscopy of *Suzaku* observation of GX 304-1 during 2010 and 2012 outbursts. The XIS (0.5-10 keV range) and PIN (10-70 keV range) pulse profiles are shown in top two panels of both sides of the figure, respectively. The left and right panels show the spectral parameters obtained from fitting of spectra with a partial covering NPEX model for first and second observations, respectively. The errors are estimated for 90% of confidence level.

icant variability with pulse-phase of the pulsar. The depth of the cyclotron absorption feature was found to be variable and single peaked. The energy of cyclotron absorption feature also showed variation over the pulse phase of the pulsar. The values of both the parameters were maximum at dip phase of the pulsar and gradually decreased to minimum value in 0.5-0.8 phase range. Data gaps in third and fourth panels in second column are due to the non-detection of cyclotron features in the spectral fitting for corresponding phase-bins. Pulsar flux in 1-10 keV and 10-70 keV shows variation with pulse phase and follows the shape of pulse profile in respective energy bands. However for second ob-

ervation, the variation in the cyclotron energy and depth were found to be similar to first observation with maximum value at close to phase 1.

4.3 Results and Discussion

Cyclotron absorption lines are unique features that directly relate the line energy to magnetic field of the pulsars. In this chapter, we have presented the detection of cyclotron lines in previously unknown sources such as 4U 1909+07 (Jaisawal, Naik and Paul, 2013) and SMC X-2 (Jaisawal and Naik, 2016). We have also discovered first harmonics of cyclotron line in Cep X-4 which appeared at less than two time of fundamental energy, showing the anharmonicity in the line energies (Jaisawal and Naik, 2015b). Phase-resolved spectroscopy of cyclotron lines was also performed for Cep X-4, GX 304-1 and SMC X-2 observed during corresponding X-ray outbursts. In case of Cep X-4 and SMC X-2, phase-resolved spectroscopy for previously unknown cyclotron lines was studied for the first time and magnetic field geometry was probed in detail. While in case of GX 304-1, phase-resolved spectroscopy of cyclotron line carried out by using data from *INTEGRAL* (Malacaria *et al.*, 2015), however, did not show any significant variation in the cyclotron line parameters. We have performed phase-resolved spectroscopy of GX 304-1 with high resolution *Suzaku* data and found significant variation of line parameters with pulsar phase (Jaisawal, Naik and Epili, 2016). In addition, positive and negative luminosity correlations for pulsars Cep X-4, SMC X-2 and GX 304-1 are also observed in our studies. As the cyclotron line was newly detected in SMC X-2, we have found negative correlation between the cyclotron line energy luminosity as a result of high luminosity in super-critical regime. All these properties are discussed in following sections.

4.3.1 Anharmonic cyclotron line energies

Cyclotron absorption features in the broad-band X-ray spectrum are originated due to the resonance scattering of photons with quantized electrons in presence

of magnetic field. Depending on the strength of the magnetic field, the states of electrons are quantized in harmonically spaced levels such that the first harmonic energy is expected to be at twice of the fundamental energy. In the present case of Cep X-4, however, the first harmonic is detected at energy which is ~ 1.7 and 1.9 times that of the fundamental line energy at low and high luminosity states, respectively. This was found to be below the ideal coupling factor of 2 that can result due to anharmonicity among the Landau energy levels. Anharmonic spacing between fundamental and harmonic lines has also been seen in a few other X-ray pulsars and described by considering the relativistic effects in photon-electron scattering for small changes in the energy ratio (Meszaros, 1984; Schönherr *et al.*, 2007). However, this may not be the only cause that can produce the anharmonicity in lines. Cyclotron absorption phenomena for fundamental and harmonic lines occurring at two different scale heights can have different optical depths and introduce the anharmonicity in the coupling factor or line energy ratio.

In detailed studies of cyclotron lines, Nishimura (2005) and Schönherr *et al.* (2007) showed that the increase in magnetic field within a line forming region can result the line ratio less than 2, as seen in 4U 0115+63 (Heindl *et al.*, 1999) and Cep X-4 (present work). At larger viewing angle $\mu=0.79$, the line ratio is expected to be 1.73 for polar cap radius of 1.5 km (Nishimura, 2013). Such decrease in energy ratio (1.57-1.73) is possible for viewing angle of 0.52-0.79 where superimposition of large numbers of fundamental line emerging from different heights of line-forming region shifts the energy to higher side with nearly constant energy for first harmonic. In a similar way, for viewing angle of $\mu=0.96$ and polar cap radius of 1.5 km, the line ratio is expected to be 1.92 as observed during the first observation of Cep X-4 (Nishimura, 2013). It indicates that viewing angle of accretion column is also evolving with the luminosity and showing a positive dependence. In case of larger viewing angle ($\mu>0.9$), it is considered that the centroid energy of fundamental and harmonic line both shifted towards the higher energy considerably. As a result, the line ratio was observed at close to 2. In another scenario, the anharmonicity in the

line ratio can be expected due to distortion or displacement from the dipole geometry of the magnetic field. In this case, both CRSFs are generated at two different poles of neutron star and produce a significant phase shift between both line parameters. Such phase-shift was not seen in Cep X-4 (Figure 4.12).

4.3.2 Luminosity dependent cyclotron line energy

The cyclotron line feature was found to show a dependence on luminosity in pulsars such as Cep X-4, GX 304-1 and SMC X-2 as studied in this thesis. In case of Cep X-4 and GX 304-1, a moderate positive correlation of cyclotron line energy with luminosity was seen. However, SMC X-2 showed a moderate negative dependence on luminosity. There are two pulsars, Her X-1 and GX 304-1 which show a positive dependence on the pulsar luminosity (Staubert *et al.*, 2007; Klochkov *et al.*, 2012). In some other cases such as 4U 0115+63 (Nakajima *et al.*, 2006; Tsygankov *et al.*, 2007), and V 0332+53 (Tsygankov, Lutovinov and Serber, 2010), a negative correlation is observed between the luminosity of pulsar and the cyclotron absorption line energy.

Attempts have been made to explain the observed positive and negative correlation between pulsar luminosity and the cyclotron line energy. A negative correlation is expected in super-critical regime where the source luminosity is higher than the critical luminosity (Becker *et al.*, 2012; Mushtukov *et al.*, 2015b). Above critical luminosity, density of infalling matter becomes so high that the particles start interacting and decelerating through the formation of a radiation-pressure dominated shock above the neutron star surface. Cyclotron scattering features most likely occur closer to the shock region. With increasing luminosity, the shock height drifts upwards in the accretion column where relatively low strength of magnetic field produces cyclotron feature at lower energy. It explains negative correlation as observed in 4U 0115+63 and V 0332+53. However, the positive correlation is predicted for a sub-critical regime e.g. below critical luminosity. The pressure of accreting matter in this regime pushes hydrodynamical shock closer to the neutron star surface where increase in the strength of magnetic field with luminosity results a positive

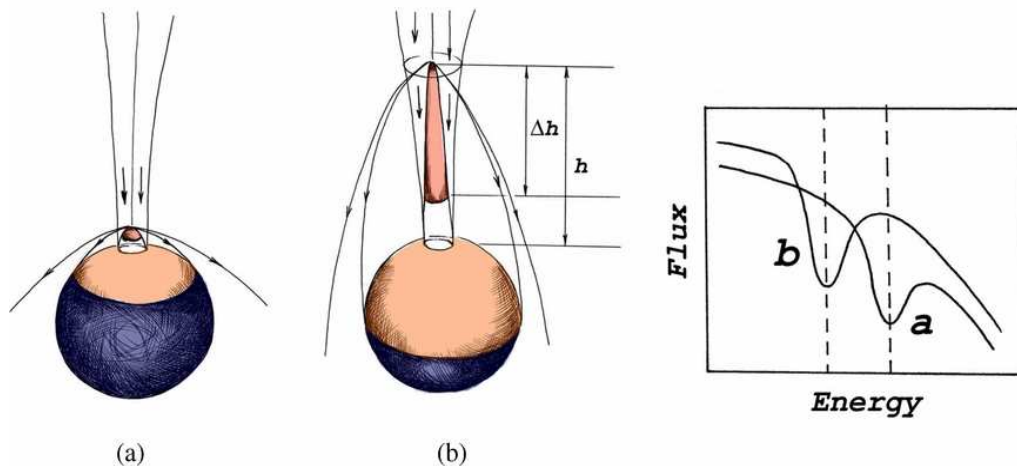


Figure 4.15: Negative dependence of cyclotron line energy with luminosity is shown. At larger accretion rate, the column height is expected to be high which results a greater illumination on the weaker magnetic field side of neutron star, producing lower cyclotron line energy. Image courtesy: Poutanen *et al.* (2013).

correlation between the cyclotron line energy and luminosity (Staubert *et al.*, 2007), as seen in Her X-1 and GX 304-1. The 1-70 keV luminosity of GX 304-1 during first and second *Suzaku* observations were estimated to be 2.3×10^{37} and 1×10^{37} ergs s^{-1} , respectively, which lies in the sub-critical regime (Mushtukov *et al.*, 2015b). Luminosity of Cep X-4 was estimated to be $< 5 \times 10^{36}$ ergs s^{-1} , which also belongs to the sub-critical regime. As a result, a positive correlation is expected in Cep X-4 and GX 304-1. However, in case of SMC X-2, the pulsar was very bright with luminosity reaching close to Eddington luminosity ($> 10^{38}$ ergs s^{-1} ; see Table 4.5). It is expected that SMC X-2 was accreting in the super-critical accretion regime during 2015 X-ray outburst. Therefore, a negative correlation is expected between these parameters as seen during our study (Jaisawal and Naik, 2016).

Poutanen *et al.* (2013) and Nishimura (2014) have proposed alternate models to describe the dependence of cyclotron absorption line energy on the source luminosity. In these models, it is argued that the formation of cyclotron line in direct spectrum is questionable due to the large gradient of magnetic field strength along line forming region in the accretion column. However, cyclotron

line (CRSF) can be formed in the reflected radiation from the surface of the neutron star where magnetic field gradient is relatively small Poutanen *et al.* (2013). It is widely believed that the accretion column height is linearly dependent on source luminosity ($>10^{37}$ ergs s^{-1}) or accretion rate. At higher luminosity, larger area on neutron star surface (from the poles with strong magnetic field towards equator with weak field strength) is expected to be illuminated for cyclotron interactions, as shown in Figure 4.15. This explains the observed anti-correlation between cyclotron line energy and luminosity, as seen in V 0332+53 and SMC X-2. However, Nishimura (2014) described the observed correlations by considering the changes in polar emission region, direction of photon propagation and the shock height. The negative correlation was interpreted in terms of shock region displacement whereas the positive correlation was explained by using the changes in beam pattern. The observed positive correlation between the cyclotron line energy and luminosity in Cep X-4 and GX 304-1, therefore, can be explained as due to the change in beam pattern, as described by Nishimura (2014). Alternatively, Mushtukov *et al.* (2015a) discussed the positive luminosity dependence of sub-critical X-ray pulsars like GX 304-1 by studying the changes of plasma velocity profile in line-forming region under the influence of radiation pressure from the hot-spot. The cyclotron line energy at a luminosity was determined by corresponding redshift from velocity profile at a given height. This model successfully predicts the positive luminosity correlation of cyclotron line energy for pulsars like Cep X-4 and GX 304-1 along with cyclotron line width dependence on luminosity and pulse phase variation of cyclotron line parameters, which were not being discussed in Nishimura (2014).

4.3.3 Pulse-phase dependence of cyclotron line parameters

Investigation of change in cyclotron line parameters with pulse phase of the pulsar provides important evidences to understand the emission geometry as

well as the magnetic field mapping around the neutron star. A comparative study of these parameters at different intensity levels during several outbursts can also yield information about the changes in emission or accretion column geometry. Change in cyclotron line parameters with pulse phase has also been seen in other X-ray pulsars such as Cen X-3 (Burderi *et al.*, 2000), GX 301-2 (Kreykenbohm *et al.*, 2004), 1A 1118-61 (Maitra, Paul and Naik, 2012), A 0535+26, XTE J1946+274, 4U 1907+09 (Maitra and Paul, 2013a), V 0332+53 (Lutovinov *et al.*, 2015) with $\sim 10\text{-}30\%$ variation in cyclotron energy.

Phase-resolved spectroscopy of cyclotron line parameters for Cep X-4, SMC X-2 and GX 304-1 showed that these parameters are variable with the pulse-phases. These variations are found to be within 30% from the phase-averaged value. Although, the cyclotron lines are expected to vary with the phases due to changes in the viewing angle. Numerous simulation works on cyclotron lines were done by considering certain sets of assumptions and geometry in line forming regions (Araya-Góchez and Harding, 2000; Schönherr *et al.*, 2007; Mukherjee and Bhattacharya, 2012). These studies predicted that the cyclotron absorption line parameters are expected to show 10-20% variation over pulse phases depending on the viewing angle of the accretion column. However, more than 30% variation in cyclotron parameters can be explained by considering distortion in the magnetic dipole geometry of the pulsar (Schönherr *et al.*, 2007; Mukherjee and Bhattacharya, 2012). In our cases, cyclotron line parameters are varying within $<30\%$ over pulse-phase which can be described in terms of the viewing angle or local distortion in magnetic field. Detailed modeling of the observed variations in cyclotron parameters would provide useful information about the neutron star magnetic field geometry, inclination and beaming or emission patterns.

Chapter 5

Time-resolved properties of OAO 1657-415 and 4U 1700-37

High energy photons emitted from the accretion column or the surface of the neutron star travel through the interstellar medium before reaching us. However, while passing through the surrounding regions of the neutron star such as accretion column, accretion wake, accretion disc, photosphere of the companion star etc., these photons interact with matter in these regions through photoelectric absorption or scattering processes. The signature of these matter can be seen in the observed X-ray spectrum of the pulsar in the form of absorption or emission lines. Investigation of these features provides a vital information about the temperature of emitting gas, nature of species, its ionization state as well as location and structure of the stellar winds. Among these, iron fluorescence emission lines are frequently observed in the pulsar spectrum due to the interaction between emitted X-ray photons and iron atoms present in these regions. The nature of interaction is governed by the photoelectric absorption which depends on energy as E^{-3} . For high energy photons, the material appears to be transparent. Although X-ray photons are able to knock out the

inner shell electron from atoms depending on their interaction probability. As a result, a vacancy is created in the inner shell of the atom that is filled by the higher shell electron through emitting a *fluorescence* photon with energy corresponding to the difference between these energy states. Iron fluorescence lines are usually observed at ~ 6.4 and 7.06 keV in spectrum of accretion powered X-ray pulsars and known to be Fe K_α and K_β lines, respectively. Sometimes absorption edges are also seen in the spectrum. These features arise when the energy of the absorbed photons corresponds to the ionization potential of the atoms. For iron, K-edge is observed at 7.1 keV. Depending on the ionization states, the energies of the fluorescence line and edges are expected to show an energy shift. At higher ionization states, the iron K-edge energy changes up to 2 keV (Kaastra and Mewe, 1993). However, for lower ionization states the energy changes are not much, ranging from a few 10 to 100 eV. To measure such energy shift precisely, high spectral resolution and well calibrated instruments such as detectors on-board *XMM-Newton* and *Chandra* are necessary.

Properties of the iron emission lines can be used to trace the distribution of stellar winds in supergiant X-ray binaries – a sub class of high mass X-ray binaries. The supergiant X-ray binaries consist of massive optical companion which is a rich source of supersonic stellar wind. A neutron star accretes a part of the dense windy matter (clump) from the companion and emits in X-rays. Depending on the mass of the clump of matter, intensity variations are observed in the light curves of these sources, showing flux variations in a time scale of a few ks to tens of ks. The physical parameters of stellar wind and its distribution can be probed by studying the timing and spectral properties of the pulsars at different orbital phases. In this chapter, we have performed time-resolved spectroscopy for two eclipsing high mass X-ray binaries OAO 1657-415 and 4U 1700-37 in order to understand the cause of intensity variability observed in the soft and hard X-ray light curves. OAO 1657-415 is an accretion powered X-ray pulsar whereas 4U 1700-37 is a high mass X-ray binary in which the nature of the compact is unclear.

Table 5.1: Log of *Suzaku* observations of eclipsing high mass X-ray binaries studied in this chapter.

Source name	ObsID	Start Date	Exposure (ks)		Period (s)
			XIS, HXD		
OAO 1657-415	406011010	2011-09-26	85, 75		36.961
4U 1700-37	401058010	2006-09-13	82, 82		No pulsation

5.1 OAO 1657-415

HMXB pulsar OAO 1657-415 was observed with *Suzaku* observatory in 2011 September 26–28 for an exposure of ~ 85 ks. A brief description on the source can be found in section 2.3.6 of Chapter 2. *Suzaku* observation of the pulsar was carried out in out-of-eclipse orbital phase range of 0.12–0.34 (considering mid-eclipse time as phase 0). *Swift*/BAT light curve of the pulsar in 15-50 keV band starting from 2011 September 16 to 2011 October 26 is shown in Figure 5.1. The horizontal line in the figure indicates the duration of the *Suzaku* observation of the pulsar. The duration of the eclipse, determined by using the orbital parameters given by (Jenke *et al.*, 2012), are also marked in the figure. *Suzaku* data were reprocessed and analyzed by following the standard procedure as mentioned in section 2.4 of Chapter-2. Source light curves and spectra were accumulated from reprocessed XIS and PIN events data. Corresponding background, response and effective area files were also obtained.

5.1.1 Pulse profiles

During the *Suzaku* observation, OAO 1657-415 was found to exhibit flux variability on several time scales. The combined XIS light curve in 0.5-10 keV range showed the presence of two extended low intensity segments and two high intensity segments as shown in Figure 5.2. The extended low flux segments were found in the light curves up to as high as ~ 50 keV. To investigate the properties of the pulsar at different flux levels, the entire observation was

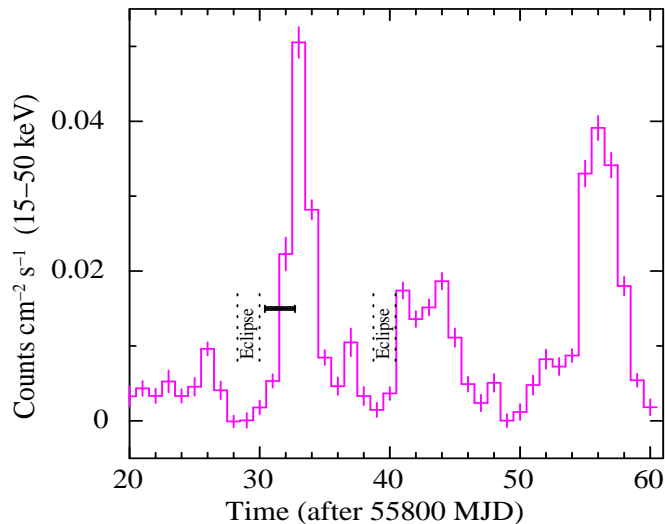


Figure 5.1: *Swift*/BAT light curve of OAO 1657-415 in 15–50 keV energy range, from 2011 September 16 (MJD 55820) to 2011 October 26 (MJD 55860). The horizontal mark shows the duration of the *Suzaku* observation of the pulsar. The durations of the eclipse are marked in the figure.

divided into four broad regions and marked as Regions-I, II, III, & IV in the top panel of Figure 5.2. Light curves were extracted from XIS and HXD/PIN data at 2 s and 1 s time resolutions, respectively, for all four segments. As the *Suzaku* observation covered about 0.2 orbital phase of the binary system, the light curves were corrected for the orbital motion by using the ephemeris given by (Jenke *et al.*, 2012). The barycentric and orbital motion corrected light curves were further used in the timing analysis of the pulsar. The pulse period of the pulsar was estimated by using the χ^2 maximization technique and found to be 36.961(1) s. Pulse profiles were generated for all four regions by folding corresponding background subtracted light curves in 0.5-5 keV, 5-10 keV, 10-25 keV, 25-50 keV and 50-70 keV ranges with the estimated pulse period and shown in Figure 5.3. Pulse profiles of the pulsar were found to be strongly energy as well as intensity dependent. The shape of the pulse profiles was complex because of the presence of several narrow absorption-like features at various pulse phases during Regions-I, II & III. At low energies, these features were more prominent compared to that at high energies. During these three regions, pulsations were detected up to ~ 50 keV. However, in the

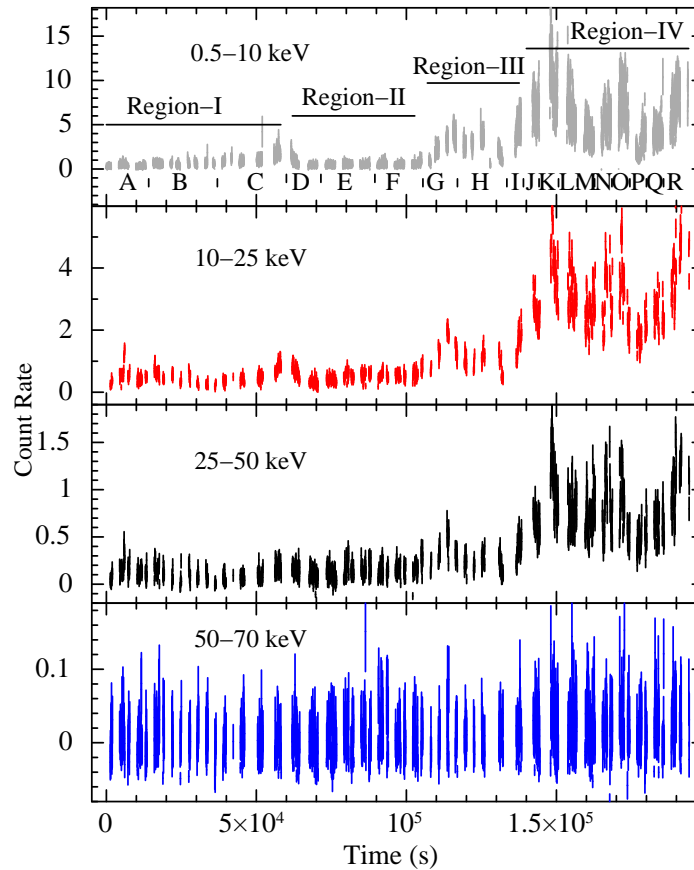


Figure 5.2: Light curves of OAO 1657-415 in 0.5-10 keV (combined data from XIS-0, 1 & 3), 10-25 keV, 25-50 keV and 50-70 keV (HXD/PIN) energy ranges obtained from the *Suzaku* observation of the pulsar in 2011 September. Depending on the variable X-ray flux during the observation, the data were divided into four broad regions as marked in the figure (top panel; Jaisawal and Naik, 2014). The acronyms in the top panel A to R show the segments of the data used for detailed time resolution spectroscopy as described in the later part of the chapter. The other panels show the presence/absence of narrow and extended low flux levels during the *Suzaku* observation. All the light curves are background subtracted.

high flux level of Region-IV, pulsations were detected up to ~ 70 keV. Though Regions-I & II were at a comparable low flux level, low signal-to-noise ratio and relatively smooth single-peaked profiles in Region-II suggest higher absorption during this segment.

Pulse profiles of OAO 1657-415 were found to be complex because of the presence of multiple absorption-like features at various spin phases of the pul-

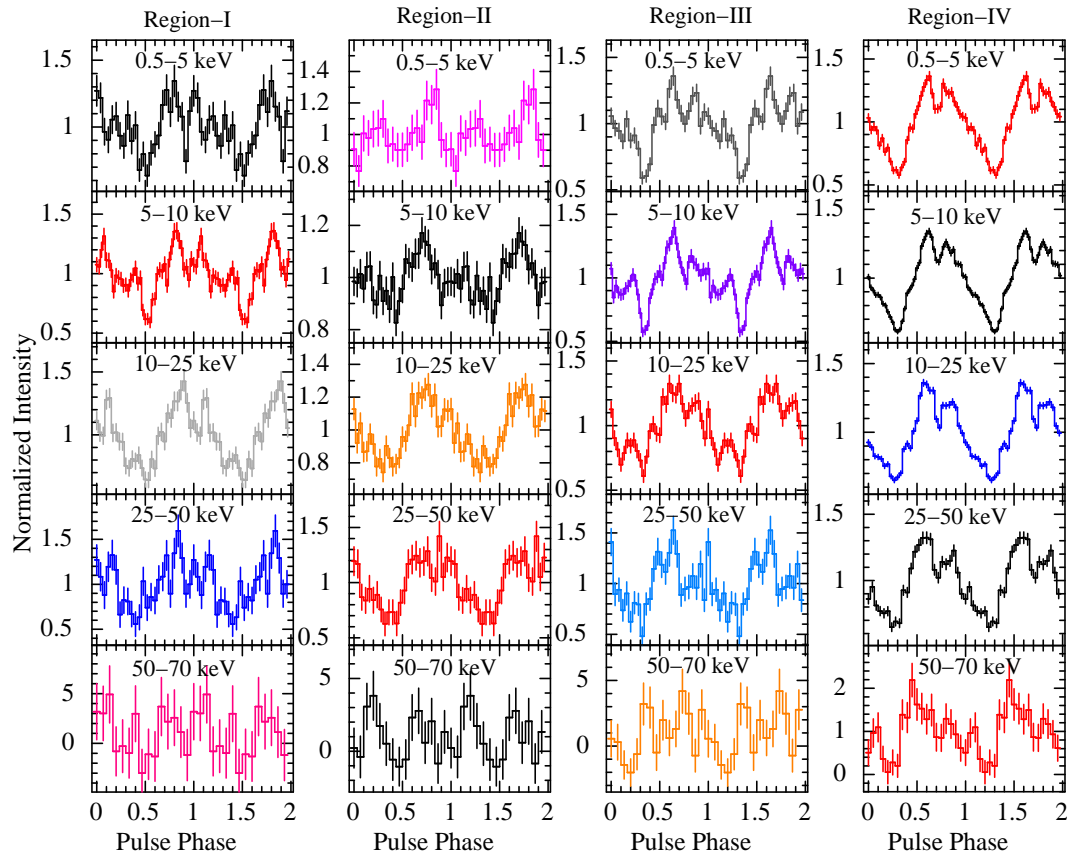


Figure 5.3: Energy-resolved pulse profiles obtained from all four region of *Suzaku* observation of OAO 1657-415 (as marked in Figure 5.2) from XIS-0 and HXD/PIN data. Complex nature of the shape of pulse profiles in soft X-ray energy ranges are clearly seen during all four regions. Pulsations can be seen up to ~ 70 keV during high flux level. The error-bars shown in the figure represent 1σ uncertainties. Two pulses are shown for clarity.

sar. As OAO 1657-415 is in a close binary system, it is subjected to dense and strong stellar wind of the high mass supergiant companion. These clumps of matter are capable of causing absorption of X-ray photons up to higher energies. Inhomogeneous nature of the stellar wind consisting of clumps of matter, therefore, can cause irregular variability in the X-ray emission from the pulsar e.g. presence of flaring episodes to short and extended duration of high and low flux levels as seen in OAO 1657-415. The presence of additional absorbing matter during this segment can be verified by investigating the spectral evolution of the pulsar during the *Suzaku* observation. In the following sec-

tion, we described the results obtained from the spectral study of the *Suzaku* observation of the pulsar.

5.1.2 Spectral analysis

To study the change in spectral properties of OAO 1657-415 in four segments of different flux levels, we extracted source and background spectra from each of XIS and PIN detectors and generated corresponding response matrices. Before carrying out spectral fitting, we generated spectral ratios between different intensity levels (regions) as marked in Figure 5.2. The spectral ratios obtained are shown in Figure 5.4. Top two panels of Figure 5.4 show continuous increase in the values of spectral ratios with energy which indicates significant decrease in the soft X-ray photons during Regions-I & II compared to that during Region-IV. This suggests that the soft X-ray photons are heavily absorbed during the low flux segments of Regions-I & II. Absence of any significant variability in the spectral ratio between Regions-III & IV (third panel of Figure 5.4) suggest that the spectral properties of the pulsar during these two regions appear similar.

Apart from the absorption of soft X-ray photons during Regions-I & II, another important feature seen in the spectral ratio plots was the presence of two iron emission lines at 6.4 keV and 7.06 keV. Second and fourth panels of Figure 5.4 show the presence of both the lines clearly in the pulsar spectrum at different segments. The low peak value of 6.4 keV line ratio (~ 0.2) suggest that the line flux during the high flux segment (Region-IV) is high (approximately by a factor of $\sim 4-5$) compared to that of during Region-II. However, the continuum flux in 2-10 keV energy range during Region-IV could be significantly high (more than an order of magnitude) compared to that during Region-II. Because of significant difference in continuum flux unlike in the case of flux of iron emission lines during Regions-II & IV, the lines are clearly seen in the spectral ratio plot (second panel). It can be seen in fourth panel that the peak of the ratio of 6.4 keV emission line is ~ 1.7 whereas the 2-10 keV continuum flux ratio varies in the range of 0.5-0.8. This indicates that though

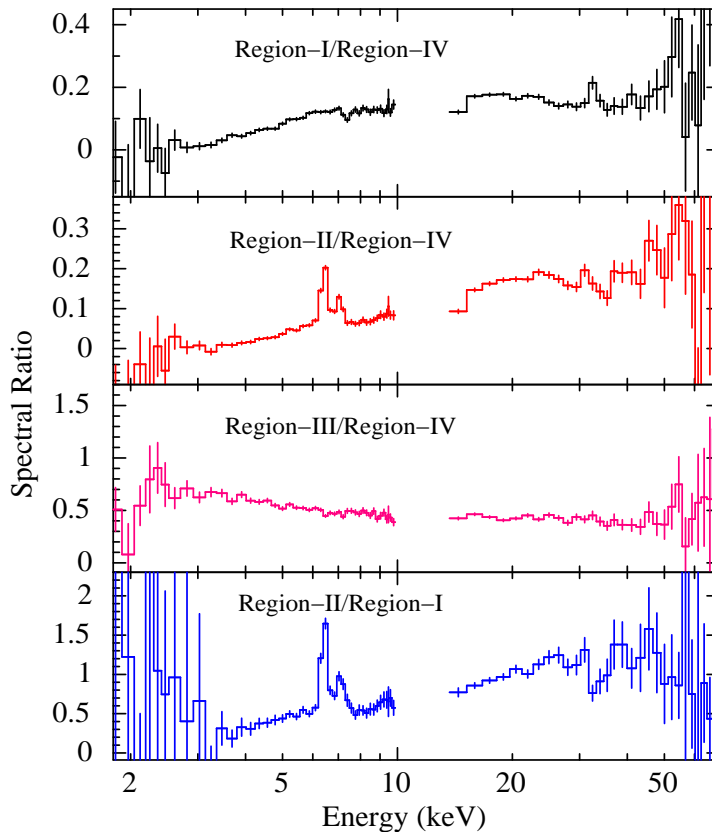


Figure 5.4: Spectral ratio in 1.8-70 keV energy range obtained for different regions of the *Suzaku* observation of OAO 1657-415. Presence of two iron fluorescent emission lines in the pulsar spectrum were clearly seen in second and fourth panels.

the 2-10 keV continuum flux is marginally higher during Region-I (as the value of the spectral ratio is less than 1; bottom panel), the flux of iron emission line is high during Region-II. These findings from the spectral ratio plots suggest different origin of the iron emission lines during the regions of different flux levels over the binary orbit. More quantitative information on the iron emission line parameters can be obtained from spectral fitting of data during different segments.

For a detailed investigation of spectral evolution of the pulsar at different flux levels during the *Suzaku* observation, we carried out simultaneous spectral fitting of data obtained from XIS-0, XIS-1, XIS-3 and HXD/PIN in 1.8-70 keV energy range. Before spectral fitting, appropriate background subtraction was done from the data obtained from all the detectors. In the beginning,

Table 5.2: Best-fitting spectral parameters obtained from the four regions seen during *Suzaku* observation of OAO 1657-415. The errors are estimated for 90% confidence level.

Parameter	Value			
	Region-I	Region-II	Region-III	Region-IV
N_H (10^{22} atoms cm^{-2})	51.33±4.09	75.74±5.91	24.81±1.67	28.45±0.93
Power-law index	1.04±0.12	1.12±0.07	1.16±0.07	0.98±0.04
Norm. ^a of Power-law (10^{-2})	1.24±0.30	1.41±0.43	3.78±0.60	5.83±0.48
kT_{BB} (keV)	0.33±0.04	0.30±0.05	0.32±0.03	0.32±0.01
Norm. ^b of kT_{BB} (10^{-2})	2.04±1.39	18.43±14.31	1.82±0.83	6.99±1.56
High energy cut-off (keV)	16.74±2.88	20.81±1.34	19.22±2.17	18.54±0.57
Folding energy (keV)	19.38±1.85	21.38±2.61	23.05±3.01	21.69±0.81
Fe K_α line Energy (keV)	6.413±0.006	6.411±0.003	6.411±0.005	6.420±0.004
Width of Fe K_α (keV)	0.01±0.03	0.01±0.01	0.01±0.01	0.03±0.02
Fe K_α eq. width (eV)	218.34±14.71	1069.38±79.61	211.46±10.49	221.42±5.82
Fe K_α line flux ^c	1.61±0.09	4.94±0.37	6.05±0.30	12.96±0.34
Fe K_β line Energy (keV)	7.077±0.057	7.072±0.009	7.07 (fr)	7.112±0.038
Width of Fe K_β (keV)	0.01±0.07	0.01±0.05	0.07±0.07	0.09±0.03
Fe K_β eq. width (eV)	66.94±13.89	267.40±21.60	46.93±18.02	66.08±11.78
Fe K_β line flux ^c	0.47±0.10	1.18±0.10	1.28±0.49	3.72±0.66
Flux ^d (in 2-10 keV range)	0.38±0.09	0.28±0.07	1.61±0.25	3.32±0.30
Flux ^d (in 10-70 keV range)	4.67±1.44	4.46±1.35	11.49±1.81	27.10±2.22
χ^2 (dof)	219 (149)	275 (148)	181 (152)	262 (142)

N_H = Equivalent hydrogen column density, ^a : photons $\text{keV}^{-1}\text{cm}^{-2}\text{s}^{-1}$ at 1 keV, ^b : in units of 10^{39} erg s^{-1} $(\text{d}/10 \text{ kpc})^{-2}$ where d is distance to the source, ^c : in 10^{-12} ergs $\text{cm}^{-2} \text{s}^{-1}$ unit, ^d : in 10^{-10} ergs $\text{cm}^{-2} \text{s}^{-1}$ unit.

we tried to fit the spectral data with standard continuum models such as HECut and NPEX model along with interstellar absorption and iron emission line at 6.4 keV. Simultaneous spectral fitting of the XIS and HXD/PIN data can describe with HECut model along with interstellar absorption and two Gaussian functions for ~ 6.4 and ~ 7.1 keV iron emission lines. A blackbody component was also added to the spectral model for the soft X-ray excess.

The emission line corresponding to the second Gaussian function in the spectral model was identified to be iron K_β fluorescent emission line. While fitting the spectra of high flux level (Region-IV), we found a weak signature of Ni K_α line at 7.48 keV in the residue. Addition of a Gaussian component

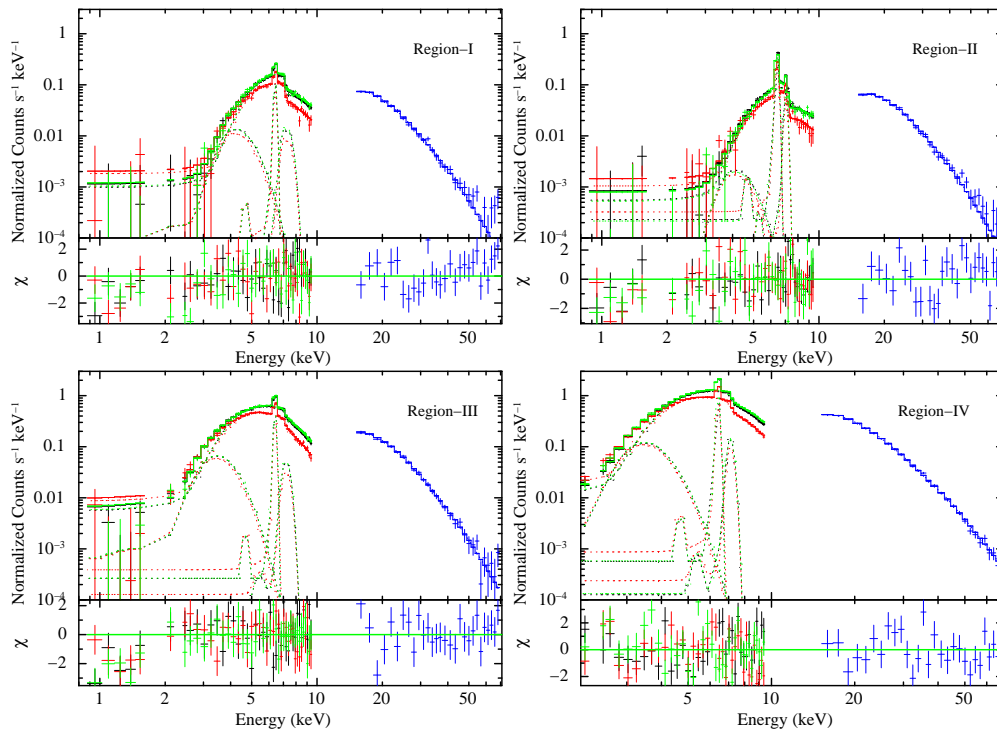


Figure 5.5: Energy spectrum of OAO 1657-415 at four different flux levels (as shown in Figure 5.2) during the *Suzaku* observation. Spectral data from XIS and HXD/PIN detectors are shown in the top panels of all four regions, along with the best-fit model comprising of a HECut with a blackbody component, interstellar absorption and two narrow iron emission lines at 6.4 keV and 7.06 keV (Jaisawal and Naik, 2014). The contributions of the residuals to the χ^2 for each energy bin for the best-fit model are shown in the second panel for corresponding regions.

at 7.48 keV improved the χ^2 value from 287 (145 dof) to 262 (142 dof). The equivalent width of Ni K_α line was estimated to be 23.7 ± 3.5 eV. This line was also detected in other source such as GX 301-2 (Suchy *et al.*, 2012). In the spectral fitting, however, there was no signature of presence of earlier reported cyclotron resonance scattering feature (CRSF) at ~ 36 keV (Orlandini *et al.*, 1999). We, therefore, did not include CRSF component in the spectral fitting. Simultaneous spectral fitting of XIS and HXD/PIN data were carried out for all four regions of the *Suzaku* observation of the pulsar and shown in Figure 5.5. The best-fit parameters (with 90% errors) obtained from simultaneous spectral fitting are given in Table 5.2. Among the four regions, the

data during Regions-I & II were found to be significantly affected by absorption with the values of absorption column density of 51×10^{22} atoms cm^{-2} and 76×10^{22} atoms cm^{-2} , respectively. Though the flux of 6.4 keV and 7.06 keV iron emission lines were maximum during the high intensity level of Region-IV, the equivalent width of these lines were significantly high during the low flux level of Region-II. The continuum flux in 2-70 keV range were found to be comparable during Regions-I & II. For a detailed understanding of the changes in the values of absorption column density, equivalent widths and flux of iron emission lines during different regions, we attempted to do time resolved spectroscopy by dividing the entire observation into 18 narrow segments (as marked at the bottom of Figure 5.2). As described earlier, XIS and HXD/PIN spectra were extracted for each of the narrow segments. Previously extracted background spectra and response files were used for the spectral fitting of XIS and HXD/PIN data during these narrow segments. Simultaneous spectral fitting was carried out by using the high energy cutoff power law model along with other components as used earlier. Iron line parameters were kept free during the spectral fitting with a lower limit of line width at 1 eV. Though, the energy and width of both Fe lines were similar during entire observation, the energy and width of Fe K_{β} line were found to be high (~ 7.28 keV and ~ 0.2 keV, respectively) during segments G & K. Therefore, the values of line energy was fixed at 7.07 keV during the segments G and K. The best-fit parameters obtained from the simultaneous spectral fitting were plotted in Figure 5.6 along with the source light curve in 0.5-10 keV range in top panels.

The value of equivalent hydrogen column density N_H (second panel; left side of Figure 5.6) was found to vary in a wide range. It was maximum in the beginning of the observation for a short duration (early part of Region-I) which decreased by a factor of ~ 4 and then increased again during the Region-II. Beyond Region-II, the value of N_H became low during the high flux segments of Regions-III and IV. The change in power law photon index was not significant enough (though a marginal decrease was seen towards the end of the observation; second panel - right side) to draw any conclusion on spectral

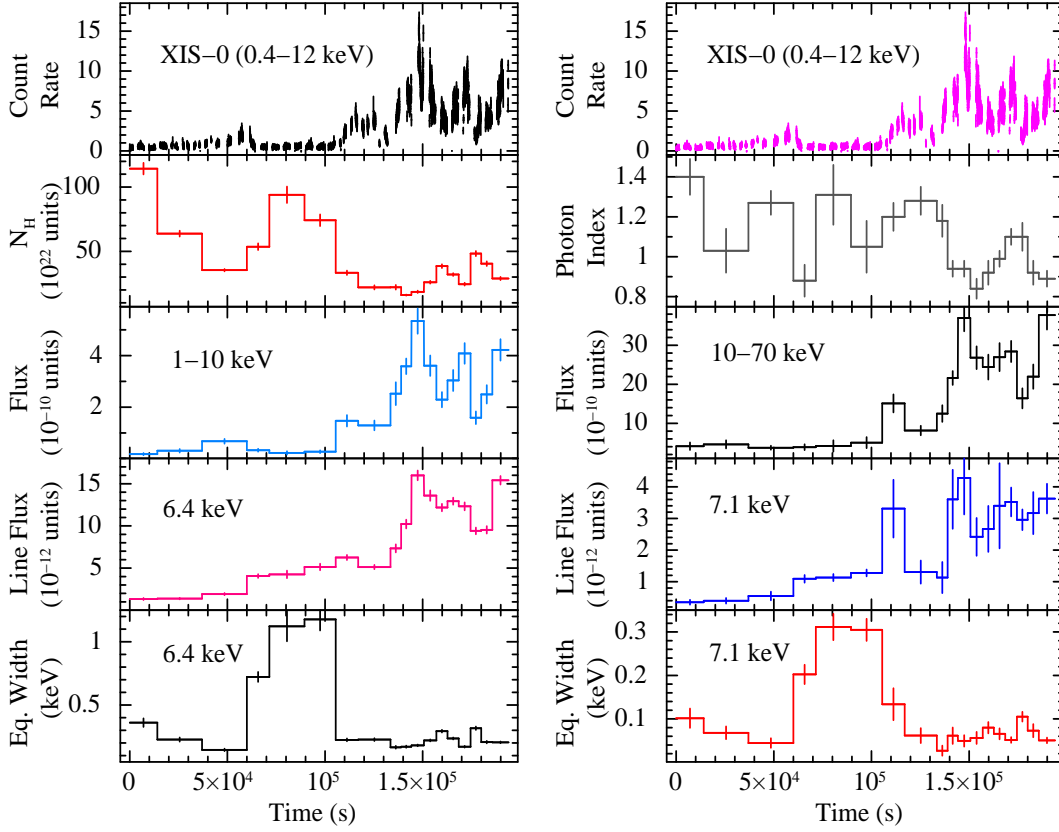


Figure 5.6: Spectral parameters obtained from the time-resolved spectroscopy of *Suzaku* observation of OAO 1657-415. The top panels in both the sides show light curves of the pulsar in 0.5-10 keV energy range. The values of N_H and power law photon index are shown in second panels in left and right side, respectively. The source flux in 2-10 keV (left side) and 10-70 keV (right side) in 10^{-10} ergs cm^{-2} s^{-1} units are shown in third panels. Fourth and fifth panels in both the sides show the line flux in 10^{-12} ergs cm^{-2} s^{-1} units and equivalent widths of 6.4 keV and 7.06 keV iron emission lines, respectively (Jaisawal and Naik, 2014). The errors shown in the figure are estimated for 90% confidence level.

state change in the pulsar. Though flux of both the iron emission lines (fourth panels from top) increased with the increase in source flux (third panels from top), equivalent width of these emission lines did not show any such change. The values of equivalent widths were significantly high during the low flux level of Region-II. To investigate changes in iron emission line parameters with the observed continuum flux, we plotted flux of iron emission lines and equivalent widths with respect to the total flux in 1.8-70 keV energy range (as shown in

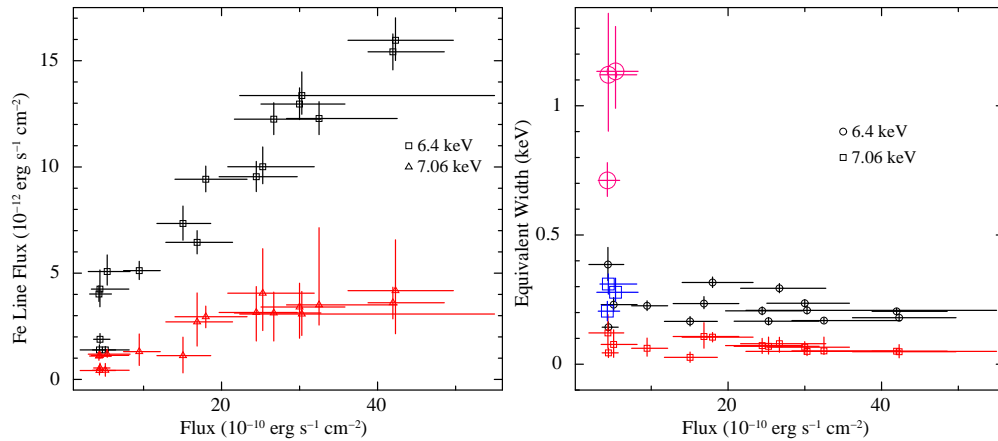


Figure 5.7: Change in the 6.4 keV and 7.06 keV iron emission line flux (left panel) and equivalent widths (right panel) with respect to the observed fluxes in 2-70 keV energy range obtained from time-resolved spectroscopy of *Suzaku* observation of OAO 1657-415. The squares and triangles in left panel represented flux for 6.4 keV and 7.06 keV iron lines, respectively. In the right panel, the circles and squares showed the equivalent widths of 6.4 keV and 7.06 keV iron lines, respectively. The markers in large sizes represented the corresponding values estimated during the low flux segment of Region-II (in Figure 5.2).

Figure 5.7). It was found that the flux of both the lines increased continuously with increase in the source flux though the increase was significantly high in case of 6.4 keV line. However, the equivalent width of both the lines were very high during the low flux segment of Region-II (shown in the right panel Figure 5.7 with larger size markers) whereas during the rest of the segments, the changes were minimal. Unusual high value of equivalent widths for both the iron emission lines during Region-II compared to that during Region-I, though both were at similar flux level, suggested the presence of significant amount of additional matter emitting iron emission lines at that orbital phase. Flux of both the lines were found to be directly correlated with the observed continuum flux (Figure 5.7). This indicates the fluorescence origin of iron lines from the cool matter surrounding the neutron star (Makishima, 1986). The direct correlation between the line flux and pulsar continuum flux also suggests that the location of reprocessing region is closer to the central source.

5.1.3 Implication of clumpy wind model

Significant flux variability in OAO 1657-415 during *Suzaku* observation can be explained by using clumpy stellar wind model (Feldmeier, Oskinova and Hamann, 2003; Oskinova, Hamann and Feldmeier, 2007). Accretion of clumps of matter onto the pulsar causes increase in source luminosity by producing flares/flare-like episodes in X-ray emission. The obstruction/absorption of X-ray photons by dense clumps of matter in the line-of-sight can also cause segments of low flux levels in X-ray light curve. Considering inhomogeneous distribution of matter in the stellar wind, the luminosity of such wind-powered HMXB pulsars depends on the density and velocity of the stellar wind through the relation (Bondi and Hoyle, 1944),

$$L_x \propto \rho v^{-3} \quad (5.1)$$

where ρ is density and v is the wind velocity as described in β -velocity law (Castor, Abbott and Klein, 1975). Any fluctuation in either density or velocity profile produces the time variability in the source luminosity.

The clumpy wind model can explain the observed variability in circumstellar absorption and source flux. By using this model, the physical parameters of the clumpy wind can be estimated from the observed time variability in the light curve of OAO 1657-415. Figure 5.2 shows the presence of a series of flares of duration of ≥ 10 ks. Considering a flare of duration $t_f \sim 10$ ks and relative wind velocity $v_{rel} \sim 250$ km s $^{-1}$ (taking an approximation of terminal velocity similar to the relative velocity; Mason *et al.* (2012)), the radius of the clump can be estimated as

$$R_c \simeq \frac{v_{rel} t_f}{2} = 1.25 \times 10^{11} \left(\frac{v_{rel}}{250 \text{ km s}^{-1}} \right) \left(\frac{t_f}{10 \text{ ks}} \right) \text{ cm} \quad (5.2)$$

Gravitational force of the neutron star on the clumps becomes effective at the accretion radius $r_{acc} \sim 2GM_{ns}/v_{rel}^2$. When a clump of matter crosses this radius, it gets accreted onto the neutron star. The accretion radius for OAO 1657-415 is calculated to be $\sim 6 \times 10^{11}$ cm by assuming typical parameters of the neutron star and relative stellar wind velocity of 250 km s $^{-1}$. Accretion

radius also imposes a constrain on upper limit of the radius of a clump that can be accreted entirely onto the neutron star. Mass of the accreted clump can be estimated by comparing the gravitational potential energy of clump to the energy released due to its accretion onto the neutron star (assuming efficiency η as 0.1) through the relation (Zel'dovich and Shakura, 1969)

$$M_c = \frac{L_x t_f R_{ns}}{\eta G M_{ns}} = 5 \times 10^{21} \left(\frac{L_x}{10^{37} \text{ erg s}^{-1}} \right) \left(\frac{t_f}{10 \text{ ks}} \right) \text{ g} \quad (5.3)$$

where M_{ns} , R_{ns} and L_x are mass, radius and X-ray luminosity of the neutron star, respectively. Therefore, for a given set of physical parameters of the spherical clump, its mean density (n_c) and radial column density (N_c) can be estimated as

$$n_c = \frac{3M_c}{4\pi m_p R_c^3} = 4 \times 10^{11} \left(\frac{L_x}{10^{37} \text{ erg s}^{-1}} \right) \times \left(\frac{t_f}{10 \text{ ks}} \right)^{-2} \left(\frac{v_{rel}}{250 \text{ km s}^{-1}} \right)^{-3} \text{ cm}^{-3} \quad (5.4)$$

$$N_c = n_c R_c = 5 \times 10^{22} \left(\frac{L_x}{10^{37} \text{ erg s}^{-1}} \right) \times \left(\frac{t_f}{10 \text{ ks}} \right)^{-1} \left(\frac{v_{rel}}{250 \text{ km s}^{-1}} \right)^{-2} \text{ cm}^{-2} \quad (5.5)$$

Using the typical parameters in Equation (5.4), the mean density of a clump can be estimated to be $4 \times 10^{11} \text{ cm}^{-3}$. However, the mean number density of the stellar wind around the neutron star is calculated to be $n \sim 4 \times 10^{10} \text{ cm}^{-3}$ by using the β -velocity law (Castor, Abbott and Klein, 1975) and the wind parameters from Mason *et al.* (2012). Stellar wind density is found to be an order of magnitude lower than the value obtained from Equation (5.4).

In the present *Suzaku* observation, the duration and luminosity of the flare (segments G & H) are about $\sim 25 \text{ ks}$ and $0.66 \times 10^{37} \text{ erg s}^{-1}$, respectively. Using these values in Equation 5.5, the clump column density (N_c) is estimated to be $1.3 \times 10^{22} \text{ cm}^{-2}$. However, the difference in the observed value of N_H (from spectral fitting) for segments F (prior to the flare) and G & H (during flare) is found to be $52 \times 10^{22} \text{ cm}^{-2}$. This value corresponds to the column

density of clump that produced a flare of ~ 25 ks duration (segments G & H). However, it is found to be ~ 40 times more than the expected column density (N_c). In case of another flare (segments I to L) with duration of ~ 24 ks and luminosity of 1.38×10^{37} erg s $^{-1}$, the clump column density (N_c) is estimated to be 2.9×10^{22} cm $^{-2}$. From spectral fitting, the difference in N_H between the flare (segments from I to L) and the segment prior to the flare (segment H) are calculated to be 1.4×10^{22} cm $^{-2}$ which is comparable to the estimated value N_c . For the flare starting from segment N to segment P, the duration and luminosity are ~ 12 ks and 1.31×10^{37} erg s $^{-1}$, respectively. Using these values, the clump column density (N_c) is estimated to be 5.4×10^{22} cm $^{-2}$. However, as calculated earlier, the clump density from spectral fitting is found to be 3.6×10^{22} cm $^{-2}$ which is also close to N_c . From these examples, it is found that the values of observed and calculated clump column densities are comparable. This supports the suggestion that the observed flux variability in the pulsar light curve can be explained by using clumpy wind hypothesis.

However, in case of the flares during segments G & H, the estimated clump column density from spectral fitting is quite high compared to the expected column density calculated by using Equation 5.5. The enhancement in the value of column density compared to the standard wind density can occur because of the instability in variable and highly structured stellar wind. As the supersonic stellar wind interacts with the neutron star, a bow shock of compressed gas forms near r_{acc} that may cause enhancement in the column density. Numerical simulation results for the wind-fed sources indicate that the regions inside the non-steady accretion wake consist of dense filaments in which the density reaches up to ~ 100 times more compared to the undisturbed stellar wind (Blondin *et al.*, 1990). Such dense clump or filament can absorb X-ray photons up to higher energies producing low flux levels in the light curve.

Interaction of X-ray photons either in dense filaments or stagnated shock front can contribute to higher value of the equivalent width. Inoue (1985) performed Monte Carlo simulation on the fluorescence emission from the neutral atom as a function of absorber density. Different model components were con-

sidered in above study. A model with a combination of direct and scattered continuum component explained the possibility of high equivalent width (up to order of keV) with change in N_H . If the absorbing matter is between the observer and the X-ray source, then the equivalent width of emission line is monotonically proportional to the column density. Observed high equivalent width (more than 100 eV) of 6.4 keV line at $N_H > 10^{23} \text{ cm}^{-2}$ can therefore be explained as due to the presence of absorbing matter between the pulsar and the observer.

In summary, we interpret our results based on the clumpy wind model. The extended low flux levels of Region-I & II can be interpreted as due to the presence of dense clump or filament of the compressed gas. The high equivalent width of Fe K_α and Fe K_β lines can be understood by the result obtained from Monte Carlo simulation (Inoue, 1985) in which the dense clump of matter obscures the direct X-rays and contributes to the high value of equivalent width as observed in Region-II. During the orbital phase 0.19-0.24 (Region-II), the clump could be situated along the line-of-sight. As the clump passes Region-II, the absorption column density decreases and causes decrease in the equivalent width of iron emission lines. Lifetime of this clump can be similar to the duration of Region-II.

5.1.4 Location of the Fe fluorescence line emitting region in OAO 1657-415

To investigate the ionization state of matter (iron) in line emitting region, the ratio of Fe K_β line flux to that of Fe K_α line was calculated for the entire *Suzaku* observation of OAO 1657-415. It was found that the value of flux ratio varies between 0.15 ± 0.11 and 0.42 ± 0.18 for all segments. The value of line flux ratio for each segment was found to be higher than the theoretically predicted value (~ 0.13) for neutral iron atom in optically thin medium (Kaastra and Mewe, 1993; Palmeri *et al.*, 2003; Han and Demir, 2009). This suggests that the line emitting region can be a mixture of neutral and ionized iron atoms. The

observed line energy and flux ratio indicate the possible existence of ionized iron atoms in ionization state between Fe VIII to Fe XVIII (Palmeri *et al.*, 2003; Mendoza *et al.*, 2004; Kallman *et al.*, 2004). Ionization of the iron atoms is characterized by the ionization parameter $\xi=L/nr^2$ and its value should be $\xi \sim 10^{2.5}$ erg cm s⁻¹ for ionization state below Fe XVIII (Tarter and Salpeter, 1969; Ebisawa *et al.*, 1996). However, the iron atoms are expected to be fully ionized at $\xi \geq 10^3$ erg cm s⁻¹ (Kallman and McCray, 1982). The peak population of ion at Fe XVIII can be expected to be ~ 0.25 (Ebisawa *et al.*, 1996). For a luminosity of 10^{37} erg s⁻¹ and column density of $10^{23} \leq N_H \leq 10^{24}$ cm⁻², the location of ionization region is found to be in range of $(0.3-3) \times 10^{11}$ cm from the neutron star. Using this method, we found that the location of ionization region lies within or closer to the accretion radius r_{acc} . Our result agrees with that obtained from earlier studies in which the location of iron fluorescence region was estimated to be within the region of 5.7×10^{11} cm (19 lt-sec; Audley *et al.*, 2006).

5.2 4U 1700-37

4U 1700-37 was observed with *Suzaku* in 2006 September 13-14. The observation was carried out during out of eclipse phase of the binary covering 0.29-0.72 orbital phase range (considering mid-eclipse time as phase zero; Rubin *et al.*, 1996). We report the time-averaged and time-resolved broadband spectroscopy of 4U 1700-37 to understand the nature of the continuum emission and its orbital dependency, flaring activities, emission lines and cyclotron features in the spectrum.

5.2.1 Timing properties

Using standard method, the source and background light curves in soft (XIS - 1 s time resolution) and hard X-ray (HXD/PIN - 0.1 s time resolution) energy ranges were extracted. Background subtracted light curves in 0.5-10 keV and 10-70 keV ranges are shown in top and middle panels of Figure 5.8. From

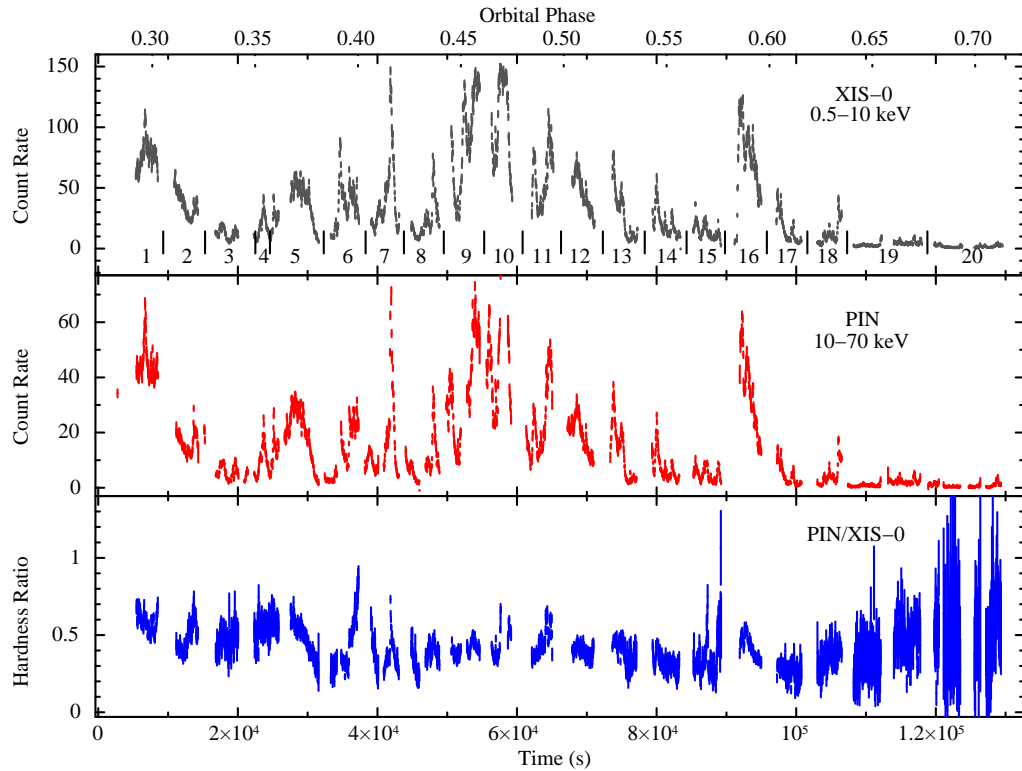


Figure 5.8: Light curves (top and middle panels) and hardness ratio (bottom panel) obtained from the *Suzaku* observation of the high-mass X-ray binary 4U 1700-37. Data from XIS-0 and HXD/PIN detectors are plotted here. Flux variability by an order of ~ 10 -15 can be seen in top and middle panels of the figure (Jaisawal and Naik, 2015a). The quoted numbers at the top panel show the duration of segments used for time-resolved spectroscopy. The orbital phases covered during the *Suzaku* observation are marked at the top of the figure.

the figure, significant and rapid flux variability by a factor of ~ 10 -15 can be seen in soft and hard X-ray bands. The presence of flaring episodes along with stable low flux segments can also be clearly seen in XIS and PIN light curves. Hardness ratio (ratio between the light curves obtained from HXD/PIN and XIS-0 event data) plot (bottom panel of Figure 5.8) was generated to check the spectral state of the source during the flaring episodes as well as low flux segments in the light curve. However, apart from marginal hardening during the extended low flux segment towards the end of the observation, any significant change in the value of hardness ratio (spectral state) was absent.

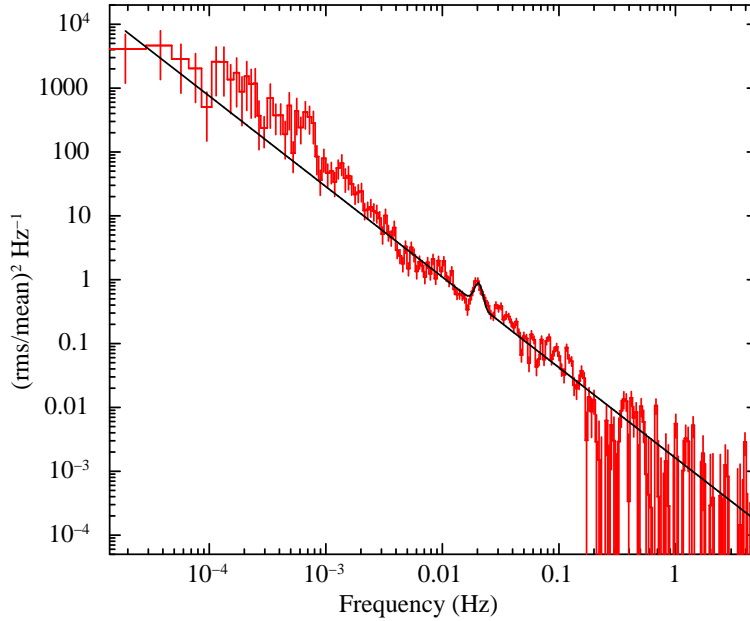


Figure 5.9: Power density spectrum (PDS) of 4U 1700-37 obtained from HXD/PIN light curve in 10-70 keV energy range. Absence of pulsations in the range of 10^{-5} Hz to 2 Hz range can be seen in the figure. A QPO at ~ 20 mHz is detected in the PDS of the X-ray source. The solid line in the figure represents the fitted model comprising of a power-law continuum and a Gaussian function at the QPO frequency.

To investigate the presence of any periodicity (pulsation) in the X-ray source, power density spectrum (PDS) was generated by using the HXD/PIN light curve with 0.1 s time resolution and shown in Figure 5.9. Absence of any clear and sharp peaks in the PDS in 0.5 s to 10^5 s range suggested the non-detection of pulsation in above time range. To confirm the non-detection of pulsation, we generated pulse profiles by assuming 50 s (corresponding to ~ 20 mHz peak in the PDS) and earlier reported 67 s (from *Tenma* observation) as the spin period of the source. We defined pulse fraction as the ratio between the difference in the maximum and minimum intensities to the sum of the maximum and minimum intensities in the pulse profile. We estimated pulse-fraction from each of the pulse profiles obtained by assuming 50 s and 67 s as spin period of the source and found to be $\sim 1\%$. The negligible values of pulse fraction indicate the non-detection of X-ray pulsation in the source. On the other hand, the observed weak and broad feature at ~ 20 mHz confirmed

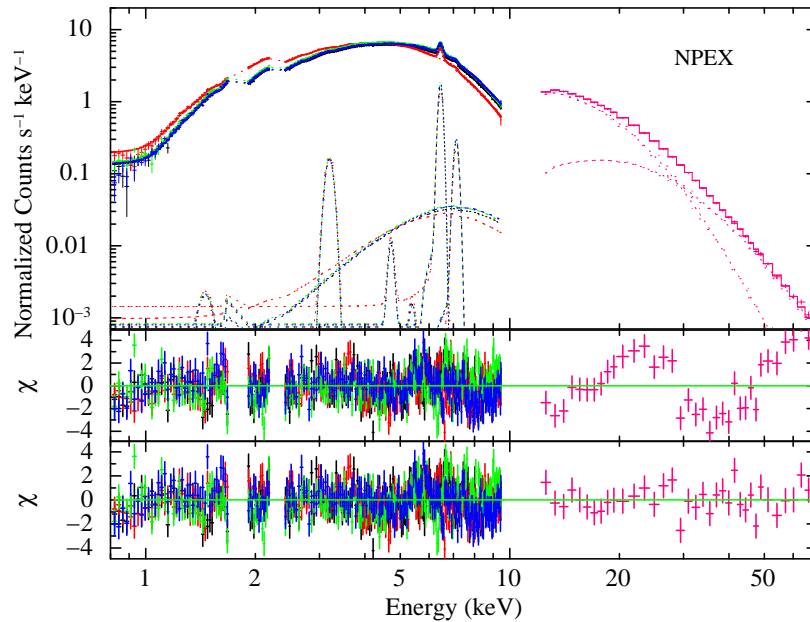


Figure 5.10: Energy spectrum of 4U 1700-37 obtained with the XISs and PIN detectors of the *Suzaku* observation, along with the best-fit model comprising a partial covering NPEX continuum model, three Gaussian functions for emission lines and a cyclotron absorption component (Jaisawal and Naik, 2015a). The middle and bottom panels show the contributions of the residuals to χ^2 for each energy bin for the partial covering NPEX continuum model without and with cyclotron component in the model, respectively.

the detection of a quasi-periodic oscillation (QPO) in the X-ray source (Jaisawal and Naik, 2015a). The significance of QPO feature was determined by fitting the PDS with a power-law continuum along with a Gaussian function at QPO frequency and found that the detection was more than 3σ level.

For spectral analysis, the source and background spectra, response matrices and effective area files for all instruments were extracted by following the standard procedures. After appropriate background subtraction, spectra from all the detectors were fitted simultaneously in 0.8-70 keV energy range by using *XSPEC* package. Standard continuum models for X-ray pulsars like HECut, FDCut, Cutoffpl, NPEX and CompTT were applied in the spectral fitting. However, HECut and NPEX model with partial covering component described the source source spectrum well.

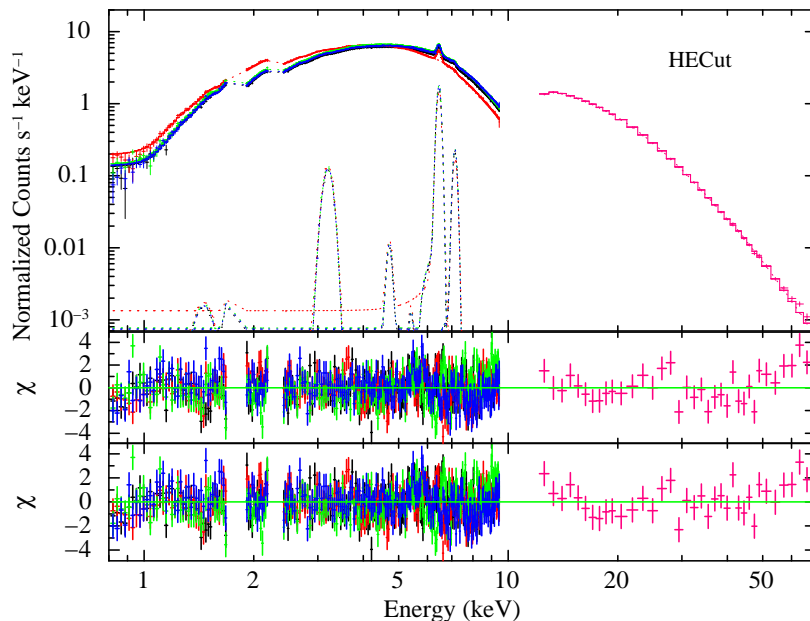


Figure 5.11: Energy spectrum of 4U 1700-37 obtained with the XISs and PIN detectors of the *Suzaku* observation, along with the best-fit model comprising a partial covering HECut continuum model, three Gaussian functions for emission lines and a cyclotron absorption component (Jaisawal and Naik, 2015a). The middle and bottom panels show the contributions of the residuals to χ^2 for each energy bin for the partial covering power law continuum model without and with cyclotron component in the model, respectively.

Addition of partial covering component to all three continuum models improved the spectral fitting yielding the reduced χ^2 values from >4 to <2 . In this model component, there are two different absorption components. Apart from these spectral components in the continuum models, the iron fluorescence lines at 6.42 keV (Fe K_α) and 7.1 keV (Fe K_β) were detected in the spectrum of 4U 1700-37. An emission line like feature at 3.19 keV was seen in the spectral residue of all three continuum models. Addition of a Gaussian component at ~ 3.19 keV to above three continuum models improved the spectral fitting further. The line at ~ 3.19 keV was identified as the fluorescence emission from S XV as seen in EXO 2030+375 (Naik *et al.*, 2013) or Ar K_β .

In contrast to earlier findings, the thermal component (soft X-ray excess) was not seen in the spectrum during the *Suzaku* observation of 4U 1700-37.

Table 5.3: Best-fitting parameters obtained from the spectral fitting of *Suzaku* observation of 4U 1700-37 with 90% errors. Model-1 : Partial covering NPEX model with Gaussian components, Model-2 : Partial covering NPEX model with Gaussian components and cyclotron absorption line, Model-3 : Partial covering HECut model with Gaussian components, Model-4 : Partial covering HECut model with Gaussian components and cyclotron absorption line.

Parameter	Value			
	Model-1	Model-2	Model-3	Model-4
N_{H1}^a	1.9±0.1	2.0±0.1	2.2±0.3	2.2±0.1
N_{H2}^b	4.1±0.1	4.5±0.2	4.9±0.1	4.9±0.1
Cov. Fraction	0.6±0.1	0.6±0.1	0.7±0.1	0.7±0.1
Photon index	0.2±0.1	0.3±0.1	1.0±0.1	1.0±0.1
E_{cut} (keV)	7.5±0.1	8.8±1.5	7.1±0.1	7.1±0.1
E_{fold} (keV)	–	–	19.1±0.1	19.7±0.4
Fe K_α line				
Line energy (keV)	6.46±0.01	6.46±0.01	6.46±0.01	6.46±0.01
Eq. width (eV)	81±2	82±3	75±2	75±2
Fe K_β line				
Line energy (keV)	7.13±0.01	7.13±0.01	7.15±0.01	7.15±0.01
Eq. width (eV)	21±2	22±2	14±1	14±1
Cyclotron line				
Line energy (keV)	–	38.9±3.2	–	38.9*
Width (keV)	–	19.3 $^{+6.1}_{-4.3}$	–	9.8 $^{+8.1}_{-5.1}$
Depth	–	0.4±0.1	–	0.1±0.1
Flux ^c (1-10 keV)	2.1±0.1	2.1±0.1	2.1±0.1	2.1±0.1
Flux ^c (10-70 keV)	5.6±0.3	5.7±0.7	5.6±0.2	5.6±0.1
χ^2 (dofs)	1551 (888)	1363 (885)	1389 (888)	1375 (886)

^a : Equivalent hydrogen column density in the source direction (in 10^{22} atoms cm^{-2} units)

^b : Additional hydrogen column density (10^{22} atoms cm^{-2} units),

^c : in 10^{-9} ergs cm^{-2} s^{-1} unit.

* : The values were fixed at the value obtained from spectral fitting with Model-2.

XMM-Newton observations of the source, however, showed the presence of soft X-ray excess over the continuum model in 0.22-0.31, 0.72-0.79 and 0.07-0.17 orbital phase ranges. Apart from the eclipse phase when two soft X-ray excess components were detected, the source showed a single and weak soft X-ray excess during other orbital phases (van der Meer *et al.*, 2005). Though the source was observed with *XMM-Newton* at four epochs, only one observation (in 0.48-0.59 phase range) overlaps partly with the binary orbital phase covered

during *Suzaku* observation. The non-detection of soft X-ray excess during *Suzaku* observation of the source, therefore, can be explained as due to the relatively low sensitivity of *Suzaku* instruments compared to that of *XMM-Newton* to detect the weak soft component in the spectrum.

Apart from the soft X-ray excess, earlier reported absorption like feature at ~ 37 keV in the source spectrum (Reynolds et al. 1999) was also marginally seen in the spectral residuals of all three continuum models in present work. However, the absorption feature was clearly detected when the source spectrum was fitted with partial covering NPEX continuum model. Addition of cyclotron absorption component to the partial covering NPEX continuum model improved the spectral fitting yielding better value of reduced χ^2 which was decreased from 1.75 to 1.54. Energy and width of the cyclotron absorption feature were found to be ~ 39 keV and ~ 19 keV, respectively. The cyclotron absorption component was added to the partial covering HECut that show a marginal improvement in the fitting. The parameters obtained from the spectral fitting of *Suzaku* observation of 4U 1700-37 are given in Table 5.3. The values of relative instrument normalizations of four XISs and HXD/PIN are also given in the table and found to be comparable to that obtained during the detector calibrations. The energy spectra of the source are shown in Figures 5.10 and 5.11 along with the best-fit models of partial covering NPEX model and partial covering HECut model, respectively. The middle and bottom panels in each figure show the residuals to the best-fit models without and with the addition of cyclotron absorption line in the continuum model, respectively.

To check the statistical significance of the absorption feature, F-test routine of *IDL*, *mpftest*¹, was applied on the χ^2 . As in case of 4U 1909+07 (Jaisawal, Naik and Paul, 2013), probability of chance improvement (PCI) was evaluated by considering the χ^2 without and with the cyclotron absorption component in continuum models (Press *et al.*, 1992). The estimated PCI was found to be 3% and 46% after adding the cyclotron component in the partial covering NPEX

¹<http://www.physics.wisc.edu/~craigm/idl/down/mpftest.pro>

and HECut models, respectively. At such high PCI value (46%), the detection of cyclotron absorption feature is statistically insignificant in spectral fitting with partial covering HECut model. Though the PCI value for partial covering NPEX model (3%) suggest the detection of cyclotron absorption feature in the source, the broad width of the feature (~ 19 keV) makes the detection tentative. Considering the different values of PCI obtained for different models, the use of F-test in checking the statistical significance of the presence of cyclotron absorption component in the spectrum of 4U 1700-37 (present case) may not be reliable enough. Observations with high sensitive hard X-ray detectors for long exposures can confirm the presence/absence of cyclotron resonance scattering feature in 4U 1700-37.

5.2.2 Time-resolved spectroscopy

During the *Suzaku* observation of 4U 1700-37, observed source flux was found to be highly variable at different time scales. Several flare like episodes lasting for ~ 10 ks and low flux segments were seen in soft and hard X-ray light curves (Figure 5.8). To probe the changes in spectral parameters during these flaring episodes and low flux segments at such short intervals, we divided the entire observation into 20 segments as marked in the top panel of Figure 5.8. As mentioned earlier, source spectra for these 20 segments were extracted from all four XISs and PIN detectors. For time-resolved spectroscopy, we used same background spectra and response matrices for corresponding detectors that were used for time-averaged spectroscopy. As all three models used in time-averaged spectroscopy well fitted the source spectrum, we choose one of the model e.g. the HECut model to fit the time-resolved spectra. Iron K_α and K_β lines were detected in each of the 20 time-resolved spectra. The best-fit spectral parameters (with 90% errors) obtained from the simultaneous spectral fitting of each of the segments are plotted in Figure 5.12 along with XIS-0 and PIN light curves in left and right top panels, respectively.

The equivalent hydrogen column density N_H was found to be high (7×10^{22} cm $^{-2}$) in the beginning of observation. However, the values of N_H gradually decreased

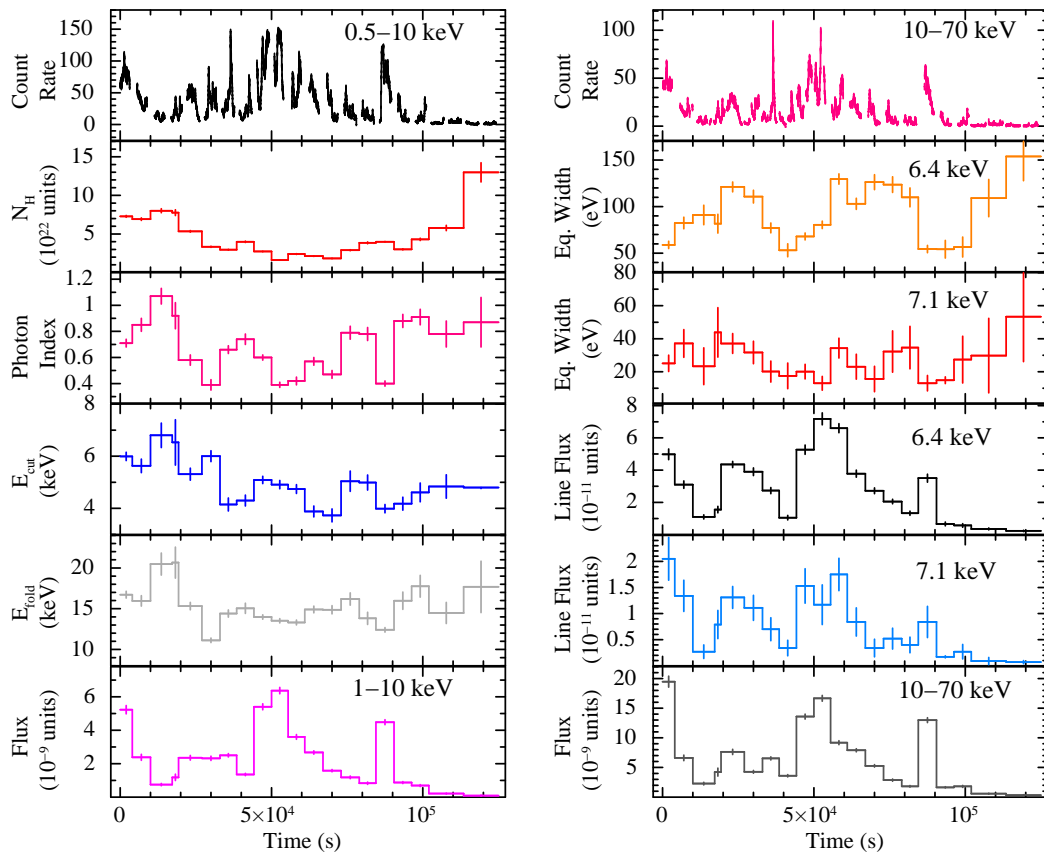


Figure 5.12: Spectral parameters obtained from the time-resolved spectroscopy for *Suzaku* observation of 4U 1700-37. The top panels in both the sides show light curves in 0.5-10 keV (XIS-0) and 10-70 keV (PIN) energy ranges. The values of N_H , power-law photon index, cutoff (E_{cut}) and folding energy (E_{fold}) are shown in second, third, fourth and fifth panels in left side, respectively. The iron emission line parameters such as the equivalent widths and flux in for 6.4 keV and 7.1 keV iron emission lines are shown in second, third, fourth and fifth panels in right side, respectively. The source flux in 1-10 keV (left side) and 10-70 keV (right side) are shown in bottom panels. The errors shown in the figure are estimated for 90% confidence level (Jaisawal and Naik, 2015a).

to a low value beyond which again showed gradual increase during the observation. The systematic and smooth variation of N_H irrespective of source intensity during the *Suzaku* observation suggested the orbital dependence of the matter distribution in 4U 1700-37. This can be confirmed with further long observations of the source with *ASTROSAT* and *NuSTAR* observatories.

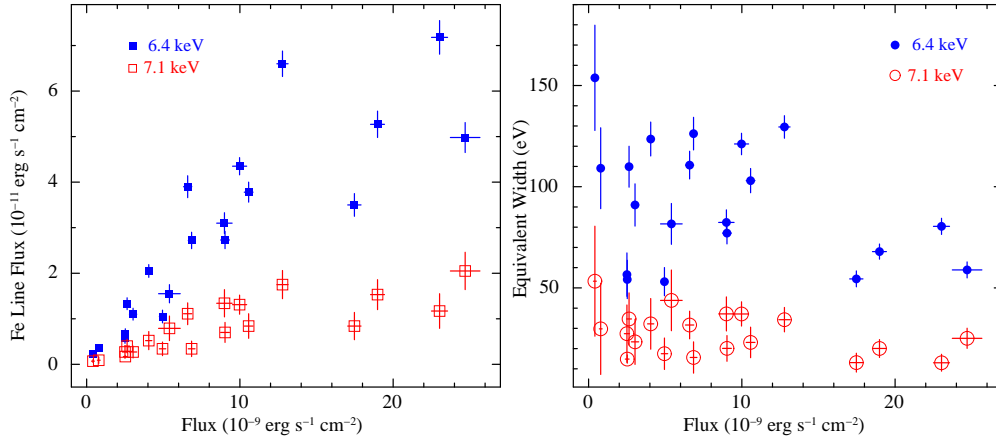


Figure 5.13: Variation in the 6.4 keV and 7.1 keV iron emission line fluxes (left panel) and equivalent widths (right panel) with respect to the estimated flux in the 8-70 keV energy range obtained from time-resolved spectroscopy of *Suzaku* observation of 4U 1700-37.

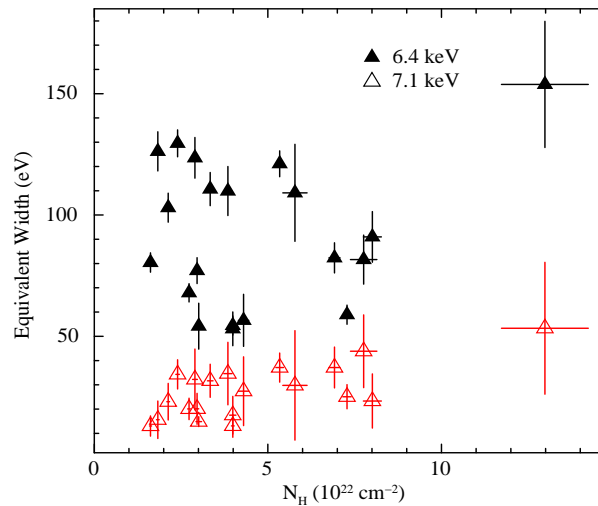


Figure 5.14: Change in the 6.4 keV and 7.1 keV iron line equivalent widths with respect to the column density during the *Suzaku* observation of 4U 1700-37.

A sharp increase in the value of N_H ($13 \times 10^{22} \text{ cm}^{-2}$) was observed during the extended low flux segment towards the end of the observation (after ~ 0.63 orbital phase). The power-law photon index was found to be variable e.g. higher during the low flux segments compared to the flaring episodes.

Flux of Iron K_α and K_β emission lines were found to vary with the source flux whereas the corresponding equivalent widths showed the opposite trend.

Source flux as well as the flux of iron emission lines were found to be low during the extended low flux segment at the end of the observation. The variation in the iron line parameters (flux and equivalent width) with the absorbed source flux in 8-70 keV are plotted in Figure 5.13. Though the flux of both the emission lines increased along with the source flux, flux of K_α line was found to increase faster compared to that of the K_β line. However, the equivalent width of both the lines showed no systematic variation with the source flux though the values were higher at low flux level. Dependence of emission line flux and equivalent width with the source flux indicates the fluorescence origin of the lines from the matter near by the neutron star. Variation of iron emission line flux and equivalent width with hard X-ray continuum flux (8-70 keV) in 4U 1700-37 are found to be similar to that found in LMX X-4 and Her X-1 (Naik & Paul 2003). In case of LMC X-4 and Her X-1, the change in iron line parameters with continuum flux was interpreted as due to the presence of precessing tilted accretion disk causing modification in the geometry and visibility of iron line emitting region in the binary systems. To investigate the geometry in 4U 1700-37 binary system, we plotted the equivalent widths of 6.4 keV and 7.1 keV iron lines with the observed column density in Figure 5.14. The equivalent widths of both the lines are found to be marginally variable with the column density. Similar kind of variation of equivalent width (below of 200 eV) with absorption column density (order of 10^{22} cm⁻²) was seen in Her X-1 and Vela X-1 (Figure 8 of Makishima, 1986). In such configuration, the X-ray source is expected to be surround by inhomogeneously distributed absorbing material that covers a fraction of radiation along the line of sight.

5.3 Results and Discussion

Photons emitted from the magnetic poles of the accretion powered X-ray pulsars interact with matter in the surrounding regions such as accretion column, accretion stream, accretion disk, dust and gas clouds, interstellar medium etc. before reaching the observer. These interactions are reflected in the observed

spectral and timing properties of these objects. Presence of several components such as soft X-ray excess, fluorescent emission lines in the spectrum are attributed to the evidence of accretion disk formation whereas detection of cyclotron absorption features leads to the estimation of surface magnetic field of the neutron star. Fluorescent iron emission lines are seen in the spectra of most of the X-ray pulsars. X-ray photons emitted from the pulsar interact with the ionized/neutral iron atoms emitting characteristic emission lines. These interactions occur at various reprocessing sites such as the atmosphere of companion star, stellar wind stagnated in shock front, accretion disk. Therefore, the investigation of iron emission lines provides powerful tool to understand the characteristics of the accretion plasma and their spatial distribution in extreme physical conditions around the neutron star. Strength of iron emission lines depend on the continuum emission and the density/amount of available line emitting materials. The change in observed values of iron emission line parameters with a short duration over orbital phase implies the presence of inhomogeneously distributed matter over the orbit of the binary pulsar.

The pulsar OAO 1657-415 showed significant flux variability during the *Suzaku* observation in 2011 September. Though the observation was carried out during out-of-eclipse phase of 10.44 d orbital period, there were two elongated segments of low flux levels followed by regions of high flux levels. Similar flux variability was seen in the light curve of another HMXB pulsar Cen X-3 (Naik, Paul and Ali, 2011a) obtained from *Suzaku* observation in 2008 December covering nearly one orbital period. Segments of low and high flux levels occurred more frequently during the *Suzaku* observation of the pulsar. The observed changes in the source flux as well as the value of absorption column density during the *Suzaku* observation of Cen X-3 was found to be comparable to that observed during the *Suzaku* observation of OAO 1657-415. This type of flux variability for extended durations at different orbital phases are rarely seen in HMXB pulsars. The low flux level segments in Cen X-3 were interpreted as due to the presence of additional absorption components compared to that during the segments of high flux levels (Naik, Paul and Ali, 2011a).

Presence of low and high flux levels were also seen in the pulsar 4U 1907+09 during *Suzaku* observations in 2006 and 2007 (Rivers *et al.*, 2010). Though the low flux levels were present in the light curves of both the observations, the one present in 2006 observation was consistent with earlier observations and interpreted as due to the change in whole continuum rather than obscuration/absorption of X-rays due to the presence of additional matter as in later case (Rivers *et al.*, 2010). The argument of presence of clump of matter causing low flux levels (dips) in the light curves during 2007 observation was supported by the enhancement in the value of absorption column density along the line of sight. In our studies, we found the clumpy wind accretion can explain the observed intensity variability in the light curves of OAO 1657-415 (Jaisawal and Naik, 2014).

In our studies, we found the clumpy wind accretion can explain the observed intensity variability in the light curves of OAO 1657-415. However, in 4U 1700-37 these variability was observed on small time scales as compared to OAO 1657-415. According to Bondi and Hoyle (1944), the source luminosity in these wind-fed systems depends on the density and velocity of stellar wind as $L_x \propto \rho v^{-3}$. Therefore, any fluctuations either in density or velocity can produce the variation in source luminosity. Flux variability in time scales of kilo-seconds as seen in 4U 1700-37, were seen in Vela X-1 and OAO 1657-415 and was explained on the basis of clumpy wind with the fluctuating density causing variation in the accretion rate (Kreykenbohm *et al.*, 2008; Odaka *et al.*, 2013). However, the variation of N_H was marginal during flare and non-flare durations. Significantly high value of N_H after orbital phase ~ 0.6 compared to rest of the segments of the *Suzaku* observation confirmed the finding from *EXOSAT* observation of the source. This high N_H value segment (beyond orbital phase of ~ 0.6) was interpreted as due to the passage of the accretion wake between the neutron star and the observer. As the neutron star moves away, the accretion wake which trails behind the neutron star during the whole orbit, crosses the line of sight of the observer at ~ 0.6 orbital phase yielding significantly high value of absorption column density.

Taam and Fryxell (1989) performed simulation to understand the interaction between asymmetric accretion flow from OB stars onto the neutron stars. The results showed that a temporary disk can be formed during the interaction of accretion flow with the shock in accretion wake region. The destruction of temporary accretion disk is associated with the reversal of storage accretion flow that increases the mass accretion rate. The flow reversal occurs in the range of few hours that generates the flares of 15 m to 1 hr time scales as seen in several segments (such as 3, 4, 7, 10 etc. in Figure 5.8). The “flip-flop instability” in the accretion disk can also explain short time flaring activities as observed in 4U 1700-37 (Matsuda *et al.*, 1991). However, in an alternate scenario, the hydrodynamics simulation results for wind-fed sources showed the formation of non-steady accretion wake consisting of dense filaments of compressed gas where the density reaches ~ 100 times more compared to undisturbed stellar wind (Blondin *et al.*, 1990). Accretion of these filaments with fluctuating density may generate the abrupt variation in the X-ray luminosity as observed in the present case.

Suzaku observation of 4U 1700-37 was carried out during out of eclipse phase of the binary. However, an eclipse-like low flux segment was observed towards the end of the observation in 0.63-0.73 orbital phase range. During this segment, an increase in column density was found. The source flux and line flux of both the iron emission lines were decreased to minimum values compared to the rest of the segments of the observation. The presence of dense matter in this orbital phase range can be the possible reason for the eclipse-like segments. Such type of eclipse-like segments (quiescence period) was also observed during *Chandra* observation of 4U 1700-37 around ~ 0.68 orbital phase (Boroson *et al.*, 2003). A significant increase in the column density after phase 0.5 was also reported earlier during the *Copernicus* observation of 4U 1700-37 (Mason, Branduardi and Sanford, 1976). During *EXOSAT* observation, an increasing column density was also noticed after 0.6 orbital phase of the binary (Haberl, White and Kallman, 1989). The sharp increase in the column density at above orbital phase range can be interpreted as the formation of accretion wake as

observed in Vela X-1 (Blondin *et al.*, 1990). Haberl, Aoki and Mavromatakis (1994) also reported the presence of accretion wake based on the temperature difference observed in the soft excess component. However, the spectroscopic evidences confirmed the formation of accretion wake at late orbital phases of binary that blocks the continuum and produces the eclipse like segments (Kaper, Hammerschlag-Hensberge and Zuiderwijk, 1994) which is seen in the present case of 4U 1700-37 (Jaisawal and Naik, 2015a).

Chapter 6

Summary and Future Work

In this thesis, timing and spectral studies of several accretion powered high mass X-ray binary pulsars have been carried out. In case of three Be/X-ray binary pulsars such as EXO 2030+375, Cep X-4 and GX 304-1, evolution of pulse profile with energy and luminosity has been investigated. The effect of cyclotron resonance scattering feature on the beam function was also examined in case of GX 304-1. Phase-averaged and phase-resolved spectral studies of Be/X-ray binary pulsars confirmed that the presence of narrow streams of matter around the neutron star causes absorption dips in the pulse profiles of these pulsars. We have detected fundamental and first harmonics of cyclotron absorption lines, for the first time, in a few X-ray pulsars. In addition, phase-resolved spectroscopy of cyclotron line was also carried out to understand the geometry of the magnetic field around the pulsar. The cause of intensity variability was also investigated in two high mass X-ray binaries OAO 1657-415 and 4U 1700-37. The results obtained from these studied are presented in the preceding Chapters. Summary and future scopes in this subject are described in the current chapter.

6.1 Summary

- In Chapter-2, the pulse profiles of Be/X-ray binary pulsars have been studied at different luminosity levels. The presence of several narrow and prominent absorption dips were found in the pulse profiles of several pulsars. At soft X-rays, these dips were frequently seen in the pulse profiles. However, with increase in energy, the depth of these dips was found to decrease gradually and finally these dips disappeared from the profiles at hard X-rays. In case of EXO 2030+375 which was studied at the peak of a intense Type I outburst in 2007 May, these dips were seen in the pulse profiles up to ~ 70 keV. Dips in the pulse profiles up to ~ 70 keV is rarely seen in the pulse profiles of accretion powered pulsars. Another observation of EXO 2030+375 during a less intense outburst in 2012 May was studied and found that the pulse profiles were relatively simple with an absorption dip up to ~ 40 keV. Energy and luminosity dependence of pulse profiles of Cep X-4 was also investigated by using *Suzaku* observations during its Type I outburst in 2014 June-July. Absorption dip was also clearly seen in the pulse profiles up to ~ 40 keV during both the observations. Beyond this energy, the pulse profile of the pulsar became simple and single-peaked. While in case of another Be/X-ray binary pulsar GX 304-1, the pulse profiles were studied with *Suzaku* at two luminosity levels during its 2010 and 2012 Type I outbursts. The pulse profiles were found to be complicated at soft X-rays due to the presence of multiple absorption dips. A peculiar phase shift of ~ 0.3 was also observed in the pulse profiles at ~ 35 keV during both observations of GX 304-1.

To understand the cause of multiple absorption dips in the pulse profiles, phase-resolved spectroscopy was carried out for each of the observations of all three pulsars EXO 2030+375, Cep X-4 and GX 304-1. Among all spectral parameters, we found that a systematic increase in the value of additional column density at the dip phases of the pulse profiles. This

indicates that the presence of additional absorbing matter in the form of narrow streams at certain pulse phases causes absorption dips at corresponding phases. These narrow streams of matter are phase-locked with the pulsar and co-rotate with along with the neutron star. Magneto Hydrodynamics (MHD) simulations for low magnetic field neutron stars showed that in case of stable accretion, the accreted matter is coupled with the pulsar magnetic field in the form of a single stream of matter through which matter is being deposited at the magnetic poles. In this type of accretion, the source light curve is expected to be smooth. However, in case of unstable accretion, the single accretion stream gets disrupted into several narrow streams which are phase-locked with the pulsar. Therefore, in case of unstable accretion, the source light is expected to be complex (Romanova, Kulkarni and Lovelace, 2008). Photons emitted from the poles of the neutron star interact with these stream causing several narrow absorption dips in the pulse profile. Depending on the density and opacity of matter in these streams, the absorption dips can be observed up to higher energies, as seen during 2007 observation of EXO 2030+375.

While in case of GX 304-1, the absorption dips were seen up to higher energies though the observed values of additional column density at dip phases were low. This suggested that absorption is not the cause of these dips in the pulse profiles of GX 304-1. However, the dips seen in soft X-ray pulse profiles were interpreted as due to the presence of narrow streams of matter that are phase-locked with the pulsar. The hard X-ray dip as seen in the pulse profiles of GX 304-1 was due to the effect of strong cyclotron line detected in the pulsar (see sections 3.3 and 4.2.3). The beam pattern of the pulsar can get changed due to the angular redistribution of X-ray photons by cyclotron resonant scattering in a strong magnetic field causing different shape of pulse profiles around the cyclotron line energy. Simulation results obtained from Schönherr *et al.* (2014) supported the finding of our study.

- Detection of cyclotron absorption features in the spectrum is a direct method to estimate the magnetic field of the accretion powered X-ray pulsars. We have studied several sources in order to search for the fundamental and harmonics of cyclotron absorption lines. Spectral properties of the high mass X-ray binary pulsar 4U 1909+07 were investigated with *Suzaku* and a cyclotron line was detected at ~ 44 keV in the pulsar spectrum. This feature was seen in a model independent manner. The Crab ratio also showed the presence of absorption feature in 40-50 keV energy range. Considering the feature as cyclotron line, corresponding magnetic field of the pulsar was estimated to be 3.8×10^{12} G. The results obtained from our work and a detailed discussion are presented in the section 4.1.1 Chapter-4 of this thesis.

The spectral properties of Cep X-4 were studied at two luminosity levels during 2014 June-July outbursts by using *Suzaku* and *NuSTAR* observations. In addition to earlier known cyclotron absorption line at ~ 28 keV, we discovered the first harmonics of cyclotron line at ~ 45 keV with *Suzaku* at a relatively low luminosity. Generally, the first harmonic of the fundamental cyclotron line is expected at an energy which is twice of the fundamental line energy. However in Cep X-4, it was detected at 1.7 times that of fundamental line energy. With *NuSTAR* observation, performed at higher luminosity phase of the outburst, the first harmonic was detected at ~ 54 keV with fundamental line at ~ 28 keV. Although the energy of first harmonic line changed with luminosity, the coupling factor e.g. the energy ratio between first harmonics and fundamental cyclotron lines, was found to be less than 2. This indicates that line forming regions are at different height of the accretion column or larger viewing angle resulting the coupling factor at < 2 (see sections 4.1.2 and 4.3.1).

SMC X-2 is one of the brightest X-ray pulsar in the Small Magellanic Cloud. The 1-70 keV broadband spectrum of the pulsar was studied for the first time with *NuSTAR* and *Swift*/XRT observations during its 2015

outburst. A cyclotron absorption line at ~ 27 keV was discovered in the pulsar. This feature was seen in a model independent manner and identified as the cyclotron absorption feature. Corresponding magnetic field of the pulsar was estimated to be 2.3×10^{12} G. The energy of cyclotron line was found to be different during all three observation, showing a negative dependence on luminosity (see section 4.1.3). In addition, the properties of cyclotron line in GX 304-1 were investigated with *Suzaku* at two luminosity levels in 2010 and 2012 outbursts. The cyclotron line energy was found to be ~ 53 and 50 keV during first and second observations, respectively. A marginal positive dependence on luminosity of cyclotron line energy was seen. The cause these correlation are discussed in detail in the section 4.3.2.

Phase-resolved spectroscopy of cyclotron absorption line is being performed for Cep X-4, SMC X-2 and GX 304-1 to understand the geometry of magnetic field around the pulsars. We found that the cyclotron line parameters were varying over pulse phases. However, these variations were found to be $< 30\%$ of their phase-averaged values. These results can be explained in terms of local perturbation in the magnetic field or effect of viewing angle of the pulsar.

- In the fifth chapter of this thesis, we investigated the cause of high intensity variability observed in the soft and hard X-ray light curves of two eclipsing high mass X-ray binaries OAO 1657-415 and 4U 1700-37 with *Suzaku*. The light curves of OAO 1657-415 showed an intensity variability on the order of 10 ks time scale. However, short duration and frequent flare-like structures were clearly seen at an order of ks time scale in the light curves of 4U 1700-37. Using time-resolved spectroscopy, we found the evidences that these systems were accreting inhomogeneous matter in the form of clumpy winds and producing variability in the light curves at longer time scales. However, short time variations in the light curves of 4U 1700-37 were explained in terms of temporary disk (see section 5.3).

In addition, the nature of compact object is unclear in 4U 1700-37 binary. We have detected a QPO at ~ 20 mHz which is frequently seen in the accretion powered X-ray pulsars. A marginal detection of cyclotron line at ~ 37 keV is also reported in our study on 4U 1700-37. On the basis of these results, we expect that 4U 1700-37 hosts a neutron star as a compact object.

Clumpy wind model is implemented on these two sources to explain the observed intensity variability in X-ray light curves. Using this, the physical parameters for clumps were estimated for OAO 1657-415. Moreover, we also estimated the iron emission line energies and determined the state of ionization of iron in the line forming regions in OAO 1657-415. It was found that emission region consisted of neutral as well ionized iron atoms. Based on this, the location of the iron emission sites was calculated to be within the accretion radius of OAO 1657-415.

6.2 Scope of future study

In future, I would focus on carrying out extensive studies of cyclotron line properties and its influences on the beam function of the accretion powered X-ray pulsars. With high resolution instruments on-board *NuSTAR* and *ASTROSAT*, I would be able to investigate the broadband continuum spectrum of several rarely studied pulsars. Several projects emerged during this thesis work are listed below.

The pulse profile of a pulsar is a unique feature of its beam pattern. Among accretion powered X-ray binary pulsars, we found that pulse profiles of Be/X-ray binary pulsars are more complicated due to the presence of sharp and narrow absorption dips at several pulse phases. These dips show energy as well as luminosity dependence and thought to be originated due to the presence of matter in form of narrow streams that are phase-locked with the neutron star. Extensive studies of the pulse profiles at various luminosity levels can provide information regarding the physical parameters of such streams. These

dips are generally observed in the pulse profile of pulsars during X-ray outbursts. Studying the pulse profiles with the *RXTE* and *ASTROSAT* at different epochs, we would be able to explore whether there is any limit in the pulsar luminosity beyond which the absorption dips start appearing in the pulse profiles. Recent studies suggest that in case of unstable accretion, the stream of matter splits into several narrow flows which appeared to be phase-locked with the pulsar. As a result, the geometry of accretion column is expected to change. With high timing sensitivity of *ASTROSAT*, such properties of the pulsars can be probed in detail.

Apart from timing properties, the cyclotron absorption line can be searched in the spectra of unexplored/rarely studied sources. *NuSTAR* is the first hard X-ray focusing observatory with unprecedented spectral resolution. Using this, the shape of cyclotron lines can also be studied to probe the asymmetric distribution of magnetic field lines. Simulation results based on the shape of the cyclotron line showed that the line profile depends on several factors such as geometry, opacity and plasma properties. Recently studied with *NuSTAR* revealed the asymmetry in cyclotron line profile of Cep X-4. The shape of cyclotron absorption line profile would be studied for several pulsars to probe the causes of the asymmetry. In addition, the correlation between cyclotron line energy and luminosity would also be studied in detail for other sources. Investigating the cyclotron line energy above and below the critical luminosity can lead towards single theoretical understanding of the causes of these correlations. Phase-resolved spectroscopy of rarely studied X-ray pulsars, as studied in this thesis, can provide important information to understand the pulsar magnetic field as well as complicated processes occurring near the magnetic poles of neutron star.

References

- Ankay, A., Kaper, L., de Bruijne, J.H.J., Dewi, J., Hoogerwerf, R., Savonije, G.J.: 2001, The origin of the runaway high-mass X-ray binary HD 153919/4U1700-37. *Astron. Astrophys.* **370**, 170–175.
- Araya, R.A., Harding, A.K.: 1996, Cyclotron line models for the X-ray pulsar A 0535+26. *Astron. Astrophys. Suppl.* **120**, 183–186.
- Araya, R.A., Harding, A.K.: 1999, Cyclotron Line Features from Near-critical Magnetic Fields: The Effect of Optical Depth and Plasma Geometry. *Astrophys. J.* **517**, 334–354.
- Araya-Góchez, R.A., Harding, A.K.: 2000, Cyclotron-Line Features from Near-critical Fields. II. On the Effect of Anisotropic Radiation Fields. *Astrophys. J.* **544**, 1067–1080.
- Audley, M.D., Nagase, F., Mitsuda, K., Angelini, L., Kelley, R.L.: 2006, ASCA observations of OAO 1657-415 and its dust-scattered X-ray halo. *Mon. Not. Roy. Astron. Soc.* **367**, 1147–1154.
- Baade, W., Zwicky, F.: 1934, Cosmic Rays from Super-novae. *Contributions from the Mount Wilson Observatory, vol. 3, pp.79-83* **3**, 79–83.
- Balona, L.A.: 2000, The Be Phenomenon¹. In: Smith, M.A., Henrichs, H.F., Fabregat, J. (eds.) *IAU Colloq. 175: The Be Phenomenon in Early-Type Stars, Astronomical Society of the Pacific Conference Series* **214**, 1.
- Basko, M.M., Sunyaev, R.A.: 1976, The limiting luminosity of accreting neutron stars with magnetic fields. *Mon. Not. Roy. Astron. Soc.* **175**, 395–417.

- Becker, P.A., Wolff, M.T.: 2005, Spectral Formation in X-Ray Pulsars: Bulk Comptonization in the Accretion Shock. *Astrophys. J.* **630**, 465–488.
- Becker, P.A., Wolff, M.T.: 2007, Thermal and Bulk Comptonization in Accretion-powered X-Ray Pulsars. *Astrophys. J.* **654**, 435–457.
- Becker, P.A., Klochkov, D., Schönherr, G., Nishimura, O., Ferrigno, C., Caballero, I., Kretschmar, P., Wolff, M.T., Wilms, J., Staubert, R.: 2012, Spectral formation in accreting X-ray pulsars: bimodal variation of the cyclotron energy with luminosity. *Astron. Astrophys.* **544**, A123.
- Bhalerao, V., Romano, P., Tomsick, J., Natalucci, L., Smith, D.M., Bellm, E., Boggs, S.E., Chakrabarty, D., Christensen, F.E., Craig, W.W., Fuerst, F., Hailey, C.J., Harrison, F.A., Krivonos, R.A., Lu, T.N., Madsen, K., Stern, D., Younes, G., Zhang, W.: 2015, NuSTAR detection of a cyclotron line in the supergiant fast X-ray transient IGR J17544-2619. *Mon. Not. Roy. Astron. Soc.* **447**, 2274–2281.
- Blondin, J.M., Kallman, T.R., Fryxell, B.A., Taam, R.E.: 1990, Hydrodynamic simulations of stellar wind disruption by a compact X-ray source. *Astrophys. J.* **356**, 591–608.
- Blum, S., Kraus, U.: 2000, Analyzing X-Ray Pulsar Profiles: Geometry and Beam Pattern of Hercules X-1. *Astrophys. J.* **529**, 968–977.
- Bodaghee, A., Tomsick, J.A., Fornasini, F.M., Krivonos, R., Stern, D., Mori, K., Rahoui, F., Boggs, S.E., Christensen, F.E., Craig, W.W., Hailey, C.J., Harrison, F.A., Zhang, W.W.: 2016, NuSTAR Discovery of a Cyclotron Line in the Accreting X-Ray Pulsar IGR J16393-4643. *Astrophys. J.* **823**, 146.
- Boerner, G., Hayakawa, S., Nagase, F., Anzer, U.: 1987, Disk formation at the magnetosphere of wind-fed pulsars - Application to VELA X-1. *Astron. Astrophys.* **182**, 63–70.
- Bondi, H., Hoyle, F.: 1944, On the mechanism of accretion by stars. *Mon. Not. Roy. Astron. Soc.* **104**, 273.

- Bonnet-Bidaud, J.M., Mouchet, M.: 1998, The identification of the transient X-ray pulsar Cepheus X-4 with a Be/X-ray binary. *Astron. Astrophys.* **332**, L9–L12.
- Bonning, E.W., Falanga, M.: 2005, INTEGRAL high energy observations of 2S 0114+65. *Astron. Astrophys.* **436**, L31–L34.
- Boroson, B., Vrtilik, S.D., Kallman, T., Corcoran, M.: 2003, Chandra Grating Spectroscopy of the X-Ray Binary 4U 1700-37 in a Flaring State. *Astrophys. J.* **592**, 516–531.
- Bulik, T., Gondek-Rosińska, D., Santangelo, A., Mihara, T., Finger, M., Cemeljic, M.: 2003, A puzzling paucity of double peaked X-ray pulsars. *Astron. Astrophys.* **404**, 1023–1032.
- Burderi, L., Di Salvo, T., Robba, N.R., La Barbera, A., Guainazzi, M.: 2000, The 0.1-100 KEV Spectrum of Centaurus X-3: Pulse Phase Spectroscopy of the Cyclotron Line and Magnetic Field Structure. *Astrophys. J.* **530**, 429–440.
- Burnard, D.J., Arons, J., Klein, R.I.: 1991, Accretion powered pulsars - Continuum spectra and light curves of settling accretion mounds. *Astrophys. J.* **367**, 575–592.
- Burnard, D.J., Klein, R.I., Arons, J.: 1988, Continuum radiative transfer in X-ray pulsar accretion columns. I - Numerical methods. *Astrophys. J.* **324**, 1001–1009.
- Burrows, D.N., Hill, J.E., Nousek, J.A., Kennea, J.A., Wells, A., Osborne, J.P., Abbey, A.F., Beardmore, A., Mukerjee, K., Short, A.D.T., Chincarini, G., Campana, S., Citterio, O., Moretti, A., Pagani, C., Tagliaferri, G., Giommi, P., Capalbi, M., Tamburelli, F., Angelini, L., Cusumano, G., Bräuning, H.W., Burkert, W., Hartner, G.D.: 2005, The Swift X-Ray Telescope. *Space Sci. Rev.* **120**, 165–195.

- Caballero, I., Kretschmar, P., Santangelo, A., Staubert, R., Klochkov, D., Camero, A., Ferrigno, C., Finger, M.H., Kreykenbohm, I., McBride, V.A., Pottschmidt, K., Rothschild, R.E., Schönherr, G., Segreto, A., Suchy, S., Wilms, J., Wilson, C.A.: 2007, A 0535+26 in the August/September 2005 outburst observed by RXTE and INTEGRAL. *Astron. Astrophys.* **465**, L21–L24.
- Casares, J., Negueruela, I., Ribó, M., Ribas, I., Paredes, J.M., Herrero, A., Simón-Díaz, S.: 2014, A Be-type star with a black-hole companion. *Nature* **505**, 378–381.
- Castor, J.I., Abbott, D.C., Klein, R.I.: 1975, Radiation-driven winds in Of stars. *Astrophys. J.* **195**, 157–174.
- Cemeljic, M., Bulik, T.: 1998, The Influence of Reprocessing in the Column on the Light Curves of Accretion Powered Neutron Stars. **48**, 65–75.
- Chakrabarty, D., Grunsfeld, J.M., Prince, T.A., Bildsten, L., Finger, M.H., Wilson, R.B., Fishman, G.J., Meegan, C.A., Paciesas, W.S.: 1993, Discovery of the Orbit of the X-ray pulsar OAO 1657-415. *Astrophys. J. Lett.* **403**, L33–L37.
- Chakrabarty, D., Wang, Z., Juett, A.M., Lee, J.C., Roche, P.: 2002, The X-Ray Position and Infrared Counterpart of the Eclipsing X-Ray Pulsar OAO 1657-415. *Astrophys. J.* **573**, 789–793.
- Clark, G., Doxsey, R., Li, F., Jernigan, J.G., van Paradijs, J.: 1978, On two new X-ray sources in the SMC and the high luminosities of the Magellanic X-ray sources. *Astrophys. J. Lett.* **221**, L37–L41.
- Clark, J.S., Goodwin, S.P., Crowther, P.A., Kaper, L., Fairbairn, M., Langer, N., Brocksopp, C.: 2002, Physical parameters of the high-mass X-ray binary 4U1700-37. *Astron. Astrophys.* **392**, 909–920.
- Coburn, W., Heindl, W.A., Gruber, D.E., Rothschild, R.E., Staubert, R., Wilms, J., Kreykenbohm, I.: 2001, Discovery of a Cyclotron Resonant

- Scattering Feature in the Rossi X-Ray Timing Explorer Spectrum of 4U 0352+309 (X Persei). *Astrophys. J.* **552**, 738–747.
- Coburn, W., Heindl, W.A., Rothschild, R.E., Gruber, D.E., Kreykenbohm, I., Wilms, J., Kretschmar, P., Staubert, R.: 2002, Magnetic Fields of Accreting X-Ray Pulsars with the Rossi X-Ray Timing Explorer. *Astrophys. J.* **580**, 394–412.
- Coe, M.J.: 2000, Be stars in X-ray binary systems. In: Smith, M.A., Henrichs, H.F., Fabregat, J. (eds.) *IAU Colloq. 175: The Be Phenomenon in Early-Type Stars, Astronomical Society of the Pacific Conference Series* **214**, 656.
- Coe, M.J., Payne, B.J., Longmore, A., Hanson, C.G.: 1988, The optical/IR counterpart to the newly-discovered X-ray source EXO 2030+375. *Mon. Not. Roy. Astron. Soc.* **232**, 865–871.
- Corbet, R.H.D.: 1986, The three types of high-mass X-ray pulsator. *Mon. Not. Roy. Astron. Soc.* **220**, 1047–1056.
- Corbet, R.H.D., Smale, A.P., Menzies, J.W., Branduardi-Raymont, G., Charles, P.A., Mason, K.O., Booth, L.: 1986, Long-term and periodic variability of 4U 1258-61 (GX304-1). *Mon. Not. Roy. Astron. Soc.* **221**, 961–973.
- Corbet, R.H.D., Marshall, F.E., Coe, M.J., Laycock, S., Handler, G.: 2001, The Discovery of an Outburst and Pulsed X-Ray Flux from SMC X-2 Using the Rossi X-Ray Timing Explorer. *Astrophys. J. Lett.* **548**, L41–L44.
- D’Ài, A., Cusumano, G., La Parola, V., Segreto, A., di Salvo, T., Iaria, R., Robba, N.R.: 2011, Evidence for a resonant cyclotron line in IGR J16493-4348 from the Swift-BAT hard X-ray survey. *Astron. Astrophys.* **532**, A73.
- Davidson, K., Ostriker, J.P.: 1973, Neutron-Star Accretion in a Stellar Wind: Model for a Pulsed X-Ray Source. *Astrophys. J.* **179**, 585–598.

- DeCesar, M.E., Boyd, P.T., Pottschmidt, K., Wilms, J., Suchy, S., Miller, M.C.: 2013, The Be/X-Ray Binary Swift J1626.6-5156 as a Variable Cyclotron Line Source. *Astrophys. J.* **762**, 61.
- Devasia, J.: 2014, Absorption in the pulse profiles of accretion powered X-ray pulsars. PhD thesis, Mahatma Gandhi University.
- Devasia, J., James, M., Paul, B., Indulekha, K.: 2011a, RXTE-PCA observations of 1A 1118-61: timing and spectral studies during an outburst. *Mon. Not. Roy. Astron. Soc.* **414**, 1023–1031.
- Devasia, J., James, M., Paul, B., Indulekha, K.: 2011b, Timing and spectral studies of the transient X-ray pulsar GX 304-1 during an outburst. *Mon. Not. Roy. Astron. Soc.* **417**, 348–358.
- Doroshenko, V., Suchy, S., Santangelo, A., Staubert, R., Kreykenbohm, I., Rothschild, R., Pottschmidt, K., Wilms, J.: 2010, RXTE observations of the 1A 1118-61 in an outburst, and the discovery of a cyclotron line. *Astron. Astrophys.* **515**, L1.
- Ebisawa, K., Day, C.S.R., Kallman, T.R., Nagase, F., Kotani, T., Kawashima, K., Kitamoto, S., Woo, J.W.: 1996, X-Ray Spectroscopy of Centaurus X-3 with ASCA over an Eclipse. *Pub. Astron. Soc. Japan* **48**, 425–440.
- Enoto, T., Makishima, K., Terada, Y., Mihara, T., Nakazawa, K., Ueda, T., Dotani, T., Kokubun, M., Nagase, F., Naik, S., Suzuki, M., Nakajima, M., Takahashi, H.: 2008, Suzaku Observations of Hercules X-1: Measurements of the Two Cyclotron Harmonics. *Pub. Astron. Soc. Japan* **60**, S57–S68.
- Feldmeier, A., Oskinova, L., Hamann, W.R.: 2003, X-ray line emission from a fragmented stellar wind. *Astron. Astrophys.* **403**, 217–224.
- Ferrigno, C., Segreto, A., Santangelo, A., Wilms, J., Kreykenbohm, I., Denis, M., Staubert, R.: 2007, INTEGRAL observation of the accreting pulsar GX 1+4. *Astron. Astrophys.* **462**, 995–1005.

- Ferrigno, C., Falanga, M., Bozzo, E., Becker, P.A., Klochkov, D., Santangelo, A.: 2011, 4U 0115+63: phase lags and cyclotron resonant scattering. *Astron. Astrophys.* **532**, A76.
- Forman, W., Jones, C., Cominsky, L., Julien, P., Murray, S., Peters, G., Tananbaum, H., Giacconi, R.: 1978, The fourth Uhuru catalog of X-ray sources. *Astrophys. J. Supplement.* **38**, 357–412.
- Frank, J., King, A., Raine, D.: 1992, *Accretion power in astrophysics.*
- Fürst, F., Kreykenbohm, I., Suchy, S., Barragán, L., Wilms, J., Rothschild, R.E., Pottschmidt, K.: 2011, 4U 1909+07: a well-hidden pearl. *Astron. Astrophys.* **525**, A73.
- Fürst, F., Pottschmidt, K., Kreykenbohm, I., Müller, S., Kühnel, M., Wilms, J., Rothschild, R.E.: 2012, Staring at 4U 1909+07 with Suzaku. *Astron. Astrophys.* **547**, A2.
- Fürst, F., Pottschmidt, K., Wilms, J., Kennea, J., Bachetti, M., Bellm, E., Boggs, S.E., Chakrabarty, D., Christensen, F.E., Craig, W.W., Hailey, C.J., Harrison, F., Stern, D., Tomsick, J.A., Walton, D.J., Zhang, W.: 2014, NuSTAR Discovery of a Cyclotron Line in KS 1947+300. *Astrophys. J. Lett.* **784**, L40.
- Fürst, F., Pottschmidt, K., Miyasaka, H., Bhalerao, V., Bachetti, M., Boggs, S.E., Christensen, F.E., Craig, W.W., Grinberg, V., Hailey, C.J., Harrison, F.A., Kennea, J.A., Rahoui, F., Stern, D., Tendulkar, S.P., Tomsick, J.A., Walton, D.J., Wilms, J., Zhang, W.W.: 2015, Distorted Cyclotron Line Profile in Cep X-4 as Observed by NuSTAR. *Astrophys. J. Lett.* **806**, L24.
- Galloway, D.K., Giles, A.B., Wu, K., Greenhill, J.G.: 2001, Accretion column eclipses in the X-ray pulsars GX 1+4 and RX J0812.4-3114. *Mon. Not. Roy. Astron. Soc.* **325**, 419–425.
- Ghosh, P., Lamb, F.K.: 1978, Disk accretion by magnetic neutron stars. *Astrophys. J. Lett.* **223**, L83–L87.

- Giacconi, R., Gursky, H., Paolini, F.R., Rossi, B.B.: 1962, Evidence for x Rays From Sources Outside the Solar System. *Physical Review Letters* **9**, 439–443.
- Giacconi, R., Gursky, H., Kellogg, E., Schreier, E., Tananbaum, H.: 1971, Discovery of Periodic X-Ray Pulsations in Centaurus X-3 from UHURU. *Astrophys. J. Lett.* **167**, L67.
- Giacconi, R., Murray, S., Gursky, H., Kellogg, E., Schreier, E., Matilsky, T., Koch, D., Tananbaum, H.: 1974, The Third UHURU Catalog of X-Ray Sources. *Astrophys. J. Supplement.* **27**, 37.
- Haberl, F., Aoki, T., Mavromatakis, F.: 1994, The soft component in the X-ray spectrum of 4U 1700-37. *Astron. Astrophys.* **288**.
- Haberl, F., White, N.E., Kallman, T.R.: 1989, An EXOSAT X-ray observation of one orbital cycle of 4U 1700-37/HD 153919. *Astrophys. J.* **343**, 409–425.
- Han, I., Demir, L.: 2009, Valence-electron configuration of Fe, Cr, and Ni in binary and ternary alloys from $K\beta$ -to- $K\alpha$ x-ray intensity ratios. **80(5)**, 052503.
- Harrison, F.A., Craig, W.W., Christensen, F.E., Hailey, C.J., Zhang, W.W., Boggs, S.E., Stern, D., Cook, W.R., Forster, K., Giommi, P., Grefenstette, B.W., Kim, Y., Kitaguchi, T., Koglin, J.E., Madsen, K.K., Mao, P.H., Miyasaka, H., Mori, K., Perri, M., Pivovarov, M.J., Puccetti, S., Rana, V.R., Westergaard, N.J., Willis, J., Zoglauer, A., An, H., Bachetti, M., Barrière, N.M., Bellm, E.C., Bhalerao, V., Brejnholt, N.F., Fuerst, F., Liebe, C.C., Markwardt, C.B., Nynka, M., Vogel, J.K., Walton, D.J., Wik, D.R., Alexander, D.M., Cominsky, L.R., Hornschemeier, A.E., Hornstrup, A., Kaspi, V.M., Madejski, G.M., Matt, G., Molendi, S., Smith, D.M., Tomsick, J.A., Ajello, M., Ballantyne, D.R., Baloković, M., Barret, D., Bauer, F.E., Blandford, R.D., Brandt, W.N., Brenneman, L.W., Chiang, J., Chakrabarty, D., Chenevez, J., Comastri, A., Dufour, F., Elvis, M., Fabian, A.C., Farrah,

- D., Fryer, C.L., Gotthelf, E.V., Grindlay, J.E., Helfand, D.J., Krivonos, R., Meier, D.L., Miller, J.M., Natalucci, L., Ogle, P., Ofek, E.O., Ptak, A., Reynolds, S.P., Rigby, J.R., Tagliaferri, G., Thorsett, S.E., Treister, E., Urry, C.M.: 2013, The Nuclear Spectroscopic Telescope Array (NuSTAR) High-energy X-Ray Mission. *Astrophys. J.* **770**, 103.
- Heindl, W.A., Coburn, W., Gruber, D.E., Pelling, M.R., Rothschild, R.E., Wilms, J., Pottschmidt, K., Staubert, R.: 1999, Discovery of a Third Harmonic Cyclotron Resonance Scattering Feature in the X-Ray Spectrum of 4U 0115+63. *Astrophys. J. Lett.* **521**, L49–L53.
- Heindl, W.A., Coburn, W., Gruber, D.E., Rothschild, R.E., Kreykenbohm, I., Wilms, J., Staubert, R.: 2001, Discovery of a Cyclotron Resonance Scattering Feature in the X-Ray Spectrum of XTE J1946+274. *Astrophys. J. Lett.* **563**, L35–L39.
- Hewish, A., Bell, S.J., Pilkington, J.D.H., Scott, P.F., Collins, R.A.: 1968, Observation of a Rapidly Pulsating Radio Source. *Nature* **217**, 709–713.
- Hutchings, J.B., Thackeray, A.D., Webster, B.L., Andrews, P.J.: 1973, Spectroscopy of HD 153919 (= 2U 1700-37). *Mon. Not. Roy. Astron. Soc.* **163**, 13P–18P.
- Iben, I. Jr.: 1991, Single and binary star evolution. *Astrophys. J. Supplement.* **76**, 55–114.
- Illarionov, A.F., Sunyaev, R.A.: 1975, Why the Number of Galactic X-ray Stars Is so Small? *Astron. Astrophys.* **39**, 185.
- Inoue, H.: 1985, TENMA observations of bright binary X-ray sources. *Space Sci. Rev.* **40**, 317–338.
- Jaisawal, G.K., Naik, S.: 2014, Investigation of iron emission lines in the eclipsing high mass X-ray binary pulsar OAO~1657-415. *Bulletin of the Astronomical Society of India* **42**, 147–164.

- Jaisawal, G.K., Naik, S.: 2015a, Broad-band spectroscopy of the eclipsing high-mass X-ray binary 4U 1700-37 with Suzaku. *Mon. Not. Roy. Astron. Soc.* **448**, 620–628.
- Jaisawal, G.K., Naik, S.: 2015b, Detection of fundamental and first harmonic cyclotron line in X-ray pulsar Cep X-4. *Mon. Not. Roy. Astron. Soc.* **453**, L21–L25.
- Jaisawal, G.K., Naik, S.: 2016, Detection of cyclotron resonance scattering feature in high-mass X-ray binary pulsar SMC X-2. *Mon. Not. Roy. Astron. Soc.* **461**, L97–L101.
- Jaisawal, G.K., Naik, S., Epili, P.: 2016, Suzaku view of the Be/X-ray binary pulsar GX 304-1 during Type I X-ray outbursts. *Mon. Not. Roy. Astron. Soc.* **457**, 2749–2760.
- Jaisawal, G.K., Naik, S., Paul, B.: 2013, Possible Detection of a Cyclotron Resonance Scattering Feature in the X-Ray Pulsar 4U 1909+07. *Astrophys. J.* **779**, 54.
- Jenke, P.A., Finger, M.H., Wilson-Hodge, C.A., Camero-Arranz, A.: 2012, Orbital Decay and Evidence of Disk Formation in the X-Ray Binary Pulsar OAO 1657-415. *Astrophys. J.* **759**, 124.
- Jones, C., Forman, W., Tananbaum, H., Schreier, E., Gursky, H., Kellogg, E., Giacconi, R.: 1973, Evidence for the Binary Nature of 2u 1700-37. *Astrophys. J. Lett.* **181**, L43.
- Kaastra, J.S., Mewe, R.: 1993, X-ray emission from thin plasmas. I - Multiple Auger ionisation and fluorescence processes for Be to Zn. *Astron. Astrophys. Suppl.* **97**, 443–482.
- Kallman, T.R., McCray, R.: 1982, X-ray nebular models. *Astrophys. J. Supplement.* **50**, 263–317.

- Kallman, T.R., Palmeri, P., Bautista, M.A., Mendoza, C., Krolik, J.H.: 2004, Photoionization Modeling and the K Lines of Iron. *Astrophys. J. Supplement.* **155**, 675–701.
- Kaper, L., Hammerschlag-Hensberge, G., Zuiderwijk, E.J.: 1994, Spectroscopic evidence for photo-ionization wakes in VELA X-1 and 4U 1700–37. *Astron. Astrophys.* **289**, 846–854.
- Kiraly, P., Meszaros, P.: 1988, TeV and PeV gamma-ray emission from accreting pulsars. *Astrophys. J.* **333**, 719–728.
- Klochkov, D., Horns, D., Santangelo, A., Staubert, R., Segreto, A., Ferrigno, C., Kretschmar, P., Kreykenbohm, I., La Barbera, A., Masetti, N., McCollough, M., Pottschmidt, K., Schönherr, G., Wilms, J.: 2007, INTEGRAL and Swift observations of EXO 2030+375 during a giant outburst. *Astron. Astrophys.* **464**, L45–L48.
- Klochkov, D., Doroshenko, V., Santangelo, A., Staubert, R., Ferrigno, C., Kretschmar, P., Caballero, I., Wilms, J., Kreykenbohm, I., Pottschmidt, K., Rothschild, R.E., Wilson-Hodge, C.A., Pühlhofer, G.: 2012, Outburst of GX 304-1 monitored with INTEGRAL: positive correlation between the cyclotron line energy and flux. *Astron. Astrophys.* **542**, L28.
- Koyama, K., Kawada, M., Tawara, Y., Kimura, K., Kitamoto, S., Miyamoto, S., Tsunemi, H., Ebisawa, K., Nagase, F.: 1991, A new X-ray pulsar GS 2138 + 56 (Cepheus X-4). *Astrophys. J. Lett.* **366**, L19–L22.
- Koyama, K., Tsunemi, H., Dotani, T., Bautz, M.W., Hayashida, K., Tsuru, T.G., Matsumoto, H., Ogawara, Y., Ricker, G.R., Doty, J., Kissel, S.E., Foster, R., Nakajima, H., Yamaguchi, H., Mori, H., Sakano, M., Hamaguchi, K., Nishiuchi, M., Miyata, E., Torii, K., Namiki, M., Katsuda, S., Matsuura, D., Miyauchi, T., Anabuki, N., Tawa, N., Ozaki, M., Murakami, H., Maeda, Y., Ichikawa, Y., Prigozhin, G.Y., Boughan, E.A., Lamarr, B., Miller, E.D., Burke, B.E., Gregory, J.A., Pillsbury, A., Bamba, A., Hiraga, J.S., Senda,

- A., Katayama, H., Kitamoto, S., Tsujimoto, M., Kohmura, T., Tsuboi, Y., Awaki, H.: 2007, X-Ray Imaging Spectrometer (XIS) on Board Suzaku. *Pub. Astron. Soc. Japan* **59**, 23–33.
- Kraus, U., Nollert, H.P., Ruder, H., Riffert, H.: 1995, Analyzing X-Ray Pulsar Profiles: Asymmetry as a Key to Geometry and Beam Pattern. *Astrophys. J.* **450**, 763.
- Kraus, U., Zahn, C., Weth, C., Ruder, H.: 2003, X-Ray Pulses from Accretion Columns: Contributions to the Energy Dependence of the Pulse Shape. *Astrophys. J.* **590**, 424–431.
- Kretschmar, P.: 1996, Hochenergie-Röntgenspektren der akkretierenden Röntgenpulsare Vela X-1 und A 0535+26. PhD thesis, Eberhard-Karls-Universität Tübingen.
- Kreykenbohm, I., Wilms, J., Coburn, W., Kuster, M., Rothschild, R.E., Heindl, W.A., Kretschmar, P., Staubert, R.: 2004, The variable cyclotron line in GX 301-2. *Astron. Astrophys.* **427**, 975–986.
- Kreykenbohm, I., Wilms, J., Kretschmar, P., Torrejón, J.M., Pottschmidt, K., Hanke, M., Santangelo, A., Ferrigno, C., Staubert, R.: 2008, High variability in Vela X-1: giant flares and off states. *Astron. Astrophys.* **492**, 511–525.
- Kuster, M.: 2004, Combined Spectral and Temporal Analysis of a Her X-1 Turn-On. PhD thesis, Eberhard-Karls-Universität Tübingen.
- La Barbera, A., Burderi, L., Di Salvo, T., Iaria, R., Robba, N.R.: 2001, The 0.1-100 KEV Spectrum of LMC X-4 in the High State: Evidence for a High-Energy Cyclotron Absorption Line. *Astrophys. J.* **553**, 375–381.
- La Palombara, N., Sidoli, L., Pintore, F., Esposito, P., Mereghetti, S., Tiengo, A.: 2016, Spectral analysis of SMC X-2 during its 2015 outburst. *Mon. Not. Roy. Astron. Soc.* **458**, L74–L78.

- Lamb, F.K., Pethick, C.J., Pines, D.: 1973, A Model for Compact X-Ray Sources: Accretion by Rotating Magnetic Stars. *Astrophys. J.* **184**, 271–290.
- Langer, S.H., Rappaport, S.: 1982, Low-luminosity accretion onto magnetized neutron stars. *Astrophys. J.* **257**, 733–751.
- Latal, H.G.: 1986, Cyclotron radiation in strong magnetic fields. *Astrophys. J.* **309**, 372–382.
- Leahy, D.A.: 1991, Modelling observed X-ray pulsar profiles. *Mon. Not. Roy. Astron. Soc.* **251**, 203–212.
- Levine, A.M., Rappaport, S., Remillard, R., Savcheva, A.: 2004, X1908+075: A Pulsar Orbiting in the Stellar Wind of a Massive Companion. *Astrophys. J.* **617**, 1284–1295.
- Lewin, W.H.G., van Paradijs, J., Taam, R.E.: 1993, X-Ray Bursts. *Space Sci. Rev.* **62**, 223–389.
- Lewin, W.H.G., van Paradijs, J., van den Heuvel, E.P.J.: 1995, X-ray binaries. *X-ray Binaries*.
- Li, J., Zhang, S., Torres, D.F., Papitto, A., Chen, Y.P., Wang, J.M.: 2012, INTEGRAL and Swift/XRT observations of IGR J18179-1621. *Mon. Not. Roy. Astron. Soc.* **426**, L16–L20.
- Liu, Q.Z., van Paradijs, J., van den Heuvel, E.P.J.: 2007, A catalogue of low-mass X-ray binaries in the Galaxy, LMC, and SMC (Fourth edition). *Astron. Astrophys.* **469**, 807–810.
- Longair, M.S.: 1994, *High energy astrophysics. Vol.2: Stars, the galaxy and the interstellar medium*.
- Lutovinov, A.A., Tsygankov, S.S., Suleimanov, V.F., Mushtukov, A.A., Doroshenko, V., Nagirner, D.I., Poutanen, J.: 2015, Transient X-ray pul-

- sar V 0332+53: pulse-phase-resolved spectroscopy and the reflection model. *Mon. Not. Roy. Astron. Soc.* **448**, 2175–2186.
- Maitra, C., Paul, B.: 2013a, Pulse-phase-dependent Variations of the Cyclotron Absorption Features of the Accreting Pulsars A0535+26, XTE J1946+274, and 4U 1907+09 with Suzaku. *Astrophys. J.* **771**, 96.
- Maitra, C., Paul, B.: 2013b, Pulse-phase-resolved Spectroscopy of Vela X-1 with Suzaku. *Astrophys. J.* **763**, 79.
- Maitra, C., Paul, B., Naik, S.: 2012, Timing and broad-band spectroscopy of 1A 1118-61 with Suzaku. *Mon. Not. Roy. Astron. Soc.* **420**, 2307–2317.
- Makishima, K.: 1986, Iron Lines from Galactic and Extragalactic X-ray Sources. In: Mason, K.O., Watson, M.G., White, N.E. (eds.) *The Physics of Accretion onto Compact Objects, Lecture Notes in Physics, Berlin Springer Verlag* **266**, 249.
- Makishima, K., Mihara, T., Ishida, M., Ohashi, T., Sakao, T., Tashiro, M., Tsuru, T., Kii, T., Makino, F., Murakami, T., Nagase, F., Tanaka, Y., Kunieda, H., Tawara, Y., Kitamoto, S., Miyamoto, S., Yoshida, A., Turner, M.J.L.: 1990, Discovery of a prominent cyclotron absorption feature from the transient X-ray pulsar X0331 + 53. *Astrophys. J. Lett.* **365**, L59–L62.
- Malacaria, C., Klochkov, D., Santangelo, A., Staubert, R.: 2015, Luminosity-dependent spectral and timing properties of the accreting pulsar GX 304-1 measured with INTEGRAL. *Astron. Astrophys.* **581**, A121.
- Manousakis, A., Beckmann, V., Bianchin, V., Brandt, S., Chenevez, J., Hermsen, W., von Kienlin, A., Krivonos, R., Mas-Hesse, M., Parmar, A., Reglero, V.: 2008, INTEGRAL hard X-ray detection of HMXB GX 304-1 and H 1417-624. *The Astronomer's Telegram* **1613**.
- Manousakis, A., Walter, R., Audard, M., Lanz, T.: 2009, Pulsed thermal emission from the accreting pulsar XMMU J054134.7-682550. *Astron. Astrophys.* **498**, 217–222.

- Mason, A.B., Clark, J.S., Norton, A.J., Crowther, P.A., Tauris, T.M., Langer, N., Negueruela, I., Roche, P.: 2012, The evolution and masses of the neutron star and donor star in the high mass X-ray binary OAO 1657-415. *Mon. Not. Roy. Astron. Soc.* **422**, 199–206.
- Mason, K.O., Branduardi, G., Sanford, P.: 1976, The X-ray behavior of 3U 1700-37. *Astrophys. J. Lett.* **203**, L29–L33.
- Mason, K.O., Murdin, P.G., Parkes, G.E., Visvanathan, N.: 1978, The optical counterpart of GX 304-1. *Mon. Not. Roy. Astron. Soc.* **184**, 45P–48P.
- Matsuda, T., Sekino, N., Sawada, K., Shima, E., Livio, M., Anzer, U., Boerner, G.: 1991, On the stability of wind accretion. *Astron. Astrophys.* **248**, 301–314.
- McBride, V.A., Wilms, J., Coe, M.J., Kreykenbohm, I., Rothschild, R.E., Coburn, W., Galache, J.L., Kretschmar, P., Edge, W.R.T., Staubert, R.: 2006, Study of the cyclotron feature in MXB 0656-072. *Astron. Astrophys.* **451**, 267–272.
- McBride, V.A., Wilms, J., Kreykenbohm, I., Coe, M.J., Rothschild, R.E., Kretschmar, P., Pottschmidt, K., Fisher, J., Hamson, T.: 2007, On the cyclotron line in Cepheus X-4. *Astron. Astrophys.* **470**, 1065–1070.
- McBride, V.A., Coe, M.J., Negueruela, I., Schurch, M.P.E., McGowan, K.E.: 2008, Spectral distribution of Be/X-ray binaries in the Small Magellanic Cloud. *Mon. Not. Roy. Astron. Soc.* **388**, 1198–1204.
- McClintock, J.E., Ricker, G.R., Lewin, W.H.G.: 1971, Rapid Fluctuations in the High-Energy X-Ray Flux from a Source in Crux. *Astrophys. J. Lett.* **166**, L73.
- McClintock, J.E., Nugent, J.J., Li, F.K., Rappaport, S.A.: 1977, Discovery of a 272 second periodic variation in the X-ray source GX 304-1. *Astrophys. J. Lett.* **216**, L15–L18.

- Mendoza, C., Kallman, T.R., Bautista, M.A., Palmeri, P.: 2004, Decay properties of K-vacancy states in Fe X-Fe XVII. *Astron. Astrophys.* **414**, 377–388.
- Meszaros, P.: 1984, Radiation from accreting magnetized neutron stars. *Space Sci. Rev.* **38**, 325–351.
- Meszaros, P.: 1992, *High-energy radiation from magnetized neutron stars*.
- Meszaros, P., Nagel, W.: 1985, X-ray pulsar models. II - Comptonized spectra and pulse shapes. *Astrophys. J.* **299**, 138–153.
- Meszaros, P., Harding, A.K., Kirk, J.G., Galloway, D.J.: 1983, Accreting X-ray pulsar atmospheres heated by Coulomb deceleration of protons. *Astrophys. J. Lett.* **266**, L33–L37.
- Mihara, T.: 1995, Observational study of X-ray spectra of binary pulsars with Ginga. PhD thesis, , Dept. of Physics, Univ. of Tokyo (M95), (1995).
- Mihara, T., Makishima, K., Ohashi, T., Sakao, T., Tashiro, M.: 1990, New observations of the cyclotron absorption feature in Hercules X-1. *Nature* **346**, 250–252.
- Mihara, T., Makishima, K., Kamijo, S., Ohashi, T., Nagase, F., Tanaka, Y., Koyama, K.: 1991, Discovery of a cyclotron resonance feature at 30 keV from the transient X-ray pulsar Cepheus X-4. *Astrophys. J. Lett.* **379**, L61.
- Mitsuda, K., Bautz, M., Inoue, H., Kelley, R.L., Koyama, K., Kunieda, H., Makishima, K., Ogawara, Y., Petre, R., Takahashi, T., Tsunemi, H., White, N.E., Anabuki, N., Angelini, L., Arnaud, K., Awaki, H., Bamba, A., Boyce, K., Brown, G.V., Chan, K.W., Cottam, J., Dotani, T., Doty, J., Ebisawa, K., Ezoe, Y., Fabian, A.C., Figueroa, E., Fujimoto, R., Fukazawa, Y., Furusho, T., Furuzawa, A., Gendreau, K., Griffiths, R.E., Haba, Y., Hamaguchi, K., Harrus, I., Hasinger, G., Hatsukade, I., Hayashida, K., Henry, P.J., Hiraga, J.S., Holt, S.S., Hornschemeier, A., Hughes, J.P., Hwang, U., Ishida, M., Ishisaki, Y., Isobe, N., Itoh, M., Iyomoto, N., Kahn, S.M., Kamae, T., Katagiri, H., Kataoka, J., Katayama, H., Kawai, N., Kilbourne,

- C., Kinugasa, K., Kissel, S., Kitamoto, S., Kohama, M., Kohmura, T., Kokubun, M., Kotani, T., Kotoku, J., Kubota, A., Madejski, G.M., Maeda, Y., Makino, F., Markowitz, A., Matsumoto, C., Matsumoto, H., Matsuoka, M., Matsushita, K., McCammon, D., Mihara, T., Misaki, K., Miyata, E., Mizuno, T., Mori, K., Mori, H., Morii, M., Moseley, H., Mukai, K., Murakami, H., Murakami, T., Mushotzky, R., Nagase, F., Namiki, M., Negoro, H., Nakazawa, K., Nousek, J.A., Okajima, T., Ogasaka, Y., Ohashi, T., Oshima, T., Ota, N., Ozaki, M., Ozawa, H., Parmar, A.N., Pence, W.D., Porter, F.S., Reeves, J.N., Ricker, G.R., Sakurai, I., Sanders, W.T., Senda, A., Serlemitsos, P., Shibata, R., Soong, Y., Smith, R., Suzuki, M., Szymkowiak, A.E., Takahashi, H., Tamagawa, T., Tamura, K., Tamura, T., Tanaka, Y., Tashiro, M., Tawara, Y., Terada, Y., Terashima, Y., Tomida, H., Torii, K., Tsuboi, Y., Tsujimoto, M., Tsuru, T.G., Turner, M.J.L., Ueda, Y., Ueno, S., Ueno, M., Uno, S., Urata, Y., Watanabe, S., Yamamoto, N., Yamaoka, K., Yamasaki, N.Y., Yamashita, K., Yamauchi, M., Yamauchi, S., Yaqoob, T., Yonetoku, D., Yoshida, A.: 2007, The X-Ray Observatory Suzaku. *Pub. Astron. Soc. Japan* **59**, 1–7.
- Morel, T., Grosdidier, Y.: 2005, Near-infrared identification of the counterpart to X1908+075: a new OB-supergiant X-ray binary. *Mon. Not. Roy. Astron. Soc.* **356**, 665–670.
- Motch, C., Janot-Pacheco, E.: 1987, The optical counterpart of the X-ray transient EXO 2030+375. *Astron. Astrophys.* **182**, L55–L58.
- Mukherjee, D., Bhattacharya, D.: 2012, A phase-dependent view of cyclotron lines from model accretion mounds on neutron stars. *Mon. Not. Roy. Astron. Soc.* **420**, 720–731.
- Müller, S., Ferrigno, C., Kühnel, M., Schönherr, G., Becker, P.A., Wolff, M.T., Hertel, D., Schwarm, F.W., Grinberg, V., Obst, M., Caballero, I., Pottschmidt, K., Fürst, F., Kreykenbohm, I., Rothschild, R.E., Hemphill, P., Núñez, S.M., Torrejón, J.M., Klochkov, D., Staubert, R., Wilms, J.:

- 2013, No anticorrelation between cyclotron line energy and X-ray flux in 4U 0115+634. *Astron. Astrophys.* **551**, A6.
- Mushtukov, A.A., Tsygankov, S.S., Serber, A.V., Suleimanov, V.F., Poutanen, J.: 2015a, Positive correlation between the cyclotron line energy and luminosity in sub-critical X-ray pulsars: Doppler effect in the accretion channel. *Mon. Not. Roy. Astron. Soc.* **454**, 2714–2721.
- Mushtukov, A.A., Suleimanov, V.F., Tsygankov, S.S., Poutanen, J.: 2015b, The critical accretion luminosity for magnetized neutron stars. *Mon. Not. Roy. Astron. Soc.* **447**, 1847–1856.
- Nagase, F.: 1989, Accretion-powered X-ray pulsars. *Pub. Astron. Soc. Japan* **41**, 1–79.
- Nagel, W.: 1981a, Radiative Transfer in a Strongly Magnetized Plasma - Part Two - Effects of Comptonization. *Astrophys. J.* **251**, 288.
- Nagel, W.: 1981b, Radiative transfer in a strongly magnetized plasma. I - Effects of anisotropy. II - Effects of Comptonization. *Astrophys. J.* **251**, 278–296.
- Naik, S., Paul, B., Ali, Z.: 2011a, X-Ray Spectroscopy of the High-mass X-Ray Binary Pulsar Centaurus X-3 over Its Binary Orbit. *Astrophys. J.* **737**, 79.
- Naik, S., Dotani, T., Terada, Y., Nakajima, M., Mihara, T., Suzuki, M., Makishima, K., Sudoh, K., Kitamoto, S., Nagase, F., Enoto, T., Takahashi, H.: 2008, Broadband X-Ray Spectroscopy of A0535+262 with Suzaku. *Astrophys. J.* **672**, 516–523.
- Naik, S., Paul, B., Kachhara, C., Vadawale, S.V.: 2011b, Suzaku observation of the transient X-ray pulsar GRO J1008-57. *Mon. Not. Roy. Astron. Soc.* **413**, 241–248.
- Naik, S., Maitra, C., Jaisawal, G.K., Paul, B.: 2013, Timing and Spectral Properties of Be/X-Ray Pulsar EXO 2030+375 during a Type I Outburst. *Astrophys. J.* **764**, 158.

- Nakajima, M., Mihara, T., Makishima, K.: 2010, Energy-Dependent Harmonic Ratios of the Cyclotron Features of X0331+53 in the 2004-2005 Outburst. *Astrophys. J.* **710**, 1755–1768.
- Nakajima, M., Mihara, T., Makishima, K., Niko, H.: 2006, A Further Study of the Luminosity-dependent Cyclotron Resonance Energies of the Binary X-Ray Pulsar 4U 0115+63 with the Rossi X-Ray Timing Explorer. *Astrophys. J.* **646**, 1125–1138.
- Negueruela, I.: 1998, On the nature of Be/X-ray binaries. *Astron. Astrophys.* **338**, 505–510.
- Nelson, R.W., Salpeter, E.E., Wasserman, I.: 1993, Nonthermal Cyclotron Emission from Low-Luminosity Accretion onto Magnetic Neutron Stars. *Astrophys. J.* **418**, 874.
- Nishimura, O.: 2005, Influence of a Non-Dipole Magnetic Field on the Peak Energies of Cyclotron Absorption Lines. *Pub. Astron. Soc. Japan* **57**, 769–778.
- Nishimura, O.: 2013, Superposition of Cyclotron Lines in Accreting X-Ray Pulsars. II. Increasing B-Field. *Pub. Astron. Soc. Japan* **65**.
- Nishimura, O.: 2014, Variations of Cyclotron Line Energy with Luminosity in Accreting X-Ray Pulsars. *Astrophys. J.* **781**, 30.
- Odaka, H., Khangulyan, D., Tanaka, Y.T., Watanabe, S., Takahashi, T., Makishima, K.: 2013, Short-term Variability of X-Rays from Accreting Neutron Star Vela X-1. I. Suzaku Observations. *Astrophys. J.* **767**, 70.
- Orlandini, M., Dal Fiume, D., Frontera, F., Del Sordo, S., Piraino, S., Santangelo, A., Segreto, A., Oosterbroek, T., Parmar, A.N.: 1998, BEPOSAX Observation of 4U 1626-67: Discovery of an Absorption Cyclotron Resonance Feature. *Astrophys. J. Lett.* **500**, L163–L166.

- Orlandini, M., dal Fiume, D., del Sordo, S., Frontera, F., Parmar, A.N., Santangelo, A., Segreto, A.: 1999, The broad-band spectrum of OAO1657-415 with it BeppoSAX: in search of cyclotron lines. *Astron. Astrophys.* **349**, L9–L12.
- Orlandini, M., Frontera, F., Masetti, N., Sguera, V., Sidoli, L.: 2012, BeppoSAX Observations of the X-Ray Pulsar MAXI J1409-619 in Low State: Discovery of Cyclotron Resonance Features. *Astrophys. J.* **748**, 86.
- Oskinova, L.M., Hamann, W.R., Feldmeier, A.: 2007, Neglecting the porosity of hot-star winds can lead to underestimating mass-loss rates. *Astron. Astrophys.* **476**, 1331–1340.
- Palmeri, P., Mendoza, C., Kallman, T.R., Bautista, M.A., Meléndez, M.: 2003, Modeling of iron K lines: Radiative and Auger decay data for Fe II-Fe IX. *Astron. Astrophys.* **410**, 359–364.
- Parkes, G.E., Murdin, P.G., Mason, K.O.: 1980, The shell spectrum of the optical counterpart of GX 304-1 /4U 1258-61/. *Mon. Not. Roy. Astron. Soc.* **190**, 537–542.
- Parmar, A.N., White, N.E., Stella, L., Izzo, C., Ferri, P.: 1989, The transient 42 second X-ray pulsar EXO 2030+375. I - The discovery and the luminosity dependence of the pulse period variations. *Astrophys. J.* **338**, 359–372.
- Paul, B., Naik, S.: 2011, Transient High Mass X-ray Binaries. *Bulletin of the Astronomical Society of India* **39**, 429–449.
- Pietsch, W., Oegelman, H., Kahabka, P., Collmar, W., Gottwald, M.: 1986, EXOSAT observations of GX 304-1 in an X-ray off state. *Astron. Astrophys.* **163**, 93–96.
- Polidan, R.S., Pollard, G.S.G., Sanford, P.W., Locke, M.C.: 1978, X-ray emission from the companion to V861Sco. *Nature* **275**, 296.
- Porter, J.M., Rivinius, T.: 2003, Classical Be Stars. *Pub. Astron. Soc. Pac.* **115**, 1153–1170.

- Pottschmidt, K., Suchy, S., Rivers, E., Rothschild, R.E., Marcu, D.M., Baragán, L., Kühnel, M., Fürst, F., Schwarm, F., Kreykenbohm, I., Wilms, J., Schönherr, G., Caballero, I., Camero-Arranz, A., Bodaghee, A., Doroshenko, V., Klochkov, D., Santangelo, A., Staubert, R., Kretschmar, P., Wilson-Hodge, C., Finger, M.H., Terada, Y.: 2012, A Suzaku view of cyclotron line sources and candidates. In: Petre, R., Mitsuda, K., Angelini, L. (eds.) *American Institute of Physics Conference Series, American Institute of Physics Conference Series* **1427**, 60–67.
- Poutanen, J., Mushtukov, A.A., Suleimanov, V.F., Tsygankov, S.S., Nagirner, D.I., Doroshenko, V., Lutovinov, A.A.: 2013, A Reflection Model for the Cyclotron Lines in the Spectra of X-Ray Pulsars. *Astrophys. J.* **777**, 115.
- Press, W.H., Teukolsky, S.A., Vetterling, W.T., Flannery, B.P.: 1992, *Numerical recipes in C. The art of scientific computing*.
- Priedhorsky, W.C., Terrell, J.: 1983, Long-term X-ray observations of CEN X-3, GX 301-2 (4U 1223-62), GX 304-1 (4U 1258-61) and 4U 1145-61. *Astrophys. J.* **273**, 709–715.
- Pringle, J.E.: 1981, Accretion discs in astrophysics. *ARA&A* **19**, 137–162.
- Protassov, R., van Dyk, D.A., Connors, A., Kashyap, V.L., Siemiginowska, A.: 2002, Statistics, Handle with Care: Detecting Multiple Model Components with the Likelihood Ratio Test. *Astrophys. J.* **571**, 545–559.
- Reig, P.: 2011, Be/X-ray binaries. *Astrophys. Space Sci.* **332**, 1–29.
- Reig, P., Coe, M.J.: 1999, X-ray spectral properties of the pulsar EXO 2030+375 during an outburst. *Mon. Not. Roy. Astron. Soc.* **302**, 700–706.
- Reig, P., Roche, P.: 1999, Discovery of two new persistent Be/X-ray pulsar systems. *Mon. Not. Roy. Astron. Soc.* **306**, 100–106.
- Reynolds, A.P., Parmar, A.N., White, N.E.: 1993, The luminosity dependence of the X-ray spectrum of the transient 42 second pulsar EXO 2030 + 375. *Astrophys. J.* **414**, 302–309.

- Rivers, E., Markowitz, A., Pottschmidt, K., Roth, S., Barragán, L., Fürst, F., Suchy, S., Kreykenbohm, I., Wilms, J., Rothschild, R.: 2010, A Comprehensive Spectral Analysis of the X-Ray Pulsar 4U 1907+09 from Two Observations with the Suzaku X-ray Observatory. *Astrophys. J.* **709**, 179–190.
- Rodes-Roca, J.J., Torrejón, J.M., Kreykenbohm, I., Martínez Núñez, S., Camero-Arranz, A., Bernabéu, G.: 2009, The first cyclotron harmonic of 4U 1538-52. *Astron. Astrophys.* **508**, 395–400.
- Romanova, M.M., Kulkarni, A.K., Lovelace, R.V.E.: 2008, Unstable Disk Accretion onto Magnetized Stars: First Global Three-dimensional Magnetohydrodynamic Simulations. *Astrophys. J. Lett.* **673**, L171.
- Rubin, B.C., Finger, M.H., Harmon, B.A., Paciesas, W.S., Fishman, G.J., Wilson, R.B., Wilson, C.A., Brock, M.N., Briggs, M.S., Pendleton, G.N., Cominsky, L.R., Roberts, M.S.: 1996, Observations of 4U 1700-37 with BATSE. *Astrophys. J.* **459**, 259.
- Schmidtke, P.C., Cowley, A.P., Udalski, A.: 2006, An Investigation of Be/X-Ray Pulsars with OGLE-III Data. *Astron. J.* **132**, 971–975.
- Schönherr, G., Wilms, J., Kretschmar, P., Kreykenbohm, I., Santangelo, A., Rothschild, R.E., Coburn, W., Staubert, R.: 2007, A model for cyclotron resonance scattering features. *Astron. Astrophys.* **472**, 353–365.
- Schönherr, G., Schwarm, F.W., Falkner, S., Dauser, T., Ferrigno, C., Kühnel, M., Klochkov, D., Kretschmar, P., Becker, P.A., Wolff, M.T., Pottschmidt, K., Falanga, M., Kreykenbohm, I., Fürst, F., Staubert, R., Wilms, J.: 2014, Formation of phase lags at the cyclotron energies in the pulse profiles of magnetized, accreting neutron stars. *Astron. Astrophys.* **564**, L8.
- Schurch, M.P.E., Coe, M.J., McBride, V.A., Townsend, L.J., Udalski, A., Haberl, F., Corbet, R.H.D.: 2011, Orbital period determinations for four SMC Be/X-ray binaries. *Mon. Not. Roy. Astron. Soc.* **412**, 391–400.

- Serlemitsos, P.J., Soong, Y., Chan, K.W., Okajima, T., Lehan, J.P., Maeda, Y., Itoh, K., Mori, H., Iizuka, R., Itoh, A., Inoue, H., Okada, S., Yokoyama, Y., Itoh, Y., Ebara, M., Nakamura, R., Suzuki, K., Ishida, M., Hayakawa, A., Inoue, C., Okuma, S., Kubota, R., Suzuki, M., Osawa, T., Yamashita, K., Kunieda, H., Tawara, Y., Ogasaka, Y., Furuzawa, A., Tamura, K., Shibata, R., Haba, Y., Naitou, M., Misaki, K.: 2007, The X-Ray Telescope onboard Suzaku. *Pub. Astron. Soc. Japan* **59**, 9–21.
- Shakura, N.I., Sunyaev, R.A.: 1973, Black holes in binary systems. Observational appearance. *Astron. Astrophys.* **24**, 337–355.
- Slettebak, A.: 1988, The Be stars. *Pub. Astron. Soc. Pac.* **100**, 770–784.
- Staubert, R., Shakura, N.I., Postnov, K., Wilms, J., Rothschild, R.E., Coburn, W., Rodina, L., Klochkov, D.: 2007, Discovery of a flux-related change of the cyclotron line energy in Hercules X-1. *Astron. Astrophys.* **465**, L25–L28.
- Stella, L., White, N.E., Rosner, R.: 1986, Intermittent stellar wind accretion and the long-term activity of Population I binary systems containing an X-ray pulsar. *Astrophys. J.* **308**, 669–679.
- Stollberg, M.T.: 1997, Determining the Orbit of the X-Ray Transient EXO 2030+375 with the Burst and Transient Source Experiment. PhD thesis, UNIVERSITY OF ALABAMA IN HUNTSVILLE.
- Suchy, S., Fürst, F., Pottschmidt, K., Caballero, I., Kreykenbohm, I., Wilms, J., Markowitz, A., Rothschild, R.E.: 2012, Broadband Spectroscopy Using Two Suzaku Observations of the HMXB GX 301-2. *Astrophys. J.* **745**, 124.
- Sugizaki, M., Yamamoto, T., Mihara, T., Nakajima, M., Makishima, K.: 2015, Luminosity and spin-period evolution of GX 304-1 during outbursts from 2009 to 2013 observed with the MAXI/GSC, RXTE/PCA, and Fermi/GBM. *Pub. Astron. Soc. Japan* **67**, 73.
- Sun, X.J., Li, T.P., Wu, M., Cheng, L.X.: 1994, The X-ray spectrum of EXO 2030 + 375. *Astron. Astrophys.* **289**, 127–130.

- Taam, R.E., Fryxell, B.A.: 1989, Numerical studies of asymmetric adiabatic accretion flow - The effect of velocity gradients. *Astrophys. J.* **339**, 297–313.
- Takahashi, T., Abe, K., Endo, M., Endo, Y., Ezoe, Y., Fukazawa, Y., Hamaya, M., Hirakuri, S., Hong, S., Horii, M., Inoue, H., Isobe, N., Itoh, T., Iyomoto, N., Kamae, T., Kasama, D., Kataoka, J., Kato, H., Kawaharada, M., Kawano, N., Kawashima, K., Kawasoe, S., Kishishita, T., Kitaguchi, T., Kobayashi, Y., Kokubun, M., Kotoku, J., Kouda, M., Kubota, A., Kuroda, Y., Madejski, G., Makishima, K., Masukawa, K., Matsumoto, Y., Mitani, T., Miyawaki, R., Mizuno, T., Mori, K., Mori, M., Murashima, M., Murakami, T., Nakazawa, K., Niko, H., Nomachi, M., Okada, Y., Ohno, M., Oonuki, K., Ota, N., Ozawa, H., Sato, G., Shinoda, S., Sugiho, M., Suzuki, M., Taguchi, K., Takahashi, H., Takahashi, I., Takeda, S., Tamura, K.I., Tamura, T., Tanaka, T., Tanihata, C., Tashiro, M., Terada, Y., Tominaga, S., Uchiyama, Y., Watanabe, S., Yamaoka, K., Yanagida, T., Yonetoku, D.: 2007, Hard X-Ray Detector (HXD) on Board Suzaku. *Pub. Astron. Soc. Japan* **59**, 35–51.
- Tanaka, Y.: 1986, Observations of Compact X-Ray Sources. In: Mihalas, D.Winkler, K.H.A. (eds.) *IAU Colloq. 89: Radiation Hydrodynamics in Stars and Compact Objects, Lecture Notes in Physics, Berlin Springer Verlag* **255**, 198.
- Tarter, C.B., Salpeter, E.E.: 1969, The Interaction of X-Ray Sources with Optically Thick Environments. *Astrophys. J.* **156**, 953.
- Tauris, T.M., van den Heuvel, E.P.J.: 2006, In: Lewin, W.H.G.van der Klis, M. (eds.) *Formation and evolution of compact stellar X-ray sources*, 623–665.
- Tendulkar, S.P., Fürst, F., Pottschmidt, K., Bachetti, M., Bhalerao, V.B., Boggs, S.E., Christensen, F.E., Craig, W.W., Hailey, C.A., Harrison, F.A., Stern, D., Tomsick, J.A., Walton, D.J., Zhang, W.: 2014, NuSTAR Discov-

- ery of a Cyclotron Line in the Be/X-Ray Binary RX J0520.5-6932 during Outburst. *Astrophys. J.* **795**, 154.
- Terada, Y., Mihara, T., Nakajima, M., Suzuki, M., Isobe, N., Makishima, K., Takahashi, H., Enoto, T., Kokubun, M., Kitaguchi, T., Naik, S., Dotani, T., Nagase, F., Tanaka, T., Watanabe, S., Kitamoto, S., Sudoh, K., Yoshida, A., Nakagawa, Y., Sugita, S., Kohmura, T., Kotani, T., Yonetoku, D., Angelini, L., Cottam, J., Mukai, K., Kelley, R., Soong, Y., Bautz, M., Kissel, S., Doty, J.: 2006, Cyclotron Resonance Energies at a Low X-Ray Luminosity: A0535+262 Observed with Suzaku. *Astrophys. J. Lett.* **648**, L139–L142.
- Titarchuk, L.: 1994, Generalized Comptonization models and application to the recent high-energy observations. *Astrophys. J.* **434**, 570–586.
- Townsend, L.J., Coe, M.J., Corbet, R.H.D., Hill, A.B.: 2011, On the orbital parameters of Be/X-ray binaries in the Small Magellanic Cloud. *Mon. Not. Roy. Astron. Soc.* **416**, 1556–1565.
- Townsend, R.H.D., Owocki, S.P., Howarth, I.D.: 2004, Be-star rotation: how close to critical? *Mon. Not. Roy. Astron. Soc.* **350**, 189–195.
- Truemper, J., Pietsch, W., Reppin, C., Voges, W., Staubert, R., Kendziorra, E.: 1978, Evidence for strong cyclotron line emission in the hard X-ray spectrum of Hercules X-1. *Astrophys. J. Lett.* **219**, L105–L110.
- Tsygankov, S.S., Lutovinov, A.A., Serber, A.V.: 2010, Completing the puzzle of the 2004-2005 outburst in V0332+53: the brightening phase included. *Mon. Not. Roy. Astron. Soc.* **401**, 1628–1635.
- Tsygankov, S.S., Lutovinov, A.A., Churazov, E.M., Sunyaev, R.A.: 2006, V0332+53 in the outburst of 2004-2005: luminosity dependence of the cyclotron line and pulse profile. *Mon. Not. Roy. Astron. Soc.* **371**, 19–28.
- Tsygankov, S.S., Lutovinov, A.A., Churazov, E.M., Sunyaev, R.A.: 2007, 4U 0115+63 from RXTE and INTEGRAL data: Pulse profile and cyclotron line energy. *Astronomy Letters* **33**, 368–384.

- Tsygankov, S.S., Lutovinov, A.A., Krivonos, R.A., Molkov, S.V., Jenke, P.J., Finger, M.H., Poutanen, J.: 2016, NuSTAR discovery of a cyclotron absorption line in the transient X-ray pulsar 2S 1553-542. *Mon. Not. Roy. Astron. Soc.* **457**, 258–266.
- Ulmer, M.P., Baity, W.A., Wheaton, W.A., Peterson, L.E.: 1973, New Transient Source, Cepheus X-4, Observed by OSO-7. *Astrophys. J. Lett.* **184**, L117.
- Usui, R., Morii, M., Kawai, N., Yamamoto, T., Mihara, T., Sugizaki, M., Matsuoka, M., Hiroi, K., Ishikawa, M., Isobe, N., Kimura, M., Kitayama, H., Kohama, M., Matsumura, T., Nakahira, S., Nakajima, M., Negoro, H., Serino, M., Shidatsu, M., Sootome, T., Sugimori, K., Suwa, F., Toizumi, T., Tomida, H., Tsuboi, Y., Tsunemi, H., Ueda, Y., Ueno, S., Yamaoka, K., Yamazaki, K., Yoshida, A.: 2012, Outburst of LS V +44 17 Observed by MAXI and RXTE, and Discovery of a Dip Structure in the Pulse Profile. *Pub. Astron. Soc. Japan* **64**.
- van der Meer, A., Kaper, L., di Salvo, T., Méndez, M., van der Klis, M., Barr, P., Trams, N.R.: 2005, XMM-Newton X-ray spectroscopy of the high-mass X-ray binary 4U 1700-37 at low flux. *Astron. Astrophys.* **432**, 999–1012.
- Wang, Y.M., Welter, G.L.: 1981, An analysis of the pulse profiles of the binary X-ray pulsars. *Astron. Astrophys.* **102**, 97–108.
- Wen, L., Remillard, R.A., Bradt, H.V.: 2000, X1908+075: An X-Ray Binary with a 4.4 Day Period. *Astrophys. J.* **532**, 1119–1123.
- Wheaton, W.A., Doty, J.P., Primini, F.A., Cooke, B.A., Dobson, C.A., Goldman, A., Hecht, M., Howe, S.K., Hoffman, J.A., Scheepmaker, A.: 1979, An absorption feature in the spectrum of the pulsed hard X-ray flux from 4U0115 + 63. *Nature* **282**, 240–243.

- White, N.E., Pravdo, S.H.: 1979, The discovery of 38.22 second X-ray pulsations from the vicinity of OAO 1653-40. *Astrophys. J. Lett.* **233**, L121–L124.
- White, N.E., Swank, J.H., Holt, S.S.: 1983, Accretion powered X-ray pulsars. *Astrophys. J.* **270**, 711–734.
- Wilson, C.A., Finger, M.H., Camero-Arranz, A.: 2008, Outbursts Large and Small from EXO 2030+375. *Astrophys. J.* **678**, 1263–1272.
- Yamamoto, T., Sugizaki, M., Mihara, T., Nakajima, M., Yamaoka, K., Matsuoka, M., Morii, M., Makishima, K.: 2011, Discovery of a Cyclotron Resonance Feature in the X-Ray Spectrum of GX 304-1 with RXTE and Suzaku during Outbursts Detected by MAXI in 2010. *Pub. Astron. Soc. Japan* **63**, S751–S757.
- Yamamoto, T., Mihara, T., Sugizaki, M., Nakajima, M., Makishima, K., Sasano, M.: 2014, Firm detection of a cyclotron resonance feature with Suzaku in the X-ray spectrum of GRO J1008-57 during a giant outburst in 2012. *Pub. Astron. Soc. Japan* **66**, 59.
- Yokogawa, J., Torii, K., Kohmura, T., Koyama, K.: 2001, ASCA Identification of SMC X-2 with the 2.37-s Pulsar Discovered by RXTE. *Pub. Astron. Soc. Japan* **53**, 227–231.
- Zeldovich, Y.B., Guseynov, O.H.: 1966, Collapsed Stars in Binaries. *Astrophys. J.* **144**, 840.
- Zel'dovich, Y.B., Shakura, N.I.: 1969, X-Ray Emission Accompanying the Accretion of Gas by a Neutron Star. *Sov. Astron.* **13**, 175.
- Ziolkowski, J.: 2002, Be/X-ray binaries. *Memorie della Societa Astronomica Italiana* **73**, 1038–1038.

List of Publications

A. Refereed Journal Publications included in the Thesis

1. “Detection of Cyclotron Resonance Scattering Feature in High Mass X-ray Binary Pulsar SMC X-2”
Jaisawal, G. K., Naik, S.
2016, *Monthly Notices of Royal Astronomical Society Letters*, **461**, L97
2. “Suzaku view of Be/X-ray binary pulsar GX 304-1 during Type I X-ray outbursts”
Jaisawal, G. K., Naik, S., Epili, P.,
2016, *Monthly Notices of Royal Astronomical Society*, **457**, 2749
3. “Detection of fundamental and first harmonic cyclotron line in X-ray pulsar Cep X-4”
Jaisawal, G. K., Naik, S.
2015, *Monthly Notices of Royal Astronomical Society Letters*, **453**, L21
4. “Suzaku Observation of Be/X-ray Binary Pulsar EXO 2030+375”
Naik, S., Jaisawal, G. K.
2015, *Research in Astronomy and Astrophysics*, **15**, 537
5. “Broadband spectroscopy of the eclipsing high mass X-ray binary 4U 1700-37 with Suzaku”
Jaisawal, G. K., Naik, S.
2015, *Monthly Notices of Royal Astronomical Society*, **448**, 620

6. **“Investigation of Iron Emission Lines in the Eclipsing High Mass X-ray Binary Pulsar OAO 1657-415”**
Jaisawal, G. K., Naik, S.
2014, *Bull. Astr. Soc. India*, **42**, 147
7. **“Possible Detection of a Cyclotron Resonance Scattering Feature in the X-Ray Pulsar 4U 1909+07”**
Jaisawal, G. K., Naik, S., Paul, B.
2013, *The Astrophysical Journal*, **779**, 54
8. **“Timing and spectral properties of Be/X-ray pulsar EXO 2030+375 during a Type I outburst”**
Naik, S., Maitra, C., Jaisawal, G. K., Paul, B.
2013, *The Astrophysical Journal*, **764**, 158

B. Additional Publications

1. **“Broad-band spectroscopy of the transient X-ray binary pulsar KS 1947+300 during 2013 giant outburst: Detection of pulsating soft X-ray excess component”**
Prahlaad, E., Naik, S., Jaisawal, G. K.
2016, *Research in Astronomy and Astrophysics*, **16**, 77
2. **“Detection of a variable QPO at ~ 41 mHz in the Be/X-ray transient pulsar 4U 0115+634”**
Dugair, M. R., Jaisawal, G. K., Naik, S., Jaaffrey, S. N. A.
2013, *Monthly Notices of Royal Astronomical Society*, **434**, 2458

C. Astronomical Circulars & Bulletins

1. **Discovery of eclipses in the X-ray transient IGR J17451-3022**
Jaisawal, G. K., Homan, J., Naik, S., Jonker, P.
2015, *The Astronomers Telegram*, **7361**

2. **Near-infrared and optical photometric observations of symbiotic star Hen 2-468**

Jaisawal, G. K., Naik, S., Kumar, V., Epili, P., Mathew, B., Ganesh, S.

2015, *The Astronomers Telegram*, **6907**

D. Conference Proceedings

1. **Detection of ~ 41 mHz quasi-periodic oscillations in 4U 0115+634 during its outbursts**

Dugair, M. R., Jaisawal, G. K., Naik, S., Jaaffrey, S. N. A.

2013, *Astronomical Society of India Conference Series*, **9**, 115

2. **Transient Be/X-ray binary pulsar EXO 2030+375 at the peak of a normal type I outburst**

Naik, S., Jaisawal, G. K., Maitra, C., Paul, B.

2013, *Astronomical Society of India Conference Series*, **9**, 84

3. **Detection of possible cyclotron resonance scattering feature in the accretion powered X-ray pulsar 4U 1909+07**

Naik, S., Jaisawal, G. K., Paul, B.

2013, *Astronomical Society of India Conference Series*, **9**, 83

E. Presentations at Conferences and Symposia

1. Contributed Oral presentation on ‘Suzaku observations of the Be/X-ray binary pulsar GX 304-1’ at the Astronomical Society of India (ASI) Meet 2016, hosted by Kashmir Univ., Srinagar during May 10-13, 2016.

2. Presented a poster on ‘Timing and spectral studies of high mass X-ray binary 4U 1700-37 with Suzaku’ at ASI 2015 Meeting held at NCRA, Pune during February 17-20, 2015.

3. Presented a poster on 'X-ray properties of the eclipsing high mass X-ray binary pulsar OAO 1657-415' at Asian Winter School 2014, held at JAXA Sagami-hara campus, Japan during January 19-21, 2015.
4. Presented a poster on 'Timing and spectral studies of high mass X-ray binary pulsar 4U 1909+07' at a conference at IUCAA, Pune during March 4-8, 2013.
5. Contributed Oral presentation on 'Detection of possible cyclotron resonance scattering feature in the accretion powered X-ray pulsar 4U 1909+07' at ASI 2013 Meeting held at Trivandrum during February 20 - 22, 2013.

Publications attached with Thesis

1. “Detection of Cyclotron Resonance Scattering Feature in High Mass X-ray Binary Pulsar SMC X-2”
Jaisawal, G. K., Naik, S.
2016, *Monthly Notices of Royal Astronomical Society Letters*, **461**, L97
2. “Detection of fundamental and first harmonic cyclotron line in X-ray pulsar Cep X-4”
Jaisawal, G. K., Naik, S.
2015, *Monthly Notices of Royal Astronomical Society Letters*, **453**, L21
3. “Possible Detection of a Cyclotron Resonance Scattering Feature in the X-Ray Pulsar 4U 1909+07”
Jaisawal, G. K., Naik, S., Paul, B.
2013, *The Astrophysical Journal*, **779**, 54

Detection of cyclotron resonance scattering feature in high-mass X-ray binary pulsar SMC X-2

Gaurava K. Jaisawal^{*} and Sachindra Naik^{*}

Astronomy and Astrophysics Division, Physical Research Laboratory, Navrangapura, Ahmedabad - 380009, Gujarat, India

Accepted 2016 May 23. Received 2016 May 23; in original form 2016 May 4

ABSTRACT

We report broad-band spectral properties of the high-mass X-ray binary pulsar SMC X-2 by using three simultaneous *Nuclear Spectroscopy Telescope Array* and *Swift*/XRT observations during its 2015 outburst. The pulsar was significantly bright, reaching a luminosity up to as high as $\sim 5.5 \times 10^{38} \text{ erg s}^{-1}$ in 1–70 keV range. Spin period of the pulsar was estimated to be 2.37 s. Pulse profiles were found to be strongly luminosity dependent. The 1–70 keV energy spectrum of the pulsar was well described with three different continuum models such as (i) negative and positive power law with exponential cutoff, (ii) *Fermi*-Dirac cutoff power law and (iii) cutoff power-law models. Apart from the presence of an iron line at ~ 6.4 keV, a model independent absorption like feature at ~ 27 keV was detected in the pulsar spectrum. This feature was identified as a cyclotron absorption line and detected for the first time in this pulsar. Corresponding magnetic field of the neutron star was estimated to be $\sim 2.3 \times 10^{12}$ G. The cyclotron line energy showed a marginal negative dependence on the luminosity. The cyclotron line parameters were found to be variable with pulse phase and interpreted as due to the effect of emission geometry or complicated structure of the pulsar magnetic field.

Key words: stars: neutron – pulsars: individual: SMC X-2 – X-rays: stars.

1 INTRODUCTION

Cyclotron absorption lines are the unique features observed in the spectrum of accretion-powered X-ray pulsars with magnetic field of the order of $\sim 10^{12}$ G. These absorption-like features are originated due to the resonant scattering between hard X-ray photons and electrons in quantized energy states (Mészáros 1992). These energy levels, known as Landau levels, are equi-spaced and depend on the strength of the magnetic field. The separation between Landau levels corresponds to the energy of the cyclotron resonance scattering feature and expressed by a relation $E_{\text{cyc}} = 11.6 B_{12} \times (1 + z)^{-1}$ (keV), where B_{12} is the magnetic field in the unit of 10^{12} G and z is the gravitational red-shift. The detection of cyclotron absorption line is therefore an unique method to directly estimate the magnetic field of the accretion-powered X-ray pulsars. Despite abundance of data from several previous X-ray missions, these features are only detected in ~ 25 accretion-powered X-ray pulsars (Pottschmidt et al. 2012 and references therein).

SMC X-2 is one of the brightest transient X-ray pulsar in the Small Magellanic Cloud (SMC). It was discovered with *SAS-3* in 1977 at a luminosity of $8.4 \times 10^{37} \text{ erg s}^{-1}$ in 2–11 keV energy band, assuming a distance of 65 kpc (Clark et al. 1978; Clark, Li & van Paradijs 1979). Since the discovery, the source was observed

with several observatories such as *HEAO*, *Einstein* and *ROSAT*, which established the transient nature of the pulsar (Marshall et al. 1979; Seward & Mitchell 1981; Kahabka & Pietsch 1996). Pulsation at ~ 2.37 s was discovered with the *RXTE* and *ASCA* observations during one of the major X-ray outburst observed in 2000 (Torii et al. 2000; Corbet et al. 2001; Yokogawa et al. 2001). The optical companion discovered by Crampton, Hutchings & Cowley (1978) was later resolved into two early spectral-type stars (Schmidtke, Cowley & Udalski 2006). The *I*-band photometric studies of these stars with Optical Gravitational Lensing Experiment revealed that the northern star is the true optical companion of SMC X-2. This conclusion was derived based on the periodic variability observed in the magnitude (up to 1 mag) at a period of 18.62 ± 0.02 d (Schurch et al. 2011). A similar value of periodicity at 18.38 ± 0.02 d was obtained from the pulse-period evolution studies of the pulsar from *RXTE* observations (Townsend et al. 2011). Observed periodicity of ~ 18.4 d from two different approaches corresponds to orbital period of binary system. McBride et al. (2008) identified the optical companion as a O9.5 III-V emission star.

Since 2000, there was no report of any major X-ray activity (outburst) detected in the pulsar. Recently, an intense X-ray outburst was detected in 2015 September during which the pulsar luminosity reached up to as high as $\sim 10^{38} \text{ erg s}^{-1}$ (Kennea et al. 2015; Negoro et al. 2015). The pulsar spectra obtained from *XMM-Newton* and *Swift*/XRT observations during this outburst were described with cutoff power-law model with a soft blackbody component

^{*} E-mail: gaurava@prl.res.in (GKJ); snaik@prl.res.in (SN)

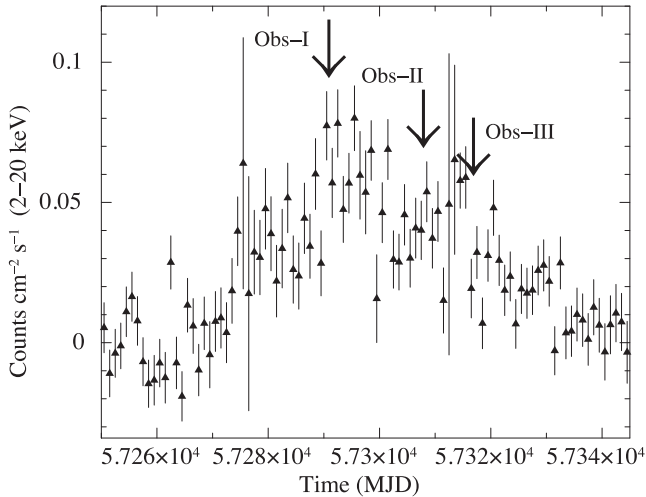


Figure 1. Light curve of the 2015 outburst of SMC X-2, observed with *MAXI* in 2–20 keV energy range covering the duration from 2015 August 16 (MJD 57250) to November 19 (MJD 57345), is shown. Arrows in the figure show the date of *NuSTAR* and *Swift*/XRT observations during the outburst.

at ~ 0.15 keV. In addition to a hard spectrum ($\Gamma \simeq 0$), several emission lines from ionized N, O, Ne, Si and Fe were detected during this outburst (La Palombara et al. 2016). We have studied the 1–70 range energy spectrum of the pulsar by using the *Nuclear Spectroscopy Telescope Array* (*NuSTAR*) and *Swift*/XRT observations during the 2015 outburst. The details on observations, results and conclusions are presented in following sections of this letter.

2 OBSERVATION AND ANALYSIS

Following the report of X-ray outburst, Target of Opportunity (ToO) observations of SMC X-2 were performed with *NuSTAR* (Harrison et al. 2013) at three different epochs in 2015 September – October as shown in Fig. 1. Simultaneous *Swift*/XRT (Burrows et al. 2005) observations were also carried out at these epochs of the outburst. The details of the observations used in this Letter are listed in Table 1. Hereafter, we used Obs-I (ObsIDs: 90102014002 and 00034073002), Obs-II (ObsIDs: 90102014004 and 00081771002) and Obs-III (ObsIDs: 90101017002 and 00034073042) to denote the first, second and third sets of *NuSTAR* and *Swift*/XRT data, respectively.

NuSTAR is the first hard X-ray focusing telescope sensitive in the 3–79 keV energy range. It consists of two independent grazing incident telescopes that focus the photons at two different focal planes, FPMA and FPMB. We have used standard *NuSTAR*DAS software v1.4.1 of HEASoft version 6.16 to generate the barycentric-

Table 1. Log of simultaneous observations of SMC X-2 with *NuSTAR* and *Swift*/XRT.

Observatory/ instrument	ObsID	Start date	Exposure (ks)
<i>NuSTAR</i>	90102014002	2015-09-25T21:51:08	24.5
<i>Swift</i> /XRT	00034073002	2015-09-25T22:32:58	1.8
<i>Swift</i> /XRT	00081771002	2015-10-12T21:30:58	1.5
<i>NuSTAR</i>	90102014004	2015-10-12T21:41:08	23
<i>Swift</i> /XRT	00034073042	2015-10-21T14:08:58	4
<i>NuSTAR</i>	90101017002	2015-10-21T21:31:08	26.7

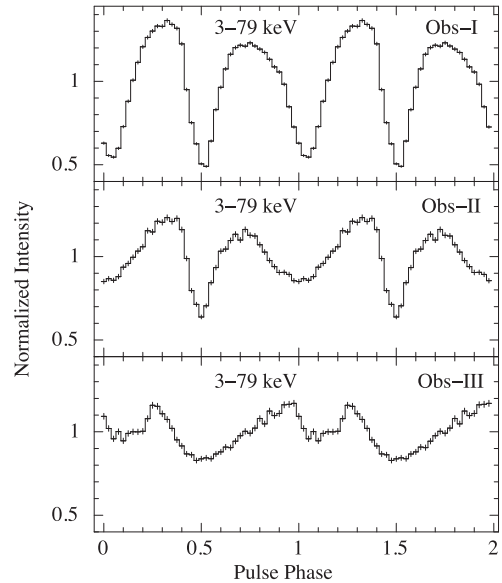


Figure 2. Pulse profiles of SMC X-2 obtained from the background-subtracted light curves of FPMA detector of *NuSTAR* during first, second and third observations, respectively. Luminosity dependence of the pulse profiles can be clearly seen. The error bars in each panel represent 1σ uncertainties. Two pulses in each panel are shown for clarity.

corrected light curves, spectra, response matrices and effective area files. The source light curves and spectra were extracted from the FPMA and FPMB data by selecting a circular region around the source centre. The radii of the circular regions used were 135, 100 and 100 arcsec for first, second and third *NuSTAR* observations, respectively. Background data products were accumulated in a similar manner by selecting circular regions of same size as quoted above and away from the source. We also used the *Swift*/XRT data for spectral analysis below 10 keV. We used the standard *XRTPIPELINE* for reprocessing the XRT data. The source and background spectra were extracted from the window timing mode event by considering the source and background regions in *XSELECT* package. The response file for XRT was generated by using the *XRTMKARF* tool.

3 RESULTS

Source and background light curves from *NuSTAR* data were extracted at 50 ms time resolution. We used the χ^2 -maximization method to estimate the barycentric-corrected pulse period of the pulsar. The pulsation period at 2.371 97(2), 2.371 41(2) and 2.372 57(2) s were detected in the X-ray light curves of the pulsar during Obs-I, Obs-II and Obs-III *NuSTAR* observations, respectively. The error in the pulse period was estimated for 1σ significance level. The pulse profiles in 3–79 keV range were generated by folding the background-subtracted light curves at corresponding estimated spin periods from these observations and shown in Fig. 2. A strong luminosity dependence of the pulse profile can be clearly seen in the figure. During Obs-I (at the peak of the outburst), the pulse profile (top panel of Fig. 2) appeared double-peaked indicating the emissions or viewing of both the poles of the pulsar. However, significantly changed pulse profiles were observed during Obs-II and III (at the declining phase of the X-ray outburst) and are shown in second and third panels of the figure.

3.1 Pulse-phase-averaged spectroscopy

Spectral properties of SMC X-2 in broad energy range (1–70 keV) have been investigated for the first time and reported in this Letter by using data from simultaneous observations with *NuSTAR* (3–70 keV range) and *Swift*/XRT (1–8 keV range). The procedure for spectral extraction was described in previous section. The source spectra were grouped to achieve >20 counts per channel bins. With appropriate background spectra, response matrices and effective area files, simultaneous spectral fitting in 1–70 keV range was carried out by using *Swift*/XRT and *NuSTAR* data for each of the three epochs of observations. XSPEC (ver. 12.8.2) package was used to do the spectral fitting. The spectral parameters were tied together during the fitting except the relative detector normalizations.

Standard continuum models such as high-energy cutoff power law (White, Swank & Holt 1983), the *Fermi*-Dirac cutoff power law (FDCut), the Negative and Positive power law with Exponential cutoff (NPEX; Makishima et al. 1999) and cutoff power law (CutoffPL) were used to fit the pulsar spectrum. We found that NPEX, FDCut and CutoffPL models can explain the pulsar continuum well for all three observations. However, an additional blackbody component was required to fit the source spectra obtained from Obs-II and Obs-III with CutoffPL model. An iron fluorescence emission line at ~ 6.4 keV was detected in the source spectrum. Apart from the iron emission line, an absorption-like feature at ~ 27 keV was also detected in the pulsar spectra obtained from all *NuSTAR* observations. This feature was detected in the source continuum in a model independent manner. We added a Gaussian absorption line (GABS) in the model to explain the absorption feature. The addition of GABS in the model improved the spectral fitting significantly yielding the reduced χ^2 close to 1. The residuals obtained from the spectral fitting with all three models are shown in Figs 3 and 4 for Obs-I and II, respectively. A strong absorption like feature can be clearly visible in 20–30 keV energy range in second, third and fourth panels of the figures. This feature was found to be model independent and clearly detected in all three *NuSTAR* observations. We identified this feature as cyclotron absorption line of the pulsar. Best-fitting parameters from the NPEX continuum model are given in Table 2 for all three observations. It can be seen that the cyclotron line energies during these observations are marginally different, showing a negative dependence on luminosity. The source flux was found to be relatively high during Obs-I compared to that during Obs-II and III. Although the cutoff energy is nearly same during these observations, the photon index is also showing a dependence on luminosity. A hard spectrum with photon index close to zero, i.e. almost flat spectrum, was observed during Obs-I.

3.2 Pulse-phase-resolved spectroscopy

Phase-resolved spectroscopy was performed to understand the variation of the parameters of cyclotron resonance scattering features with the pulse phase of the pulsar. As the pulsar was relatively bright during the first observation, we accumulated the phase-resolved spectra in eight pulse-phase bins from the first *NuSTAR* observation. Using corresponding background, response and effective area files, the phase-resolved spectroscopy was carried out in the 3–70 keV energy range. The NPEX continuum model was used to fit the phase-resolved spectra. The absorption-like feature, as seen in phase-averaged spectra, was also clearly detected in each of the phase-resolved spectra. A GABS component was included in the continuum model for the cyclotron absorption line. While fitting, the equivalent hydrogen column density (N_{H}), iron line parameters

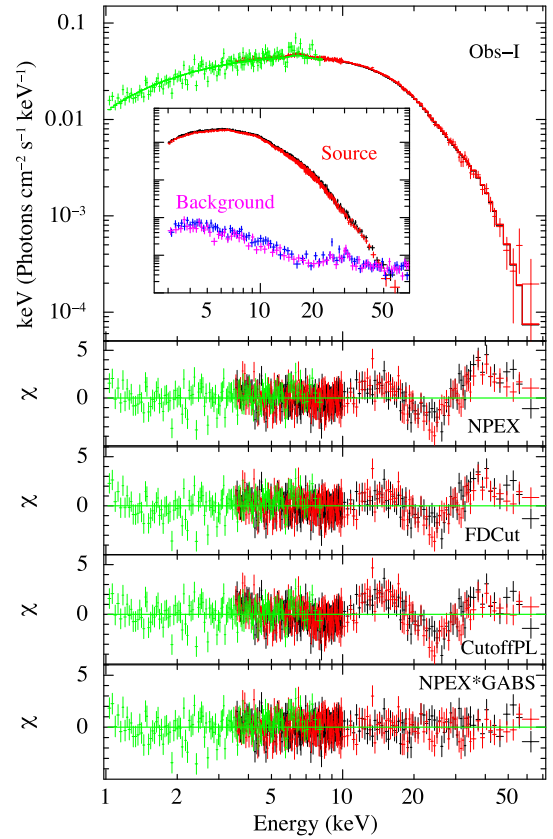


Figure 3. The energy spectrum of SMC X-2 in 1–70 keV range obtained from FPMA and FPMB detectors of *NuSTAR* and *Swift*/XRT data during the first observation along with the best-fitting model comprising an NPEX continuum model with an iron emission line and a Gaussian absorption component for cyclotron resonance scattering feature. The second, third and fourth panels show the contributions of the residuals to χ^2 when pulsar continuum was fitted with NPEX, FDCut and CutoffPL models, respectively. In all these panels, an absorption like feature in 20–30 keV range is clearly visible. The fifth panel shows the residuals for NPEX model after including a GABS component for cyclotron line. The background-subtracted source spectra and background spectra are shown in the inset. It can be seen that the background is relatively much lower than the source counts during the observation.

and cyclotron width were fixed to corresponding phase-averaged values as given in Table 2.

The cyclotron line parameters such as line energy and strength obtained from the phase-resolved spectroscopy are shown in Fig. 5. Both the parameters are marginally variable with pulse-phases of the pulsar. The energy of cyclotron line was found to be variable between 23 and 28 keV (<20 per cent of phase-averaged value) with maximum at around 0.5 pulse phase. The strength of cyclotron line was found to be varying between 4 and 8 and following similar pattern to that of cyclotron line energy. The errors in the figure are estimated for 90 per cent confidence level. We also checked the variation of cyclotron line energy with pulse phase by fixing the line strength at the phase-averaged value and vice versa. However, there was no notable change in the pulse-phase dependence of these parameters apart from a marginal improvement in the estimated errors at each of the pulse phase values.

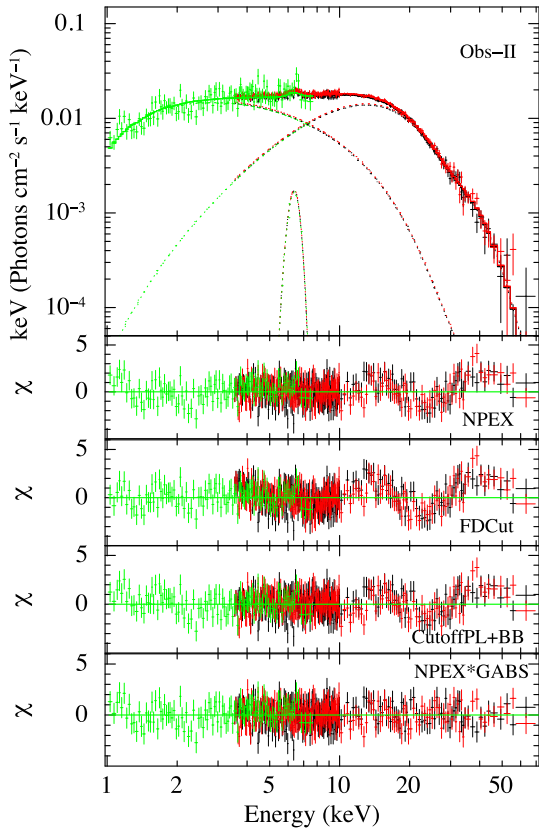


Figure 4. The energy spectrum of SMC X-2 in 1–70 keV range obtained from FPMA and FPMB detectors of *NuSTAR* and *Swift*/XRT data during second observation along with the best-fitting model comprising a NPEX model with an iron emission line and a Gaussian absorption component for a cyclotron line. The second, third and fourth panels show the contributions of the residuals to χ^2 when the continuum was fitted with NPEX, FDCut and CutoffPL (with blackbody) models, respectively. In all these panels, an absorption like feature in 20–30 keV range is clearly visible. The fifth panel shows the residuals for NPEX model after including a GABS component for cyclotron line.

4 DISCUSSION AND CONCLUSIONS

As the magnetic field of accretion-powered binary X-ray pulsars is of the order of 10^{12} G, the cyclotron resonance scattering features

Table 2. Best-fitting parameters (with 90 per cent errors) obtained from the spectral fitting of three *NuSTAR* and *Swift*/XRT observations of SMC X-2 during 2015 outburst with the NPEX continuum model with an iron emission line and cyclotron absorption line.

Parameter	Obs-I		Obs-II		Obs-III	
	NPEX	NPEX×GABS	NPEX	NPEX×GABS	NPEX	NPEX×GABS
N_H^a	$0.1^{+0.03}_{-0.1}$	0.18 ± 0.06	0.7 ± 0.1	0.5 ± 0.1	0.8 ± 0.1	0.6 ± 0.1
Photon index	-0.1 ± 0.02	0.04 ± 0.04	0.78 ± 0.05	0.62 ± 0.08	1.05 ± 0.09	0.81 ± 0.09
E_{cut} (keV)	4.4 ± 0.1	4.8 ± 0.1	4 ± 0.1	4.6 ± 0.2	4 ± 0.1	4.5 ± 0.2
Fe line energy (keV)	6.42 ± 0.08	6.42 ± 0.08	6.32 ± 0.09	6.35 ± 0.08	6.31 ± 0.15	6.34 ± 0.1
Fe line eq. width (eV)	47 ± 10	72 ± 14	88 ± 18	83 ± 18	70 ± 20	70 ± 20
Cycl. line energy (E_c) (keV)	–	27.2 ± 0.9	–	29 ± 1.6	–	$29.8^{+2.7}_{-1.7}$
Cycl. line width (σ_c) (keV)	–	6.4 ± 1.0	–	7 ± 1.5	–	$7.2^{+2.3}_{-1.4}$
Cycl. line strength (τ_c)	–	6 ± 2	–	9^{+5}_{-3}	–	9^{+9}_{-4}
Luminosity ^b (1–70 keV)	–	5.5 ± 0.5	–	2.7 ± 0.3	–	1.8 ± 0.2
Reduced- χ^2 (dofs)	1.55 (582)	1.04 (579)	1.29 (551)	1.02 (548)	1.27 (596)	1.08 (593)

Notes. ^aEquivalent hydrogen column density (in 10^{22} atoms cm^{-2});

^bLuminosity in 10^{38} erg s^{-1} , assuming a distance of 61 kpc (Hilditch, Howarth & Harries 2005).

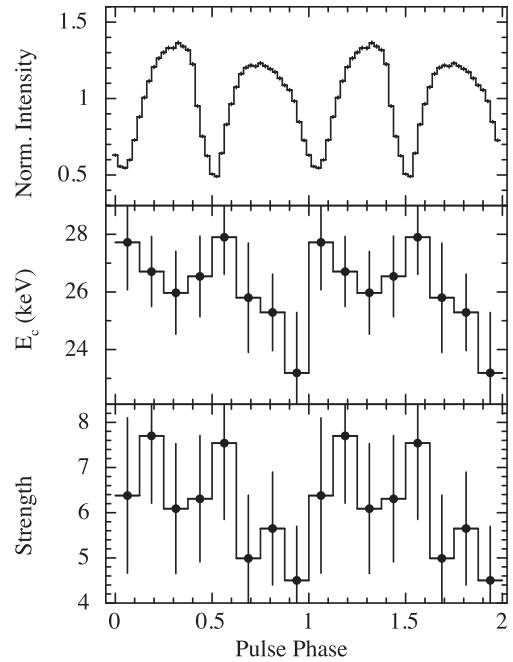


Figure 5. Spectral parameters (with 90 per cent errors) obtained from the phase-resolved spectroscopy of SMC X-2 during first *NuSTAR* observation. Top panel shows the pulse profile in the 3–79 keV energy range. The values of cyclotron line parameter such as energy E_c and strength τ are shown in second and third panels, respectively.

are expected to be detected in hard X-ray (10–100 keV) ranges. Therefore, the possibility of detection of such features in the hard X-ray spectrum becomes high when the source is very bright. During the 2015 giant X-ray outburst, the luminosity of SMC X-2 was estimated to be significantly high ($\sim 5.5 \times 10^{38}$ erg s^{-1}) compared to earlier reported values. This high-luminosity phase of SMC X-2 enabled us to detect the presence of cyclotron resonance scattering feature at ~ 27 keV for the first time in the pulsar spectrum which has not been reported earlier. As mentioned earlier, the cyclotron resonance scattering features are directly related to the magnetic field strength of the pulsar. Corresponding to the detected cyclotron line energy of ~ 27 keV, the magnetic field of SMC X-2 was estimated to be $\sim 2.3 \times 10^{12}$ G. Although the cyclotron lines are rarely detected in the broad-band spectrum of accretion-powered binary

X-ray pulsars, the hard X-ray focusing capability of *NuSTAR* remarkably contributed in the discovery of cyclotron lines in new sources. This helped in increase of the number of cyclotron sources to about 25.

During *NuSTAR* observations, the luminosity of the pulsar was very high ($>10^{38}$ erg s $^{-1}$). It is possible that SMC X-2 was accreting in the supercritical accretion regime during 2015 X-ray outburst. At such high-luminosity state, a radiation-dominated shock can be formed above the neutron star surface which decelerates infalling matter before settling on to the surface (Becker et al. 2012). Cyclotron lines are expected to be formed close to the shock region. As the luminosity increases, the shock region shifted upwards in the accretion column where relatively low value of cyclotron line energy is observed. This results a negative dependence between cyclotron line energy and luminosity. We observed the expected negative correlation during *NuSTAR* observations of SMC X-2. This can be explained in terms of changes in shock height or line forming region with luminosity. Only two X-ray pulsars such as 4U 0115+63 (Nakajima et al. 2006) and V 0332+53 (Tsygankov, Lutovinov & Serber 2010) are known showing such negative correlation.

For the first time, we presented a detailed phase-resolved spectroscopy of cyclotron parameters for SMC X-2. The cyclotron line energy and its strength were found to be marginally variable with pulse-phase of the pulsar. Numerical simulations based on cyclotron line features suggest that the 10–20 per cent variation in the cyclotron line parameters can be attributed to the viewing angle of the emission geometry. However, >30 per cent variation in parameters can be expected from distortion in magnetic dipole geometry of the pulsar (Schönherr et al. 2007; Mukherjee & Bhattacharya 2012). During *NuSTAR* observations, the cyclotron line energy was variable within 20 per cent of the phase-averaged value which can be explained as the effect of viewing angle or local distortion in the magnetic field, as seen in other X-ray binary pulsars such as Cep X-4 (Jaisawal & Naik 2015) and GX 304-1 (Jaisawal, Naik & Epili 2016).

In summary, we report the discovery of cyclotron absorption line at ~ 27 keV in SMC X-2 with *NuSTAR* and *Swift*/XRT observations at three epochs during 2015 X-ray outburst. The cyclotron line was detected in all three observations in a model independent manner. Using the detected cyclotron line parameters, the magnetic field of the pulsar was estimated to be $\sim 2.3 \times 10^{12}$ G. A negative dependence between cyclotron line energy and luminosity in SMC X-2 can be explained as due to the change in the shock height or line forming region with luminosity. The phase-resolved spectroscopy from first *NuSTAR* observation also revealed the presence of cyclotron line at different phases. The pulse-phase variation of the cyclotron parameters can be attributed as the effect of viewing angle or role of complicated magnetic field of the pulsar.

ACKNOWLEDGEMENTS

We sincerely thank the referee for his/her valuable comments and suggestions which improved the Letter. The research work at Phys-

ical Research Laboratory is funded by the Department of Space, Government of India. The authors would like to thank all the *NuSTAR* and *Swift* team members for ToO observations. This research has made use of data from HEASARC Online Service, and the NuSTAR Data Analysis Software (NUSTARDAS) jointly developed by the ASI Science Data Center (ASDC, Italy) and the California Institute of Technology (USA).

REFERENCES

- Becker P. A. et al., 2012, *A&A*, 544, A123
 Burrows D. N. et al., 2005, *Space Sci. Rev.*, 120, 165
 Clark G., Doxsey R., Li F., Jernigan J. G., van Paradijs J., 1978, *ApJ*, 221, L37
 Clark G., Li F., van Paradijs J., 1979, *ApJ*, 227, 54
 Corbet R. H. D., Marshall F. E., Coe M. J., Laycock S., Handler G., 2001, *ApJ*, 548, L41
 Crampton D., Hutchings J. B., Cowley A. P., 1978, *ApJ*, 223, L79
 Harrison F. A. et al., 2013, *ApJ*, 770, 103
 Hilditch R. W., Howarth I. D., Harries T. J., 2005, *MNRAS*, 357, 304
 Jaisawal G. K., Naik S., 2015, *MNRAS*, 453, L21
 Jaisawal G. K., Naik S., Epili P., 2016, *MNRAS*, 457, 2749
 Kahabka P., Pietsch W., 1996, *A&A*, 312, 919
 Kennea J. A. et al., 2015, *Astron. Telegram*, 8091, 1
 La Palombara N., Sidoli L., Pintore F., Esposito P., Mereghetti S., Tiengo A., 2016, *MNRAS*, 458, L74
 Makishima K., Mihara T., Nagase F., Tanaka Y., 1999, *ApJ*, 525, 978
 Marshall F. E., Boldt E. A., Holt S. S., Mushotzky R. F., Pravdo S. H., Rothchild R. E., Serlemitsos P. J., 1979, *ApJS*, 40, 657
 McBride V. A., Coe M. J., Negueruela I., Schurch M. P. E., McGowan K. E., 2008, *MNRAS*, 388, 1198
 Mészáros P., 1992, *High-energy Radiation from Magnetized Neutron Stars*. Univ. Chicago Press, Chicago, IL
 Mukherjee D., Bhattacharya D., 2012, *MNRAS*, 420, 720
 Nakajima M., Mihara T., Makishima K., Niko H., 2006, *ApJ*, 646, 1125
 Negoro H. et al., 2015, *Astron. Telegram*, 8088, 1
 Pottschmidt K. et al., 2012, in Petre R., Mitsuda K., Angelini L., eds, *AIP Conf. Proc. Vol. 1427, Suzaku 2011: Exploring the X-ray Universe: Suzaku and Beyond*. Am. Astron. Soc., Melville, NY, p. 60
 Schmidtke P. C., Cowley A. P., Udalski A., 2006, *AJ*, 132, 971
 Schönherr G., Wilms J., Kretschmar P., Kreykenbohm I., Santangelo A., Rothschild R. E., Coburn W., Stauber R., 2007, *A&A*, 472, 353
 Schurch M. P. E., Coe M. J., McBride V. A., Townsend L. J., Udalski A., Haberl F., Corbet R. H. D., 2011, *MNRAS*, 412, 391
 Seward F. D., Mitchell M., 1981, *ApJ*, 243, 736
 Torii K., Kohmura T., Yokogawa J., Koyama K., 2000, *IAU Circ.*, 7441, 2
 Townsend L. J., Coe M. J., Corbet R. H. D., Hill A. B., 2011, *MNRAS*, 416, 1556
 Tsygankov S. S., Lutovinov A. A., Serber A. V., 2010, *MNRAS*, 401, 1628
 White N. E., Swank J. H., Holt S. S., 1983, *ApJ*, 270, 711
 Yokogawa J., Torii K., Kohmura T., Koyama K., 2001, *PASJ*, 53, 227

This paper has been typeset from a $\text{\TeX}/\text{\LaTeX}$ file prepared by the author.

Detection of fundamental and first harmonic cyclotron line in X-ray pulsar Cep X-4

Gaurava K. Jaisawal^{*} and Sachindra Naik^{*}

Astronomy and Astrophysics Division, Physical Research Laboratory, Navrangapura, Ahmedabad 380009, Gujarat, India

Accepted 2015 July 13. Received 2015 July 10; in original form 2015 June 1

ABSTRACT

We report the broad-band spectral properties of the X-ray pulsar Cep X-4 by using a *Suzaku* observation in 2014 July. The 0.8–70 keV spectrum was found to be well described by three continuum models – Negative and Positive power-law with Exponential cut-off (NPEX), high-energy cut-off power-law and CompTT models. Additional components such as a cyclotron line at ~ 28 keV and two Gaussian components for iron lines at 6.4 and 6.9 keV were required in the spectral fitting. Apart from these, an additional absorption feature at ~ 45 keV was clearly detected in residuals obtained from the spectral fitting. This additional feature at ~ 45 keV was clearly seen in phase-resolved spectra of the pulsar. We identified this feature as the first harmonic of the fundamental cyclotron line at ~ 28 keV. The ratio between the first harmonic and fundamental line energies (1.7) was found to be in disagreement with the conventional factor of 2, indicating that the heights of line-forming regions are different or viewed at larger angles. The phase-resolved spectroscopy of the fundamental and first harmonic cyclotron lines shows significant pulse-phase variation of the line parameters. This can be interpreted as the effect of viewing angle or the role of complicated magnetic field of the pulsar.

Key words: stars: neutron – pulsars: individual: Cep X-4 – X-rays: stars.

1 INTRODUCTION

Cyclotron resonance scattering features (CRSFs) are generally seen in the hard X-ray spectrum (10–100 keV) of the accretion powered X-ray pulsars with surface magnetic field of $\sim 10^{12}$ G. These are absorption like features which appear due to the resonant scattering of photons with electrons in quantized Landau levels (Mészáros 1992). The energy difference between these levels depends on the strength of magnetic field and expressed through the relation $E_{\text{cyc}} = 11.6 B_{12} \times (1 + z)^{-1}$ keV (without relativistic correction), where B_{12} is the magnetic field in the unit of 10^{12} G and z is the gravitational redshift. Detection of fundamental CRSF in the spectra of accretion powered X-ray pulsars provides the direct estimation of local magnetic field of the neutron stars in line-forming region. At the same time, the study of the harmonics (multiples of fundamental cyclotron line) gives crucial information about the optical depth of the line-forming region (Araya-Góchez & Harding 2000; Schönherr et al. 2007; Nishimura 2013). As of now, CRSF has been seen in about 20 accretion powered X-ray pulsars. However, the harmonics of the fundamental cyclotron line are detected only in a few cases (Pottschmidt et al. 2012 and references therein).

The transient X-ray pulsar Cep X-4 (GS 2138+56) was discovered at a position near the galactic plane with *OSO-7* in 1972 (Ulmer et al. 1973). X-ray pulsations were detected in the source at ~ 66 s during its 1988 March outburst with *Ginga* (Makino et al. 1988; Koyama et al. 1991). A cyclotron absorption line feature at ~ 30 keV was discovered in 1.2–37 keV range spectrum obtained from *Ginga* observation of the pulsar (Mihara et al. 1991). An optical star of 14.2 mag was identified as the companion of Cep X-4 (Roche, Green & Hoenig 1997). Detailed optical spectroscopy showed the presence of Balmer emission lines that characterized the companion as Be star of type B1–B2V. The distance of the binary was estimated as 3.8 kpc (Bonnet-Bidaud & Mouchet 1998).

The presence of cyclotron line at ~ 30 keV was confirmed with the 2002 June *RXTE* observations of Cep X-4 (McBride et al. 2007). However, there were no significant changes in cyclotron line energy with source luminosity observed during these observations. The pulsar was observed with *NuSTAR* during the 2014 June–July outburst. First observation was carried out near the peak of the outburst whereas the second was at the declining phase of the outburst (Fürst et al. 2015). The 1–50 keV combined spectra from *Swift*/XRT and *NuSTAR* were described by Fermi–Dirac cut-off power-law (FDCUT) model along with an absorption component at ~ 30 keV. Addition of a simple absorption component or a pseudo-Lorentzian profile was failed to explain the cyclotron absorption feature properly because of the asymmetric nature of the line profile. Along

^{*} E-mail: gaurava@prl.res.in (GKJ); snaik@prl.res.in (SN)

with this asymmetry profile, an absorption like feature at ~ 19 keV was also detected in the spectrum. A marginal positive dependence of cyclotron line energy with the pulsar luminosity was seen during the *NuSTAR* observations.

In this work, we used *Suzaku* observation of the pulsar during 2014 outburst to study its spectral properties. The broad-band coverage and low background capability (up to 70 keV) of detectors onboard *Suzaku* provided best opportunity to investigate cyclotron absorption line parameters in binary X-ray pulsars. Using *Suzaku* observation of Cep X-4, we detected a cyclotron line at ~ 28 keV along with another absorption like feature at ~ 45 keV. We interpret the absorption lines at ~ 28 keV and at ~ 45 keV as the fundamental and first harmonic cyclotron absorption lines, respectively. Details on the observations, analysis procedures, results and conclusions are presented in following sections of this Letter.

2 OBSERVATION AND ANALYSIS

A Target of Opportunity observation of Cep X-4 was carried out with *Suzaku* (Mitsuda et al. 2007) in July 01–02 during its 2014 June–July outburst. The pulsar was observed for exposures of ~ 60 ks with XIS-3 and ~ 81 ks with HXD during the decay phase of the outburst. Among three active XISs (XIS-0, 1 and 3), data from the XIS-3 was used in our analysis as XIS-0 and XIS-1 were exposed for ~ 100 s short durations. The XIS-3 was operated in ‘normal’ clock mode with ‘1/4’ window option yielding 2 s time resolution. The observation was carried out in ‘XIS nominal’ position. We used publicly available data (Obs. ID: 909001010) in the present study. Calibration data base (CALDB) files released on 2015 January 05 (XIS) and 2011 September 13 (HXD) were applied during reprocessing of data in *HEASOFT* (version 6.16) analysis package.

The ‘aepipeline’ task of *FTOOLS* was used to reprocess the unfiltered XIS and HXD events. Clean events generated after the reprocessing were used in our study. Barycentric correction was applied on these XIS and PIN clean events by using ‘aebarycen’ package. XIS data were checked for the attitude and pile-up effects by applying *S-LANG* scripts (*aeattcor.sl* and *pile_estimate.sl*), respectively. We found a pile-up of ~ 8 per cent at the centre of XIS-3 that was reduced to ≤ 4 per cent by choosing the events only from an annulus region with inner and outer radii of 10 and 180 arcsec, respectively. The source light curves and spectra from XIS-3 were extracted by using *XSELECT* package of *FTOOLS*. Background light curves and spectra for XIS-3 were created from a circular region away from the source. Response matrix and effective area files for XIS-3 were generated from ‘resp = yes’ command in *XSELECT*. Source light curves and spectra for PIN were extracted from cleaned event data by using *XSELECT*. However, HXD/PIN background light curves and spectra were accumulated in a similar manner from simulated non-X-ray background event file provided by the instrument team. The cosmic X-ray background correction was included in PIN non-X-ray background spectrum. Epoch 11 PIN response file (20110601) was used in spectral analysis.

3 RESULTS

Source and background light curves with 2 s and 1 s time resolution were extracted from the barycentric corrected XIS-3 and PIN event data, respectively. The χ^2 -maximization technique was used to estimate the pulse period of the pulsar. The pulsation was detected at a period of 66.334 ± 0.004 s from background subtracted light curves of XIS-3 and PIN. Above pulsation period was used to generate pulse profiles in soft (0.5–10 keV) and hard X-rays (10–70 keV)

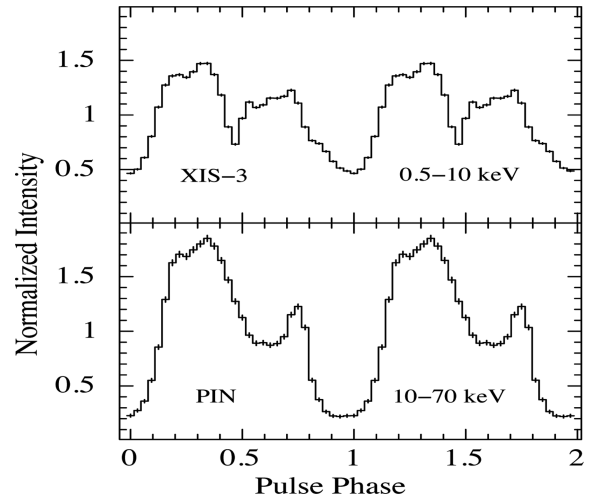


Figure 1. Pulse profiles of Cep X-4 obtained from XIS-3 and HXD/PIN light curves during the *Suzaku* observation in 2014 July. The presence of absorption dip in soft X-ray pulse profile in 0.4–0.5 phase range can be seen. The error bars represent 1σ uncertainties. Two pulses in each panel are shown for clarity.

and are shown in Fig. 1. Strong energy dependence of pulse profiles with energy can be seen in the soft and hard X-rays pulse profiles. A dip like feature in soft X-rays (top panel) in 0.4–0.5 phase range disappeared from the hard X-ray pulse profile. Therefore, it is interesting to investigate spectral properties of the pulsar at different pulse phases.

3.1 Spectral analysis

3.1.1 Pulse-phase-averaged spectroscopy

To study the broad-band spectral characteristics of the pulsar, phase-averaged spectroscopy was carried out by using the source and background spectra accumulated from the XIS-3 and PIN event data. The procedure for spectral extraction was described earlier. The 0.8–70 keV spectra, obtained from XIS-3 and PIN data were simultaneously fitted by using *XSPEC* (ver. 12.8.2) package. Appropriate background spectra, response matrices and effective area files for corresponding detectors were used in the spectral fitting. Spectral data in 1.7–1.9 keV and 2.2–2.4 keV ranges were ignored in the fitting due to presence of known artificial emission features in the spectrum. XIS-3 spectrum was binned by a factor of 6, whereas PIN spectrum was binned by a factor of 2 up to 30 keV, a factor of 4 from 30 to 50 keV and a factor of 6 from 50 to 70 keV. All the spectral parameters were tied during the fitting, except the normalization constant of detectors which were kept free.

Continuum models used to describe spectra of accretion powered X-ray pulsars such as high-energy cut-off power-law (White, Swank & Holt 1983), cut-off power-law, Negative and Positive power-law with Exponential cut-off (NPEX; Makishima et al. 1999), FDCUT and CompTT (Titarchuk 1994) were used to fit the 0.8–70 keV spectrum of Cep X-4. Investigating the residuals, we added two Gaussian functions at 6.4 and 6.9 keV for iron emission lines in the source spectrum. As in case of Be/X-ray binary pulsars, a partial covering absorption component (Paul & Naik 2011 and references therein) was used in the spectral model along with the interstellar absorption component. A strong absorption like feature at ~ 28 keV was clearly seen in the spectrum. Addition of a CRSF component at above energy was added to all continuum models. Simultaneous

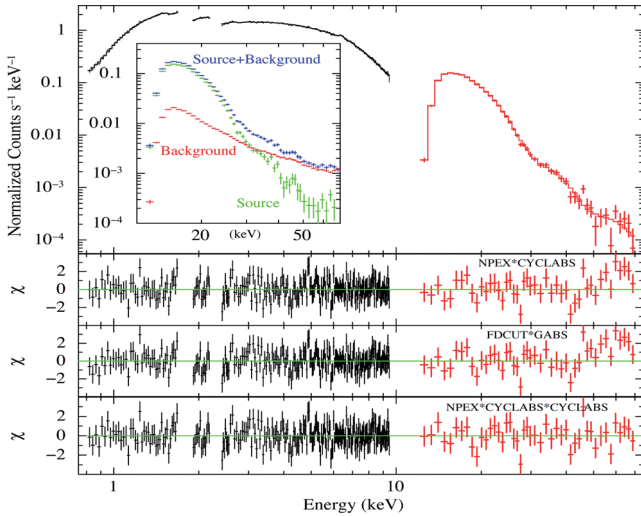


Figure 2. Energy spectrum of Cep X-4 in 0.8–70 keV range obtained from XIS-3 and HDX/PIN data, along with the best-fitting model comprising a partial covering NPEX model, two Gaussian functions for iron emission lines and two cyclotron absorption components. The second and fourth panels show the contributions of the residuals to χ^2 for each energy bin for the partial covering NPEX continuum model with one and two cyclotron absorption components, respectively. The third panel shows the residuals for FDCUT model with one GABS component. The inset shows the HDX/PIN spectrum of the pulsar with background, without background and the simulated HDX/PIN background spectrum.

spectral fitting of XIS-3 and HDX/PIN data in 0.8–70 keV range showed that partial covering NPEX continuum model, partial covering high-energy cut-off power-law model and partial covering CompTT model describe the spectrum well with acceptable values of reduced χ^2 (< 1.5).

Apart from ~ 28 keV cyclotron line, we found an additional absorption like feature at ~ 45 keV in the residues obtained from all three continuum models. This feature was clearly seen at same energy range and was model independent (third panel in Fig. 2). The inset in Fig. 2 shows the HDX/PIN spectrum of the *Suzaku* observation of the pulsar with background, without background and simulated PIN background spectrum. The absorption-like feature at ~ 45 keV can be clearly seen in the background subtracted spectrum. The inclusion of additional CRSF component at this energy in the model fitted the XIS-3 and HDX/PIN spectra well with significant improvement in the values of χ^2 . Absorption feature at ~ 45 keV can be considered as the first harmonic of the ~ 28 keV cyclotron absorption line. Ideally, the ratio between the energy of first cyclotron harmonic and fundamental line is expected to be a value closer to 2. However, in present case, the ratio was estimated to be $\sim 1.7 \pm 0.1$, which can be acceptable in current understanding of the cyclotron physics. Best-fitting parameters obtained from simultaneous spectral fitting are given in Table 1. The energy spectra of the pulsar along with all three best-fitting model components resemble similar absorption features in the spectral residues. Energy spectra obtained from simultaneous fitting of the XIS-3 and HDX/PIN data are shown in Fig. 2. The second and fourth panels in figure show the residuals to the best-fitting model with one and two cyclotron lines in the continuum model, respectively. As in the case of *NuSTAR* observations, a weak absorption like feature can be seen at ~ 19 keV in the spectral residue (third and fourth panels of Fig. 2). Addition of an absorption component at ~ 19 keV, however, did not show any significant improvement in the spectral fitting. Negligible strength

Table 1. Best-fitting parameters (with 90 per cent errors) obtained from the spectral fitting of *Suzaku* observation of Cep X-4 in 2014 July. Model-1 and Model-2 consist of the partial covering NPEX and CompTT model with two Gaussian and two cyclotron lines, respectively. Model-3 is combination of FDCUT model with blackbody, two Gaussian and one *gabs* components.

Parameter	Model-1	Model-2	Model-3
N_{H1}^a	0.78 ± 0.03	0.77 ± 0.03	0.71 ± 0.02
N_{H2}^b	3.7 ± 0.6	2.6 ± 0.3	–
Cov. fraction	0.28 ± 0.06	0.41 ± 0.08	–
Photon index	1.04 ± 0.09	–	1.01 ± 0.05
BB temp. (keV)	–	–	1.08 ± 0.06
BB norm. (10^{-4})	–	–	4.8 ± 0.6
E_{cut} (keV)	9.5 ± 2.1	–	25.1 ± 4.0
E_{fold} (keV)	–	–	6.8 ± 1.1
CompTT $_{70}$ (keV)	–	$0.21^{+0.6}_{-0.21}$	–
CompTT kT (keV)	–	11.6 ± 2.3	–
CompTT τ	–	4.4 ± 0.4	–
<i>Fe line parameters</i>			
Energy (keV)	6.41 ± 0.03	6.41 ± 0.03	6.42 ± 0.03
Eq. width (eV)	32 ± 8	27 ± 7	34 ± 8
Energy (keV)	6.97 ± 0.16	6.98 ± 0.22	6.95 ± 0.14
Eq. width (eV)	13 ± 6	9 ± 6	14 ± 7
<i>Cyc. line parameters</i>			
Energy (E_{c1}) (keV)	27.5 ± 0.4	27.7 ± 0.4	29.6 ± 0.5^d
Width (σ_{c1}) (keV)	8.9 ± 1.0	6.1 ± 0.8	4.8 ± 0.5^d
Depth (D_{c1})	2.3 ± 0.3	1.8 ± 0.3	$17^{+5}_-3^d$
Energy (E_{c2}) (keV)	45.4 ± 2.8	43.0 ± 3.6	–
Width (σ_{c2}) (keV)	10.3 ± 4.6	11.9 ± 4.2	–
Depth (D_{c2})	1.8 ± 0.7	1.8 ± 0.4	–
Flux ^c (1–10 keV)	3.1 ± 0.5	3.1 ± 0.7	3.1 ± 0.4
Flux ^c (10–70 keV)	5.5 ± 1.1	5.6 ± 1.2	5.5 ± 1.4
χ^2 (dofs)	254 (244)	261 (244)	303 (247)

Notes. ^aEquivalent hydrogen column density. ^bAdditional hydrogen column density (in 10^{22} atoms cm^{-2}); ^cabsorption uncorrected flux (in 10^{-10} ergs cm^{-2} s^{-1}); ^dcyclotron parameters are given for *gabs* component.

and width of the ~ 19 keV line against other two absorption lines at ~ 28 and ~ 45 keV, therefore, makes it difficult to accept the earlier feature as the fundamental cyclotron absorption line. Therefore, we did not include any spectral component for this feature in our fitting.

To verify the ~ 45 keV feature as additional absorption feature detected in *Suzaku* spectra, we fitted XIS-3 and HDX/PIN spectra with the spectral model (FDCUT model along with blackbody and Gaussian absorption (*gabs*) components) as used by Fürst et al. (2015) to fit spectra obtained from *Swift* and *NuSTAR* observations of the source. Though the data shown in fig. 2 of Fürst et al. (2015) were up to 50 keV, we used *Suzaku* data in 0.8–70 keV range to compare both the results. The spectral parameters obtained from our fitting were found to be comparable (within errors) with the parameters obtained from the *NuSTAR* observations and given in Table 1. While fitting *Suzaku* data with the model was used by Fürst et al. (2015), an absorption like feature at ~ 45 keV was also seen (third panel of Fig. 2). A careful look at the trend of distribution of points at ~ 45 –50 keV in the residuals obtained from the spectral fitting of Obs.1 data (second and third panels of fig. 2 of Fürst et al. 2015) indicates a hint of presence of an absorption-like feature.

Statistical significance of ~ 45 keV absorption feature was tested by using *XSPEC* script *simfrest* as applied in the case of IGR J17544–2619 (Bhalerao et al. 2015). Including systematic uncertainty of 0.3 per cent (15–40 keV) and 1.9 per cent (40–70 keV) in PIN background model, we simulated 1000 fake spectra for partial

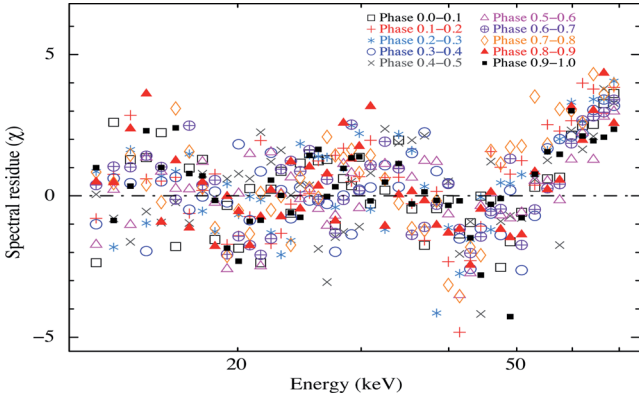


Figure 3. Spectral residuals obtained from the phase-resolved spectra while fitted with partial covering NPEX continuum model with a fundamental cyclotron absorption line at ~ 28 keV. An absorption like feature in ~ 40 – 50 keV range is clearly seen in each of the phase intervals of the pulsar.

covering NPEX model and estimated the differences in χ^2 ($\Delta\chi^2$) without and with ~ 45 keV cyclotron absorption line. The maximum value of $\Delta\chi^2$ from 1000 simulations was found to be 17.8 which is less than observed $\Delta\chi^2 = 27.2$ for three degree of freedom in real data. Corresponding to this, we confirmed the significant detection of ~ 45 keV absorption feature at $>4\sigma$ level.

3.1.2 Pulse-phase-resolved spectroscopy

We performed phase-resolved spectroscopy to understand the change in cyclotron absorption line parameters with the pulse phase of the pulsar. Another motivation in doing phase-resolved spectroscopy was to study the presence of ~ 45 keV absorption line as well as its dependence on pulse-phases of the pulsar. Detection of absorption feature at ~ 45 keV at each pulse-phase bins can confirm the detection of first cyclotron harmonic in Cep X-4. For this, the phase-resolved spectroscopy was carried out by accumulating source spectra in 10 pulse-phase bins. XIS-3 and PIN phase-resolved spectra were extracted by applying phase filter in `XSELECT`. Using the same background, response and effective area files as used in phase-averaged spectroscopy, the phase-resolved spectroscopy was carried out in 0.8–70 keV range. Partial covering NPEX model with a cyclotron component at ~ 28 keV was used to describe the phase-resolved spectrum. While fitting, the normalization constants, equivalent hydrogen column density (N_{HI}), iron line parameters and cyclotron width were fixed to the corresponding phase-averaged values as given in Table 1.

Spectral residues obtained from fitting all phase-resolved spectra with above model are shown in Fig. 3. Presence of an additional significant absorption feature in ~ 40 – 50 keV range can be clearly seen in each phase intervals. Detection of the ~ 45 keV absorption line in phase-averaged as well as phase-resolved spectra ensures that this feature is not spurious and model dependent. This feature can be interpreted as the first cyclotron harmonic of the ~ 28 keV fundamental line. Inclusion of a CRSF at this energy improved the spectral fitting significantly as in the case of phase-averaged spectroscopy. During the fitting, widths of both cyclotron lines were frozen at phase-averaged value to constrain the absorption features. Variation of best-fitting cyclotron line parameters with pulse phase are shown in Fig. 4 along with hard X-ray source flux.

Cyclotron parameters such as depth and energy of both the lines were found significantly variable with pulse phase with maximum

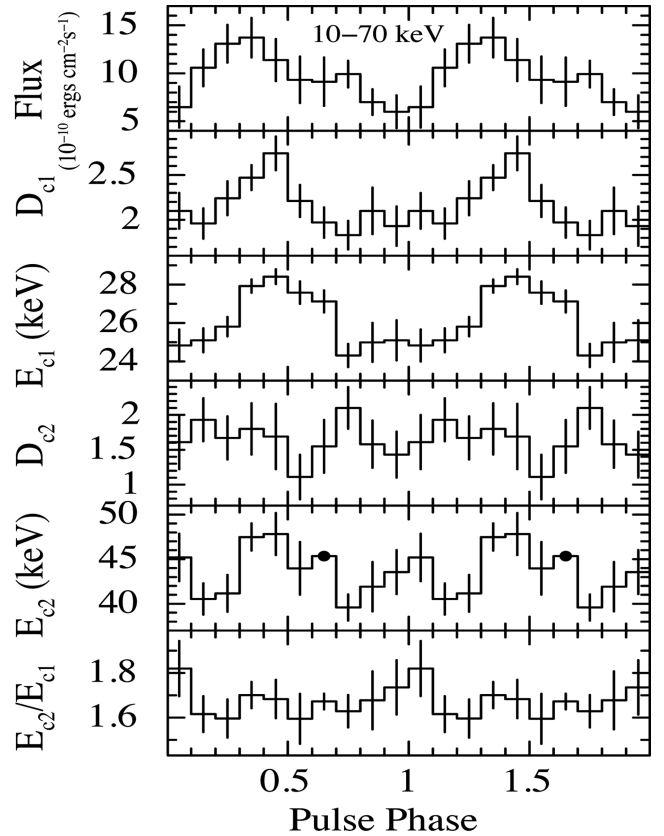


Figure 4. Spectral parameters (with 90 per cent errors) obtained from the phase-resolved spectroscopy of Cep X-4. Top panel shows estimated source flux in 10–70 keV energy range. The values of cyclotron line parameters such as depths and energies for fundamental and first harmonic and ratio between harmonic and fundamental line energies (E_{c2}/E_{c1}) are shown in second, third, fourth, fifth and sixth panels, respectively. Solid circles in the fifth panel indicate that the cyclotron line energy was fixed for corresponding phase-bin at the phase-averaged value.

values in 0.3–0.6 phase range. However, the peak values of these parameters were slightly phase shifted (0.1 phase) with the peaks of 10–70 keV pulse profile and source flux. Depth of fundamental line was variable in the range of 1.8–2.7 (~ 20 per cent of the phase-averaged value). Depth of first cyclotron harmonic was found to be marginally variable with the pulse phase of the pulsar. The variation of the energy of the first harmonic was found to be double (~ 8 keV) of that of the fundamental line (~ 4 keV). However, while computing the ratio between the energy of the first harmonic and the fundamental cyclotron line, it was found to be in ~ 1.6 – 1.8 range. Source flux in 10–70 keV range was found to follow similar pattern as the pulse profile in same energy band.

4 DISCUSSION AND CONCLUSIONS

We report the detection of first harmonic of the cyclotron absorption line in Cep X-4. Though the pulsar was observed with *NuSTAR* during same outburst, data from *Suzaku* observation with longer exposure (twice that of *NuSTAR*) confirmed the detection of the harmonic at ~ 45 keV. The harmonic feature was found to be model independent and also present in each bin of the phase-resolved spectra of the pulsar. Statistical tests on the *Suzaku* data also confirmed the detection of the harmonic of the cyclotron line at ~ 45 keV. Though *NuSTAR* has better effective area at ~ 50 keV than *Suzaku*,

long exposure of the *Suzaku* observation detected the additional feature at ~ 45 keV.

Cyclotron absorption features in the broad-band X-ray spectrum originate due to the resonance scattering of photons with quantized electrons in the presence of magnetic field. Depending on the strength of the magnetic field, the states of electrons are quantized in harmonically spaced levels such that the first harmonic energy is expected to be at twice of the fundamental energy. In the present case of Cep X-4, however, the first harmonic is detected at an energy which is ~ 1.7 times that of the fundamental line which is less than the ideal coupling factor of 2. An-harmonic spacing between fundamental and harmonic lines has also been seen in a few other X-ray pulsars and described by considering the relativistic effects in photon–electron scattering for small changes in the energy ratio (Mészáros 1992; Schönherr et al. 2007). However, this may not be the only cause that can produce the anharmonicity in lines. Cyclotron absorption phenomena for fundamental and harmonic lines occurring at two different scaleheights can have different optical depths and introduce the anharmonicity in the coupling factor or line energy ratio. In detailed studies of cyclotron lines, Nishimura (2005) and Schönherr et al. (2007) showed that the increase in magnetic field within a line-forming region can result the line ratio less than 2, as seen in 4U 0115+63 (Heindl et al. 1999) and Cep X-4 (this work). At larger viewing angle $\mu = 0.79$, the line ratio is expected to be 1.73 for polar cap radius of 1.5 km (Nishimura 2013). Such decrease in energy ratio (1.57–1.73) is possible for viewing angle of 0.52–0.79 where superimposition of large numbers of fundamental line emerging from different heights of line-forming region shifts the energy to higher side with nearly constant energy for first harmonic. In another scenario, the anharmonicity in the line ratio can be expected due to distortion or displacement from the dipole geometry of the magnetic field. In this case, both CRSFs are generated at two different poles of neutron star and produce a significant phase shift between both line parameters. Such phase-shift was not seen in Cep X-4 (Fig. 4).

For the first time, we present the detailed analysis of fundamental cyclotron line with previously unknown first cyclotron harmonic in Cep X-4. Numerous simulation works on cyclotron lines were done by considering certain sets of assumptions and geometry in line-forming regions (Araya-Góchez & Harding 2000; Schönherr et al. 2007; Mukherjee & Bhattacharya 2012). These studies predicted that the cyclotron absorption line parameters are expected to show 10–20 per cent variation over pulse phases depending on the viewing angle of the accretion column. However, more than 30 per cent variation in cyclotron parameters can be explained by considering distortion in the magnetic dipole geometry of the pulsar (Schönherr et al. 2007; Mukherjee & Bhattacharya 2012). In Cep X-4, both cyclotron line parameters are varying within 20 per cent over pulse phase, which can be described in terms of the viewing angle or local distortion in magnetic field. Detailed modelling of the observed variations in cyclotron parameters would provide useful information

about the neutron star magnetic field geometry, inclination and beaming or emission patterns. However, these works are beyond the scope of this Letter.

In summary, we report the detection of the first harmonic of ~ 28 keV fundamental cyclotron absorption feature at ~ 45 keV in Cep X-4. This feature was clearly seen in the phase-averaged and phase-resolved spectra from the *Suzaku* observation in 2014 July. The values of the energy of first harmonic with fundamental line were found anharmonic with ratio of 1.7. Parameters of both the fundamental and first harmonic lines were variable within 20 per cent with pulse phase which is explained as the effect of viewing angle or local perturbation in magnetic field of line-forming region.

ACKNOWLEDGEMENTS

We sincerely thank the anonymous referee for valuable comments which improved this Letter significantly. This research has made use of *Suzaku* data obtained through HEASARC Online Service.

REFERENCES

- Araya-Góchez R. A., Harding A. K., 2000, *ApJ*, 544, 1067
 Bhalerao V. et al., 2015, *MNRAS*, 447, 2274
 Bonnet-Bidaud J. M., Mouchet M., 1998, *A&A*, 332, L9
 Fürst F. et al., 2015, *ApJ*, 806, L24
 Heindl W. A., Coburn W., Gruber D. E., Pelling M. R., Rothschild R. E., Wilms J., Pottschmidt K., Staubert R., 1999, *ApJ*, 521, L49
 Koyama K. et al., 1991, *ApJ*, 366, L19
 McBride V. A. et al., 2007, *A&A*, 470, 1065
 Makino F., Ginga Team, 1988, *IAU Circ.*, 4575
 Makishima K., Mihara T., Nagase F., Tanaka Y., 1999, *ApJ*, 525, 978
 Mészáros P., 1992, *High-energy Radiation from Magnetized Neutron Stars*. Univ. Chicago Press, Chicago, IL
 Mihara T., Makishima K., Kamijo S., Ohashi T., Nagase F., Tanaka Y., Koyama K., 1991, *ApJ*, 379, L61
 Mitsuda K. et al., 2007, *PASJ*, 59, 1
 Mukherjee D., Bhattacharya D., 2012, *MNRAS*, 420, 720
 Nishimura O., 2005, *PASJ*, 57, 769
 Nishimura O., 2013, *PASJ*, 65, 84
 Paul B., Naik S., 2011, *Bull. Astron. Soc. India*, 39, 429
 Pottschmidt K. et al., 2012, in Petre R., Mitsuda K., Angelini L., eds, *AIP Conf. Proc. Vol. 1427, Suzaku 2011: Exploring the X-ray Universe: Suzaku and Beyond*. Am. Astron. Soc., Melville, NY, p. 60
 Roche P., Green L., Hoenig M., 1997, *IAU Circ.*, 6698
 Schönherr G., Wilms J., Kretschmar P., Kreykenbohm I., Santangelo A., Rothschild R. E., Coburn W., Staubert R., 2007, *A&A*, 472, 353
 Titarchuk L., 1994, *ApJ*, 434, 313
 Ulmer M. P., Baily W. A., Wheaton W. A., Peterson L. E., 1973, *ApJ*, 184, L117
 White N. E., Swank J. H., Holt S. S., 1983, *ApJ*, 270, 711

This paper has been typeset from a $\text{\TeX}/\text{\LaTeX}$ file prepared by the author.

POSSIBLE DETECTION OF A CYCLOTRON RESONANCE SCATTERING FEATURE IN THE X-RAY PULSAR 4U 1909+07

GAURAVA K. JAISAWAL¹, SACHINDRA NAIK¹, AND BISWAJIT PAUL²

¹ Astronomy & Astrophysics Division, Physical Research Laboratory, Ahmedabad 380009, India; gaurava@prl.res.in

² Raman Research Institute, Sadashivnagar, C. V. Raman Avenue, Bangalore 560080, India
Received 2013 April 22; accepted 2013 September 28; published 2013 November 25

ABSTRACT

We present timing and broad band spectral studies of the high-mass X-ray binary pulsar 4U 1909+07 using data from *Suzaku* observations during 2010 November 2–3. The pulse period of the pulsar is estimated to be 604.11 ± 0.14 s. Pulsations are seen in the X-ray light curve up to ~ 70 keV. The pulse profile is found to be strongly energy-dependent: a complex, multi-peaked structure at low energy becomes a simple single peak at higher energy. We found that the 1–70 keV pulse-averaged continuum can be fit by the sum of a blackbody and a partial covering Negative and Positive power law with Exponential cutoff model. A weak iron fluorescence emission line at 6.4 keV was detected in the spectrum. An absorption-like feature at ~ 44 keV was clearly seen in the residuals of the spectral fitting, independent of the continuum model adopted. To check the possible presence of a cyclotron resonance scattering feature (CRSF) in the spectrum, we normalized the pulsar spectrum with the spectrum of the Crab Nebula. The resulting Crab ratio also showed a clear dip centered at ~ 44 keV. We performed statistical tests on the residuals of the spectral fitting and also on the Crab spectral ratio to determine the significance of the absorption-like feature and identified it as a CRSF of the pulsar. We estimated the corresponding surface magnetic field of the pulsar to be 3.8×10^{12} G.

Key words: pulsars: general – stars: individual (4U 1909+07) – stars: neutron – X-rays: stars

1. INTRODUCTION

Accretion-powered X-ray binary pulsars, which were discovered in the early 1970s (Giacconi et al. 1971), are among the brightest X-ray sources in the sky. These binary systems consist of a neutron star with a strong magnetic field ($B \sim 10^{12}$ G) and a supergiant or a Be star as an optical companion. Mass transfer from the companion star to the neutron star takes place through Roche lobe overflow (in the case of low-mass X-ray binaries such as Her X-1; Reynolds et al. 1997) and/or capture of stellar wind (in high-mass X-ray binary (HMXB) systems). The accreted matter is channeled toward the magnetic poles of the neutron star by its strong magnetic field and forms accretion columns from where the gravitational energy of accreted matter is being dissipated in the form of X-rays. Most accretion-powered X-ray pulsars belong to the group of HMXB systems. Based on spectral and luminosity class of companion stars, the HMXBs are further classified into two subgroups: (1) supergiant X-ray binary (SGXB) systems and (2) Be/X-ray binary systems. In case of SGXBs, the optical companion is an OB supergiant star whereas the Be/X-ray binary systems associate with non-supergiant B-type stars that show Balmer emission lines in their spectra.

The energy spectra of accretion-powered X-ray pulsars are generally described by phenomenological models consisting of a power law with a photon index ~ 1 , a high energy cutoff (dal Fiume et al. 1998), and a Gaussian function at 6.4 keV for the presence of iron fluorescence emission. In some cases, a blackbody or bremsstrahlung component is required to describe the presence of excess emission at soft X-rays (Paul et al. 2002; Naik & Paul 2004a, 2004b; Hickox et al. 2004). The broadband X-ray spectra of some pulsars have been described with the Negative and Positive power law with EXponential cutoff (NPEX) continuum model, which is an approximation of the unsaturated thermal Comptonization in hot plasma (Makishima et al. 1999). The NPEX continuum model reduces

to a simple power law with a negative slope at low energies that is often used to describe the spectra of accretion-powered X-ray pulsars. In the case of transient Be/X-ray binary pulsars, these continuum models are marginally modified to describe the presence of absorption features at certain pulse phases. A partial covering, high-energy cutoff power-law model is being used to describe the broadband spectrum of many transient pulsars (Paul & Naik 2011; Naik et al. 2011, and references therein). This model consists of two power-law continua with a common photon index but with different hydrogen-absorbing column densities. Several emission lines due to fluorescence from ions at different ionization levels and broad absorption-like features due to cyclotron resonance scattering are often seen in the pulsar spectrum. The magnetic field strength B and the cyclotron resonance energy E_a are related through the relation $E_a = 11.6 B_{12} (1 + z_g)^{-1}$ (keV), where z_g is the gravitational redshift and B_{12} is the magnetic field strength in units of 10^{12} G. Detection of a cyclotron scattering resonance feature (CRSF) in the spectrum, therefore, provides the direct measurement of the strength of the pulsar magnetic field. The CRSFs have been detected in the spectrum of about 19 X-ray pulsars (Coburn et al. 2002; Staubert 2003; Pottschmidt et al. 2012) using data from several X-ray observatories. The harmonics of fundamental cyclotron absorption lines are also detected in some pulsars (Nakajima et al. 2006; Orlandini et al. 2012).

The HMXB pulsar 4U 1909+07 was discovered with the *Uhuru* satellite and referenced as 3U 1912+07 in third *Uhuru* catalog (Giacconi et al. 1974). The position of the pulsar was refined and the source was renamed 4U 1909+07 in the fourth catalog (Forman et al. 1978). The presence of many other sources in the intensity range of 2–12 mCrab and the 2–10 keV energy range was reported at nearby coordinates of 4U 1909+07 through observations with different missions such as *OSO7*, *Ariel5*, *HEAO – 1*, and *EXOSAT*. Wen et al. (2000) recognized that all the sources such as 4U 1909+07, 3A 1907+074, 1H 1907+074, GPS 1908+075, 1E 1908.4+0730,

and X1908+075 reported through various surveys are consistent to within an uncertainty of $1'$. The orbital period of the binary system was reported to be 4.4 days using *Rossi X-Ray Timing Explorer (RXTE)* All-Sky Monitor data (Wen et al. 2000). Using *RXTE* Proportional Counter Array observations of 4U 1909+07, pulsations with a 605 s period were detected in the X-ray flux (Levine et al. 2004). The orbital inclination, orbital separation, and mass of the companion star were estimated to be in the range of 38° – 72° , 60–80 lt-s, and 9–31 M_\odot , respectively (Levine et al. 2004). The detection of an OB star in the near-infrared within the X-ray error box of the pulsar confirmed the system to be an OB supergiant-neutron star HMXB (Morel & Grosdidier 2005). The distance of the binary system was estimated to be ~ 7 kpc (Morel & Grosdidier 2005). *RXTE* and *INTEGRAL* observations of the pulsar showed that the 605 s pulsation in the X-ray flux is not stable; it changes erratically on time scales of years (Fürst et al. 2011). The pulse profile was found to be strongly energy-dependent. The phase-averaged spectrum, obtained from the above observations, was well described by a power law with a high-energy cutoff continuum model along with a blackbody component (Fürst et al. 2011). Fürst et al. (2012) also analyzed data from *Suzaku* observations of the pulsar and described the spectrum using the same model as was used in their earlier work. In both cases, there was no detection of CRSF in the pulsar spectrum. Data from *Suzaku* observation were used in later case and the high energy data were truncated at 40 keV in the spectral fitting. However, using the same data set up to high energy ranges, we detected an absorption-like feature at ~ 44 keV and interpreted it as possible CRSF in the pulsar spectrum. The details of analysis and results we obtained are described in the following sections.

2. OBSERVATION AND ANALYSIS

The HMXB pulsar 4U 1909+07 was observed with *Suzaku* on 2010 November 2–3. We used the publicly available archival data of processing version 2.5.16.28 in the present work to investigate the timing and spectral properties of the pulsar. The observations were carried out at the “XIS nominal” pointing position for effective exposures of ~ 30 ks and ~ 22 ks for the X-ray Imaging Spectrometer (XIS) and the Hard X-ray Detector (HXD), respectively. XIS was operated with “normal” clock mode in the “1/4 window” option. In this operational mode, the time resolution and field of view (FoV) of XIS are 2 s and 17.8×4.4 , respectively.

Suzaku, the fifth Japanese X-ray astronomy satellite, was launched by the Japan Aerospace Exploration Agency (JAXA) on 2005 July 10 (Mitsuda et al. 2007). The instruments on board *Suzaku* cover the 0.2–600 keV energy range through two sets of instruments, XIS (Koyama et al. 2007) and HXD (Takahashi et al. 2007). XIS consists of imaging CCD cameras that are located at the focal plane of the X-Ray Telescope (XRT). Among the four XISs, XIS-0, XIS-2, and XIS-3 are front illuminated (FI), whereas XIS-1 is back illuminated (BI). In full-window mode, the effective area of XIS is 340 cm^2 for front illumination and 390 cm^2 for back illumination at 1.5 keV. Due to large charge leakage in the imaging region, XIS-2 has not longer been operational since 2007 September. The non-imaging detector HXD consists of two types of instruments such as silicon PIN diodes covering the 10–70 keV energy range and the GSO crystal scintillator covering the 30–600 keV energy range. The effective area of PIN is 145 cm^2 at 15 keV and for the effective area of GSO is 315 cm^2 at 100 keV. The FoVs of XIS and PIN are $18' \times 18'$ and $34' \times 34'$ in open window

mode, respectively. GSO has same FoV as PIN up to 100 keV. As XIS-2 is no longer operational, the data from the other 3 XISs, PIN, and GSO are used in the present analysis.

For analysis, we used HEASoft software package (version 6.12). The calibration database (CALDB) files, released in 2012 February 10 (for XIS) and 2011 September 13 (for HXD) by the instrument teams are used for data reduction. The unfiltered event files are reprocessed using the “aepipeline” package of FTOOLS. These reprocessed cleaned event files are used for further analysis. The arrival times of X-ray photons were converted to arrival times at the solar system barycenter by applying the “aebarycen” task of FTOOLS on the reprocessed cleaned event files of XIS, PIN, and GSO. Source light curves and spectra were accumulated from XIS reprocessed cleaned event data by selecting a circular region with a $3'$ diameter around the central X-ray source. The XIS background spectra were extracted from the same event files by selecting circular regions away from the source position. By using the “xisrmfgen” and “xissimarfgen” tasks of FTOOLS, the response files and effective area files for each XIS were generated for spectral fitting. Using reprocessed and cleaned HXD data, light curves and spectra were accumulated by using the task “XSELECT” of FTOOLS. Simulated background event data (provided by the instrument teams) were used to estimate the HXD/PIN and HXD/GSO backgrounds for 4U 1909+07 observations. The response files released in 2010 July (for HXD/PIN) and 2010 May (for HXD/GSO) were used for spectral analysis. An additional effective area file, released in 2010 May, was used for HXD/GSO.

3. RESULTS AND DISCUSSION

3.1. Timing Analysis

As described above, source light curves with time resolutions of 2 s, 1 s, and 1 s were extracted from barycenter-corrected XIS, HXD/PIN, and HXD/GSO reprocessed event data. The orbital period of the binary system is short (4.4 days) and *Suzaku* observations of the pulsar spanned a significant part of the binary orbit, so it is possible that the X-ray pulsations got smeared. To neutralize the effect of orbital motion on the X-ray pulsations, the photon arrival times in each of the light curves were corrected for the binary motion using the ephemeris given by Levine et al. (2004). The orbital motion and barycenter-corrected light curves were used for timing studies of the pulsar. By applying pulse folding and the χ^2 maximization technique, the pulse period of the pulsar was estimated to be 604.11 ± 0.14 s for XIS-0 and 604.08 ± 0.13 s for HXD/PIN. The pulse period of 604.11 s estimated from the XIS light curve was used to generate pulse profiles of the pulsar in the 0.4–12 keV, 10–70 keV, and 40–200 keV energy ranges using background-subtracted XIS, HXD/PIN, and HXD/GSO light curves, respectively. The corresponding pulse profiles are shown in Figure 1. From this figure, it is seen that the pulse profiles are strongly energy-dependent. In soft X-rays (top panel of the figure), the shape of the profile is found to be complex because of the presence of dip-like features, whereas it becomes a single peaked profile in the 10–70 keV (HXD/PIN) energy range (middle panel). The pulsations are either absent or marginal in the 40–200 keV (HXD/GSO) energy range (bottom panel). To investigate the evolution of pulse profile with energy, several energy-resolved light curves were extracted from the barycenter-corrected XIS, HXD/PIN, and HXD/GSO event data. An orbital correction was applied to all the light curves before generating the pulse

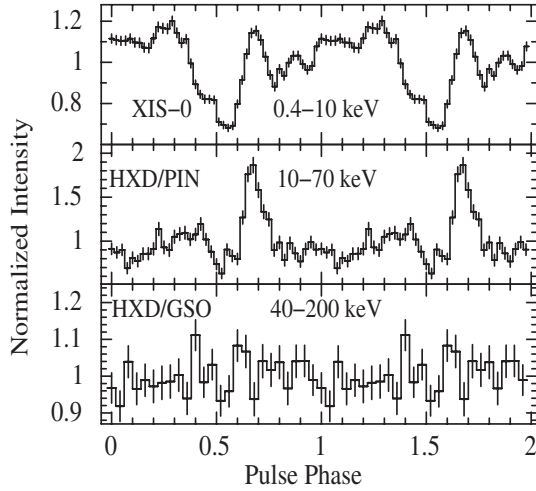


Figure 1. Pulse profiles of the HMXB pulsar 4U 1909+07 in 0.4–12 keV (XIS-0), 10–70 keV (HXD/PIN), and 40–200 keV (HXD/GSO) energy ranges are shown. The profiles are obtained from corresponding light curves by estimated 604.11 s pulse period of the pulsar. The errors shown in the figure are estimated for 1σ confidence level. Two pulses are shown for clarity.

profiles. The corresponding energy-resolved pulse profiles are shown in Figure 2. The evolution of pulse profile from a complex shape at soft X-rays to a single-peaked profile up to ~ 70 keV can be clearly seen in Figure 2. It can be seen that the 604.11 s pulsation is present in GSO light curves up to 70 keV energy range, beyond which it is absent.

The pulse profiles of the HMXB pulsar 4U 1909+07 strongly depend on energy. At low energies (≤ 10 keV), the shape of the profile is found to be complex because of the presence of several dip-like structures. These structures disappear at high energies, making the pulse profile single-peaked in the 10–70 keV energy range, beyond which the pulsations are absent in the pulsar. Energy-dependent dips or dip-like features in the pulse profile are seen in many accretion-powered X-ray pulsars such as

4U 0115+63 (Tsygankov et al. 2007), A 0535+262 (Naik et al. 2008), 1A 1118–61 (Maitra et al. 2012, and references therein), GRO J1008–57 (Naik et al. 2011), EXO 2030+375 (Naik et al. 2013), etc. Detailed pulse-phase resolved spectral analysis of many HMXB pulsars such as GRO J1008–57 (Naik et al. 2011), 1A 1118–61 (Devasia et al. 2011a; Maitra et al. 2012), GX 304-1 (Devasia et al. 2011b), EXO 2030+375 (Naik et al. 2013), etc. showed complex pulse profile structure, which was interpreted as being due to the presence of an additional stream of matter at certain pulse phases, which are phase locked to the neutron star. Absorption of soft X-ray photons by the additional matter in narrow streams causes dips or dip-like features in the pulse profiles.

3.2. Spectral Analysis

A pulse-phase averaged spectral analysis of 4U 1909+07 was performed using spectra accumulated from the XIS-0, XIS-1, XIS-3, PIN, and GSO detectors. The corresponding background spectra and response files were obtained as described above. Spectra from both FI CCDs (XIS-0 and XIS-3) and corresponding background spectra and response files were merged together by applying the task “addascaspec.” Simultaneous spectral fitting was carried out by using the spectrum, background, and response data files of merged FI CCDs (0.8–10 keV), XIS-1 (0.8–10 keV), HXD/PIN (12–70 keV), and HXD/GSO (40–100 keV) with the software package XSPEC v12.7. Because of the presence of known artificial structures in XIS energy spectra around the Si and Au edge, data in the 1.7–1.9 keV and 2.2–2.4 keV energy ranges were ignored in the spectral fitting. XIS spectra were re-binned by a factor of 8 from 0.8 keV to 2 keV and by a factor of 6 from 2 keV to 10 keV. The HXD/PIN spectrum was re-binned by a factor of 2 from 25 keV to 40 keV and by a factor of 6 from 40 keV to 70 keV. The binning of GSO spectrum was suggested by the instrument team. All spectral model parameters except for the relative instrument normalizations were tied together in the spectral fitting. We attempted to fit the broadband continuum

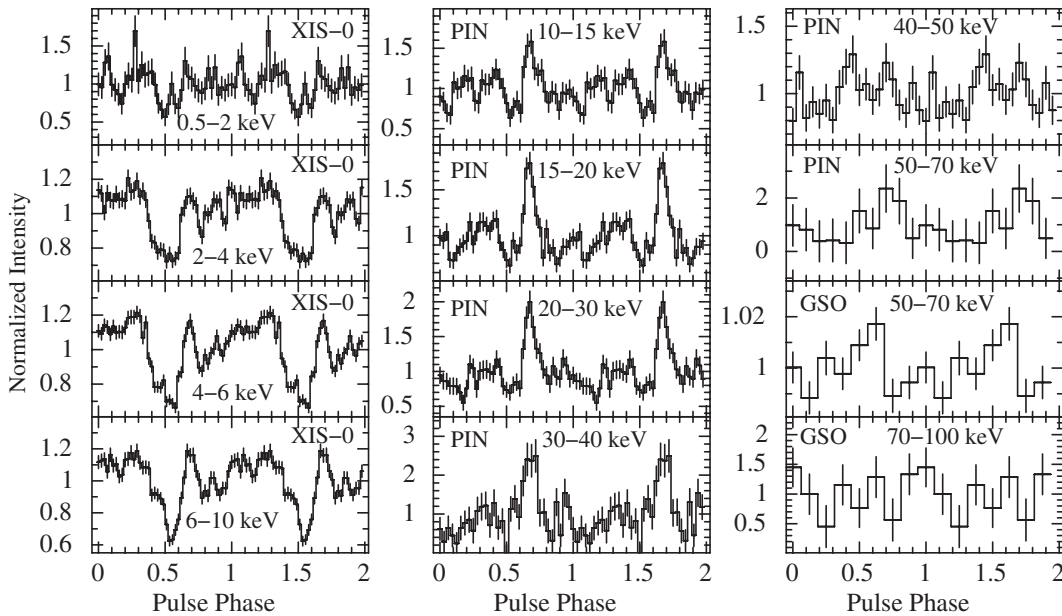


Figure 2. Energy-resolved pulse profile of 4U 1909+07 at different energy bands obtained from XIS-0, HXD/PIN, and HXD/GSO data. The evolution of the pulse profile from a complex shape in soft X-ray energy ranges to a single-peaked profile up to ~ 40 keV can be clearly seen. The pulsation in GSO can be seen up to ~ 70 keV.

Table 1
Best-fit Parameters of the Phase-Averaged Spectra for 4U 1909+07 from *Suzaku* Observations with 1σ Errors

Parameter	Value					
	Model 1	Model 2	Model 3	Model 4	Model 5	Model 6
N_{H1} (10^{22} atoms cm^{-2})	6.16 ± 0.17	5.95 ± 0.19	7.50 ± 0.21	7.53 ± 0.25	7.09 ± 0.20	7.05 ± 0.19
N_{H2} (10^{22} atoms cm^{-2})	9.71 ± 0.95	8.20 ± 1.28	32.19 ± 8.20	34.01 ± 7.82	38.78 ± 7.89	39.71 ± 7.90
Covering fraction	0.52 ± 0.03	0.47 ± 0.05	0.18 ± 0.04	0.18 ± 0.03	0.19 ± 0.03	0.20 ± 0.03
kT_{BB} (keV)	3.38 ± 0.21	2.71 ± 0.23	0.19 ± 0.01	0.19 ± 0.01	0.20 ± 0.01	0.20 ± 0.01
Norm. ^a of kT_{BB} (10^{-3})	1.50 ± 0.14	1.18 ± 0.18	10.59 ± 3.25	11.07 ± 3.10	5.65 ± 1.70	5.27 ± 1.82
Iron line energy (keV)	6.39 ± 0.01	6.39 ± 0.01	6.39 ± 0.01	6.39 ± 0.01	6.39 ± 0.01	6.39 ± 0.01
Iron line width (keV)	0.01 ± 0.01	0.01 ± 0.01	0.01 ± 0.01	0.01 ± 0.01	0.01 ± 0.01	0.01 ± 0.01
Iron line eq. width (eV)	73 ± 3	72 ± 3	68 ± 3	68 ± 3	69 ± 3	68 ± 3
Power-law index	1.91 ± 0.03	1.77 ± 0.05	1.43 ± 0.05	1.44 ± 0.04	1.05 ± 0.06	1.01 ± 0.07
Norm. ^b of power law (10^{-2})	7.40 ± 0.51	5.36 ± 0.71	4.16 ± 0.50	4.26 ± 0.52		
High energy cutoff (keV)			7.34 ± 0.28	7.37 ± 0.16	13.98 ± 1.77	12.78 ± 1.58
Folding energy (keV)			23.42 ± 1.51	24.23 ± 1.10		
Cyclotron line E_a (keV)		43.75 ± 1.51		43.10 ± 2.09		43.85 ± 1.58
Width of cyclotron line (keV)		4.72 ± 2.58		$1.0^{+2.5}_{-1.0}$		2.04 ± 2.02
Depth of cyclotron line		1.25 ± 0.50		1.01 ± 0.83		1.57 ± 0.89
Flux ^c (in the 1–10 keV range)	1.51 ± 0.10	1.51 ± 0.03	1.51 ± 0.18	1.51 ± 0.16	1.51 ± 0.15	1.51 ± 0.14
Flux ^c (in the 10–70 keV range)	4.22 ± 0.29	4.14 ± 0.40	3.76 ± 0.42	3.76 ± 0.38	3.94 ± 0.69	4.01 ± 0.75
$C_{\text{XIS-03}}/C_{\text{XIS-1}}/C_{\text{PIN}}$	$1.0/0.94/1.11$	$1.0/0.94/1.22$	$1.0/0.94/1.18$	$1.0/0.94/1.17$	$1.0/0.94/1.13$	$1.0/0.94/1.13$
χ^2 (degrees of freedom)	609 (489)	587 (486)	576 (487)	573 (484)	578 (487)	570 (484)

Notes. Model 1: partial-covering, power-law model with blackbody and Gaussian components. Model 2: partial-covering power-law model with blackbody and Gaussian components and a cyclotron line. Model 3: partial-covering, high-energy cutoff power-law model with blackbody and Gaussian components. Model 4: partial-covering, high-energy cutoff power-law model with blackbody and Gaussian components and a cyclotron line. Model 5: partial-covering NPEX model with blackbody and Gaussian components. Model 6: partial-covering NPEX model with blackbody and Gaussian components and a cyclotron line.

N_{H1} , equivalent hydrogen column density; N_{H2} , additional hydrogen column density.

^a In units of 10^{39} erg s^{-1} ($\text{d}/10 \text{ kpc}$) $^{-2}$, where d is the distance to the source.

^b Photons $\text{keV}^{-1} \text{cm}^{-2} \text{s}^{-1}$ at 1 keV.

^c Absorption uncorrected flux (in units of 10^{-10} erg $\text{cm}^{-2} \text{s}^{-1}$).

spectrum of the pulsar with (1) a simple power-law model, (2) a high-energy cutoff power-law model, (3) the NPEX model, and (4) a Comptonization continuum model (Sunyaev & Titarchuk 1985). A partial covering absorption component *pcfabs* was also applied to the above continuum models in spectral fittings. Apart from these, additional components such as photoelectric absorption, a Gaussian function for an iron emission line, and a blackbody component for soft X-ray excesses were needed to describe the continuum spectrum. All of these models produced reasonable fits up to ~ 40 keV, beyond which significant anomalous residuals was noted in the spectral fitting. We tried to obtain a suitable model that described the broadband spectrum of the pulsar in the 0.8–100 keV energy range. While fitting XIS, HXD/PIN, and HXD/GSO spectra simultaneously, we noted that the relative normalization for the HXD/GSO detector was high (≥ 2) compared with XIS and HXD/PIN for all of the above continuum models. The relative normalizations for HXD/PIN and HXD/GSO should be the same or comparable according to the HXD calibration. Apart from high values of the relative instrument normalization for HXD/GSO, the spectrum beyond 100 keV also showed patterns similar to the modeled GSO background spectrum. As the pulsar is very weak in hard X-rays and there is a background-like pattern in 100–150 keV source spectrum after background subtraction, it is likely that the HXD/GSO background is underestimated for this *Suzaku* observation. Considering this, we did not use the HXD/GSO spectrum in spectral fitting and fit the 0.8–70 keV spectrum extracted from XIS and HXD/PIN data by using the above models.

The partial covering power-law continuum model with iron emission lines and a blackbody component with a temperature of

~ 3 keV fit the pulsar spectrum well. A blackbody component with a high temperature as high as ~ 3 keV is unusual in the case of accretion-powered X-ray pulsars. The addition of a high-energy cutoff to the partial covering power-law model fit the data well with a blackbody temperature of ~ 0.2 keV. The parameters obtained by fitting the partial-covering, high-energy cutoff power-law model to the spectrum are in good agreement with Table 2 of Fürst et al. (2012). However, the partial-covering NPEX continuum model with iron lines and a blackbody component described the spectrum better, yielding an acceptable blackbody temperature of 0.2 keV. An absorption-like feature was seen in the pulsar spectrum and in the residuals at ~ 44 keV that allowed us to add a CRSF component in the spectral model. The addition of a CRSF component to the above continuum models improved the χ^2 values for each model (as given in Table 1). The count rate spectra of the pulsar 4U 1909+07 are shown in Figure 3 (for partial covering the partial-covering, power-law model), Figure 4 (for the partial-covering, high-energy cutoff power-law model), and Figure 5 (for the partial-covering NPEX model) along with the model components (top panels). The middle panels in the above three figures show the residuals to the fitted models without the CRSF whereas the bottom panels show the residuals to the best-fitting model using the CRSF component in the spectral models. The presence of an absorption feature at ~ 44 keV can be clearly seen in the middle panels of all figures.

To test the statistical significance of the χ^2 improvement due to the addition of the CRSF component, we performed an F -test. In the case of emission line features (additive components in *XSPEC*), the F -test routine incorporated in the *XSPEC* package should be the best suited to perform the

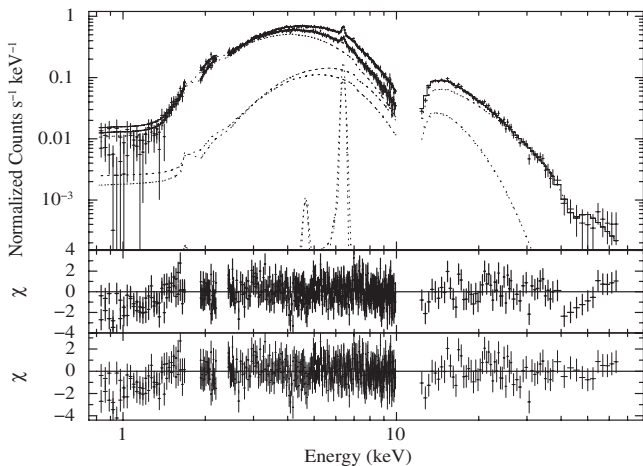


Figure 3. Energy spectrum of 4U 1909+07 obtained with the XIS and HXD/PIN detectors of the *Suzaku* observations, along with the fitted model comprising a partial-covering, power-law continuum model along with a blackbody component, narrow iron line emission, and a CRSF. The middle and bottom panels show the contributions of the residuals to χ^2 for each energy bin for the partial-covering, power-law continuum model without and with a CRSF component in the model, respectively.

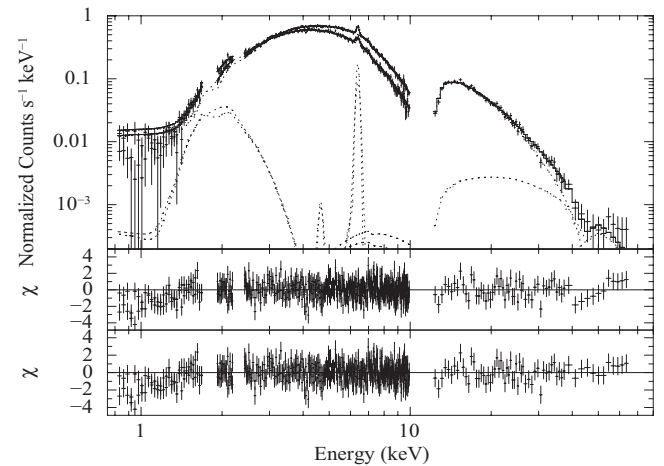


Figure 5. Energy spectrum of 4U 1909+07 obtained with the XIS and HXD/PIN detectors of *Suzaku* observations, along with the best-fit model comprising a partial-covering NPEX continuum model along with a blackbody component, narrow iron line emission, and a CRSF. The middle and bottom panels show the contributions of the residuals to χ^2 for each energy bin for the partial-covering NPEX continuum model without and with a CRSF component in the model, respectively.

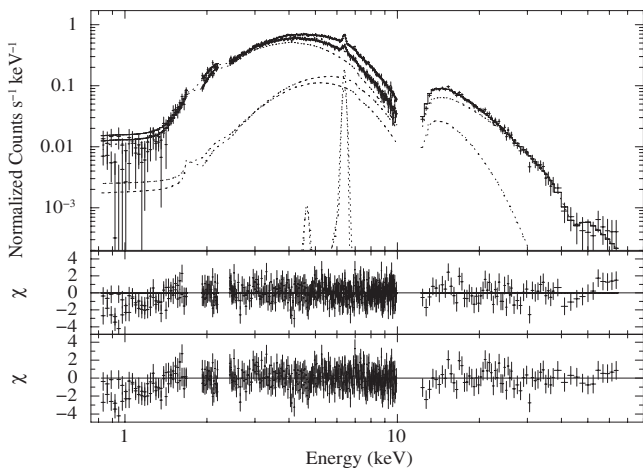


Figure 4. Energy spectrum of 4U 1909+07 obtained with the XIS and HXD/PIN detectors of *Suzaku* observations, along with the fitted model comprising a partial-covering, high-energy cutoff power-law continuum model along with a blackbody component, narrow iron line emission, and a CRSF. The middle and bottom panels show the contributions of the residuals to χ^2 for each energy bin for the partial-covering power-law continuum model without and with a CRSF component in the model, respectively.

significance test (although care should be taken while using this; see Protassov et al. 2002). However, in the case of multiplicative components such as CRSF, the F -test in *XSPEC* is inappropriate for performing the null hypothesis test. The F -test in *XSPEC* is based on the assumption that the inclusion of the new component does not alter the continuum. This is true if the component is added to the continuum model, whereas this is not correct if the component is multiplied by the continuum. Therefore, we used a different F -test, as described in Press et al. (2007), to test the statistical significance of the CRSF component in the spectrum of 4U 1909+07 (see, e.g., Orlandini et al. 2012). The F -test routine is available in the IDL package (named *mpftest*³) and was used for significance tests of multiplicative components such as CRSF or Gaussian

absorption features (Decesar et al. 2013). The probability of chance improvement (PCI) is evaluated for each of the three models used to fit the pulsar spectrum without and with the CRSF component. The estimated PCI values after the addition of the CRSF component to the (1) partial-covering, power-law model with black-body a blackbody, (2) the partial-covering, high-energy cutoff power-law model with a blackbody, and (3) the partial-covering NPEX model with a blackbody are found to be 37%, 51%, and 47%, respectively. Considering the high value of PCI for all three models, the CRSF is found to not be statistically significant. But the residuals shown in the middle panels of Figures 3–5 clearly show an absorption-like feature at ~ 44 keV. It may be noted that the goodness-of-fit estimator chosen here to assess the statistical significance of the CRSF (χ^2) is not the best suited as it does not take into account the “shape” of the residuals. Considering the identical distribution of residuals around 40 keV (the middle panels of Figures 3–5), we applied the run-test (also called the Wald-Wolfowitz test) on the residuals obtained from the spectral fitting by using above three continuum models. The IDL routine for the run-test⁴ was used to derive the null hypothesis of the randomness in the residuals of spectral fitting in the 37–65 keV energy range. It was found that the number of data points used for the run test in the 37–65 keV energy range is 12 (6 points below zero and 6 points above zero), 13 (4 points below zero and 9 points above zero), and 13 (6 points below zero and 7 points above zero) for partial covering the partial-covering power-law, partial-covering, high-energy cutoff, and partial-covering NPEX continuum models, respectively. The probability of getting 3 runs in above the energy range was estimated to be 0.8%, 0.7%, and 0.5%, respectively. The marginal difference in the probability values is because of the use of different continuum models that can affect the residuals in the spectral fitting. The computed probability of $\leq 1\%$ for all three continuum models rejects the hypothesis of random sampling of the detected absorption feature in the pulsar spectrum. Among the three continuum models, it is found

³ <http://www.physics.wisc.edu/~craigm/idl/download/mpftest.pro>

⁴ http://www.astro.washington.edu/docs/idl/cgi-bin/getpro/library07.html?R_TEST

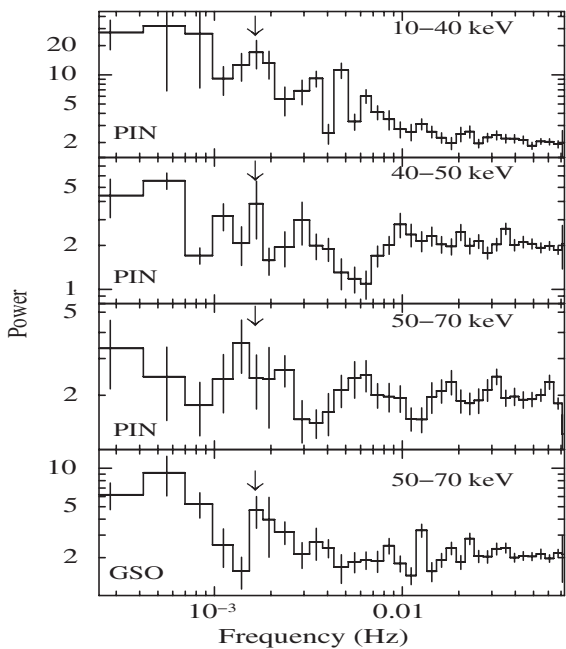


Figure 6. Power density spectra of the HMXB pulsar 4U 1909+07 in the 10–40 keV (top panel), 40–50 keV (second panel), and 50–70 keV (third and fourth panels) ranges. Background-subtracted and orbital-corrected HXD/PIN and HXD/GSO light curves were used to generate power density spectra in each energy range. The arrows indicate the spin period of the pulsar. Additional power can be seen at ~ 1.65 mHz (spin frequency of the pulsar) in all panels.

that the NPEX continuum model with a blackbody, a Gaussian function, and a CRSF feature at ~ 44 keV yields the best fit to the 0.8–70 keV data. The presence of an absorption feature at ~ 44 keV in the residuals of all the models suggest that the CRSF is indeed required in the spectral fitting. The best-fit spectral parameters obtained by using three different continuum models along with additional components are given in Table 1. It can be seen from the table that the addition of a CRSF at ~ 44 keV improved the spectral fitting in all cases.

The same *Suzaku* observations were analyzed, although with the ISIS package, by Fürst et al. (2012). These authors did not use HXD/GSO data because of possible contamination from the nearby source GRS 1915+105 and therefore performed their spectral analysis in the 1–40 keV energy range. Considering the earlier result, the possible CRSF feature at ~ 44 keV was carefully examined by different approaches. As the pulsar is weak in hard X-ray energy ranges, we tried to establish that the observed photons in the spectrum beyond ~ 40 keV are not affected by detector energy response uncertainties. We extracted pulsar light curves in 10–40 keV, 40–50 keV, and 50–70 keV energy ranges from HXD/PIN and HXD/GSO reprocessed event data. The corresponding background light curves were also extracted from the simulated background event data (as described in the previous section). The background-subtracted and orbital-corrected light curves in the above energy ranges were used to generate power density spectra. The energy-resolved power density spectra of 4U 1909+07, as shown in Figure 6, show additional power (peaks) at ~ 1.65 mHz (the spin frequency of the pulsar) in the 10–40 keV (top panel), 40–50 keV (second panel), and 50–70 keV (third and fourth panels) energy ranges. The power density spectra shown in the top three panels were extracted from the corresponding light curves obtained from HXD/PIN data whereas the spectrum shown in the bottom panel was extracted from HXD/GSO data.

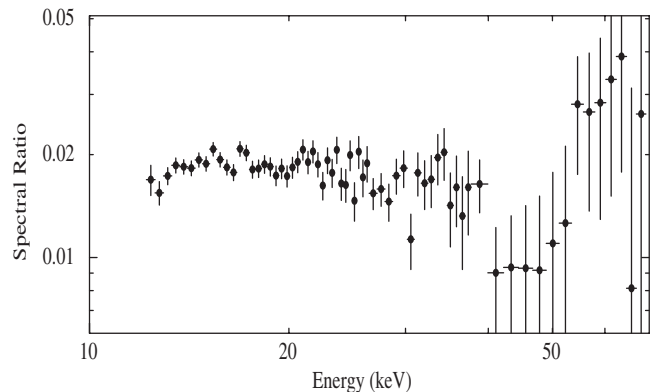


Figure 7. Ratio between the background-subtracted HXD/PIN spectra of the HMXB pulsar 4U 1909+07 and the Crab Nebula. The absorption feature at ~ 44 keV is clearly seen.

The presence of additional power at ~ 1.65 mHz in the power density spectra at 40–50 keV and 50–70 keV confirms that photons beyond 40 keV in the spectrum are not associated with any energy response uncertainties.

To establish the absorption-like feature seen at ~ 44 keV in the pulsar spectrum as CRSF, we evaluated the energy spectra of the pulsar 4U 1909+07 in a model-independent manner. We attempted to normalize the pulsar spectrum with that of the Crab Nebula, the spectrum of which is a featureless power law with a photon index of ~ 2.1 . The normalization (Crab ratio) has the advantage of minimizing the effects due to the detector response and the uncertainties in the energy response. To generate the Crab ratio, we used a Crab observation with *Suzaku* (on 2010 April 5) that is nearest to the observation of the pulsar 4U 1909+07. Data reduction and background estimation for the Crab HXD/PIN data were done as described above and the Crab ratio was obtained to investigate the presence of the absorption feature in the pulsar spectrum. The resulting Crab ratio in the 12–70 keV energy range is shown in Figure 7. The presence of the absorption feature at ~ 44 keV, as was seen in the spectral fitting (middle panels of Figures 3–5), can be clearly seen in the figure. It should be noted here that the shape of this CRSF-like feature in the Crab ratio is very similar to that seen in the middle panels of the above figures. In order to evaluate the statistical significance of the absorption feature, we performed a run test on the Crab ratio data. It was found that in the 37–65 keV energy range in the Crab ratio, there are 13 data points with 3 runs in which 7 points are above zero and 6 points are below zero. The probability of obtaining 3 runs is only $\sim 1\%$. This result, together with the results obtained from the analysis on the spectral residuals, strongly supports the genuine presence of an absorption feature in the Crab ratio at ~ 44 keV. It confirms the presence of CRSF at ~ 44 keV in the HMXB pulsar 4U 1909+07.

4. CONCLUSIONS

In this work, we have studied the timing and spectral properties of the HMXB pulsar 4U 1909+07 using data from *Suzaku* observations. The pulse profiles strongly depend on energy and evolve from a complex shape at lower energy to a single-peaked profile at higher energy. Broadband spectroscopy of the HMXB pulsar 4U 1909+07 in the 1–70 keV energy range is reported here for the first time. Although the pulsar is very weak in hard X-rays, the high sensitivity of the HXD on board *Suzaku* helped in performing phase-averaged spectroscopy at

energies up to 70 keV. The energy spectrum of the X-ray pulsar is well described by a partial-covering NPEX model with a blackbody component. For the first time, we report the possible detection of CRSF at ~ 44 keV in this pulsar. Based on this detection, the magnetic field strength at the neutron star surface is estimated to be $\sim 3.8 \times 10^{12}$ G. It is seen that the values of CRSF detected in accretion-powered X-ray pulsars follow a continuum distribution starting from as low as ~ 11 keV for 4U 0115+634 (Nakajima et al. 2006) to as high as ~ 76 keV for GRO J1008–57 (Yamamoto et al. 2013). Nevertheless, a CRSF at ~ 100 keV is reported in LMC X-4 (La Barbera et al. 2001), but it is yet to be confirmed. Considering the confirmed values of CRSF in X-ray pulsars, the CRSF detected in the pulsar 4U 1909+07 in the present work falls in the higher side. It is to be noted that we report the detection of CRSF at ~ 44 keV in the spectrum of 4U 1909+07, obtained from a ~ 22 ks of exposure with HXD. *Suzaku* observations with long exposures are required to confirm the presence of the absorption feature in this pulsar. The LAXPC instrument on the upcoming *Astrosat* mission will also provide a very good opportunity to establish the CRSF feature in the slow HMXB pulsar 4U 1909+07.

We thank the anonymous referee for constructive comments and suggestions that improved the contents of the paper. The research work at the Physical Research Laboratory is funded by the Department of Space, Government of India. The authors thank all the members of *Suzaku* for their contributions in the instrument preparation, spacecraft operation, software development, and in-orbit instrumental calibration. This research has made use of data obtained through HEASARC Online Service, provided by NASA/GSFC, in support of NASA's High Energy Astrophysics Programs.

REFERENCES

- Coburn, W., Heindl, W. A., Rothschild, R. E., et al. 2002, *ApJ*, **580**, 394
- dal Fiume, D., Orlandini, M., Cusumano, G., et al. 1998, *A&A*, **329**, L41
- Decesar, M. E., Boyd, P. T., Pottschmidt, K., et al. 2013, *ApJ*, **762**, 61
- Devasia, J., James, M., Paul, B., & Indulekha, K. 2011a, *MNRAS*, **414**, 1023
- Devasia, J., James, M., Paul, B., & Indulekha, K. 2011b, *MNRAS*, **417**, 348
- Forman, W., Jones, C., Cominsky, L., et al. 1978, *ApJS*, **38**, 357
- Fürst, F., Kreykenbohm, I., Suchy, S., et al. 2011, *A&A*, **525**, 73
- Fürst, F., Pottschmidt, K., Kreykenbohm, I., et al. 2012, *A&A*, **547**, 2
- Giacconi, R., Gursky, H., Kellogg, E., Schreier, E., & Tananbaum, H. 1971, *ApJL*, **167**, L67
- Giacconi, R., Murray, S., Gursky, H., et al. 1974, *ApJS*, **27**, 37
- Hickox, R. C., Narayan, R., & Kallman, T. R. 2004, *ApJ*, **614**, 881
- Koyama, K., Tsunemi, H., Dotani, T., et al. 2007, *PASJ*, **59**, 23
- La Barbera, A., Burderi, L., Di Salvo, T., Iaria, R., & Robba, N. R. 2001, *ApJ*, **553**, 375
- Levine, A. M., Rappaport, S., Remillard, R., & Savcheva, A. 2004, *ApJ*, **617**, 1284
- Maitra, C., Paul, B., & Naik, S. 2012, *MNRAS*, **420**, 2307
- Makishima, K., Mihara, T., Nagase, F., & Tanaka, Y. 1999, *ApJ*, **525**, 978
- Mitsuda, K., Bautz, M., Inoue, H., et al. 2007, *PASJ*, **59**, 1
- Morel, T., & Grosdidier, Y. 2005, *MNRAS*, **356**, 665
- Naik, S., Dotani, T., Terada, Y., et al. 2008, *ApJ*, **672**, 516
- Naik, S., Maitra, C., Jaisawal, G. K., & Paul, B. 2013, *ApJ*, **764**, 158
- Naik, S., & Paul, B. 2004a, *ApJ*, **600**, 351
- Naik, S., & Paul, B. 2004b, *A&A*, **418**, 655
- Naik, S., Paul, B., Kachhara, C., & Vadawale, S. V. 2011, *MNRAS*, **413**, 241
- Nakajima, M., Mihara, T., Makishima, K., & Niko, H. 2006, *ApJ*, **646**, 1125
- Orlandini, M., Frontera, F., Masetti, N., et al. 2012, *ApJ*, **748**, 86
- Paul, B., Nagase, F., Endo, T., et al. 2002, *ApJ*, **579**, 411
- Paul, B., & Naik, S. 2011, *Bull. Astron. Soc. India*, **39**, 429
- Pottschmidt, K., Suchy, S., Rivers, E., et al. 2012, in *AIP Conf. Ser.* 1427, *Suzaku 2011: Exploring the X-ray Universe: Suzaku and Beyond* (Melville, NY: AIP), 60
- Press, W. H., Teukolsky, S. A., Vetterling, W. T., & Flannery, B. P. 2007, *Numerical Recipes: The Art of Scientific Computing* (Cambridge: Cambridge Univ. Press), 730
- Protassov, R., van Dyk, D. A., Connors, A., Kashyap, V. L., & Siemiginowska, A. 2002, *ApJ*, **571**, 545
- Reynolds, A. P., Quintrell, H., Still, M. D., et al. 1997, *MNRAS*, **288**, 43
- Staubert, R. 2003, *ChJAS*, **3**, 270
- Sunyaev, R. A., & Titarchuk, L. G. 1985, *A&A*, **143**, 374
- Takahashi, T., Abe, K., Endo, M., et al. 2007, *PASJ*, **59**, 35
- Tsygankov, S. S., Lutovinov, A. A., Churazov, E. M., & Sunyaev, R. A. 2007, *AstL*, **33**, 368
- Yamamoto, T., Mihara, T., Sugizaki, M., et al. 2013, *ATel*, **4759**
- Wen, L., Remillard, R. A., & Bradt, H. V. 2000, *ApJ*, **532**, 1119

